STRENGTH AND CREEP TESTING FOR ARTIFICIAL GROUND FREEZING

by

CHRISTOPHER N. HAMPTON, B.Sc

Thesis submitted to the University of Nottingham for the degree of Doctor of Philosophy

OCTOBER 1986

TABLE OF CONTENTS

ABSTRACT

Artificial ground freezing (AGF) provides a means by which excavations can be given temporary or permanent structural support. It may also be used to control the movement of groundwater without the risk of pollution of potable aquifers.

As AGF is called upon to strengthen ground at ever increasing depths, the design process needs to be adapted to account for the greater stresses encountered. In strong materials, the prime consideration is the short term strength of the materials and closed-form formulae can be used in design. In weaker materials, the time dependent creep behaviour of the frozen ground predominates and more complex analysis techniques have been devised (e.g. finite elements). Previous works in this field have been chiefly concerned with uniaxial states of stress. In this thesis, consideration is given to the problem of modelling creep under triaxial stress conditions.

An introduction is followed by an outline of the general applications and design procedures currently used in ice wall design. Descriptions are then given of a selection of soils and weakly cemented rocks which have been incorporated into a programme of tests to investigate both short and long term strength behaviour. The apparatus available at the start of this project was suitable for uniaxial and low pressure triaxial tests only. Equipment subsequently developed to extend the confining pressure capability to 12 MPa, is described in detail.

Short term strength tests show the increase in strength on freezing of ground materials is almost entirely due to the cohesion contributed by the ice matrix. Analysis of the creep test results leads to the development of a new empirically based triaxial creep equation for frozen soils. A sensitivity analysis of the parameters in this equation is followed by its application to a simplified design. Suggestions for further work in this field are included.

ACKNOWLEDGEMENTS

This thesis has been produced at the culmination of a research project based at the University of Nottingham. The author wishes to thank Professor P.S. Pell for making available the facilities of the Civil Engineering Department for the project which was funded by the Science and Engineering Research Council in co-operation with the British Drilling and Freezing Company (formerly Foraky Ltd).

Special thanks are due to Dr. R.H. Jones (academic supervisor) and Mr. J.S. Harris (industrial supervisor) for their invaluable contributions to the project. The author is also indebted to Dr. A.O. Tan for his contributions to the development of the specimen preparation techniques and for the provision of valuable test data on LAL sand.

The author acknowledges the assistance given by the staff and technicians in both the Civil Engineering and Engineering Faculty Workshops during the development of laboratory equipment. Special thanks are extended to Mr. G. Barnes and Mr. R. Collins for their continued involvement.

Finally, I would like to thank Beverly Tribbick for her efficiency and patience in typing this thesis.

NOTATION

a	inner radius of ice wall
a	intercept of K_f failure line
A	creep equation parameter (Klein, Hampton)
ASR	applied stress ratio
b	outer radius of ice wall
b	creep equation parameter
B	creep equation parameter (Klein, Hampton)
c	cohesion
c	creep equation parameter (Gardner)
C	creep equation parameter (Klein, Fish)
$\tilde{C}$	creep equation parameter (Fish)
E	activation energy
G	shear modulus
h	Planck's constant
H	creep equation parameter (Hampton)
H	depth of shaft
k	creep equation parameter (Vyalov)
K	unconfined compressive strength
K	Boltzmann's constant
K	$A\ (\Delta\sigma)^B$ - creep equation parameter (Hampton)
K_o	
m	failure point in creep (Subscript)
m	creep equation parameter (Vyalov, Fish, Jessberger)
n	porosity
n	rate process equation parameter
n	creep equation parameter (Fish, Jessberger)
N	creep equation parameter (Hampton)

p	creep equation parameter (Jessberger)
ps	primary-secondary transition point in creep (Subscript)
P_o	overburden pressure
q	external pressure on ice wall
R	universal gas constant
s	radius of plastic zone in ice wall
s	strength-temperature equation parameter
s	creep equation parameter (Jessberger)
S_i	degree of ice saturation
S_r	degree of saturation
t	ice wall thickness
t	duration of freeze
t	time since stress application in creep test
t_o	Frenkel's relaxation time
t_r	time to rupture
t_N	normalised time (wrt time to failure, t_m)
T	absolute temperature
T_m	absolute melting temperature
U	pore pressure
w	moisture content
w	creep equation parameter (Vyalov)
α	slope of K_f failure line
γ	bulk unit weight
δ	creep equation parameter (Fish)
ΔG	activation energy
ΔS	change of entropy
$\Delta\sigma$	deviator stress
$\Delta\sigma_f$	deviator stress at failure (CDR tests)

ε	true strain
ε_o	pseudo-instantaneous strain
ε_f	strain at failure (CDR tests)
ε_{Nt}	calculated strain normalised w.r.t. actual strain at time t
$\dot{\varepsilon}$	true strain rate
Θ	temperature below freezing point in °C
λ	creep equation parameter (Vyalov, Fish)
ν	Poisson's ratio
ρ_d	dry density
σ	total stress
σ'	effective stress
σ_3	confining pressure
σ_f	failure stress
σ_L	longitudinal stress
σ_o	ultimate strength
σ_r	radial stress
σ_t	tangential stress
σ_v	vertical stress
σ_Θ	tangential stress
τ	normalised time
ϕ	angle of shearing resistance
ψ	integration factor in creep equation (Fish)

CHAPTER 1

INTRODUCTION

1.1 GENERAL INTRODUCTION

Artificial ground freezing (AGF) is a construction technique used to provide temporary support of excavations in low strength water bearing strata (e.g. soils and weak rocks). Freezing is effected by circulating a coolant through double walled pipes (freeze tubes) installed in the ground around the intended excavation. The coolant induces the freezing of pore water around the freeze tubes and an impermeable barrier is established. The AGF process has been recorded in use as far back as 1862 in a coalfield in South Wales.

Applications of AGF have mainly centred on the construction of tunnels, shafts and in-ground storage facilities for liquified gases. The limiting factor in its use is the presence of sufficient water in the pore spaces of the soil to give the required strength and impermeability. The advantages that AGF has over most other geotechnical dewatering processes include suitability to almost all soils, its limitation to localised effects, the non-toxic nature of the treatment and its reversibility (i.e. freezing is a temporary treatment for the duration of a project). This allows AGF to be used safely through aquifers bearing potable water supplies without permanent obstruction or pollution which may be associated with processes such as grouting.

An important characteristic of the mechanical behaviour of soils when frozen is the phenomenom of creep. Creep is the deformation of a material with time under steady state conditions such as constant stress. It has been most extensively studied with respect to metals and many theories have been advanced on the various mechanisms involved.

The upper limit of strength of a crystalline solid is determined by the stress required to shear one plane of atoms relative to another. The is recognised to be of the order of G/20 where G is the shear modulus. The fact that metals deform at stresses lower than this value is a result of the presence of

dislocations and vacancies within the crystal lattice (Gittus 1975). In well ordered crystalline solids creep can be considered a function of the gradual migration of crystal defects or dislocations under the influence of a shear stress. The structure is considerably weakened by their presence as the shear stress need only move single atoms rather than whole planes (the strength can be reduced from G/20 by a factor of 10^3 to 10^4, Sully 1949). The process of dislocation migration is shown schematically in Fig. 1.1. A secondary consideration is the slip that occurs along the grain boundaries which form between adjacent crystals. The effect of grain boundaries on creep is temperature dependent and below 0.5 T_m (the absolute melting temperature) can lead to a decrease in the steady-state creep rate (Bernasconi and Piatti, 1979).

The primary stage of creep is characteristic of strain hardening which, in metals, is caused by the generation and movement of dislocations. At temperatures above 0.4 T_m, dislocation creep settles to a constant rate (secondary creep stage) when the rate of generation of dislocations is balanced by the recovery processes such as climb and cross slip (diffusion processes). Microstructural instability (grain growth, recrystallisation) or mechanical instability (necking, development of cracks) can disrupt these steady state conditions to produce accelerated or tertiary creep and eventually rupture (Evans and Wilshire, 1985).

Frozen soil creep relies on the inhomogeneous nature of the material. Essentially consisting of a mixture of soil grains and ice the stress distribution through frozen soil is uneven and local concentrations of stress are exerted on the ice between adjacent soil particles. Ice is susceptible to pressure melting and as a result of the concentration of stress, this can occur on a microscopic scale within the soil structure. The resulting flow of melted ice away from this zone of high pressure allows the soil particles to reorientate themselves and relieve the stress. The melted ice flows to adjacent regions of lower stress where it refreezes, (Fig. 1.2). On the microscopic scale this produces creep deformation with time.

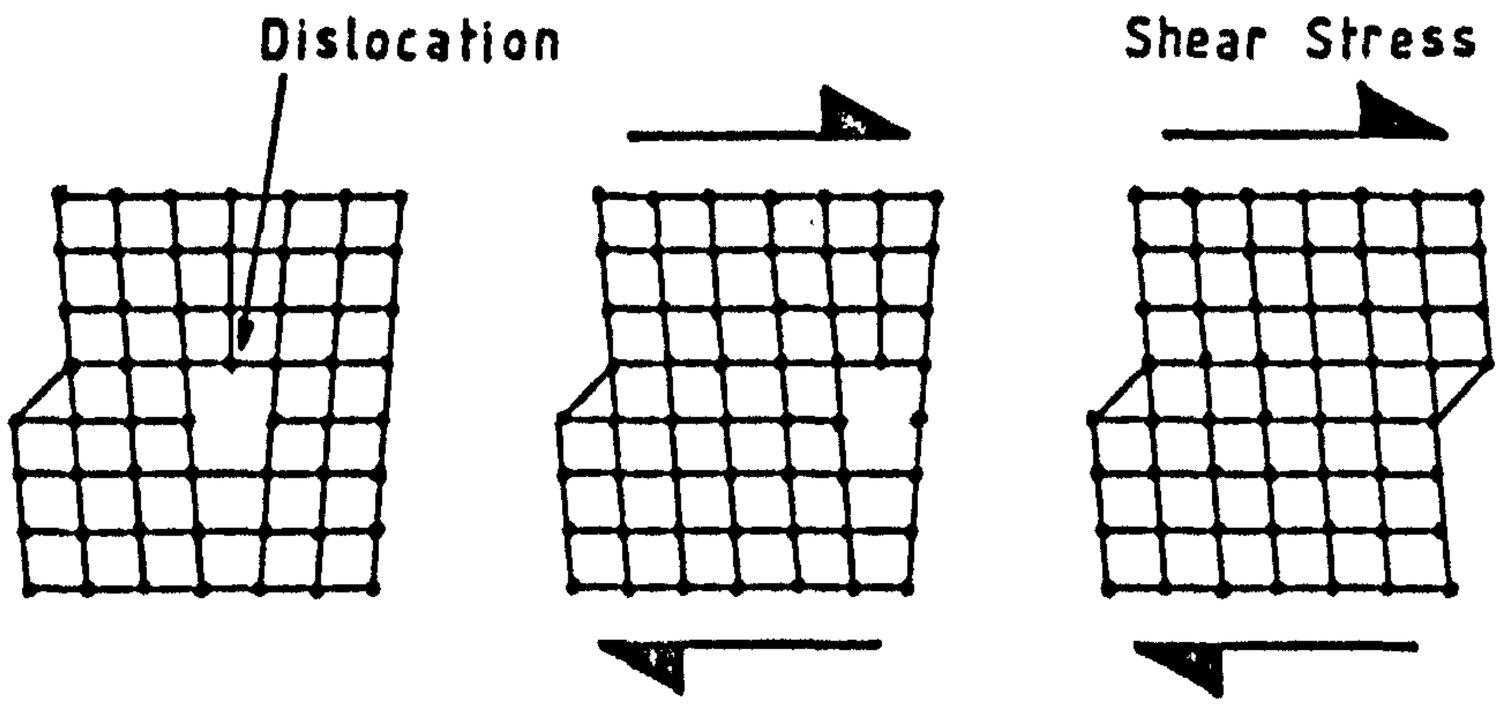

Fig. 1·1 Shear of metal crystal lattice by dislocation migration.

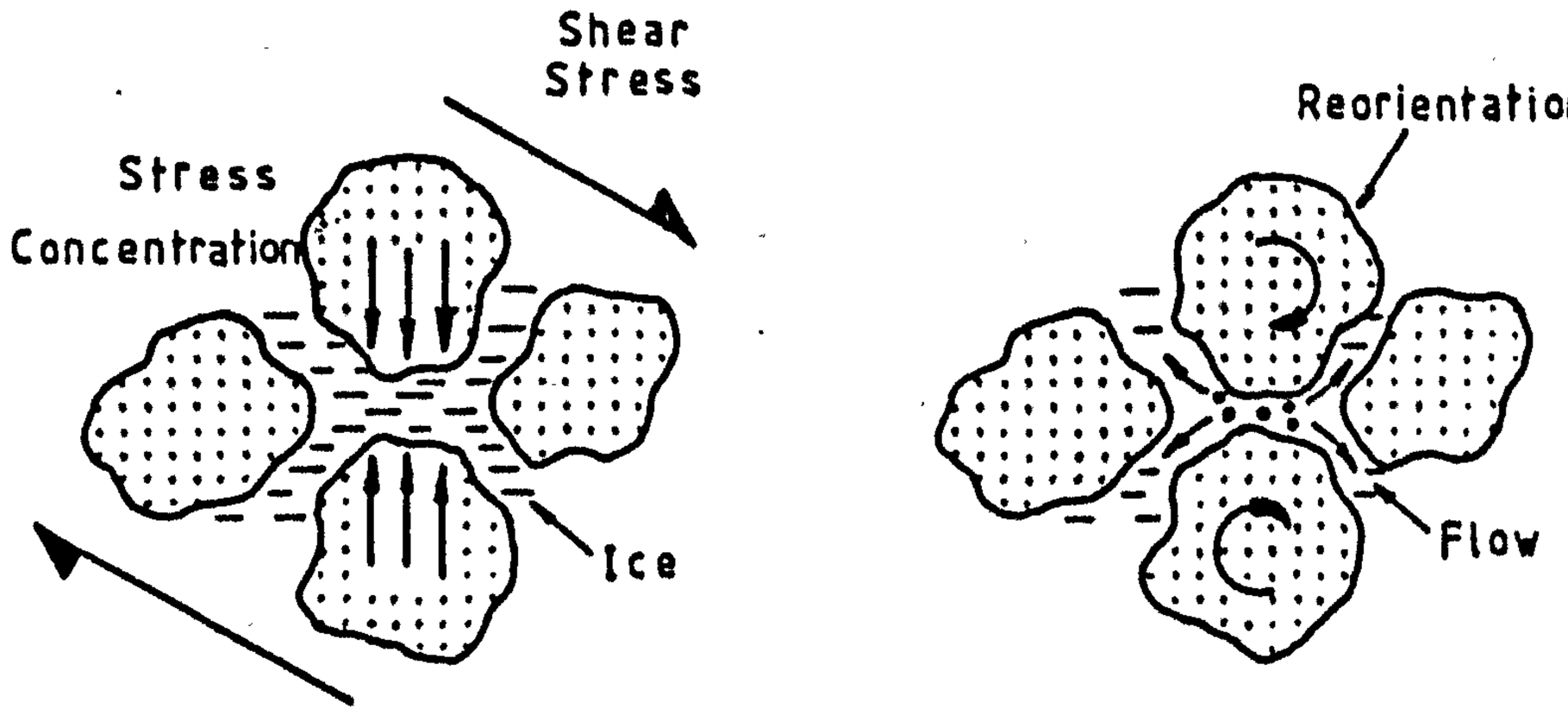

a)

Inhomogenous material.
Stress concentration between soil grains.

b)

Pressure melting of ice.
Flow to regions of lower stress.
Reorientation of soil grains.

Fig. 1·2 Shear of frozen soil matrix by pressure melting of ice.

1.2 Objectives and scope of thesis

The scope for research into AGF can be classified under three headings.

(i) Field instrumentation and monitoring of construction.
(ii) Field and laboratory testing.
(iii) Methods of analysis and design.

Research into any one of these classifications can emphasise the need for research in the other two so that they are all interlinked, as shown in Fig. 1.3.

Monitoring the behaviour of the soil during a construction can yield valuable information on both the condition of the excavation and the appropriateness of the design method. The main areas of interest in field monitoring of frozen soil constructions are summarised by Jones (1984) and include temperature distributions, geostatic and pore water pressures and movements of both the ground surface and the excavation walls. To investigate the whole history of a site during both freezing and construction, the necessary instruments must be installed in vertical boreholes and reliable instruments are available for these investigations (Hanna, 1973, Jessberger, 1980). The expense involved in extensive projects of this nature is restrictive but the results of some field research during construction through frozen ground is available in the literature (Aerni and Mettier 1980, Altounyan et al 1982, Funcken et al 1980, 1983, Neerdael et al 1983). The results of a field monitoring exercise can affect not only the way in which future projects are designed but can also influence the type and magnitude of testing used to provide design parameters.

The properties of frozen soil are known to be both stress and temperature dependent and information gained on their relative magnitudes from field monitoring exercises can influence the way in which future designs are approached. Investigations into the mechanical response of frozen ground materials, either in the

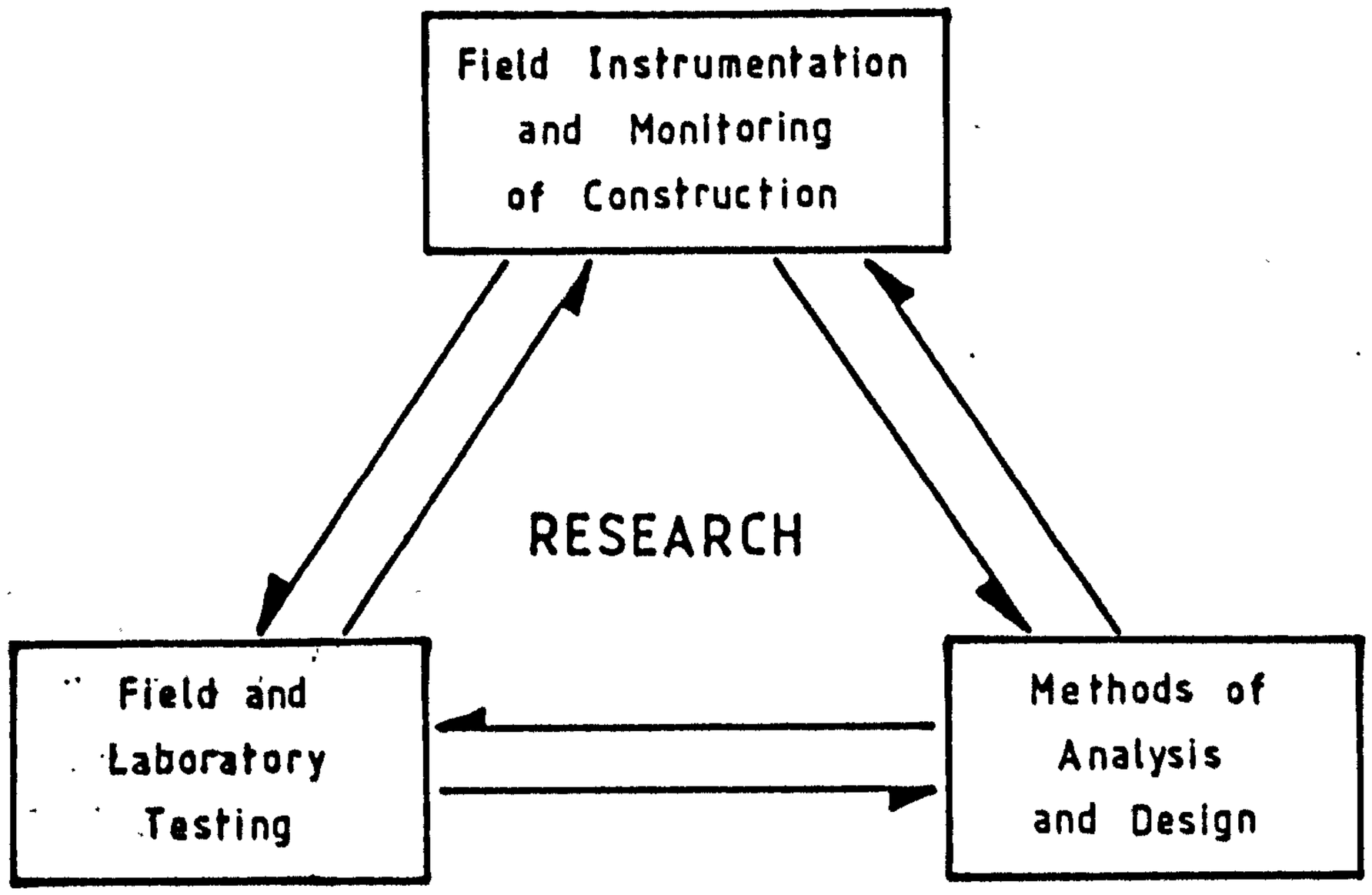

Fig. 1·3 The AGF research triangle

field or in the laboratory, can also affect the design procedure and it is this aspect of the AGF research triangle which is addressed in this thesis.

Research into testing techniques covers both the development of apparatus and proof of its suitability to a range of materials. For this thesis, materials were chosen which were representative of the soils and rocks lying above the coal measures in the Nottingham region as water exclusion by freezing has frequently been employed during shaft sinking (the most recent examples being Selby mine in N. Yorkshire and the Asfordby mine currently being constructed in N.E. Leicestershire). In Chapter 3, these materials, which include a silty sand, clay and some weak rocks, are described and the results of the appropriate index tests tabulated. Also described are the Brussels sand used by Gardner (1985) and a surrogate obtained from the same geological formation in Scotland.

Field testing as a preliminary to design is not generally practical as it involves the early installation of equipment on site. A recent example of field testing resulted from the recourse to freezing to provide a strengthened roof over the excavation of the Louise metro station in Brussels (Gonze et al, 1985). The natural moisture content of this Brussels sand was just 4% (i.e. 21% saturated) and the freezing trial demonstrated the need for irrigation of the sand during the main freeze. Field testing is beyond the scope of this thesis.

Testing in the laboratory is more generally employed and is preferred here. Field frozen material is not generally available and most research relies on laboratory preparation and freezing of suitably sized specimens. The techniques developed at Nottingham for producing frozen specimens of the four soils studied are described in Chapter 3 along with some details of the equipment used. The integrity of the resulting specimens is tabulated with a statistical analysis of repeatability and quality.

The main emphasis in this study was placed on the further development of testing equipment at the University. In Chapter 4, the full extent of the facilities available is described. At the start of this project there existed a single computer controlled refrigerated triaxial cell which had been successfully used for both short and long term strength tests at temperatures down to -10°C. The versatility of this apparatus made it an ideal initial development but as the demands put on the facility increased, the limitations of operating a single piece of equipment for all tests were exposed. The options available at this stage were,

(i) Straight duplication of the existing apparatus.
(ii) Duplication with modifications and improvements.
(iii) Diversification into specialised cells with the degree of sophistication balanced against the requirements of specific tests.

The new apparatus developed during the current research programme can be seen to combine the latter two options to provide two types of specialist cells for short term strength determinations, and an enhanced design of computer controlled cell for more complex work.

The new computer controlled triaxial cell extends the confining pressure range of the creep testing facility to 12 MPa from the previous limit of 1.8 MPa. The refrigerated Hoek cell offers a similar increase for short term strength tests and this allows the stress conditions found at greater depths of excavation to be modelled. This is an important development, as the depth to which excavations requiring AGF as a temporary support are proceeding means that the stresses imposed on soil elements within the ice wall are increasing. At these greater depths, the ice wall needs to provide a considerable strength component to support the sides of the excavation while it is temporarily unlined.

The results of short term strength tests are commonly used for

two purposes. The first of these is to provide strength parameters for the closed-form solutions to ice wall design (Chapter 2) and the second to determine the upper limit for loading in creep tests. In Chapter 5, the results of short term strength tests at constant deformation rates and constant stress rates are presented and discussed for all the test materials. In this thesis these results are chiefly used as a preliminary for the creep tests which follow in Chapter 6. Using the new computer controlled cell allowed creep testing to extend across a wide range of confining pressures and the results show a confining pressure dependence of the point of material failure.

Analysis of these results leads to the presentation of a new triaxial creep equation which is demonstrated to be valid over pressures ranging from 0 to 11.2 MPa. The implications of these findings, with particular emphasis on their engineering value, are discussed in Chapter 7. A brief examination of the effects of incorrect parameter determination follows.

Chapter 8 lists the main conclusions to emerge from this study and makes some suggestions for further work.

CHAPTER 2

APPLICATION OF THE AGF PROCESS

2.1 INTRODUCTION

An important aspect of most civil engineering projects is the need to provide a bond between the new structure and the earth. Formation level for most constructions will be below the normal ground level and this will often involve interception of the water table. When this occurs, a dewatering process is necessary to allow construction to proceed.

Many techniques have been developed to effect dewatering. The direct approach is drainage of the soil which can lower the water table over an extensive area if required. Two methods of drainage frequently employed are open sumps and well points with their associated pumping facilities. The effect of lowering the water table on the foundations of neighbouring structures must be considered and installation of a coffer-dam to localise drainage may be necessary.

Underground excavations such as tunnels and shafts may be drained in another way. By using a suitable system of air locks, excavation can proceed in a compressed air environment which prevents flooding and drives moisture from the pores of the surrounding soil. Two main problems are associated with compressed air work. These are the need to pass all personnel, equipment and waste materials through air locks to maintain pressure at the work face, and the health hazards resulting from changes in air pressure on leaving the chamber. Working at 1 atmosphere above normal air pressure requires a decompression cycle of 10 minutes for safety. At greater depths of excavation, or where ground water flow rates are high, pressures over 2½ atmospheres (38psi) are common and the decompression period rises to 2 hours.

An alternative to drainage is grouting. This involves the injection of a slurry into the pore spaces to replace the ground water and provide an impermeable barrier when set. Grouting is a non-reversible process but has the advantage of strengthening the ground as well as dewatering. A wide range of grouts are

commercially available and are generally suited to coarser grained soils which allow the grout slurry to flow freely on injection. Fig. 2.1 shows the particle size range over which each dewatering process is generally applied.

Artificial ground freezing is shown in Fig. 2.1 to be a versatile process applicable to almost all soil types which contain, or can be made to contain, water in their pore spaces.

This chapter will look in detail at the principles involved in ground freezing and the applications to which it has been put. Important aspects of the design of an ice wall are then discussed along with the procedures employed to satisfy the design constraints. The chapter concludes by considering the information required from laboratory testing to enable design to commence, and that required from field instrumentation for justification of the procedures used.

2.2 Principle of ground freezing

On freezing, the groundwater is converted to interstitial ice and this has the twin effects of strengthening the soil and forming a water impermeable barrier. This is usually a temporary treatment, although the thawing process may reveal changes in moisture content, density and particle orientation.

The ground freezing technique avoids the settlement problems of sheetpiling, which are associated with vibration, and is non-toxic, making it better suited than grouting when penetrating potable water aquifers.

Ground freezing is effected by installing and interconnecting a series of freeze tubes around the intended excavation. A freeze tube consists of two concentric pipes and the refrigerant is supplied from a ring main to the inner pipe of each tube. It returns through the annulus to be vented to the atmosphere or recirculated to a compressor unit.

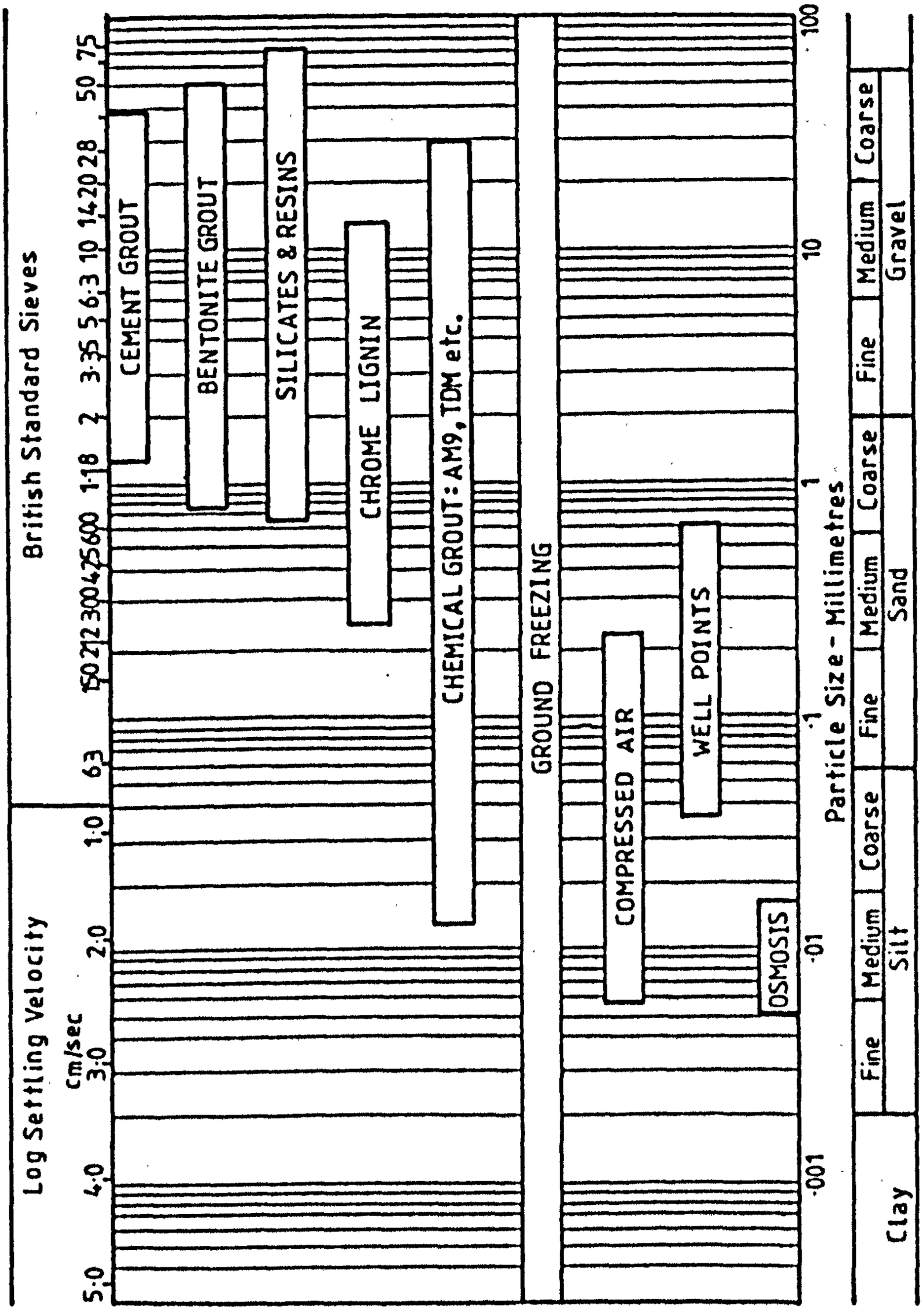

Fig. 2·1 Applicability of Geotechnical Processes

On refrigeration, a column of ice will build up around each freeze tube. When these columns merge an ice wall is established. The method of circulation of refrigerant through each tube dictates that the far end will be coldest and a 'pear' shaped column often develops with brine systems. Typical temperatures are -25°C at the base, rising to -23°C at the top.

A faster freezing cycle can be achieved with liquid nitrogen. A liquid nitrogen reservoir is connected to the ring main and the cryogenic liquid extracts its latent heat of vaporisation from the soil at the base of the freeze tube. The cold vapour then passes up the annulus, still cooling the soil, before venting to the atmosphere. Ice columns formed in this way are more bulbous and temperatures range from -196°C at the base, to typically -120 to -20°C on the surface. Fig. 2.2 shows the stages involved in ice wall growth.

The use of cryogenic systems is generally limited by cost to small scale projects and/or where speed is critical.

2.3 Applications

Artificial ground freezing (AGF) is most commonly used for temporary stabilisation and strengthening of soils. Fig. 2.3 shows some arrangements of freeze tubes designed to provide temporary support. Fig. 2.3a shows a freeze tube pattern established to provide a stiff, impermeable wall and floor to an excavation. The main details of this arrangement are a double ring of freeze tubes providing the wall and a regular pattern within these rings providing the floor. If the excavation is large, the core may be unfrozen at the start, but in many cases will be frozen (Braun et al, 1978).

A special case of this method is shown in Fig. 2.3b where a bottom cut-off is provided by an impermeable layer of soil or rock. AGF is only needed here to provide a cylindrical wall of ice. The freeze tubes should penetrate into the impermeable

a)

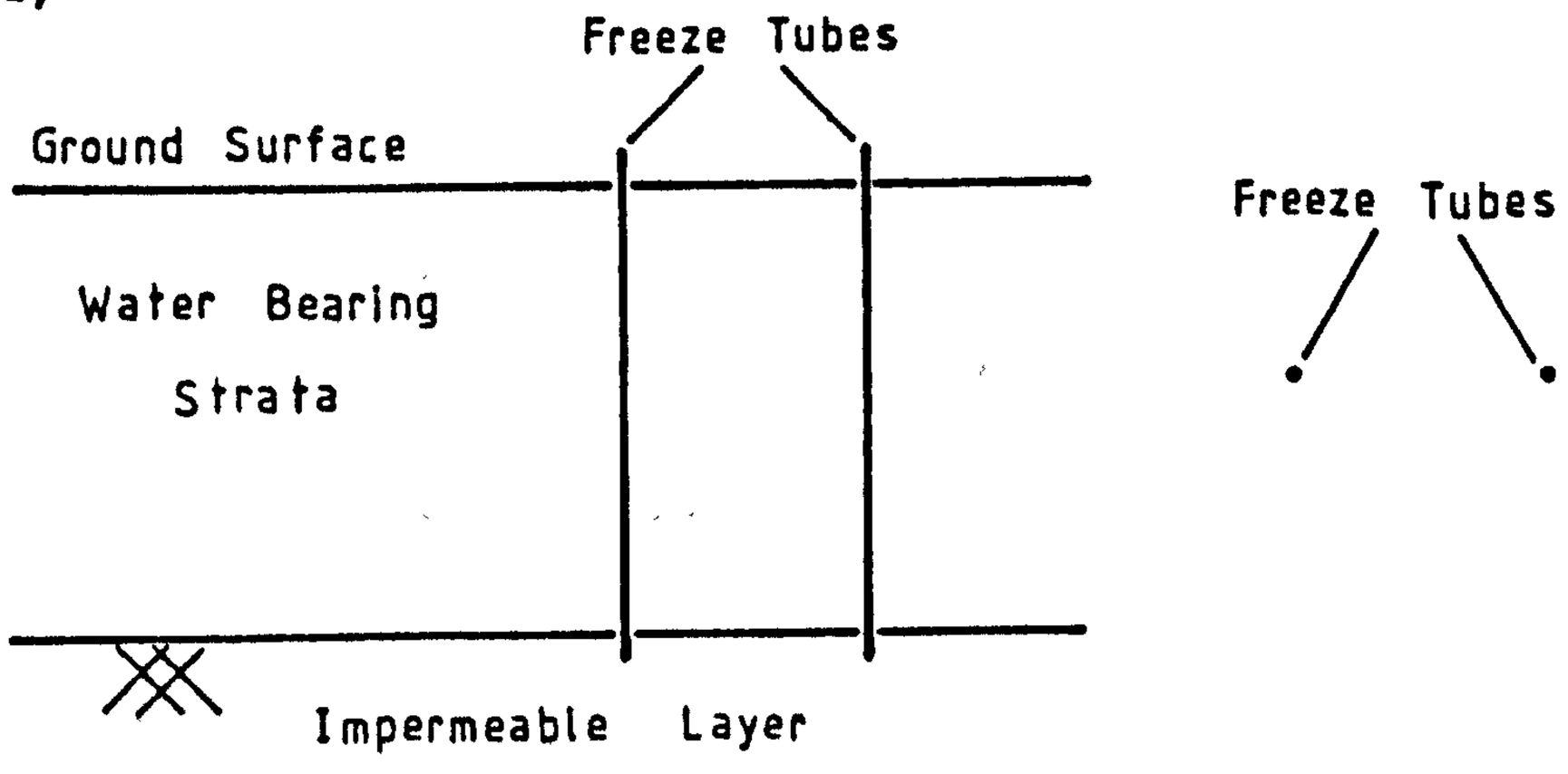

b)

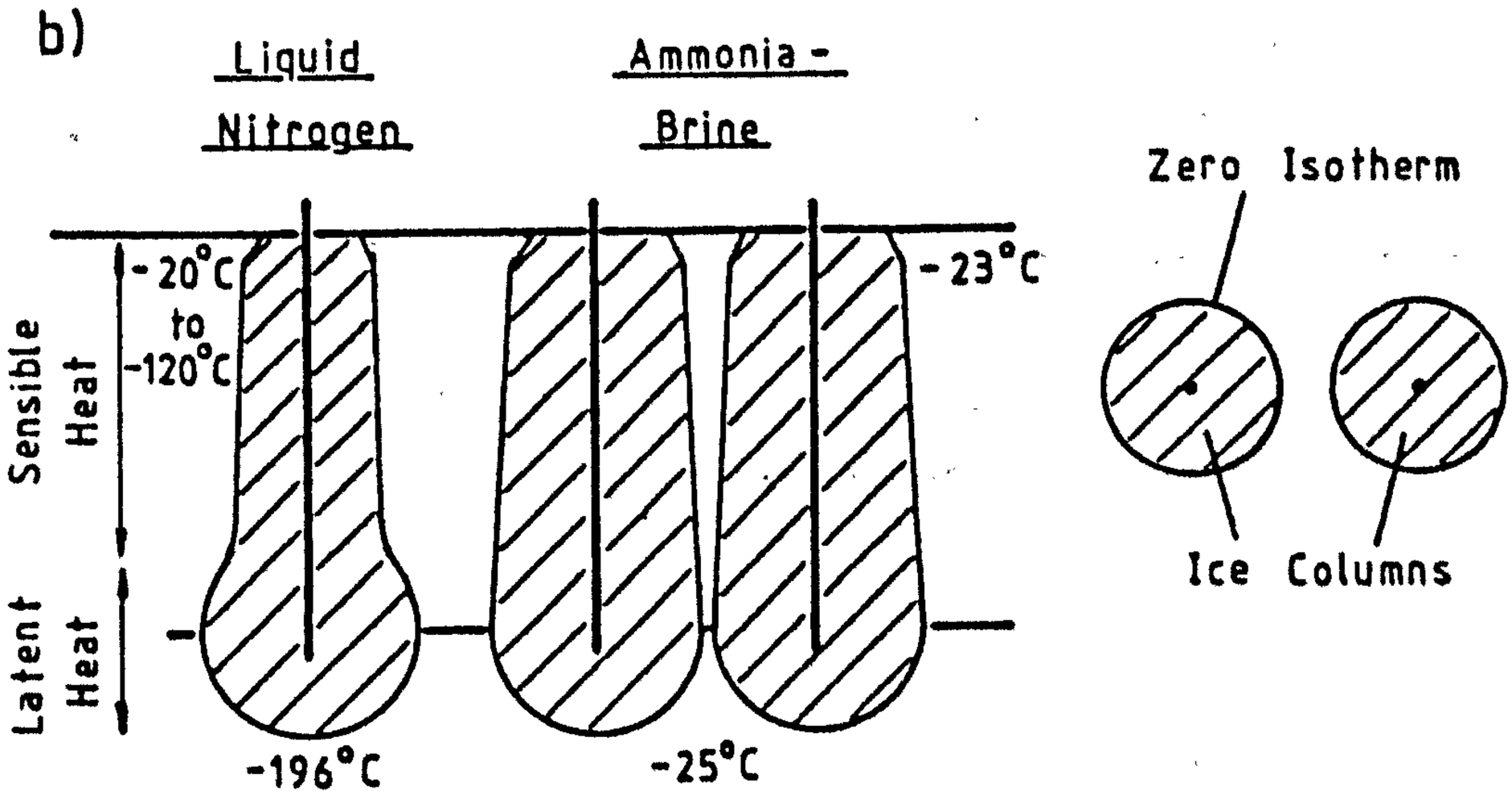

c)

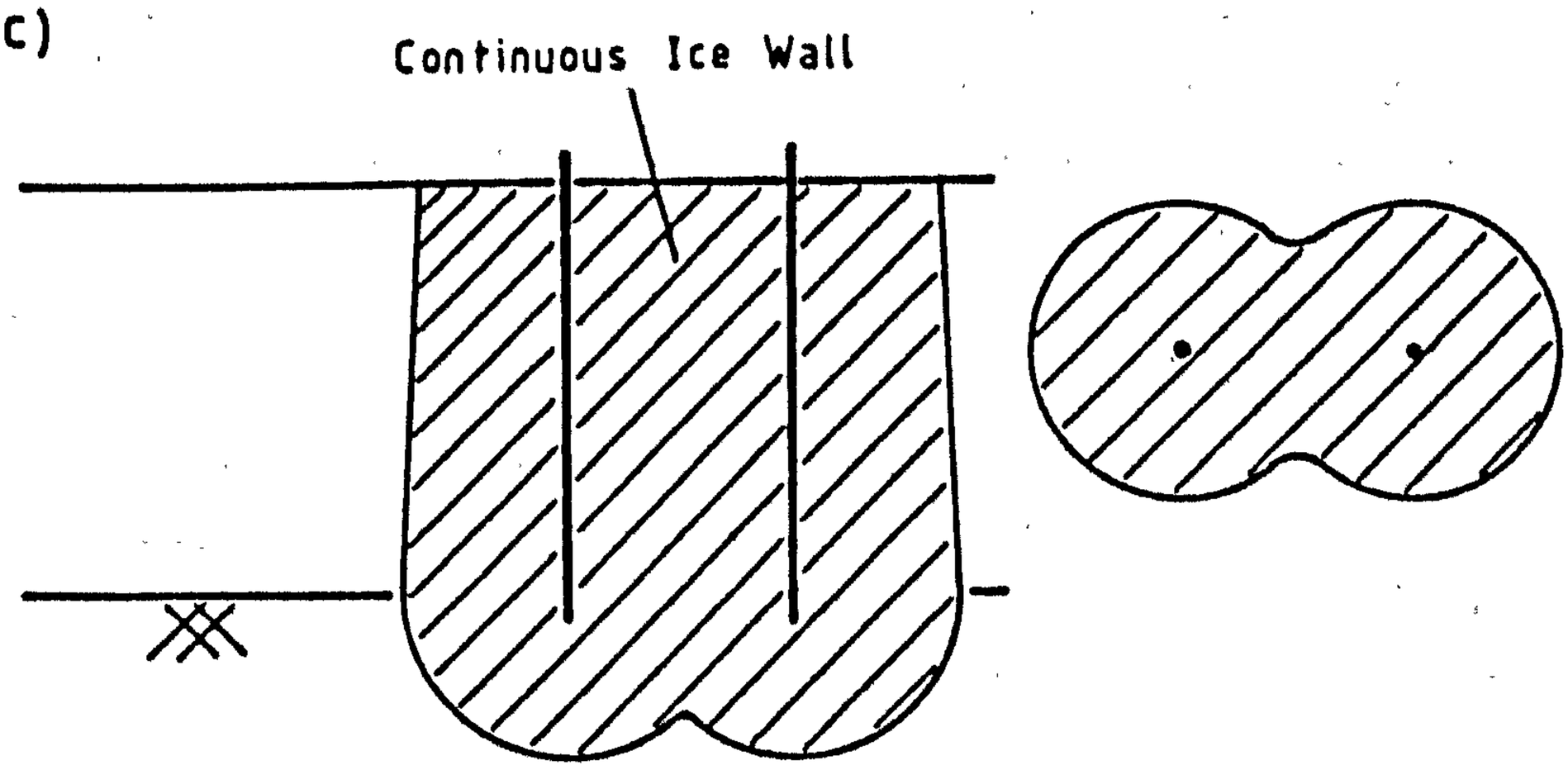

Fig. 2·2 The Ground Freezing Sequence

layer to reduce the risk of leaving an unfrozen window in the ice wall.

In tunnelling applications both horizontal and vertical freeze tubes can be used. Fig. 2.3c shows an example of this where short lengths of ground are surrounded by near horizontal freeze tubes and a cut-off established before excavation of the tunnel. This process is repeated until competent ground is reached. This method of freezing was used on the Milchbuck tunnel (Schmid 1981).

The final example shown in Fig. 2.3d is one of underpinning. The frozen ground temporarily stabilises the foundations of an existing building to allow the encroachment of a new excavation. Details of the underpinning process are given by Harris (1985).

The above examples have shown AGF in use as a temporary measure. In all these cases, permanent lining with concrete or steel would follow and, once this is in place, refrigeration stopped. Recovery of freeze tubes is not always possible but if left in place they are sealed to close a possible flow channel for groundwater and reduce the risk of contamination of aquifers.

AGF has also been used as a permanent lining technique for liquified gas storage tanks. These inground structures are excavated after an ice wall and floor have been established and the refrigeration maintained until the tanks are commissioned. At this stage, the ice wall is cooled by the liquified gas and the tanks become self supporting. At Canvey Island in Essex, Natural Gas tanks were constructed by this method and the ice wall growth arrested by the installation of a thermal barrier consisting of conventional freeze tubes circulating a warm brine solution. The differential thermal properties of the three strata through which the tanks were constructed caused cracks to occur and the tanks to leak when greater than half full. The tanks thus become uneconomic to maintain and have been abandoned.

One other important application of AGF is as a remedial measure

a) Large Excavation

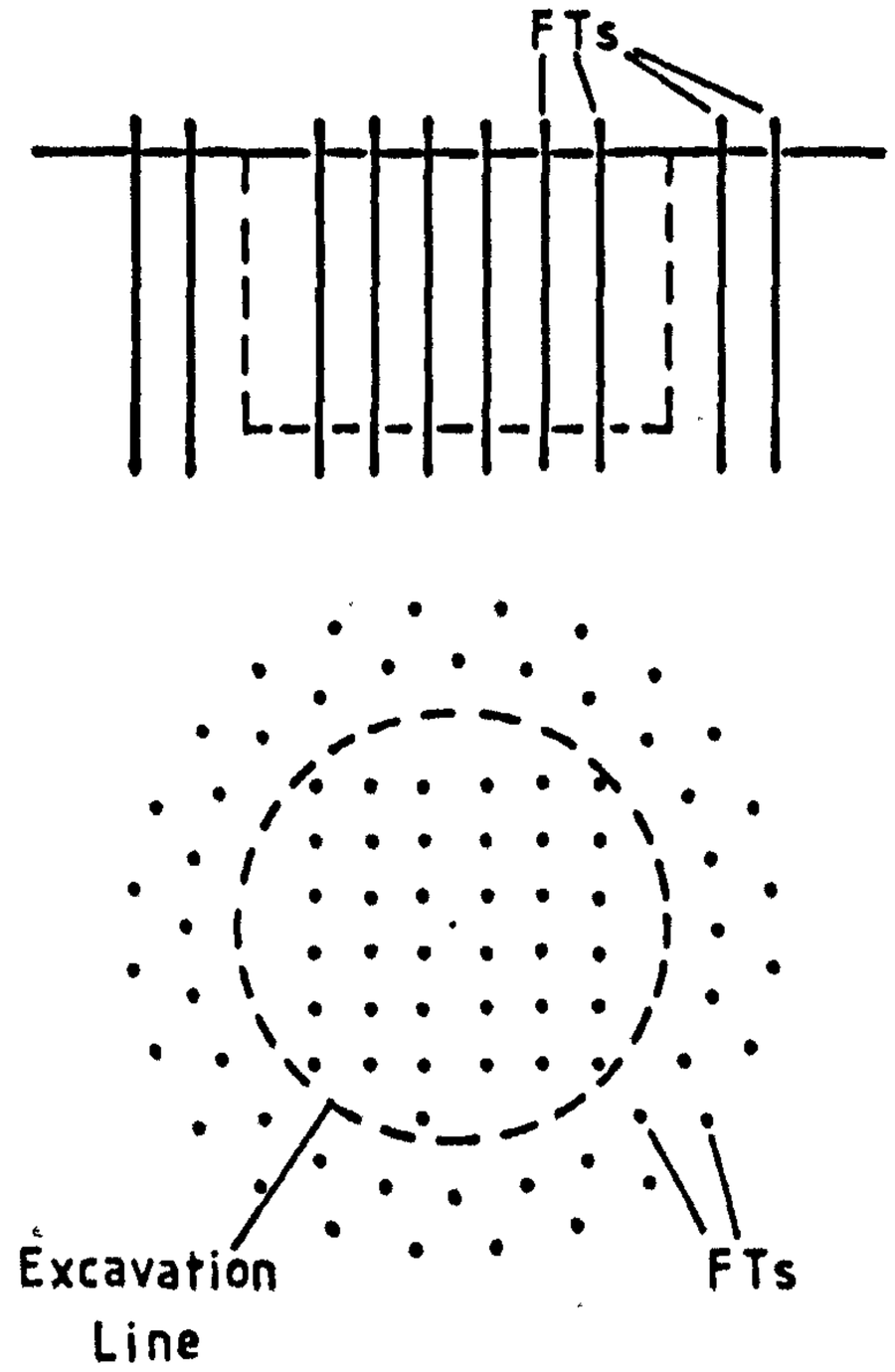

b) Narrow Shaft

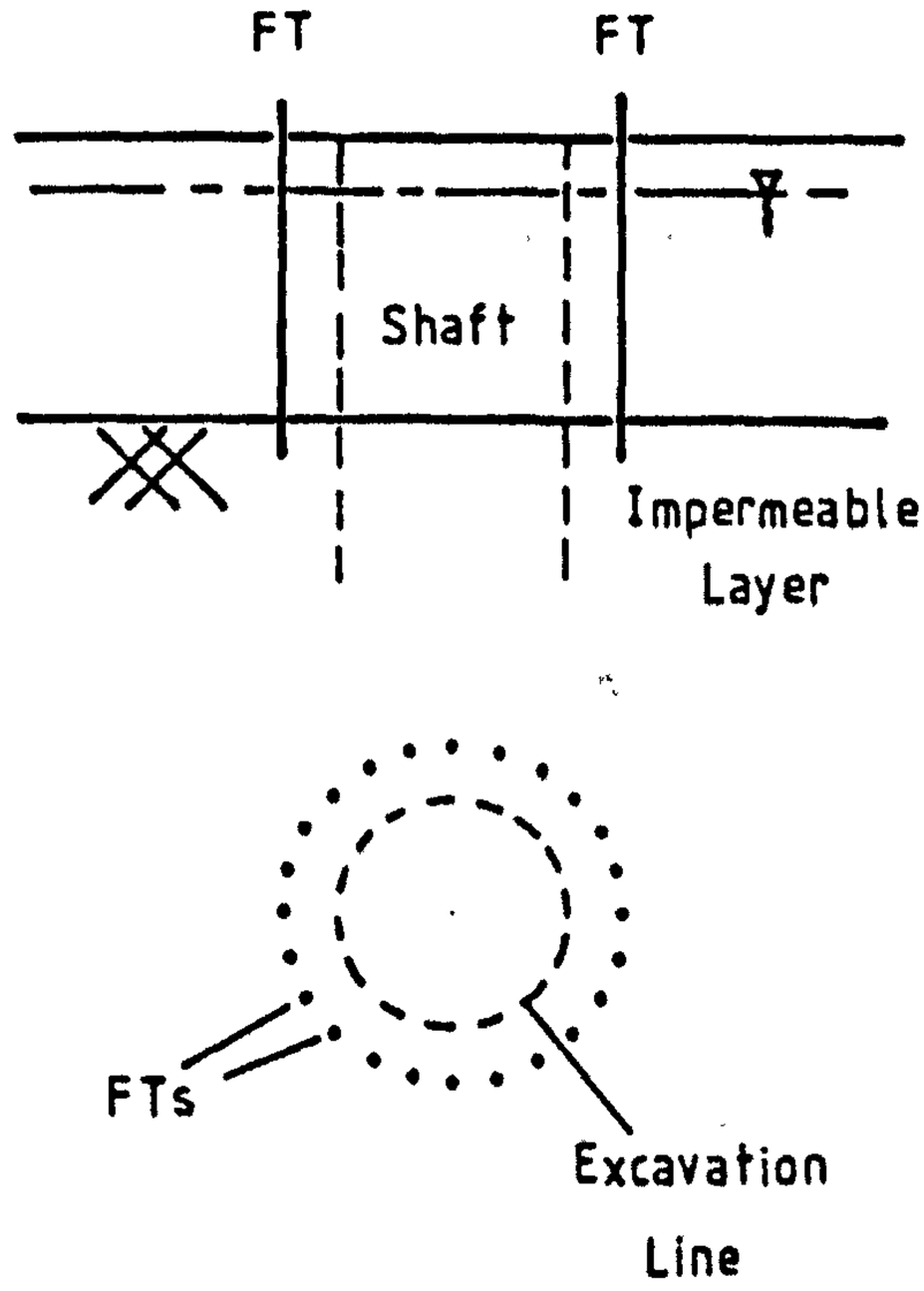

c) Segmentally Frozen Tunnel

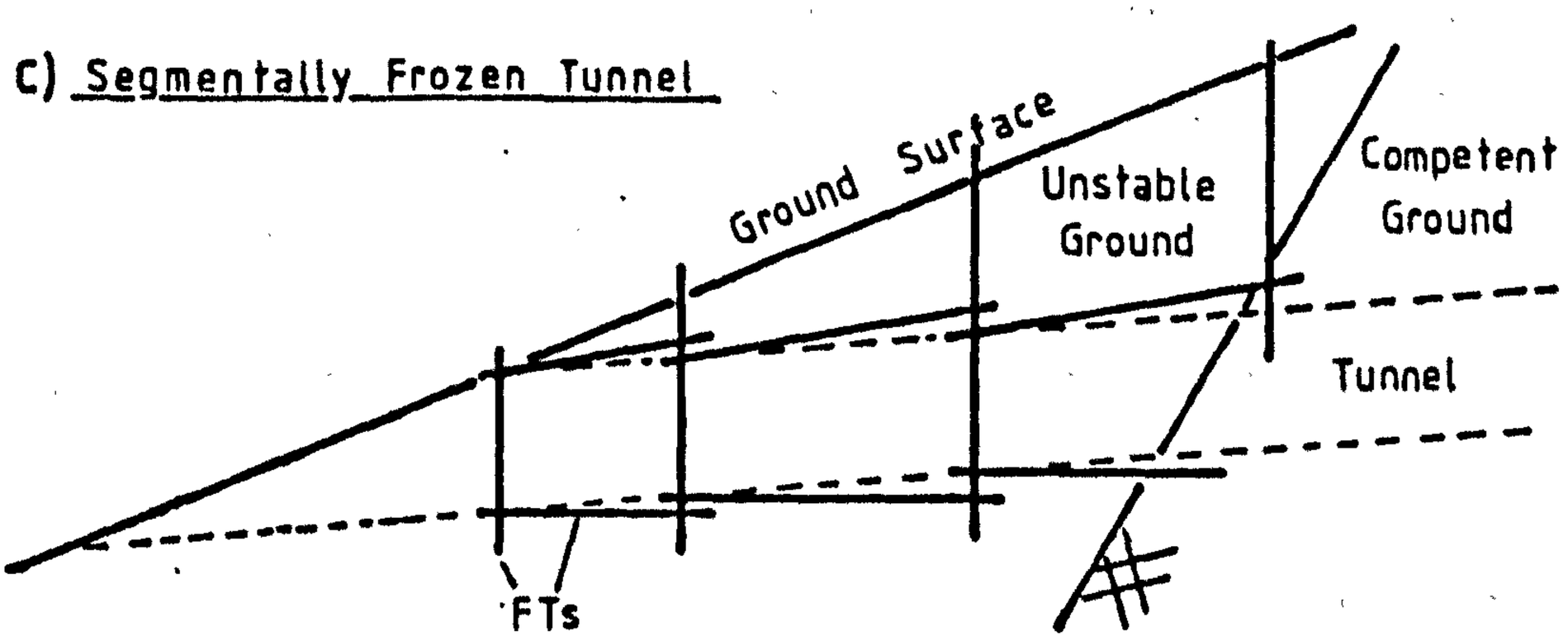

d) Underpinning and
Retaining Wall

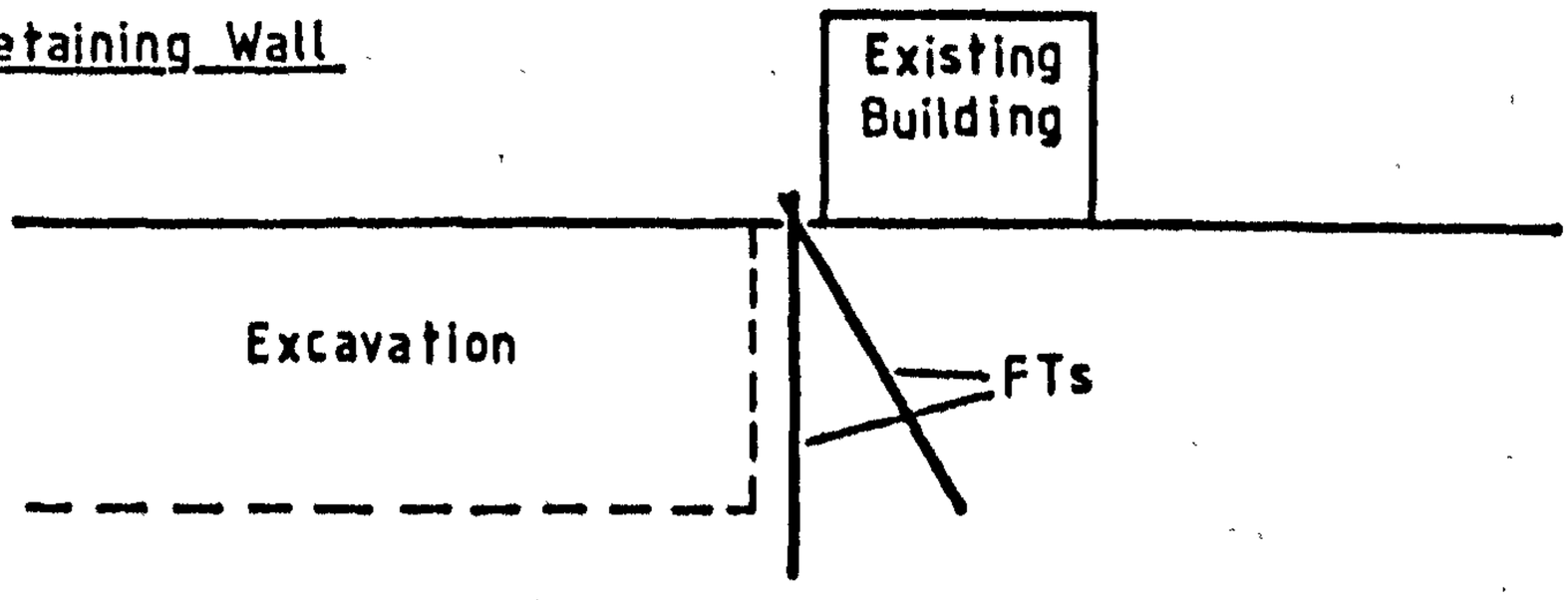

Fig. 2·3 Applications of Ground Freezing and Freeze Tube (FT) Arrangements

to counter tunnel collapses. Liquid nitrogen charged AGF can quickly be installed and ground water flows stemmed. Excavation and lining of the tunnel through the troublesome strata can then be safely continued.

Other specialist applications of AGF include slope stability and mine capping, an example being the sealing of a disused and flooded shaft on the line of the Wrexham bypass (Gregory and Maishman , 1973).

2.4 Design considerations

Before entering in to any detailed design the local ground conditions need to be investigated and a series of boreholes usually meet this need. For ground freezing design, the main interests are the properties of the geological strata, the position of the water table and the location, if any, of impermeable or strong rock layers.

The extent of the zone to be frozen will be decided by the properties of the strata such as porosity and strength. Borehole logs used in conjunction with an established data base can usually achieve this.

The water table position is important as free water must be available in the soil or rock voids for freezing to succeed. Harris and Pollard (1985) give a moisture content of 11% as the normal minimum required. Below this level, irrigation may be introduced as at the Louise metro station in Brussels (Gonze et al, 1985).

Examples of the use of impermeable or strong layers are given in Figs. 2.3b and c. These layers act as cut-offs for the frozen zone and reduce the number of freeze tubes needed to produce a safe working environment.

The adverse effects of freezing the ground must also be

considered and principal amongst these is frost heave. Frost heave arises from the growth of lenses of ice within the soil at the position of the zero isotherm or freezing front. Frost susceptible soils are generally characterised by a fine grading which allows high suction forces to be generated in the presence of a free water supply. The effects of frost heave are reviewed by Jones (1982) and include disruption of foundations and lifting of buildings.

The thermal properties of the soils to be frozen must be considered when designing the ice wall growth. Thermal aspects dictate the rate of advance of the freezing front and therefore closure of the ice wall. The freeze tube spacing and choice of refrigerant will be affected by this.

Time also becomes important when considering the deformation properties of frozen ground. Frozen soils and ice are subject to creep deformation under relatively low stresses and this can affect the time an excavation can be left open unsupported.

The principal design considerations can therefore be summarised under three headings. The first is to take account of the existing ground conditions, the mechanical and hydrological properties of the soil and rock layers through which the excavation must pass. The second is to look at the effects of freezing on the soil behaviour, its strength and creep properties and the adverse effects of heaving forces. The third is to consider the rate at which the ice columns and, on closure, the ice wall will advance.

2.5 Design procedures

The AGF design process is often initiated by calculating an approximate ice wall thickness based on elastic or elastic/plastic deformation. Various models have been proposed for this calculation when dealing with circular excavations and these have been conveniently assembled by Auld (1985). The

particular design problem often reduces to either an unlined short thick cylinder of ice wall (normal shaft sinking procedure in the U.K.) or a lined long thick cylinder (normal German procedure). These two design problems are shown in Fig. 2.4.

In the case of Fig. 2.4a, if the length of excavation left open between lining stages is considerable, then the ice wall thickness can be approximately designed using the elastic approach of Lamé and Clapeyron (1833),

$$t = a\left(\sqrt{\frac{K}{K-2P_o}} - 1\right) \qquad 2.1$$

where t is the ice wall thickness, a the internal diameter of the wall, P_o the external pressure and K the unconfined compressive strength of the frozen ground (Fig. 2.5a). An improvement to this approximation was made by Domke (1915) who introduced a plastic deformation zone at radius, s (Fig. 2.5b),

$$t = a\left[0.29\left(\frac{P_o}{K}\right) + 2.30\left(\frac{P_o}{K}\right)^2\right] \qquad 2.2$$

with $s = \sqrt{ab}$ and b being the outer radius of the ice wall.

The approximate solution obtained for the ice wall thickness forms the basis of both the thermal and structural analyses which follow. Thermal analysis is chiefly concerned with the positioning of freeze tubes to meet both temperature and time requirements. As the pattern of freeze tubes is normally regular, analysis is based on the smallest segment of common symmetry, which, for a circular shaft, may be the ice wedge shown in Fig. 2.6a. This wedge has a width of one half of the freeze tube spacing at the radius of the freeze tube circle. Simple techniques for thermal design are given by Sanger (1968)

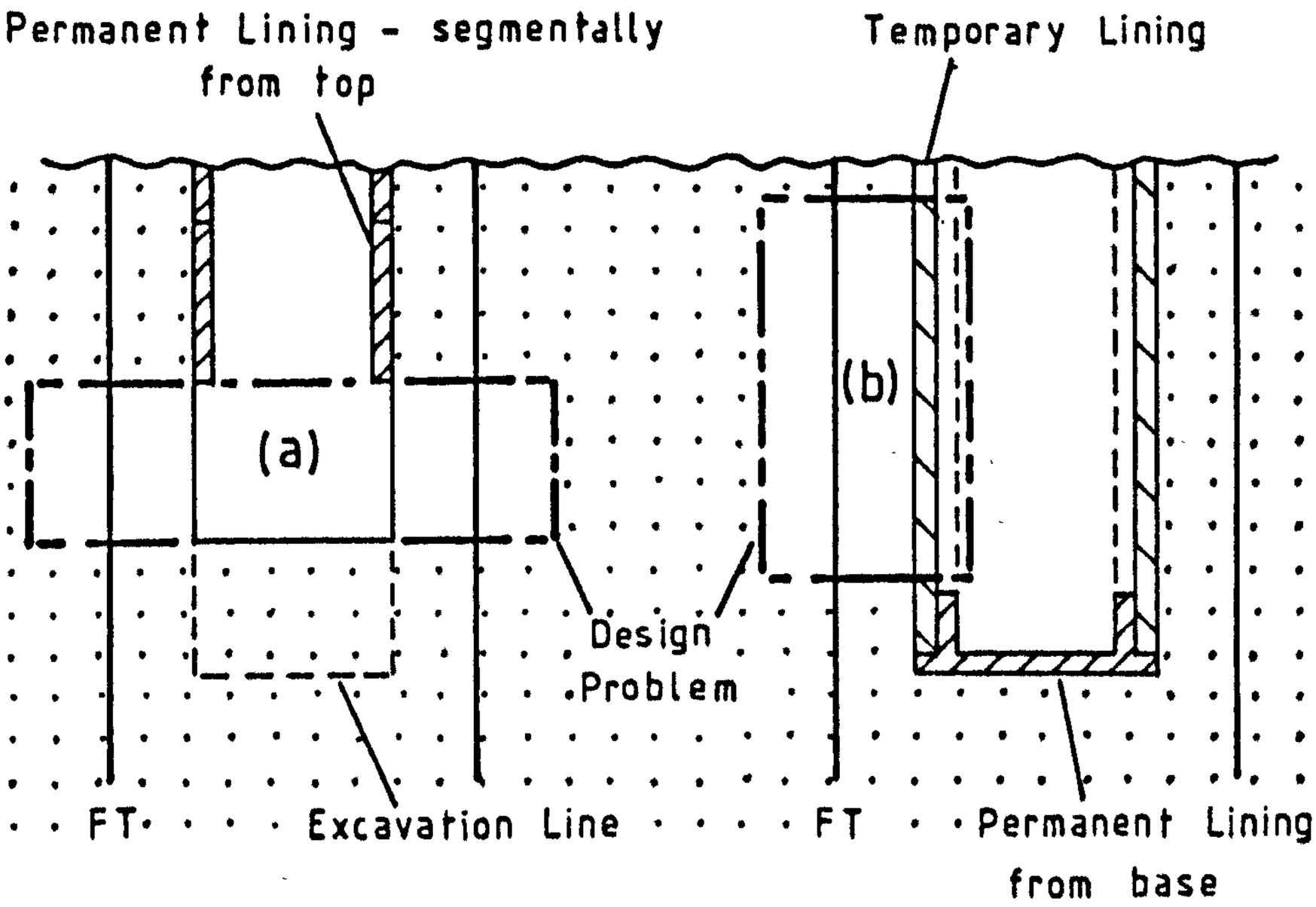

a) Unlined Short Thick Cylinder b) Lined Long Thick Cylinder

Fig. 2·4 Design Problems in Shaft Sinking

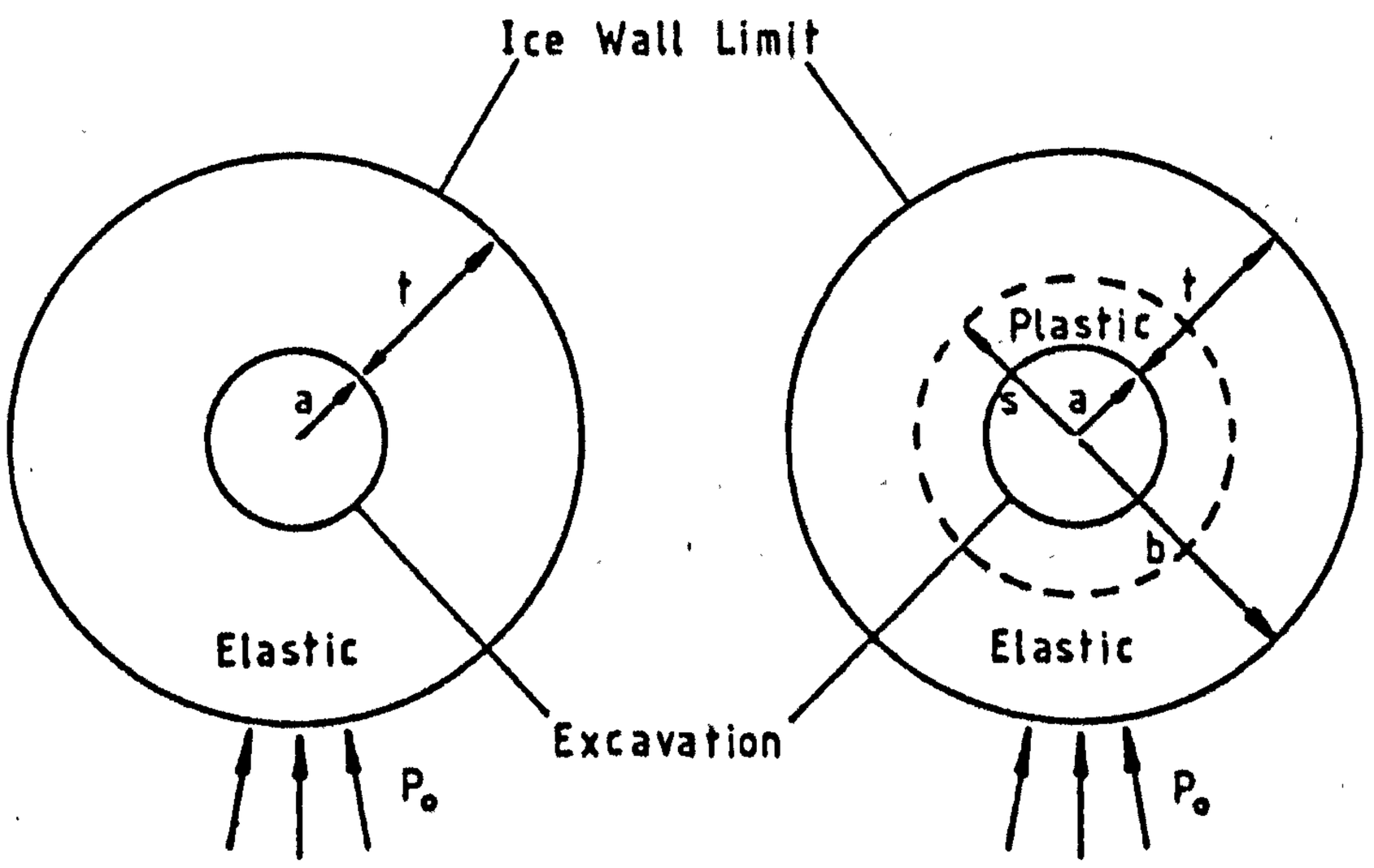

a) Lamé b) Domke

Fig. 2·5 Notation for Design Formulae

but with the introduction of computers into design offices, finite element methods (FEM) can be applied. An example FEM mesh is also shown in Fig. 2.6a.

The temperature distribution with time depends on the excavation geometry and the properties of both the soil and the refrigerant. The approximate wall thickness, t, and the excavation diameter, a, will allow a freeze tube spacing and circle diameter to be assumed. The rate at which heat is extracted from the ground by this particular freeze tube pattern will then be governed by the flow rate and temperature of the refrigerant. Ice column growth and closure to form an ice wall will follow at a rate determined by the thermal properties of the soil. For design purposes, these include thermal conductivities both frozen and unfrozen, specific heat capacity, quartz content and moisture content. The quartz content greatly affects the thermal conductivity.

The results of a finite element thermal analysis can be presented in the form shown in Fig. 2.6b and 2.6c. Isotherms are plotted to represent the temperature distribution after set time periods and the progress of the zero isotherm can be observed. On closure of the ice wall, the temperature profile may be similar to that shown in Fig. 2.6d.

The final stage of the design procedure is to check the deformation of the frozen material under both instantaneous and time dependent loading. Design formulae for radial deformation have again been assembled by Auld (1985) for the two design problems of Fig. 2.4. An alternative and more intensive analysis is available using FEM, and a tunnelling example is given by Gardner (1985).

The outcome of the deformation analysis may require a reassessment of the particular solution chosen in the wall thickness and thermal analysis stages of the design.

a)

FEM Net

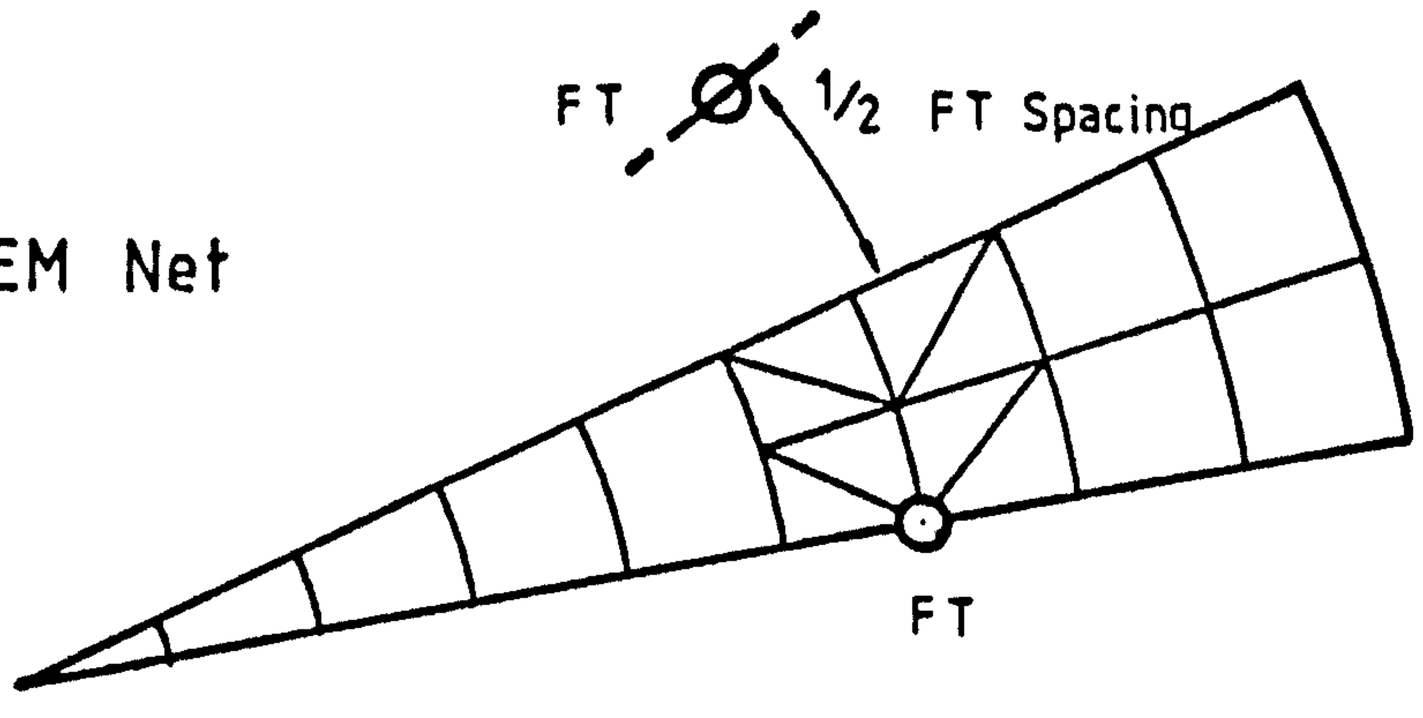

b) Isotherms for Ice Column

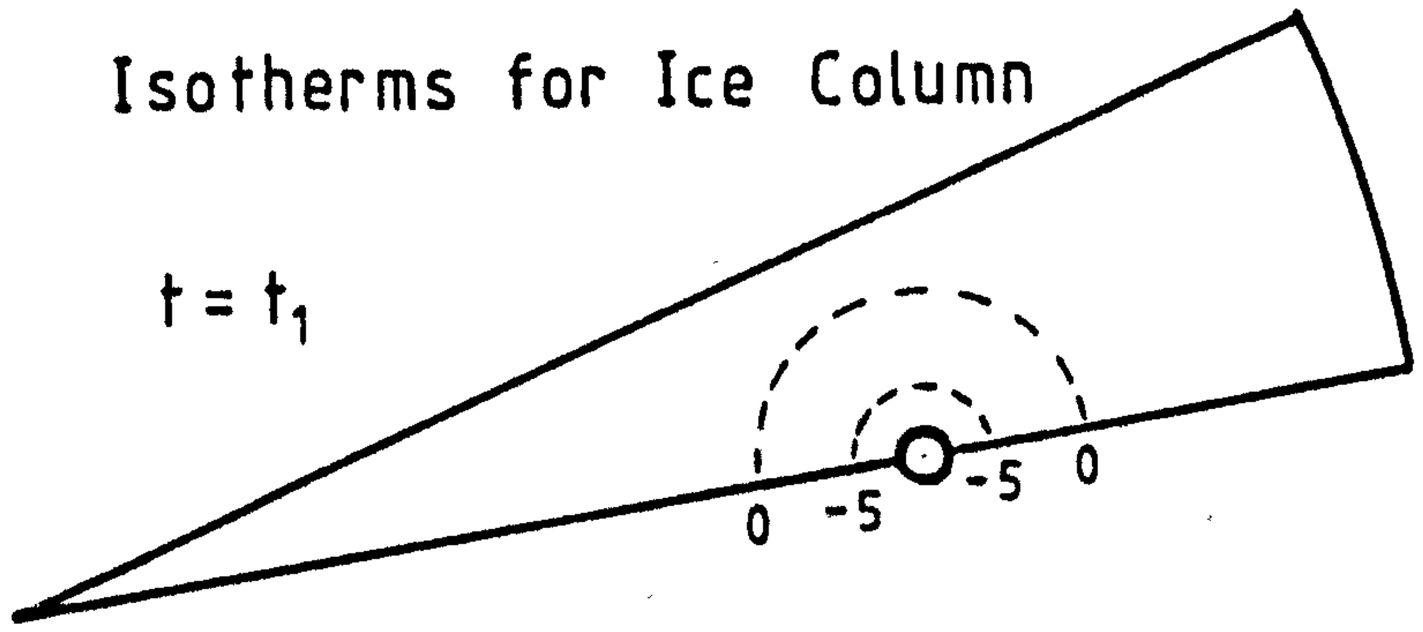

c) Isotherms for Ice Wall

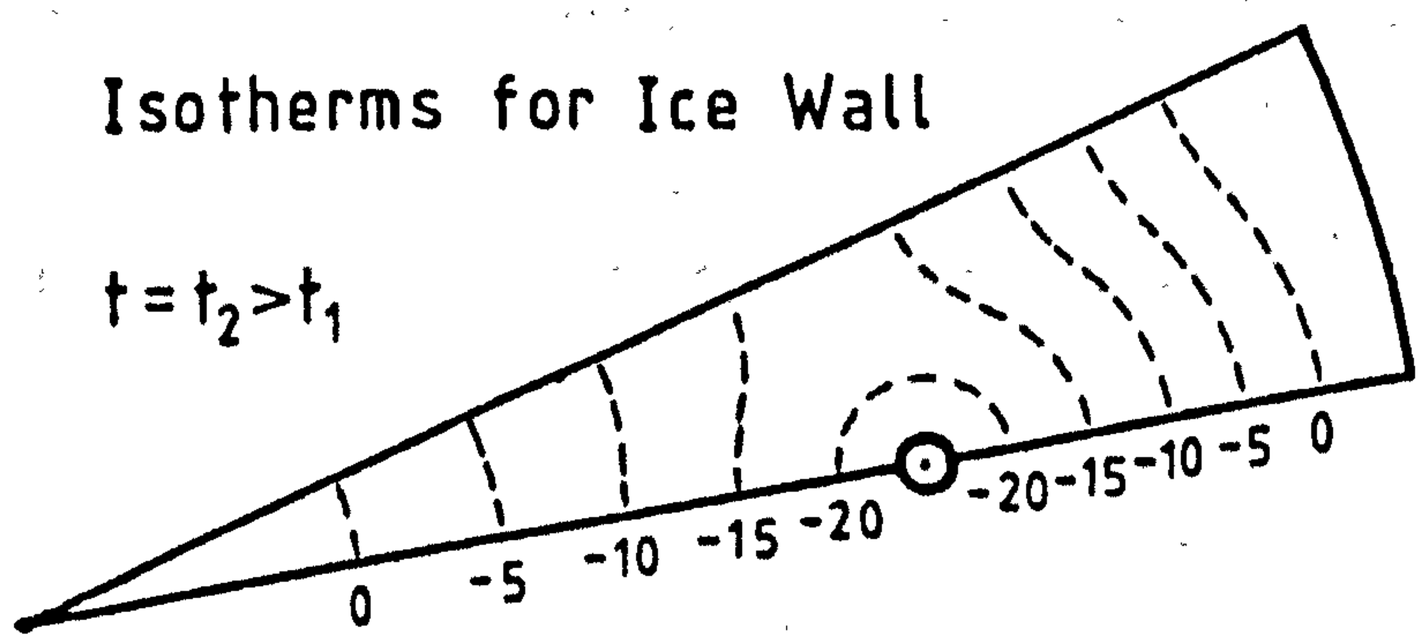

d) Temperature Profile

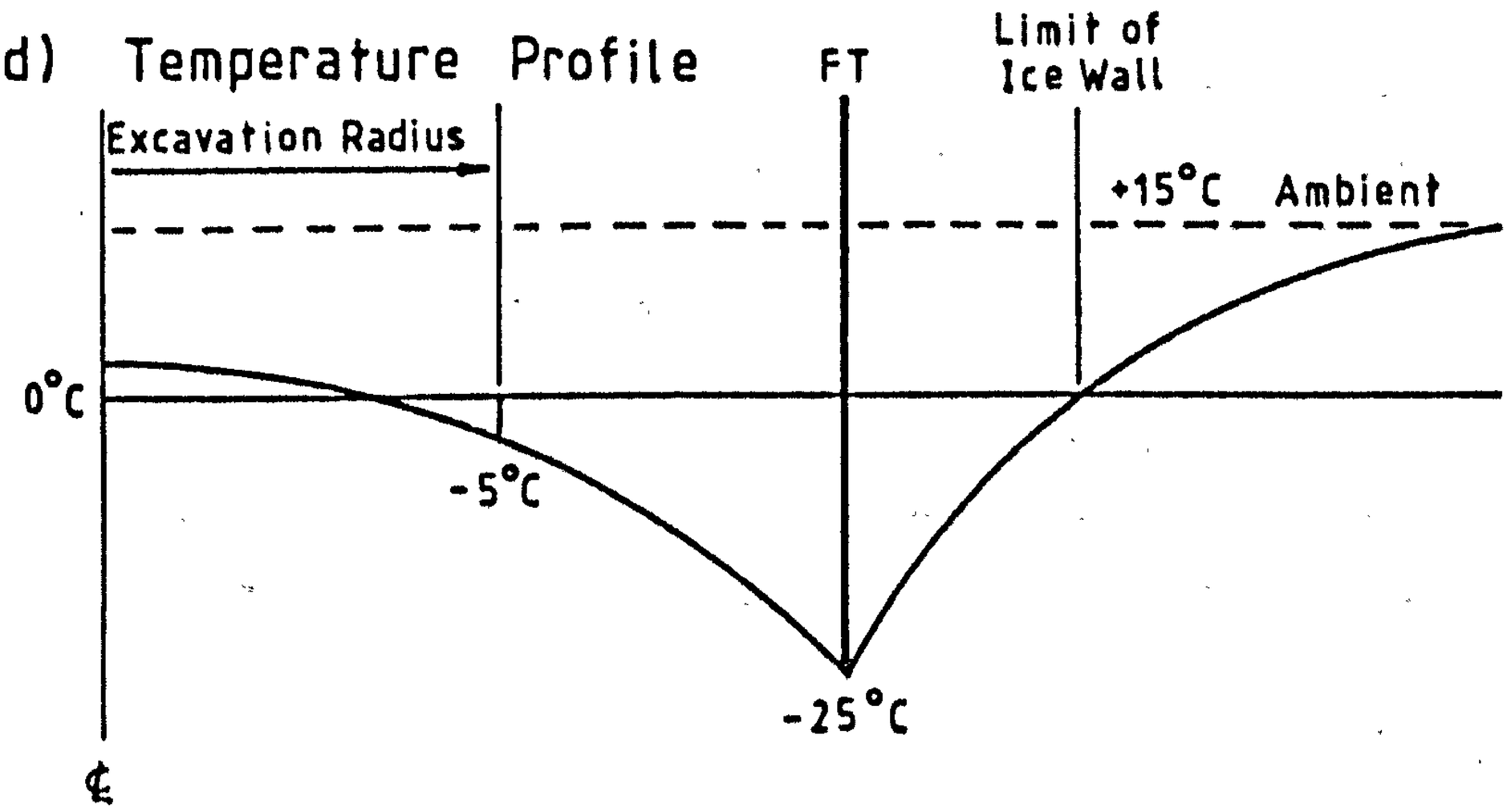

Fig. 2·6 Thermal Analysis of Ice Wall

2.6 Laboratory test requirements

At each stage of the design procedure described in the previous section, information has been required about the general properties of the soil to be frozen. Laboratory testing normally supplies this information.

The unconfined compressive strength, K, in equations 2.1 and 2.2, can be obtained from uniaxial compression tests in refrigerated triaxial cells (Chapter 4). Ideally, field frozen material should be used in all the laboratory tests but this is unlikely to be available at the design stage.

A mineralogical analysis of the soil can determine the quartz content which has a significant influence on the thermal properties, specifically the heat flow rate. The ability of the soil to conduct heat away from a source will affect the time to closure of the ice wall and laboratory measurements of the thermal conductivity are required. These can be made by monitoring the temperature change with time adjacent to a line source heater inserted into a sample of the soil. The thermal conductivity is temperature dependent and both frozen and unfrozen values are normally measured. Methods of determining thermal conductivities are summarised by Farouki (1981).

The other thermal property needed for design is the specific heat capacity. This is a measure of the heat input required to raise unit mass of the soil through 1°C and again has implications for the ice wall growth rate.

For the deformation analysis the time dependent properties of the soil can be determined from laboratory creep tests. Creep tests are typically conducted under constant stress conditions using specialised refrigerated equipment (Chapter 4). Analysis of the test results allows parameters to be evaluated for the chosen creep model (Chapter 6).

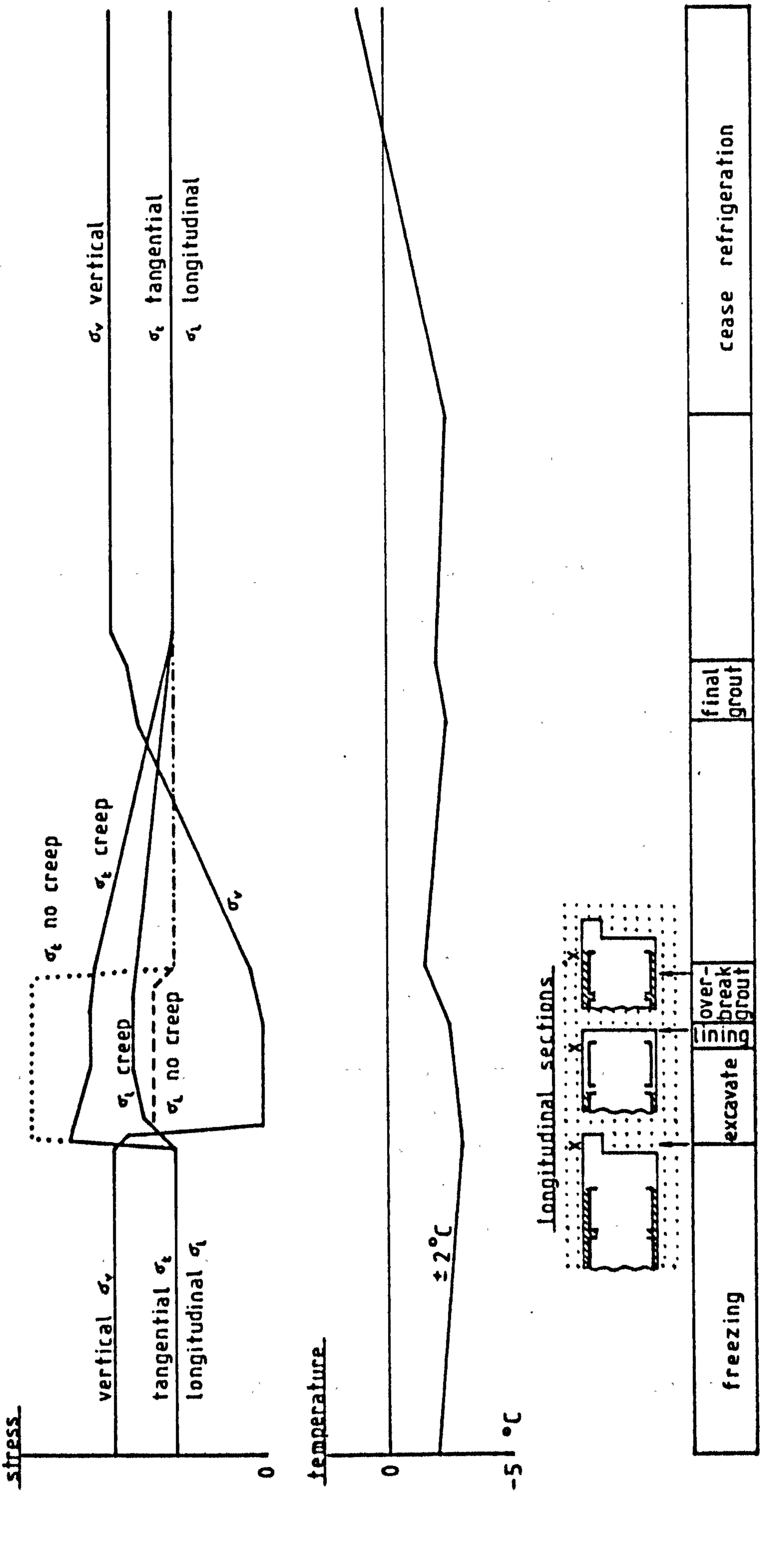
stress
vertical σ_v
tangential σ_t
longitudinal σ_l
0
σ_t no creep
σ_t creep
σ_l creep
σ_l no creep
σ_v
temperature
0
-5 °C
±2°C
Stress and Temperature variations for soil element (x) in crown of tunnel, during construction using AGF
Longitudinal sections
excavate
lining
over-break grout
final grout
freezing
ceased refrigeration

Fig: 2:7

2.7 Stress and temperature during construction

During the excavation of a shaft or tunnel in frozen ground the stress and temperature distributions in the surrounding soil do not remain constant. Attempts have been made to monitor construction temperatures by installing arrays of thermocouples in the ground but no similar exercises involving earth pressure cells are recorded. In an attempt to illustrate the need for such field instrumentation, a postulative distribution of stress and temperature with time is presented in Figs. 2.7 and 2.8 for the cases of a tunnel and a shaft through frozen ground.

Fig. 2.7 studies a soil element in the line of the crown of a frozen tunnel as the excavation approaches, remains open for a period, and is lined. Three mutually perpendicular stress directions are considered and as the excavation reaches the soil element the principal stresses rotate as the vertical stress drops to zero and the longitudinal and tangential stresses increase. Creep deformation during the open period will allow some relaxation of the stresses in the crown. When the lining has been placed and back grouting completed, the vertical stress will return and all three stresses may reach their original levels as the ground thaws.

In the shaft example of Fig. 2.8 the element studied is adjacent to the wall of the shaft which is being excavated and lined in stages from the surface. Here, the radial stress must decrease to zero until the lining is in place and consequently the tangential stress must increase to provide the wall support. The vertical stress is shown to remain constant throughout and the others to return to their original levels on thawing.

Approximate temperature distributions for brine freezing accompany both Figs. 2.7 and 2.8 to highlight the warming effects of excavation and of hydration of concrete and cement.

Full instrumentation of a ground freezing site would provide valuable information about the stresses experienced during

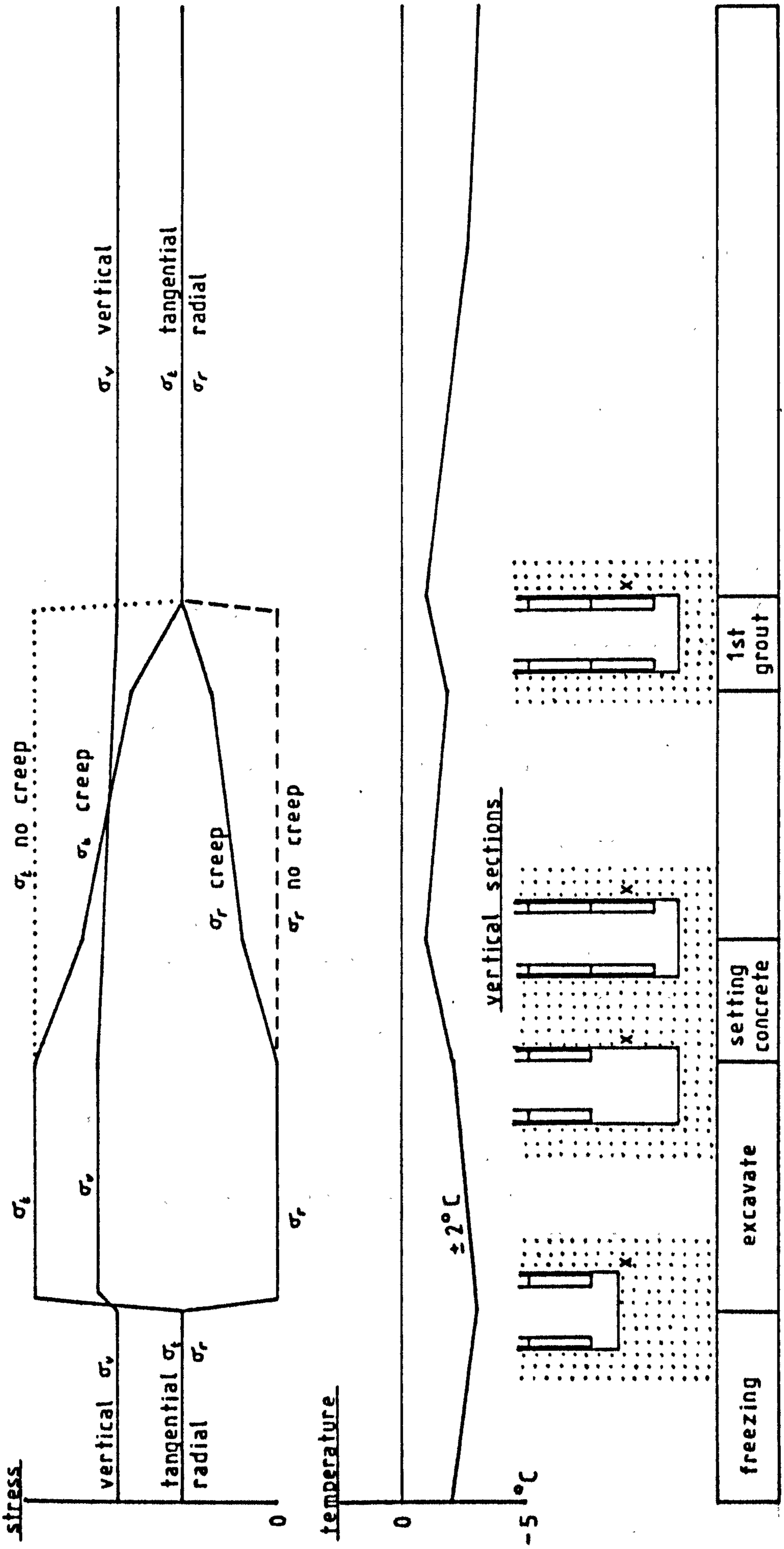
stress
vertical
tangential
radial
σ_v
σ_t
σ_r
σ_t no creep
σ_t creep
σ_r creep
σ_r no creep
temperature
+2°C
0
-5°C
vertical sections
x
H
freezing
excavate
setting concrete
1st grout
Stress and Temperature variations for soil element adjacent to shaft wall, during construction using AGF

Fig. 2-8

freezing and excavation to quantify this postulative study. This would also be beneficial to the design procedure which relies on the input of applied stresses for calculating the ice wall thickness.

2.8 Summary

This chapter has covered the general uses of artificial ground freezing and shown its versatility over a range of geotechnical materials. The applications highlighted include both temporary and permanent strengthening of the ground, and water exclusion by a well formed ice wall.

The design procedure for an ice wall around a proposed shaft can be considered to involve three stages. An approximate solution is used to obtain an ice wall thickness and this is followed by thermal and deformation analyses to determine freeze tube spacings and suitability of the solution chosen. The results of laboratory tests are required by the design process and the need to choose suitable stresses to apply in these tests has led to the postulative analysis in section 2.7.

Figs. 2.7 and 2.8 attempt to show how the stresses vary during an excavation. The relative magnitudes of the stresses shown are not indicative of true values as no documented information from field instrumentation is available. The importance of this analysis is reflected by the rotation of the principal stresses on excavation, a process which can cause great changes in material properties. A better understanding of the mechanisms involved in the excavation process could greatly improve the whole design procedure.

CHAPTER 3

MATERIALS AND SPECIMEN PREPARATION

3.1 INTRODUCTION

The mechanical properties of frozen ground materials tested in the laboratory are dependent on the quality of the specimens. In order that individual influences on strength and deformation, such as stress and temperature , can be investigated, it is important that variations in the internal structure of the test specimens are minimised. For the purposes of research it is therefore beneficial to manufacture specimens and carefully control both the density and water content.

To meet this condition, three soils have been chosen to supplement the studies on Brussels sand reported by Gardner (1985). The materials are described in section 3.2 and represent contrasting soil types which range from silty clay to a medium sand. Also described are a set of triassic rocks, mainly sandstone, siltstone and mudstone which, in many ways, represent typical materials as recovered from the field. These materials are generally more variable in content than those with laboratory controlled structures and, as such, produce more erratic test results when examined as small specimens.

In section 3.3 a review is made of the various preparation stages and techniques used to obtain laboratory frozen specimens. Each technique is limited in its application to a certain range of materials and examples from the literature are given where appropriate. Leading from this review, section 3.4 looks at the methods applied to the materials of this study after preliminary experimentation had identified the most suitable approach. Some reference is made to the laboratory equipment either specially designed or adapted for use for these purposes.

In conclusion, a short statistical analysis of the quality of the specimens produced, demonstrates the success of the adopted methods.

3.2 Materials studied

Three soils have been investigated during this research programme and details of their properties are given in Table 3.1. Most work has involved an uncemented lower mottled sandstone from the Lenton Abbey formation (LAF sand), which is a red, very silty sand with clay outcropping in the Nottingham area. Keuper Marl (KM) was used to develop the sample preparation technique for clay soils and to prove the versatility of the test facility over a range of materials. A second sand (LAL), from Loch Aline in Scotland, was introduced to supplement the work on Brussels sand (B). Gradings for these soils are shown in Fig. 3.1 where the similarity in particle size distribution between LAL and B can be appreciated. Under microscopic analysis, the particle size and shapes of the two materials are similar, both consisting mainly of single sized rounded grains.

The properties listed in Table 3.1 were obtained by laboratory tests in accordance with BS1377 (1975). The 4.5 kg rammer test was used to determine the dry density/moisture content relationship for KM as this method was to be employed for compacting dense clay specimens during the main test programme. The high proportion of fines in LAF suggested that Atterberg limits could be obtained and test 2(A) produced a liquid limit value. No plastic limit could be obtained and LAF is classified as non-plastic.

In addition to the work on soils, some weakly cemented Triassic rocks were recovered for testing from an NCB exploratory borehole at the Asfordby mine site in N.E. Leicestershire. The rocks consisted mainly of sandstone, siltstone and mudstone but included a few conglomerates and breccias. Table 3.2 shows the geological strata encountered by the borehole and indicates their approximate depths below ground surface level.

Table 3.1 *Physical properties of test materials*

Material	Classification Letters (BS 5930)	BS 1377 Specific Gravity	Optimum Moisture Content	Maximum Dry Density	Liquid Limit	Plastic Limit
LAF	SM	2.64 Test 6(B)	13 Test 12	1.74 Test 12	26 Test 2(A)	- Test 3
LAL	SPu	2.64 Test 6(B)	4 Test 12	1.68 Test 12	-	-
KM	CI	2.61 Test 6(B)	22 Test 13	1.61 Test 13	37 Test 2(A)	18 Test 3
B	SPu	2.63	-	-	-	-
		Mg/m^3	%	Mg/m^3	%	%

Notes: Test 6(B) - Specific Gravity, density bottle method
Test 12 - 2.5 kg rammer compaction
Test 13 - 4.5 kg rammer compaction
Test 2(A) - cone penetrometer method for Liquid Limit
Test 3 - Plastic Limit test

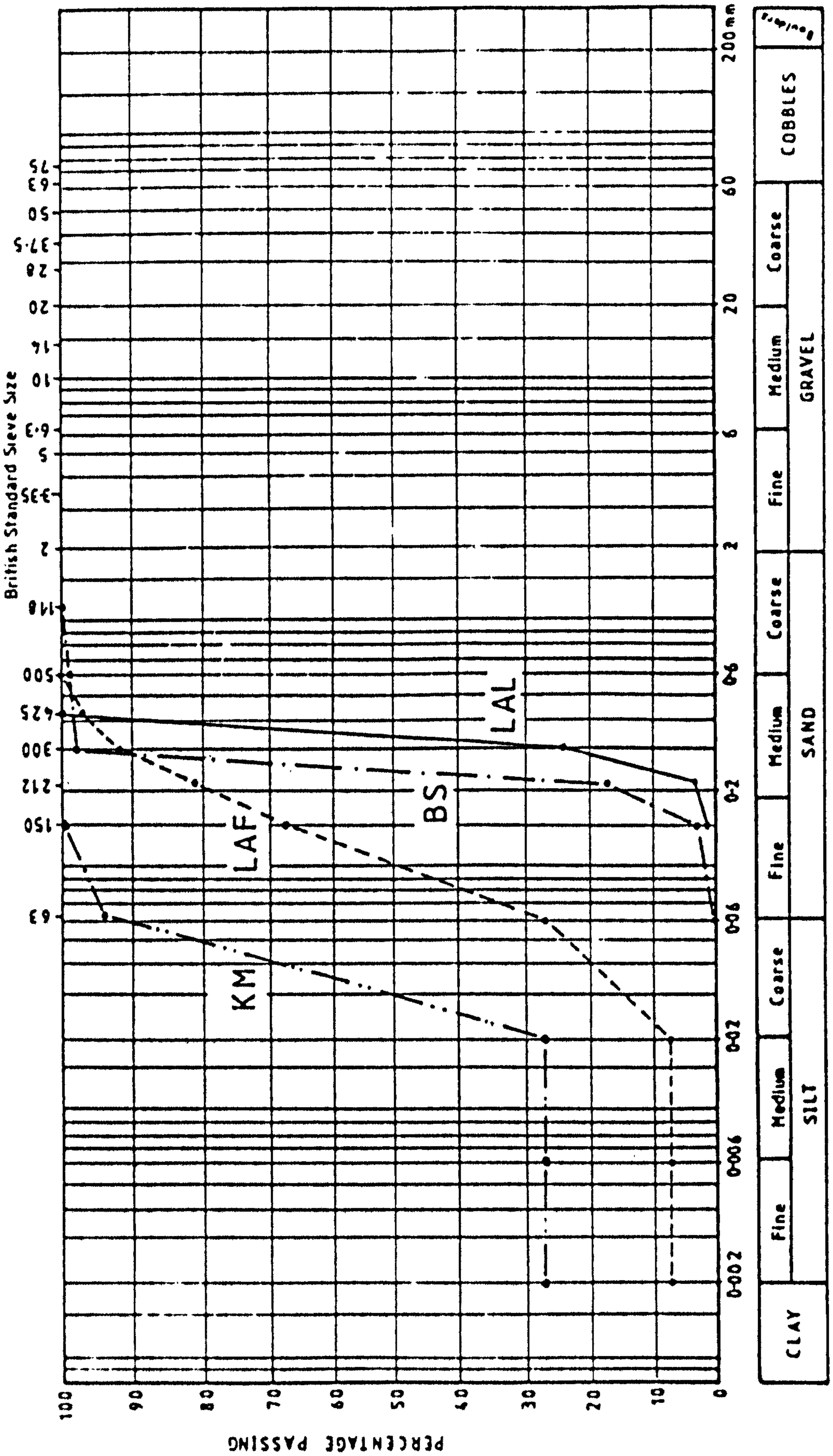

Fig. 3·1 Particle size distribution curves

Table 3.2 Geological strata encountered by Asfordby borehole

Geological Strata	Depth (m)
Keuper Mudstone	314.5 ↓ 318.0
Waterstones	323.2 ↓ 359.3
Basement Beds	362.8 ↓ 371.2
Bunter	372.8 ↓ 389.1
Basal Breccia	392.5 ↓ 392.7
Coal Measures	396.7 ↓ 399.1

Table 3.3 Mean values of specimen properties for the three test soils when frozen

Material	Dry Density ρ_d	Moisture Content w	Degree of Saturation S_r	Porosity n	Height/ Diameter Ratio
LAF	1.53	24.1	96	42	76/38
KM	1.61	22.0	99	38.3	76/38
LAL	1.68	19.2	98	36.4	76/38

3.3 Literature review on preparation methods

Laboratory testing of frozen soils for engineering design purposes will generally involve the freezing and subsequent testing of cores of unfrozen material recovered relatively undisturbed from an exploratory borehole. Some machining of specimens into suitable shapes for testing may be necessary and this can conveniently be undertaken when frozen. Occasionally, material may be recovered in a field frozen condition as in the case of the Brussels sand work of Gardner (1985). For research purposes it is often necessary to be able to strictly control the macroscopic structure and recompacted specimens of suitably graded material will frequently be used.

The first stage of preparation of laboratory specimens is to select a material with a grading which is reproducable in sufficient quantities to complete the test schedule. The size and shape of the particles will dictate the way that the soil compacts, which in turn, affects the porosity and moisture/ice content. Small changes in the soil composition can have great effects on the mechanical properties of manufactured specimens.

Test specimens are often formed from oven dry material which is compacted into split moulds to a predetermined density. Sayles and Epanchin (1966) and Alkire and Andersland (1973) describe this process and vibrate a measured quantity of sand in the moulds until the specimen height is reduced to give the required dry density. An alternative technique (Sayles 1968) is to tamp sand samples into the moulds in layers as this helps ensure a uniform density distribution throughout. A standard number of blows is used on each layer (Sayles - 10 blows on each of 6 layers) for consistency, and continuity is achieved by scarifying the top surface of each layer.

In 1976 the vibration technique was recommended for preparing sand specimens in the ASTM publication STP 599 (Baker 1976). The same report laid down a procedure to be used for producing hand tamped samples of air dried soil which was consistent with that

attributed to Sayles above. Zhu and Carbee (1983) used this procedure for preparing specimens of Fairbanks silt.

Recently, Baker and Konrad (1985) have reported the use of a pluviation technique to produce specimens over a range of dry densities. An even rain is obtained by allowing the sand to fall through a series of sieves which cause dispersion of the grains over the cross-section of the mould. The specimen density was found to be related to the size of aperture in a funnel directing the sand from a hopper to the sieves.

Wet compaction of soils into suitable moulds provides an alternative method which is well suited to producing clay specimens for freezing. Andersland and Akili (1967) mixed air dried Sault ste. Marie clay, with preselected quantities of distilled water, then allowed a two day equilibration period in a sealed container before statically compacting the moist clay into moulds. The procedure followed is fully described by Leonards (1955). A somewhat different approach by Perkins and Ruedrich (1973) produced synthetic permafrost specimens by filling a metal mould with distilled water and adding the soil in layers whilst tamping to produce a dense pack.

Sand specimens have also been produced in a moist condition. Rein et al (1975) compacted a layer of dry sand into a mould and then added a measured quantity of distilled water. The now moist layer was further tamped and then the whole process repeated until the desired specimen height was reached. Parameswaran (1980) and Parameswaran and Jones (1981) produced Ottawa sand specimens by compacting in layers at the optimum moisture content. A similar method has been adopted by Diekmann and Jessberger (1982) for forming sandy silt specimens. Diekmann and Jessberger claim that this technique gives the best reproducibility.

Having produced samples of known dry density it is then important to control the moisture content, often to the extent of obtaining 100% saturation. Alkire and Andersland (1973)

produced specimens which were 97% saturated by adding pre-cooled de-aired distilled water to their dry vibrated sand. It is thought that air inclusions within the sample prevented 100% saturation being obtained. By the same technique, 55% saturation was obtained with uniform moisture distribution throughout the specimen.

In his recommendations to ASTM, Baker (1976) suggests that specimens should be subjected to a vacuum for 2 hours prior to any attempt at saturation. It is suggested that this should remove any air from the specimen voids and when a de-aired water supply is introduced to one end, the vacuum will draw up water to saturate. A slow saturation rate should ensure that piping does not occur. Once visible signs of excess water appear, Baker suggests a further period of 1 hour under a 0.5m head of water to encourage complete saturation.

The vacuum saturation technique was used by Parameswaran and Jones (1981) in an attempt at completely saturating Ottawa sand specimens prepared at optimum moisture content. This method is less likely to achieve 100% saturation than that proposed by Baker as air voids may remain trapped within the specimen by the surrounding moist sand.

Sandy silt (Diekmann and Jessberger 1982) and silt (Zhu and Carbee 1983), have also been shown to be amenable to the vacuum saturation technique.

The next preparation stage is that of freezing. The freezing process in soils is accompanied by redistribution of free water under the influence of pressure differences between pore water and ice, and this needs to be accounted for in the specimen preparation procedure. One method is to freeze the specimens quickly by exposing all the surfaces to low temperatures. This promotes a rapid advance of the freezing front towards the centre of the specimen and in the ideal case a three dimensionally symmetrical distribution of ice throughout. O'Connor and Mitchell (1982) used such a multiaxial freeze

method on river silt specimens in a consolidated saturated state but report no details of either the method employed or any difficulties encountered.

One drawback with the multiaxial freeze method results from the natural 9% volume increase on freezing of water to ice. A water saturated specimen subjected to freezing temperatures must expel moisture from its pore spaces in advance of the ice front to maintain a constant dry density. In the multiaxial freeze method, where the ice front is advancing inwards from all surfaces, this can result in a saturated unfrozen core surrounded by an ice saturated frozen wall. Further freezing will inevitably result in the build up of high internal stresses. This may be avoided by controlling the progress of the freezing front through the specimen in a unidirectional manner.

The uniaxial freezing method simulates conditions found in practice where heat is extracted from the neighbouring soil elements by a freeze tube. Laboratory uniaxial freezing apparatus are normally designed to allow the freezing front to advance along the major axis of a cylindrical specimen. Rein et al (1975) stood sand samples on a cold plate at -25°C and with the provision of lateral insulation, advanced the ice front to the top surface. Excess water was allowed to drain out of the specimens at all times up to the completion of the freezing process. The direction of freezing was inverted by Parameswaran and Jones (1981) and the warmer temperature of -6°C used to promote freezing from the top surface.

Free movement of moisture, rather than uniaxial drainage, can be obtained through an open system. Open systems include a reservoir of water which allows the specimen to take up water in response to suction forces set up in the freezing zone. Sayles (1968) used an open system which froze Ottawa sand specimens unidirectionally from the top surface and incorporated an external reservoir to supply de-aired water to the base. This system corresponds to the recommendations set out by Baker (1976).

The open freezing system is ideal for use with sandy materials where 100% saturation is desired. Any moisture deficiency in the pore spaces may be made up during the freezing cycle to produce ice saturated materials. It is, however, important to note that frost susceptible materials will allow the development of ice lenses within a specimen unless heaving is restrained. Zhu and Carbee (1983) successfully froze silt samples using an open system by encouraging a fast rate of freezing which restricted the magnitude of the suctions developed.

The final stage in the preparation process is to shape the specimens to meet the test requirements. For strength and creep testing, this normally involves forming true cylindrical specimens with smooth coplanar ends. Shaping normally takes place in a cold room and Baker (1976) suggests -5°C as a temperature which prevents surface thawing of specimens but also provides for personnel comfort. A rotary lathe is ideally suited to finishing specimens but simpler techniques, using hand tools and shaping jigs, may suffice. Whichever method is employed, it is important that all equipment to be brought in contact with the test specimens should be stored in the cold room to avoid localised thawing damage when in use.

3.4 Preferred preparation methods

3.4.1 Preliminary experimentation

The quality of the test specimens is sensitive to the soil types and some preliminary experimentation is often needed to find an ideal combination of soil and preparation technique. When recompacting soils, the first problem is one of obtaining a uniform density through the specimen and this can be achieved by vibrating the mould or by dynamically or statically compacting the soil in bulk or in layers. These techniques were attempted for the three soils LAF, LAL and KM and the method adopted in each case gave the most consistent values of dry density both through the specimen and between individual specimens. The

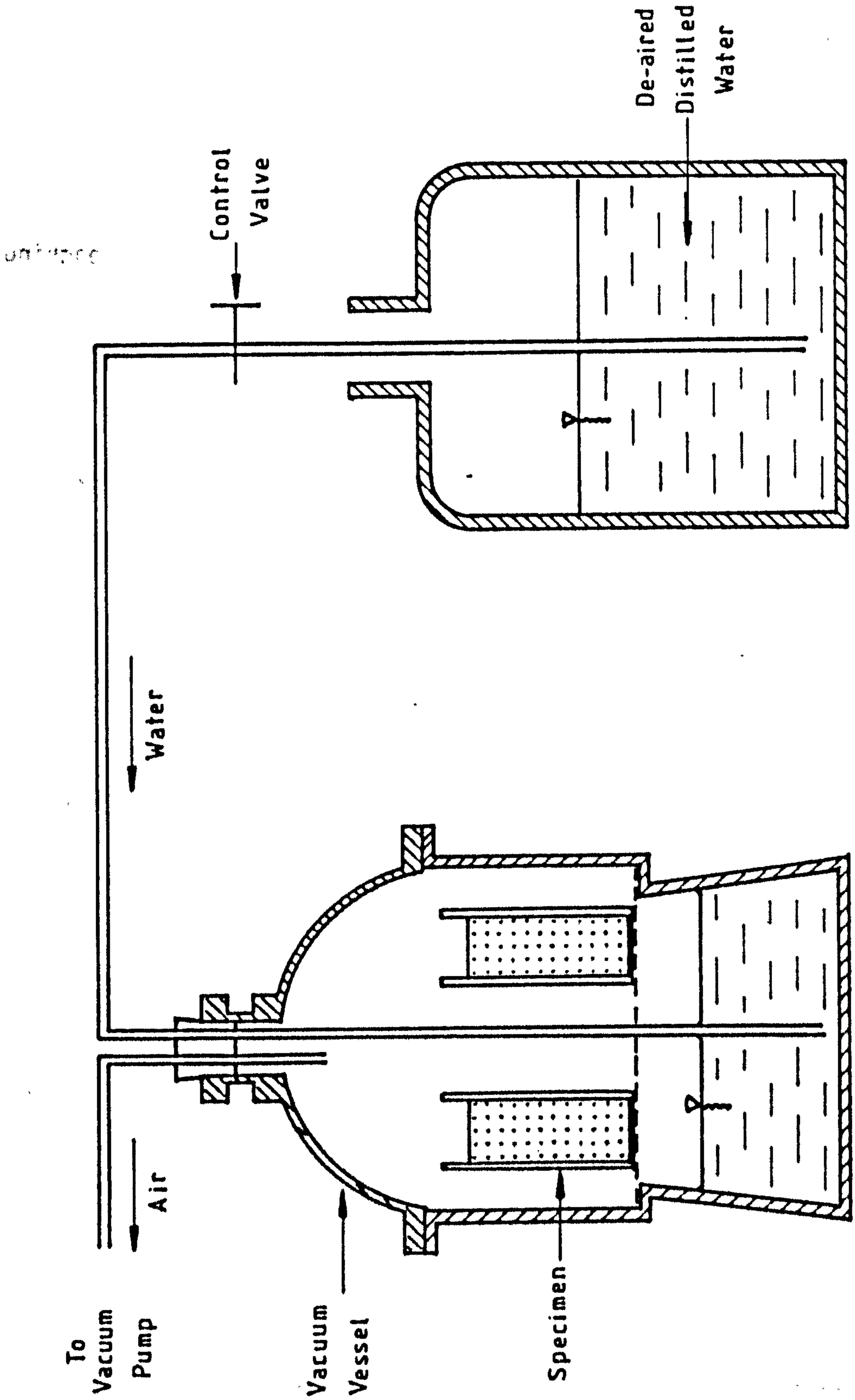

Fig. 3·2 Apparatus for saturating soil and rock specimens

methods adopted are described in subsection 3.4.2 and were only suited to providing one particular specimen density for each material.

A target saturation level of 100% was set for the research programme and this led to the development of both saturation and resaturation techniques. The basic technique was to evacuate the pore spaces in the specimens prior to introducing de-aired water to the base to allow unidirectional saturation (Fig. 3.2). The fine material in LAF was found to be susceptible to migration out of the top of the specimens when saturated under vacuum and it was therefore necessary to revert to a capillary rise method for this material. Most of the rock specimens were successfully resaturated under vacuum but some siltstones and mudstones suffered from slaking effects. These materials were successfully resaturated and frozen by Marchina (1984) after development of a new apparatus based on the standard triaxial cell. Both KM and LAL specimens were nominally saturated from the compaction stage and no further saturation process was deemed necessary.

The options considered for freezing the specimens were free draining and open uniaxial systems. The free draining system (Fig. 3.3) had been developed by Gardner (for freezing 21% saturated Brussels sand) and was found to be well suited to the freezing of nominally saturated materials where a net expulsion of water results from the volume expansion to ice. The open system was developed through several stages which incorporated thermostatically controlled water reservoirs and recirculatory systems. The final version (Fig. 3.4) simply relies on good lateral insulation to ensure that the zero isotherm penetrates through the specimens before the reservoir water freezes. Specimens of plaster, sandstone and LAF sand, embedded with thermocouples along their central axes, were used to verify this behaviour.

The open freezing system is shown with three specimens in place in Plate 1. The vermiculite insulation has been removed to expose the brass tank.

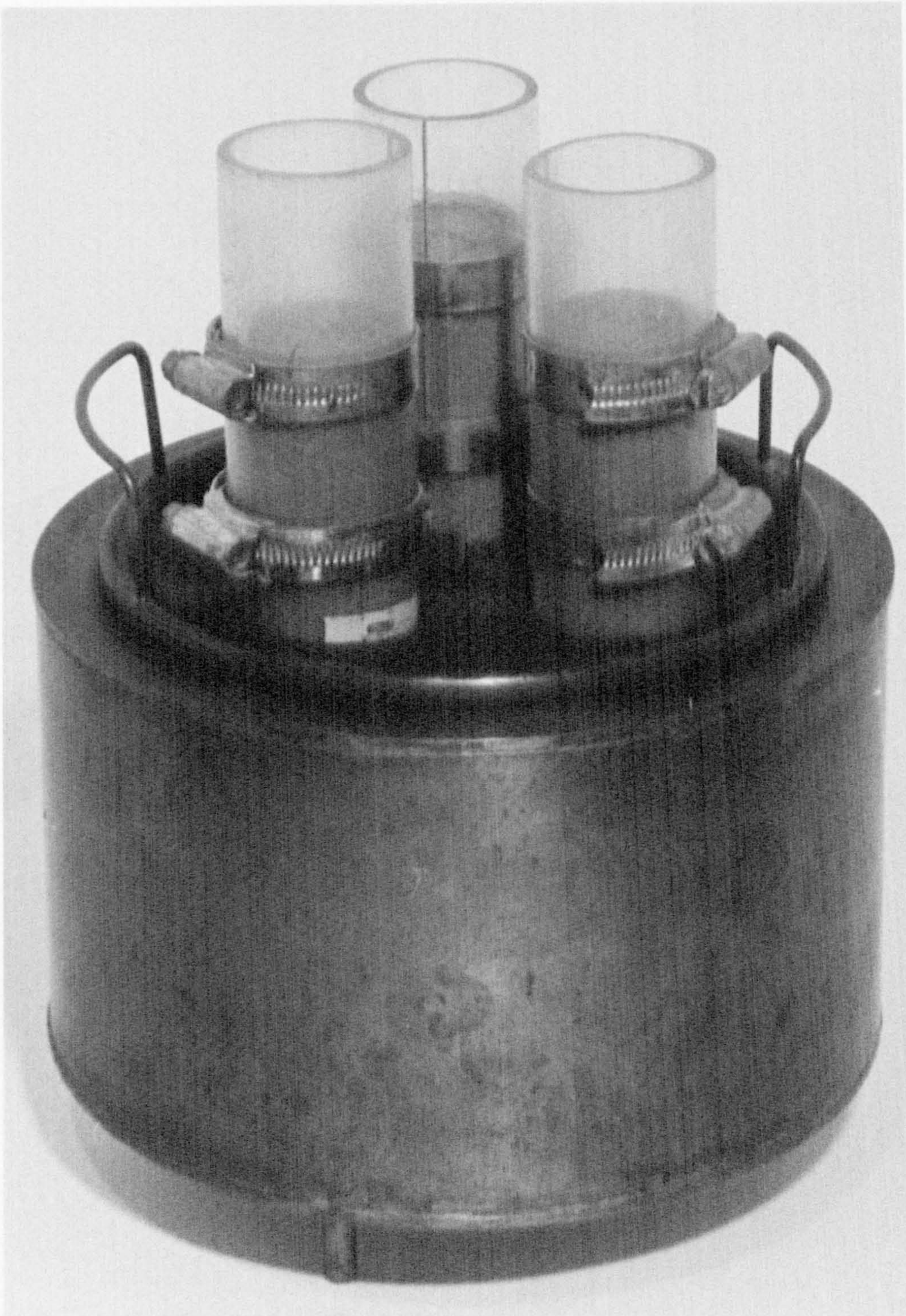

Plate 1 Open Freezing Apparatus

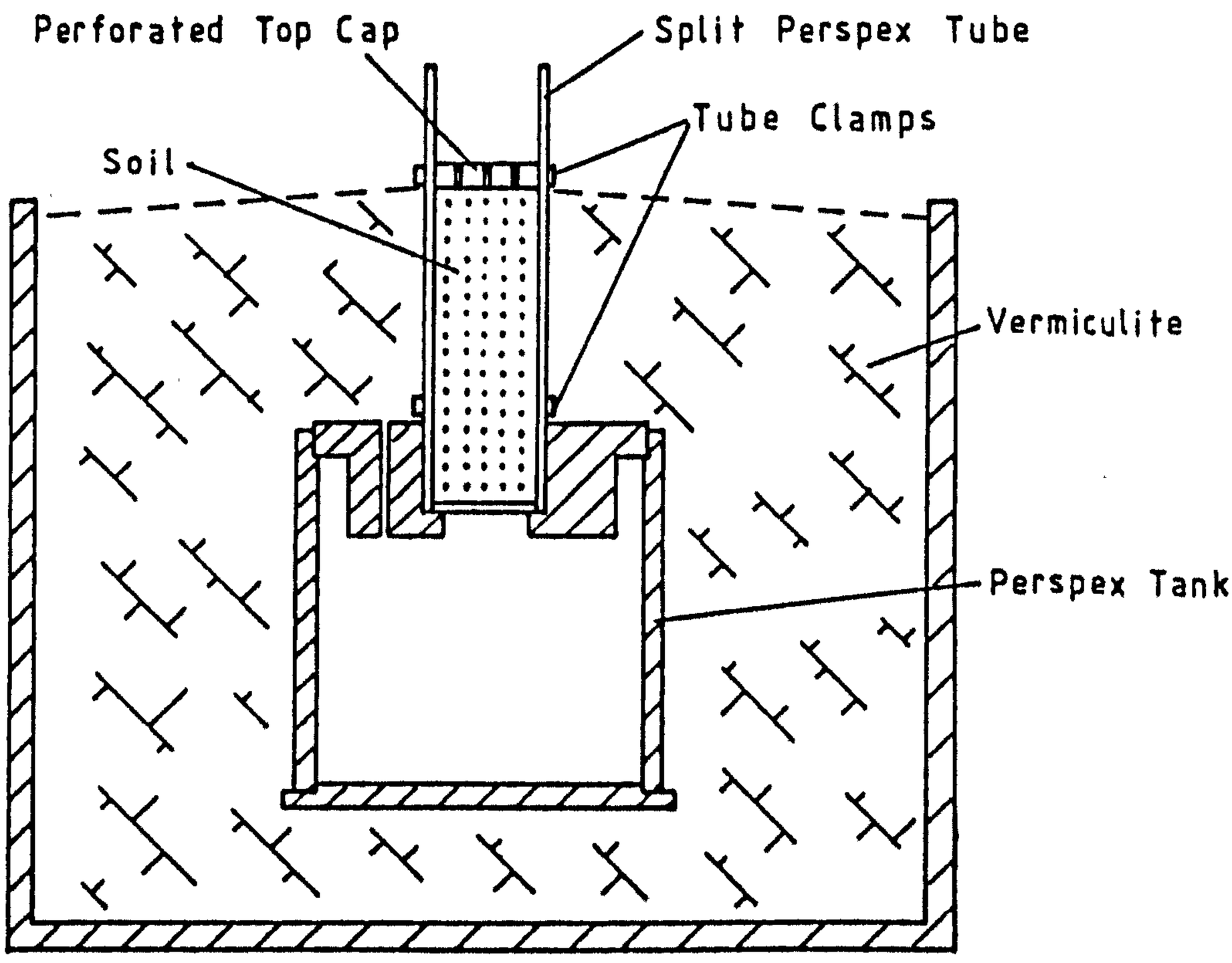

Fig. 3·3 Free draining freezing apparatus

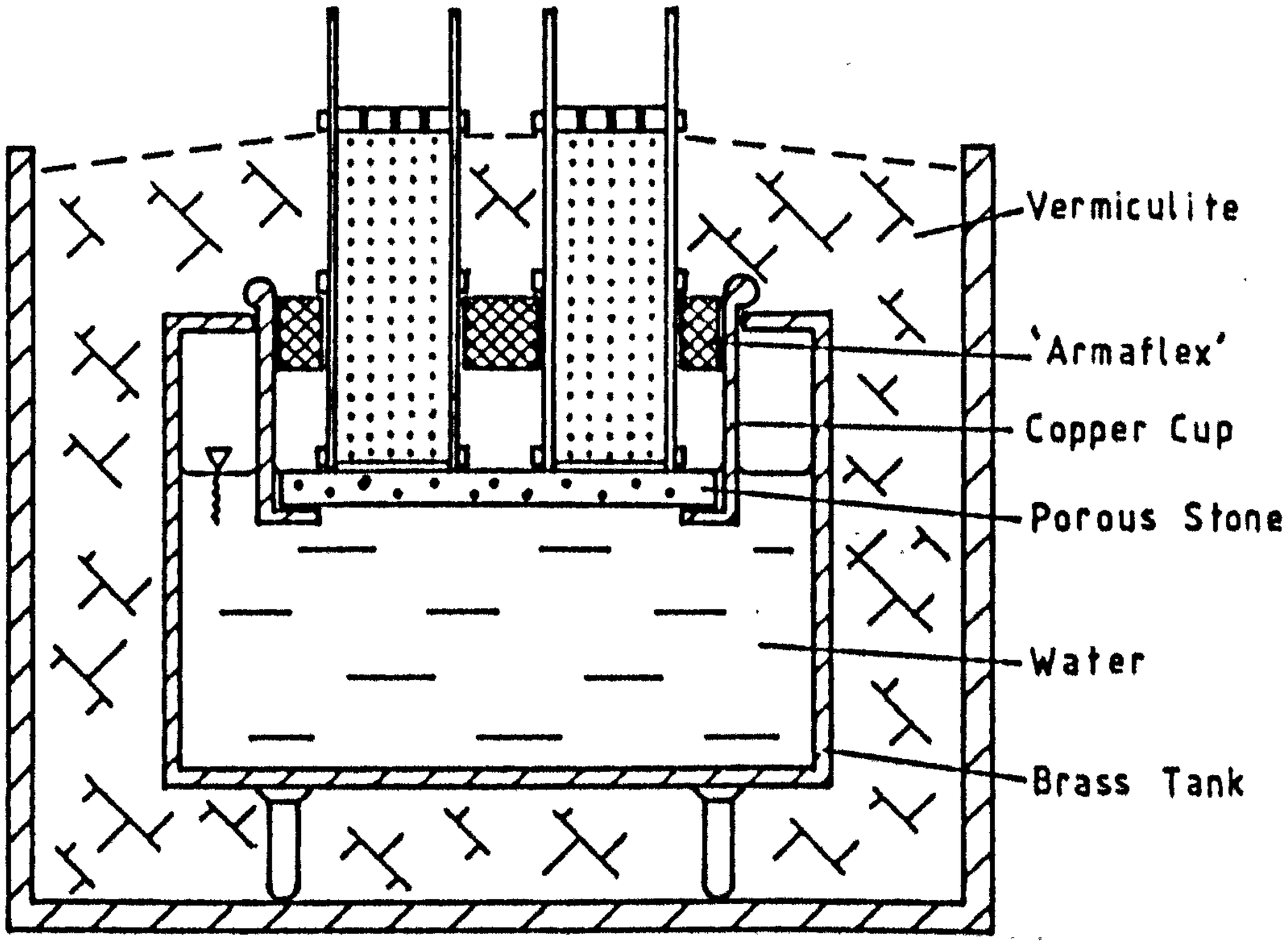

Fig. 3·4 Open freezing apparatus

3.4.2 Methods adopted

The procedures described in this section were used to produce 38mm diameter frozen soil specimens and 30mm diameter (AX core size) frozen rock specimens. 38mm diameter split perspex tubes with sintered bronze porous discs clamped across the bottom end, were used to form the soil specimens.

3.4.2.1 LAF sand

200g of oven dried sand passing a 600μm sieve was poured into each tube and the whole vibrated using a Burgess engraving tool with an 80mm diameter footing. Vibration continued until the height of sand within the mould reduced to a height appropriate to the target density of 1.53 Mg/m^3. A perforated perspex top cap was then clamped in place and each tube stood in a shallow water bath for 24 hours to allow saturation by capillary rise. The open freezing system was used to freeze three specimens over a 48 hour period in a cold room at -17°C. The frozen specimens were then trimmed to a height of 76mm using hand tools and a jig to ensure end squareness. Material was removed from both ends to avoid possible freezing and sublimation effects on the test specimens.

A trimmed specimen is shown in Plate 2 along with the end platens, membrane and 'o' rings necessary for protection during a test.

3.4.2.2 LAL sand

200g of dry LAL sand was poured into the moulds which were submerged in water. Vibration using the engraving tool continued until no further decrease in specimen height could be observed. No saturation period was needed for this procedure and the specimens were frozen then trimmed as for LAF sand.

Plate 2 Specimen, End Platens and Membrane

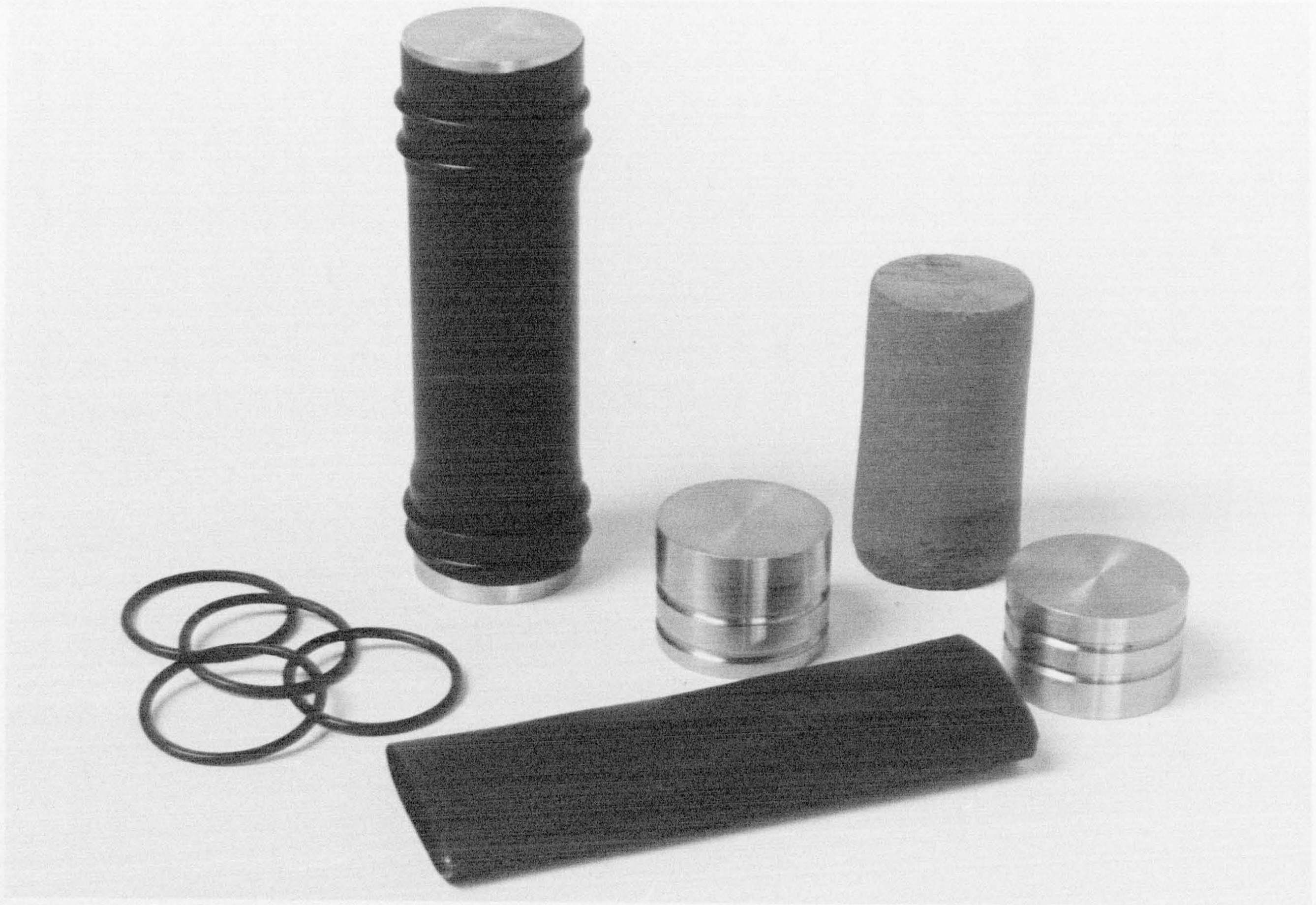

3.4.2.3 KM clay

KM was mixed to its optimum moisture content and then compacted into a standard proctor mould using a 4.5 kg rammer. The clay cake was then extruded into 38mm diameter steel tubes and transferred from these to the split moulds for freezing. Freezing took place in the free drainage apparatus of Fig. 3.3. End preparation followed the same procedures as for the sands.

3.4.2.4 Triassic rocks

The rock specimens were received at nominal dimensions of 30mm diameter by 60mm high and were tested at these sizes. Each specimen was wrapped in wax paper, with just the ends exposed, to minimise any damage in handling. Vacuum saturation was preferred but specimens which were susceptible to slaking were frozen as received. The open freezing apparatus was used in all cases.

3.4.3 Quality of specimens

The properties of the frozen soil specimens prepared by the methods described above are summarised in Table 3.3. Mean values are given but the degree of scatter about the means is not high. The variations in dry density are shown in Fig. 3.5 and statistical analyses of these distributions show the standard deviation about the mean to be 0.02 in each case. The mean value for LAF dry densities is the target value of 1.53 Mg/m^3 but for KM the maximum dry density of 1.61 Mg/m^3 was not consistently attainable. Each LAL sample was compacted to the maximum attainable density and Fig. 3.5c shows reproducibility to be good by this method. Further details on the quality of LAL specimens is given by Tan (1985).

The degree of ice saturation (s_i) for each LAF specimen was evaluated after testing. The calculations were based on the

pre-test volume and post-test oven dry weight and gave the frequency distribution shown in Fig. 3.6. These results are surprisingly consistent as calculated s_i values were shown by Marchina (1984) to be susceptible to errors giving accuracies of ± 16% of the true value for specimens of this size.

3.5 Summary

Three soils, LAF, LAL and KM, have been described and their general properties determined in accordance with BS1377. LAF and KM have been selected to extend the range of soils over which the test apparatus has been proven and LAL introduced as a replacement for the Brussels sand used in previous studies. Some weakly cemented triassic rocks are also described in terms of their geological horizons and sampling depths in a borehole at Asfordby in N.E. Leicestershire.

The specimen preparation process can be divided into five stages.

1. Selection of a suitable material grading, taking account of the relative sizes of soil grains and finished specimens (e.g. Brown 1983 suggests a 10:1 ratio between specimen diameter and maximum grain size).

2. Forming of the specimen by compaction or consolidation.

3. Control of the moisture content to attain the required degree of saturation.

4. Control of the freezing process to ensure that the specimens are not subjected to high internal stresses or ice lens formation.

5. Shaping to the required tolerances on size and shape.

A literature review has shown the methods used to complete these stages which may in some cases be combined (e.g. compaction of

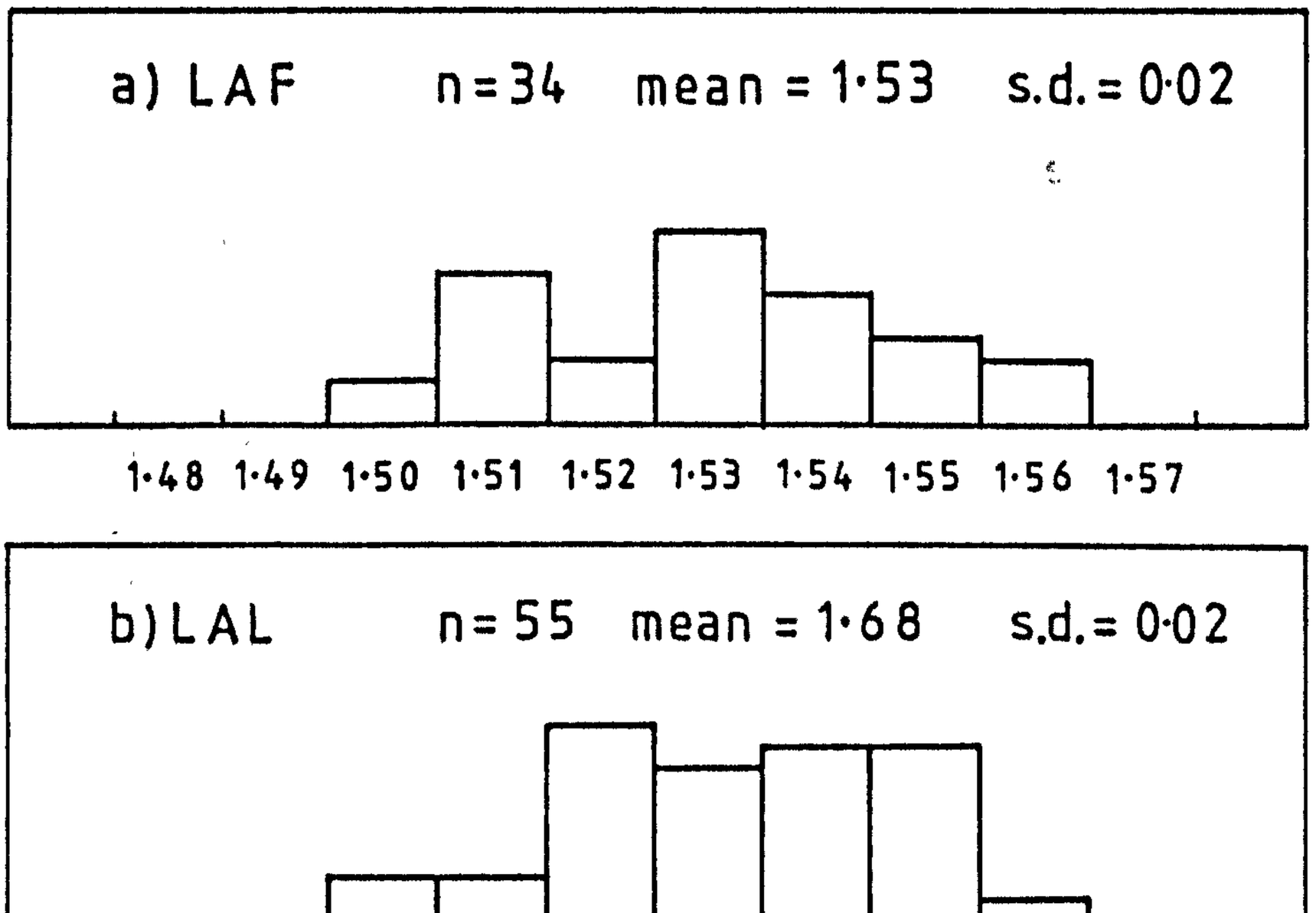

Fig. 3·5 Frequency distribution of dry densities using preferred preparation methods

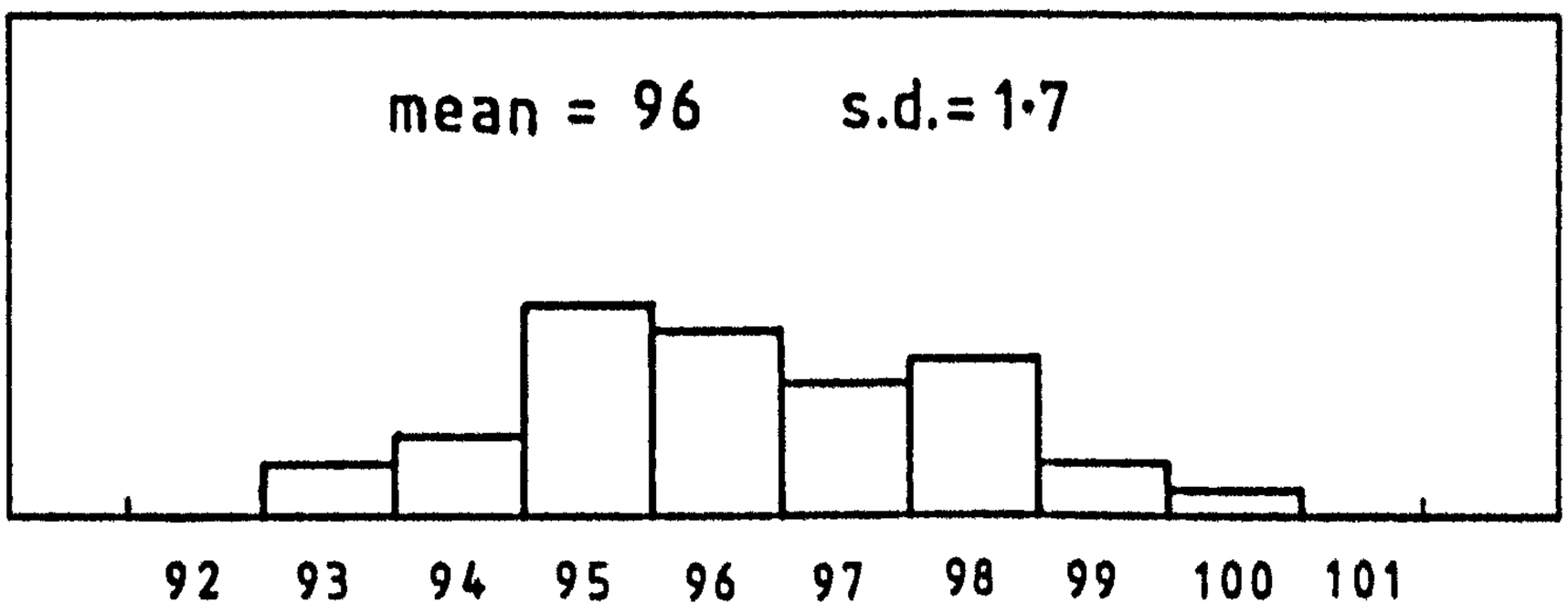

Fig. 3·6 Frequency distribution of degree of ice saturation for LAF sand

moist soil or consolidation from a slurry combine stages 2 and 3).

Reproducibility is an important aspect of any specimen preparation method and some flexibility in approach is required to suit individual soils. The methods used for each material in this study have been given in detail and the reproducibility demonstrated by examining the distribution of dry density and degree of saturation between specimens. Statistical analyses of the dry densities show the standard deviations about the mean to be 0.02 in each case and only one KM specimen lies outside the limit of ± 2 standard deviations from the mean.

CHAPTER 4

SHORT AND LONG TERM STRENGTH TEST EQUIPMENT

4.1 INTRODUCTION

The design procedures described in Chapter 2 require information about the strength and deformation properties of the frozen materials. Soils are not of regular composition and documentation of frozen properties is not as yet available in any great quantities, making laboratory testing necessary in many cases. The equipment is readily available for testing the strength and deformation properties of soils at ambient temperatures, but the adaptation of such equipment to sub-zero temperatures can be approached in a number of ways.

The triaxial compression test cell is able to yield information on the elastic modulus, Poisson's ratio, ultimate strength and creep strain limits, making it an ideal basis for the development of a frozen test facility. At Nottingham University, the initial development of a versatile computer controlled cell has now been supplemented by further equipment which has extended the capability to greater confining pressures and soil strengths.

The original cell was designed to withstand confining pressures upto 1.8 MPa and to apply deviator stress consistent with a vertical load limit of 35 kN. The computer control includes both short and long term strength test programmes. To develop the facility further, specialist test cells have been preferred to enable simple tests to be performed as easily and efficiently as possible. The designs are detailed in section 4.3 and consist of a uniaxial test cell and an adaptation of an existing triaxial cell made suitable for low temperature work. The triaxial cell can operate at very high pressures and the limit of 12 MPa required by the present research is well within its operating range.

The advantage of developing specialist short term strength cells is in the release of more complex apparatus for creep testing. In section 4.4, the design of a second computer controlled apparatus is given. The aim is once again to increase the

confining pressure range to 12 MPa and a number of innovative deviations from the low pressure cell design provide a more versatile apparatus in terms of load capacity and control.

In section 4.5 the limits to which the four main test cells have been taken are described for each of the soils of Chapter 3. Each cell is shown to perform well, within its design limitations, over a range of soil and rock types. The chapter closes with a brief summary.

4.2 Review of low temperature strength test equipment

Equipment and test procedures for investigating the mechanical properties of soils at ambient temperatures are well established. Many tests involve the use of the standard triaxial cell, which can impose deviatoric stress conditions on a soil specimen, with the method of stressing affecting the type of information obtained.

To adapt this equipment for testing frozen soils, a means of maintaining a constant sub zero temperature is required. This can be achieved by installing the test facility into a cold room with a heat exchanger and forced air flow regulating the temperature. Sayles (1963) reports the use of such a facility at the U.S. Army Cold Regions Research and Engineering Laboratory (USA CRREL) and a similar unit has been established at the University of Karlsruhe (Eckardt 1979, 1982). Problems arising from this approach principally concern the forced air flow which can cause temperature instability and induce sublimation. Sublimation involves the conversion of pore ice to water vapour and the redeposition of the vapour as frost on the heat exchanger where the air temperature is lowest. Sublimation problems can be eliminated by wrapping specimens during storage and installing a protective sheath during testing.

Temperature stabilisation can be achieved by introducing an enclosed test chamber which provides a localised stable

environment. Close control of test temperatures was achieved at the CRREL facility by back heating the enclosed chamber (Sayles 1968, Fish and Sayles 1981). Parameswaran (1980) used a kerosene bath with an immersed heat exchange coil to provide local temperature control. In both these cases, the main refrigeration is provided by the cold room and stability by small heat exchangers around the specimen.

A progression from the cold room approach is to construct small temperature controlled test chambers to provide localised refrigeration whilst allowing the bulk of the apparatus to remain at room temperature. Sanger and Kaplar (1963) used an air filled freezing cabinet to house a creep test facility and similar systems mounted in standard testing machines are reported by Parameswaran and Jones (1981) and Perkins and Ruedrich (1973). In each of these apparatus, the specimens were cooled by static air. A recirculating air system was introduced by Mellor and Cole (1982) along with an independent means of refrigerating the test cell base platen. Refrigerating the base platen minimises the temperature gradients within the specimens which would otherwise result from the flow of heat from the test machine. To test specimens down to -160°C, a low temperature cabinet charged with nitrogen has been used by Bourbonnais and Ladanyi (1985a, 1985b). At these temperatures, the insulation of the cabinet from both the test machine and the outside air, becomes critical if temperature instability is to be avoided.

Similar to the gas cooled temperature cabinets are constant temperature baths. A portable refrigeration unit can be used to cool the oil, kerosene, or anti freeze solution in the bath and good thermal contact between this solution and the test specimen allows close temperature control (Andersland and Alnouri, 1970). Alkire and Andersland (1973) then pressurised the bath fluid in an enclosed chamber to allow the apparatus to be used for triaxial strength tests. This effectively now becomes a self-contained refrigerated triaxial cell.

At Nottingham University, a specialist triaxial cell which

includes an internal coil of copper pipe has been developed (Gardner et al, 1982). A methanol refrigerant is circulated through the copper coil by a chiller/circulator unit and a silicon oil, used as the confining medium, readily transfers heat from the specimen to the coil. More details of this apparatus are given in section 4.4. Other test cells with built in refrigeration capabilities have preferred the use of double walled pressure vessels to copper coils (Jessberger and Jordan 1982, Simonsen et al, 1974).

The way in which frozen soil specimens are loaded has a considerable effect on the mechanical response. Tests can be categorised under the two headings short and long term strength with the latter being concerned with the time dependent creep behaviour of the material. For short term strength, stress or strain is controlled while the other is monitored.

Constant deformation rate (CDR) tests are most frequently used for short term strength determination. In terms of engineering or conventional strain (defined as change of length/original length), a CDR is a constant strain rate. However, true or natural strain (change of length/instantaneous length) rate increases during a CDR test in compression. Reference to constant strain rate (CSR), implies true strain rate in this thesis.

CDR test apparatus for frozen soils are generally based upon universal testing machines with the addition of one of the means of refrigeration discussed above. CDR tests approximate to CSR tests when the material fails at a low strain and it is often the average strain rate that is quoted. Materials showing less brittle behaviour cannot be treated in the same way and Andersland and Alnouri (1970) adopted the practice of periodically adjusting the deformation rate to approximate a strain rate of 5×10^{-5} s^{-1}.

Less frequently used in soil mechanics are constant load rate and constant stress rate tests. In rock mechanics, a stress

rate of 1 MPa/s is recommended by the ISRM, (Brown, 1983) and this is most conveniently achieved through a hydraulic loading system with periodic adjustments to the load rate. Constant stress rate tests on frozen rocks are reported in Chapter 5 and by Marchina (1984) with both studies using this technique. The refrigerated test cell is detailed in section 4.3.

Long term strength testing requires that a specimen be subjected to steady state conditions for an extended period of time. The simplest form of loading which can approach this condition is the imposition of a constant load. For applying small loads, a dead weight system can be used but physical constraints on the size and stability of the load pan limits this technique. Sanger and Kaplar (1963) used a dead load apparatus with bags of lead shot providing a maximum vertical force of 2.1 kN. Screw jacks supported the load box when not in use and allowed a rapid but controlled load application to the specimen. Higher loads can be obtained by incorporating a series of levers between the load and the specimen. The system devised by Akagawa et al (1982) includes motor driven fulcrums for the two lever arms to ensure that the load remains vertical through the specimen. The system was designed for a 20 kN capacity. High loads may also be applied using hydraulic systems and Perkins and Ruedrich (1973) adopted such a system for testing permafrost specimens.

A closer approximation to steady state conditions can be achieved through the constant stress (CS) creep test. To calculate the load necessary to maintain a constant stress, certain assumptions need to be made about the deformation behaviour of the specimen. Most commonly, this involves assuming the specimen deforms as a right cylinder of constant volume ($\nu = 0.5$) such that the cross-sectional area is constant throughout the length. This area may then be calculated from measurements of lateral strain or from the vertical deformation. These assumptions are valid for most materials at low longitudinal strains.

To maintain a constant stress using a hydraulic system, Eckardt

(1979) manually increased the load in response to each 1.3% increase in cross-sectional area. Similar stepped increases of load have been adopted by others with just the step length (tolerance) and loading method varying. Andersland and Alnouri (1970) used the dead load system and added lead shot to the load pan as required.

Lever loading systems offer a choice of two methods for maintaining constant stress. Increases in the dead load account for one and adjustment of the lever arm length the other. Sayles (1963) used the latter method and incorporated a programming wheel or cam to provide automatic adjustment. The cam served to change the lever arm length in response to specimen deformation and different shaped cams could be fitted to suit a variety of specimen sizes and test stress paths.

More versatile programmable systems have evolved from the gradual transition from mechanical to electrical devices for monitoring test conditions. Closed loop electrohydraulic systems can adjust applied loads in response to time or deformation signals and this allows a great variety of load types to be imposed. Jessberger (1977) reports the use of a closed loop electrohydraulic system for maintaining constant stress in a creep test and Jessberger and Jordan (1982) included a servohydraulic actuator to apply wave form loading. Microcomputer control systems have been developed to control apparatus based on electrohydraulic principles and the type of test then becomes software dependent (Gardner et al 1982, Gardner 1985).

The advantages of computer controlled and servohydraulic test apparatus lie in their versatility and adaptability. At Nottingham University, the apparatus developed by Gardner has been supplemented by a second computerised triaxial cell to operate at higher confining pressures and by two types of refrigerated test cells suitable for short term strength testing. These strength test cells provide an alternative means of obtaining strength parameters whilst the more complex

apparatus is dedicated to long term creep strength.

4.3 Short term strength test equipment

The short term strength test cells were designed specifically for testing frozen soils and weak rocks on a commercial basis. Sufficient instrumentation was included to enable peak stress, initial tangent modulus and the shear strength parameters c and ϕ to be measured. The cells were designed to be used with an independent loading device which adds to the versatility of the test facility. Deformation measurements can be made using a dial gauge or linear motion potentiometer (LMP) bearing on the crosshead of the machine and load measurements through a proving ring or load cell. The load cell and LMP can be used with an X-Y chart recorder to automatically produce load-deformation recordings.

The strength test facility is made up of four cells for testing in unconfined compression (UNC cells) and three for triaxial compression (Hoek cells). The main features of both types of cell are described in this section.

4.3.1 UNC Cells

The UNC cells were originally designed to accommodate 30mm diameter specimens (AX core size) with the specification that the design should allow for rapid placement and removal of specimens. The main features of the design are shown in Fig. 4.1 and consist of a steel top plate which acts as a piston housing, suspended on three threaded rods above a steel base plate. Grade 316 stainless steel base platens of 30mm and 38mm diameter have been manufactured and these locate in the centre of the base plate. A 2mm diameter hole passing through the end platens and the cell base, allows access for a thermocouple at the specimen/platen interface.

The top plate houses a linear bearing which accepts a 30mm diameter piston. The piston has a concave end face which matches the convex face of the specimen top platen. The radius of curvature of these faces is centred on the specimen/platen interface to allow rotation of the end during specimen failure. Both the piston and the top platens (30 and 38mm diameter) are of stainless steel.

One of the UNC cells has been modified as a result of temperature anomalies observed during tests on LAL sand. The three threaded rods have been replaced by a cylindrical aluminium wall with a removable section to allow specimen placement. This produces a more stable environment for the specimen and reduces the magnitude of the temperature gradient along the specimen principal axis to a minimum. Temperature conditions become similar to those of the Hoek cell.

Both types of UNC cell are shown in Plate 3.

4.3.2 Hoek Cells

The Hoek cell is a standard piece of rock mechanics equipment suitable for triaxial testing up to confining pressure of 70 MPa. The cell was originally designed for use in the field where materials recovered from a borehole could be quickly trimmed and tested with minimal disturbance. The main feature of the cell was the ease of specimen placement which required neither drainage nor dismantling of the cell (Hoek and Franklin, 1968). This is achieved by the inclusion of a thick walled membrane which effects a fluid tight seal when bearing on the cell end plates. The main components of the Hoek cell are shown in Fig. 4.2.

Two 30mm and one 38mm diameter Hoek cells have been used and base plates have been manufactured for each. The base plates incorporate end platens with similar thermocouple access ports to those of the UNC cells. The top platen and loading piston

Plate 3 UNC Strength Test Cell

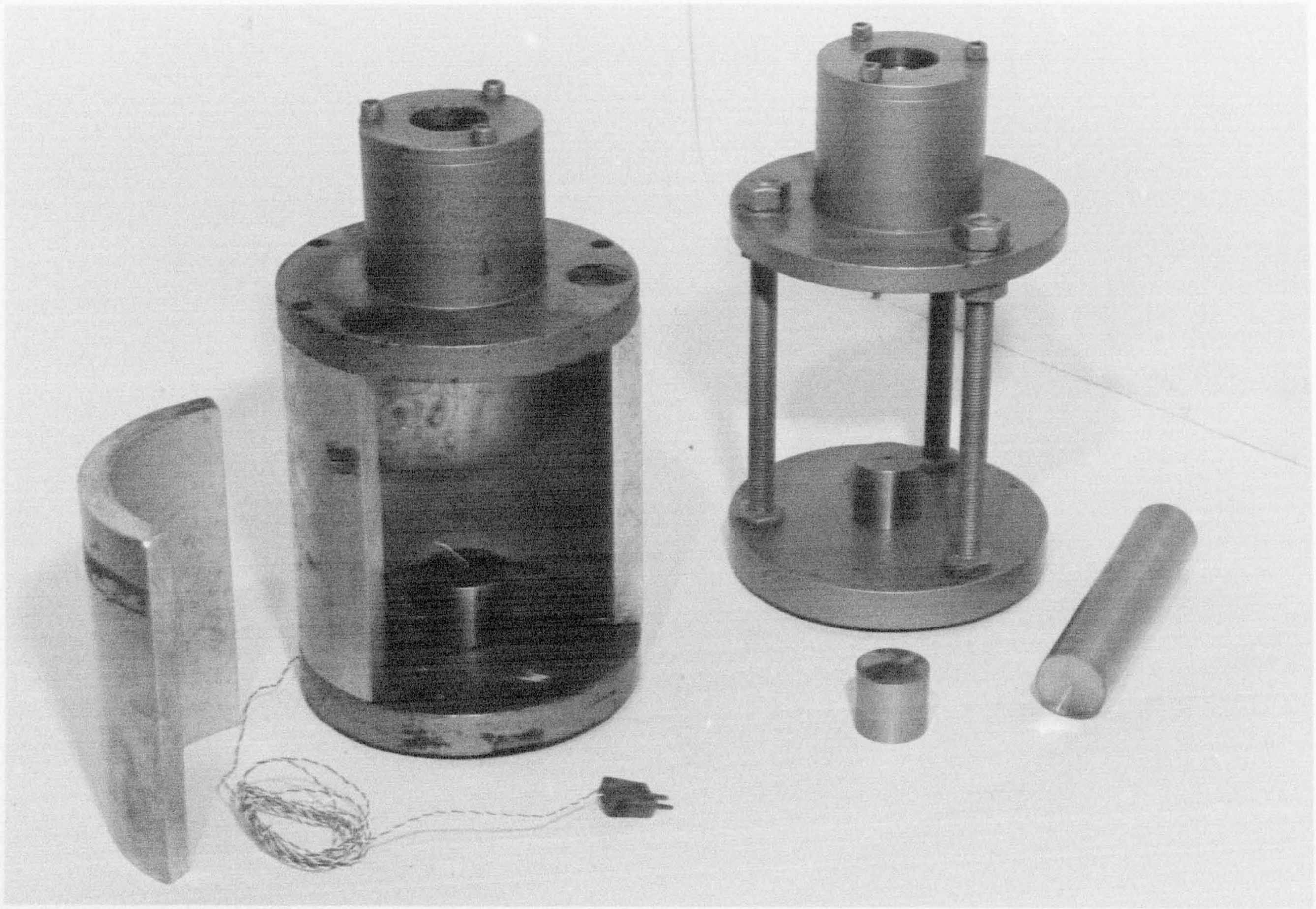

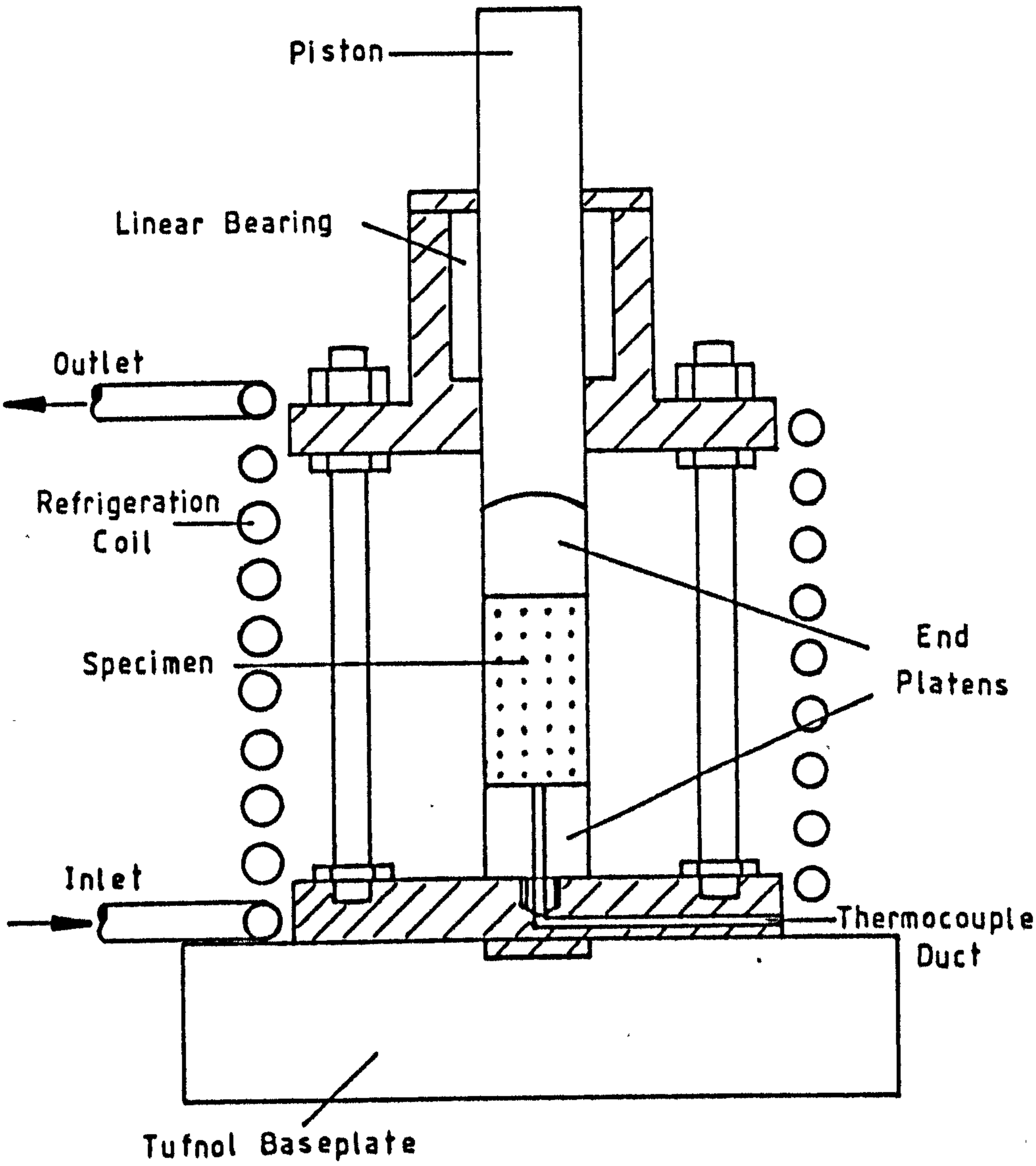

Fig. 4·1 Uniaxial compressive strength cell

are also of similar style to their UNC counterparts. Plate 4 shows the two types of Hoek available.

4.3.3 Hoek cell pressure system

For the envisaged test programme, an oil pressure system capable of supplying and maintaining confining pressures up to 14 MPa was required. The four component parts of the system are the Hoek cell, pressure transducer, bleed valve and pump which are combined in the manner shown in Fig. 4.3.

The system was initially built around a hand operated pressure pump which required a separate isolator valve to prevent the cell pressure from dissipating. This was later replaced by a Madan Unicub model C pressure multiplier pump which actively maintains the cell pressure to a preset level. The pump multiplies a low air pressure (nominal 150 psi or 1.05 MPa) up to a high oil pressure with a maximum multiplication factor of 27. Pressure is preset by a regulator valve on the low pressure side of the pump. The oil pressure is monitored by an electronic pressure transducer giving an output of 200mV at 2000 psi (14 MPa) from a 10V d.c. power supply. The transducer used was a model P102 manufactured by Maywood Instruments.

During deformation of the test specimen, lateral strains cause the oil chamber in the Hoek cell to decrease in volume and this increases the confining pressure. To relieve this pressure, a fine needle valve was included in the system and adjusted manually in response to changes in the transducer readout. This valve also allowed the pressure to dissipate at the end of each test.

4.3.4 Refrigeration of UNC and Hoek cells

Both types of cell are refrigerated in the same way. The main components of each system are a coil of copper pipe, a portable

Plate 4 Hoek Cells

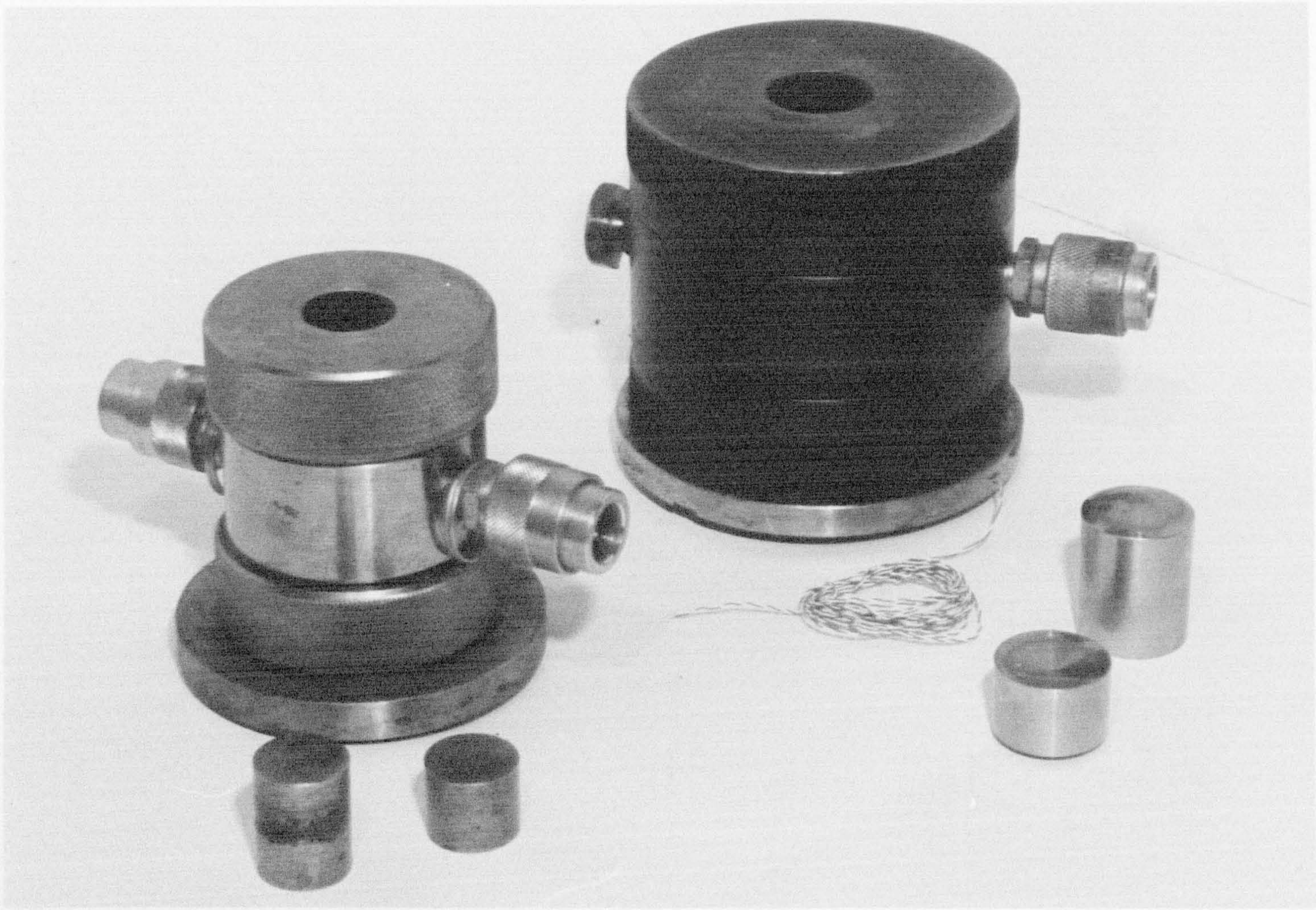

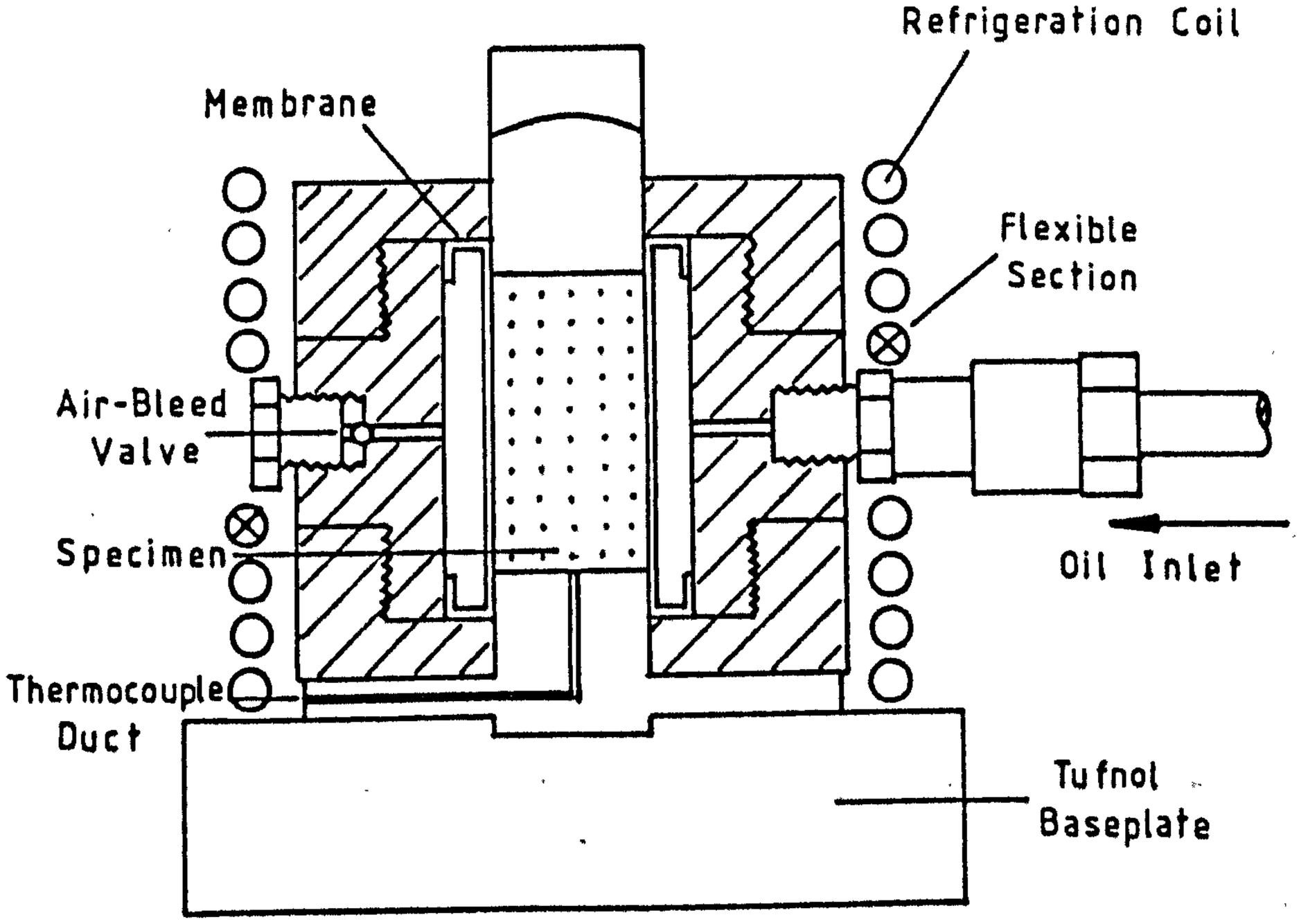

Fig. 4·2 Refrigerated Hoek cell

refrigeration unit and the appropriate insulation. The copper coils are formed to circulate a methanol refrigerant around the outside of the cells. The Hoek cell coils include a flexible section in the middle which enables the cell to be removed without disconnecting the pressure connections.

Flexible pipes lead from the coils to the refrigeration unit. This is a Freon charged Churchill model 05/CTCV chiller/ circulator capable of refrigerating a methanol solution down to -30°C. A heater system within the unit allows the temperature to be maintained at a set value. The pipes running between the Churchill unit and the coils are insulated using 'Armaflex', a rubber based product available in sheets and in preformed tubes. 'Armaflex' sheeting has been cut to shape and fitted closely around the cell coils and across the cell tops. Insulation between the cell base plate and the test machine needs to be both strong and resistant to deformation. A 50mm thick sheet of Tufnol meets these requirements.

Refrigeration time of the two cell types varies, mainly due to the greater thermal mass of the Hoek cells. Using one refrigeration unit with two UNC cell coils connected in series, it was possible to test up to six specimens a day (at -16°C). Optimum output for the Hoek cell was obtained with just one cell and coil per refrigeration unit, yielding a maximum of two tests per day.

4.4 Programmable strength test equipment

By October 1982, the creep test facility developed by Gardner had been commissioned and used for triaxial testing to 1 MPa confining pressure at -10°C (Gardner et al 1982, Gardner 1985). The apparatus was designed for both short and long term strength tests with a Commodore PET microcomputer controlling and monitoring each test.

The cell is made of steel and supported on a lightweight frame

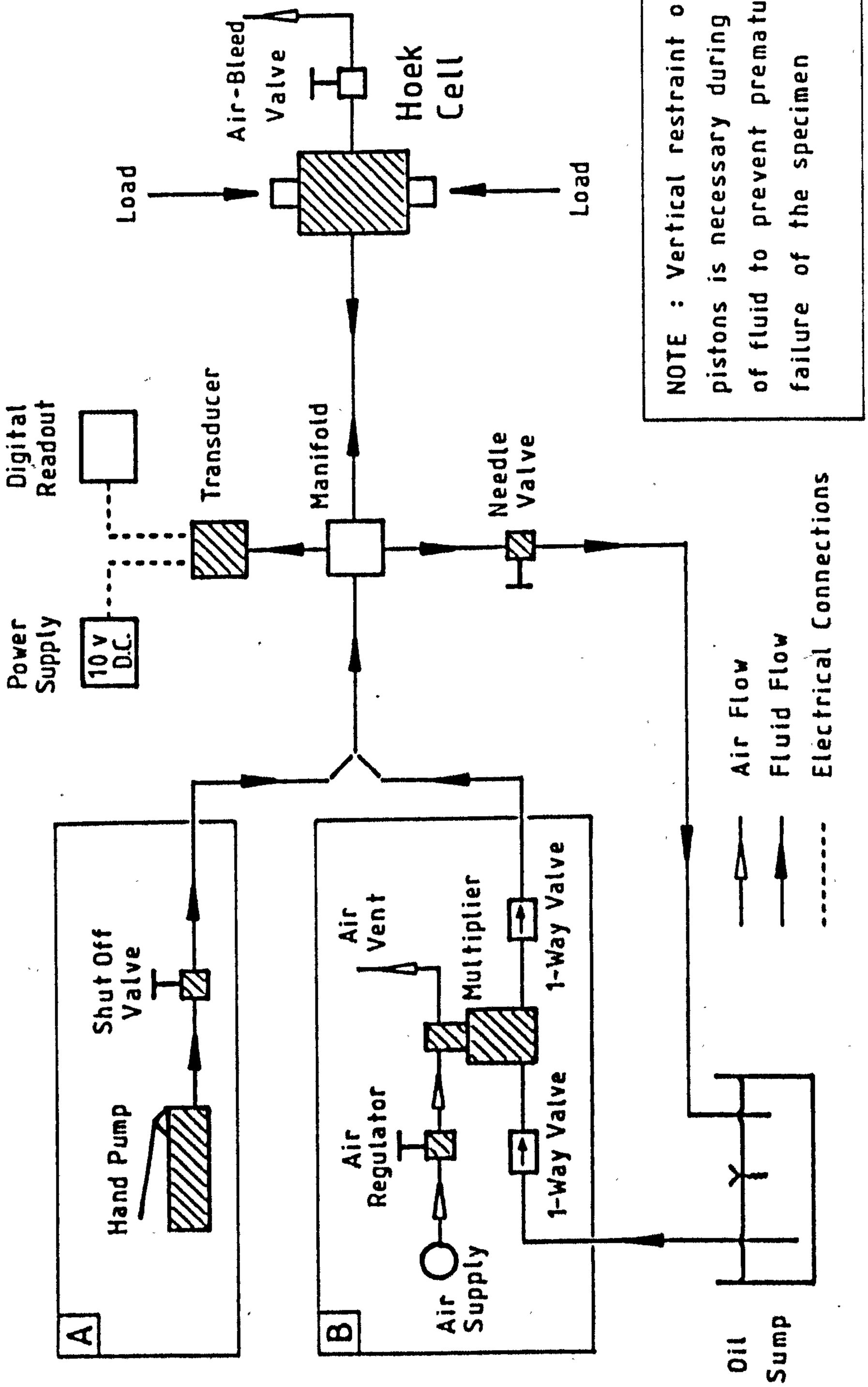

Fig. 4.3 Oil pressure system for Hoek cell

which also houses a Bellofram loading cylinder (Fig. 4.4). The Bellofram cylinder acts on a piston passing through the base of the cell and loads 38mm diameter soil specimens which react against the cell top cap. A load cell is incorporated in the top cap and electrical signals from this are sent to an amplifier and conditioning unit. Refrigeration of the cell is by circulation of a methanol solution through a coil of copper pipe secured inside the cell. A Churchill refrigeration unit similar to those used for the UNC and Hoek cells cools the methanol. Temperatures are monitored by copper/constantan thermocouples mounted adjacent to the specimen.

Silicon oil is used as the confining medium as this fluid has a low electrical conductivity and provides good thermal contact between the specimen and the cooling coils. The fluid may be pressurised during triaxial tests by regulating the compressed air pressure acting on an air/oil interface. A similar system is used for pressurising the hydraulic oil in the Bellofram cylinder but with the regulator valve driven by an electric motor controlled by the microcomputer.

Deformation of the specimen is monitored by a linear motion potentiometer (LMP) with the signals sent via an analogue to digital (A-D) convertor to the computer. The load cell output follows a similar path from the conditioning unit to the computer where software interprets the information and calculates any changes in load which may be necessary. Signals can then be sent by the computer to a digital to analogue (D-A) convertor and on to the motor to regulate the air supply.

The system will be referred to as the Low Pressure Computer Controlled (LPCC) apparatus in the following text. A new apparatus was designed to extend the confining pressure range from its 1 MPa limit on the LPCC upto 12 MPa, a pressure roughly equivalent to ground pressures at a depth of 600m. A correspondingly greater load capacity was required to provide deviator stresses in an acceptable range for testing frozen soils and rocks at these pressures.

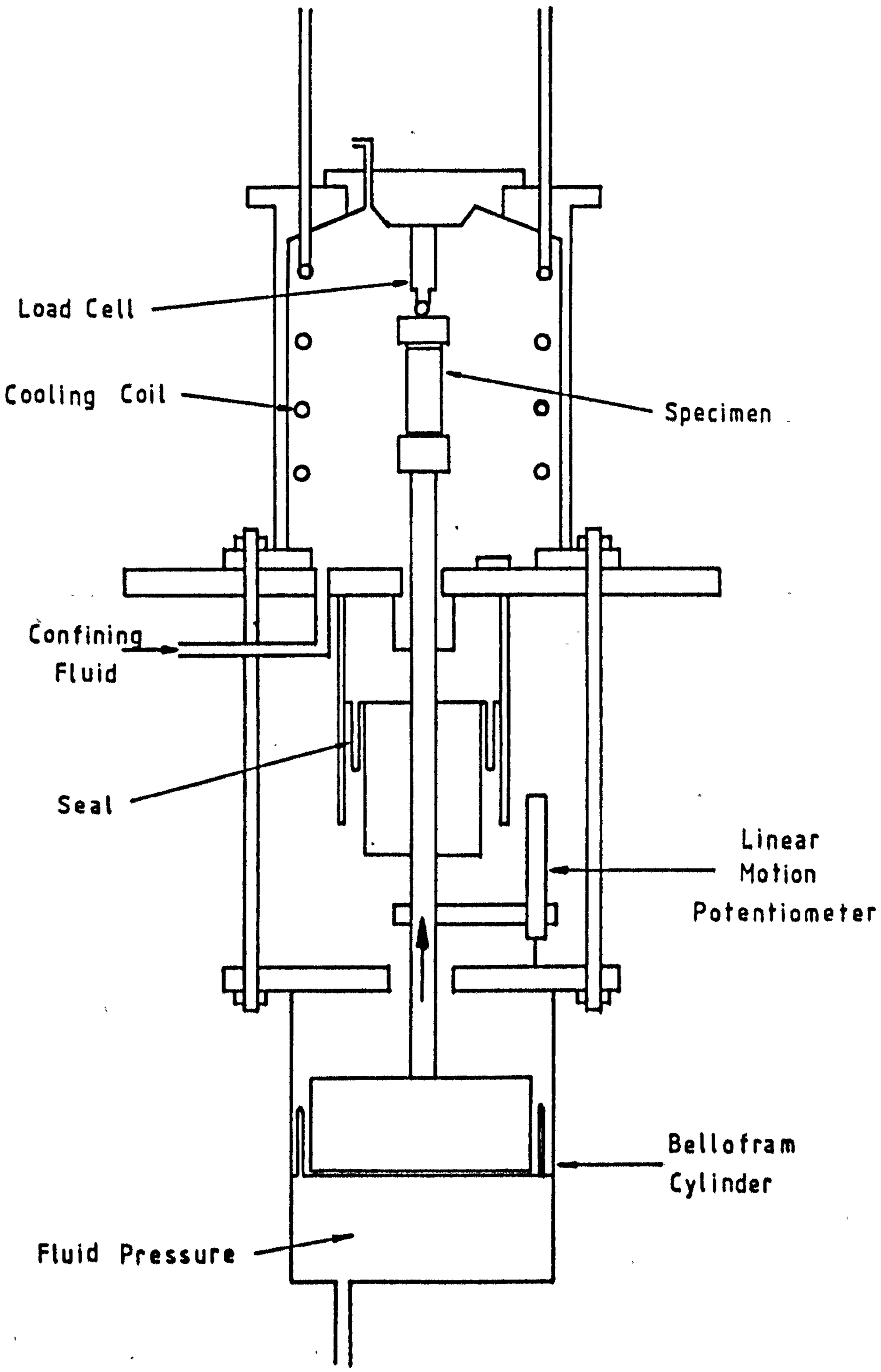

Fig. 4·4 Low pressure computer controlled triaxial cell

4.4.1 High Pressure Computer Controlled (HPCC) cell

The main body of the triaxial cell is a 150mm internal diameter cylinder of grade 316 austenitic stainless steel. This grade steel combines high strength, which increases with drop in temperature, and good corrosion resistance, to improve on the materials chosen for the LPCC cell. The wall thickness is 25mm and at each end of the cylinder the external diameter increases to 310mm to form flanges for the securing of end plates. The two end plates are secured by six 30mm diameter bolts and are a minimum of 50mm thick to minimise the bending of the plates when the cell is pressurised. A central hole through the top plate houses seals and bearings for a 40mm diameter stainless steel piston. The base plate is generally 100mm thick to allow room for the service ducts bringing fluids and electrical connections to the outside of the cell. Fig. 4.5 shows a section through the cell.

The interfaces between the flanges and the end plates are sealed against leakage of cell fluid using sealing rings of composite construction. A section through the seals is shown in Fig. 4.6a. At low pressures, the seal is effected by the spring within the 'v' section PTFE ring pushing outwards against the stainless steel faces. The PTFE ring is deformable and can shape itself to the contours of these faces. At higher pressures, the confining fluid improves the quality of the seal by acting on the inner surfaces of the PTFE and increasing the contact pressure.

The piston housing in the top plate incorporates both seals and bearings to prevent leakage of fluid along the sides of the piston. The exact arrangement is shown in Fig. 4.6b. PTFE stepseals bear on the piston and the seal is activated by compression of a rubber 'o' ring between the seal and its housing. One seal is sufficient to prevent leakage but a second is included as back-up. PTFE bearing rings ensure that the piston travels linearly through the top plate.

69

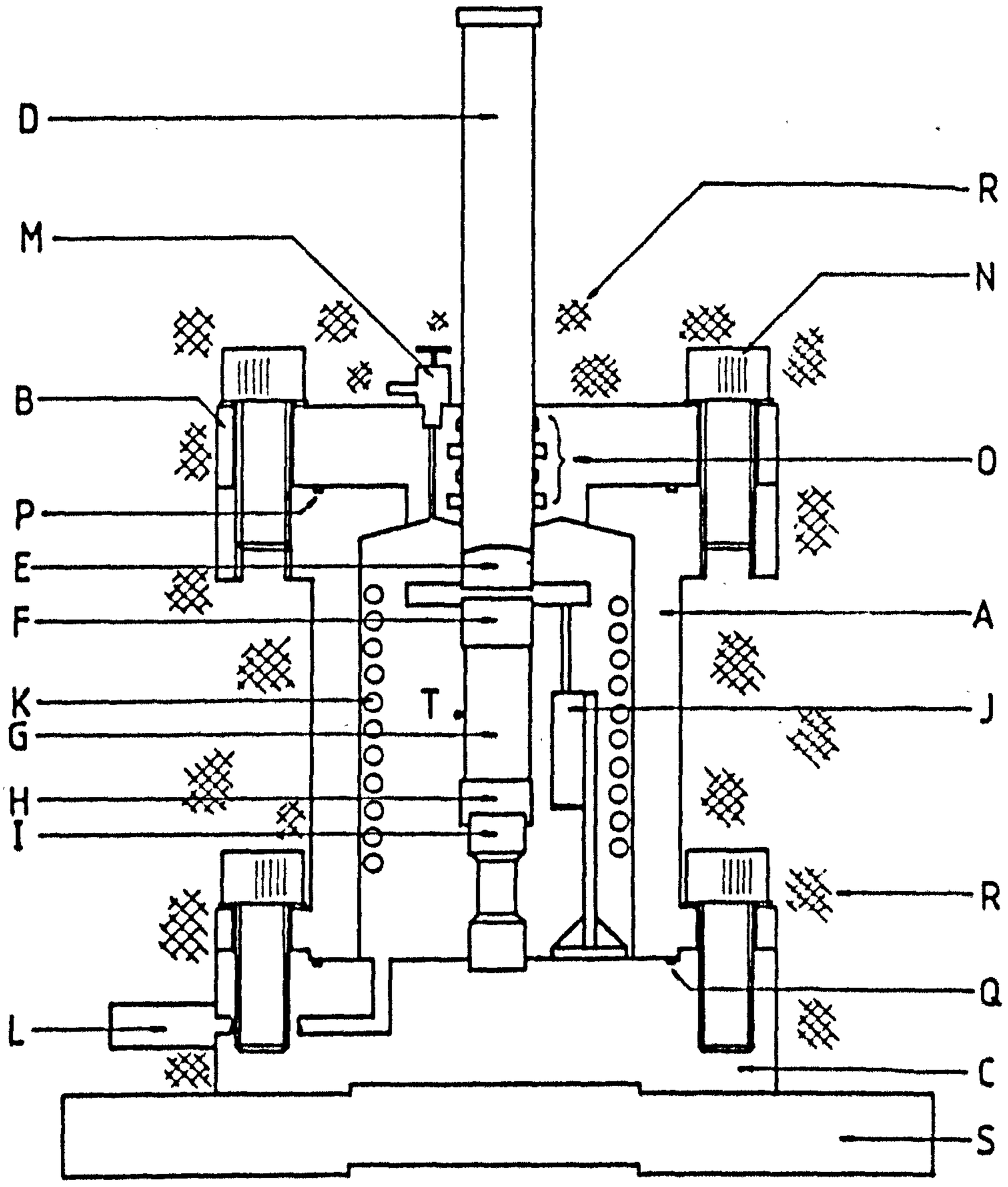

Fig. 4·5

High Pressure Triaxial Cell

A	MAIN BODY WALL	K	COOLING COIL
B	TOP PLATE	L	PRESSURE TRANSDUCER
C	BASE PLATE	M	AIR BLEED VALVE
D	LOADING PISTON	N	RETAINING BOLTS
E	SPHERICAL SEAT	O	PISTON SEALS AND BEARINGS
F	TOP PLATEN	P	TOP PLATE SEALS
G	SAMPLE	Q	BOTTOM PLATE SEAL
H	BOTTOM PLATEN	R	SHEET INSULATION
I	LOAD CELL	S	BASE PLATE INSULATION
J	LINEAR MOTION POTENTIOMETER	T	THERMOCOUPLE

4.4.2 Confining pressure system

Two major changes were needed to upgrade the confining pressure system of the LPCC cell to one suitable for higher pressures. Firstly, the compressed air line could not provide high enough pressures to act directly on an air/oil interface and secondly, the flexible Enots tubing had to be replaced by rigid 10mm internal diameter copper pipe. A two tier pressure system was built to allow the cell to operate at both high and low pressures. The low pressure system uses an air/oil interface whilst high pressures are obtained through a Unicub C multiplier pump as on the Hoek cell system. The pressure system is shown in Fig. 4.7. Non-return valves on the entry and exit of the pump ensure that the high pressures generated by the pump do not feed back into the low pressure system.

The pressure in the triaxial cell is maintained to a minimum level by the air regulators in each supply system. An upper limit is set separately by a manually adjustable relief valve mounted on the outlet side of the cell. The relief valve is made necessary by the decrease in volume and, hence, the increase in cell pressure as the piston enters the cell during a test. The cracking pressure of the valve is determined by the choice of spring and the precompression applied.

The cell pressure is measured by a Druck model PDCR 10 pressure transducer which is mounted on the outside of the base plate at the end of a fluid duct from the inside. The operating range for this device is 0 to 13.5 MPa and the electrical output is linear in the temperature range -20 to +80°C. The low pressure system also includes an air pressure gauge to monitor the pressure independently. Silicon oil is used to charge the pressure system with the normal test procedure being to fill the cell with precooled oil after placement of the specimen. When the top cap is in place, and the piston restrained from moving, the low pressure system is activated to expel any remaining air through the bleed valve.

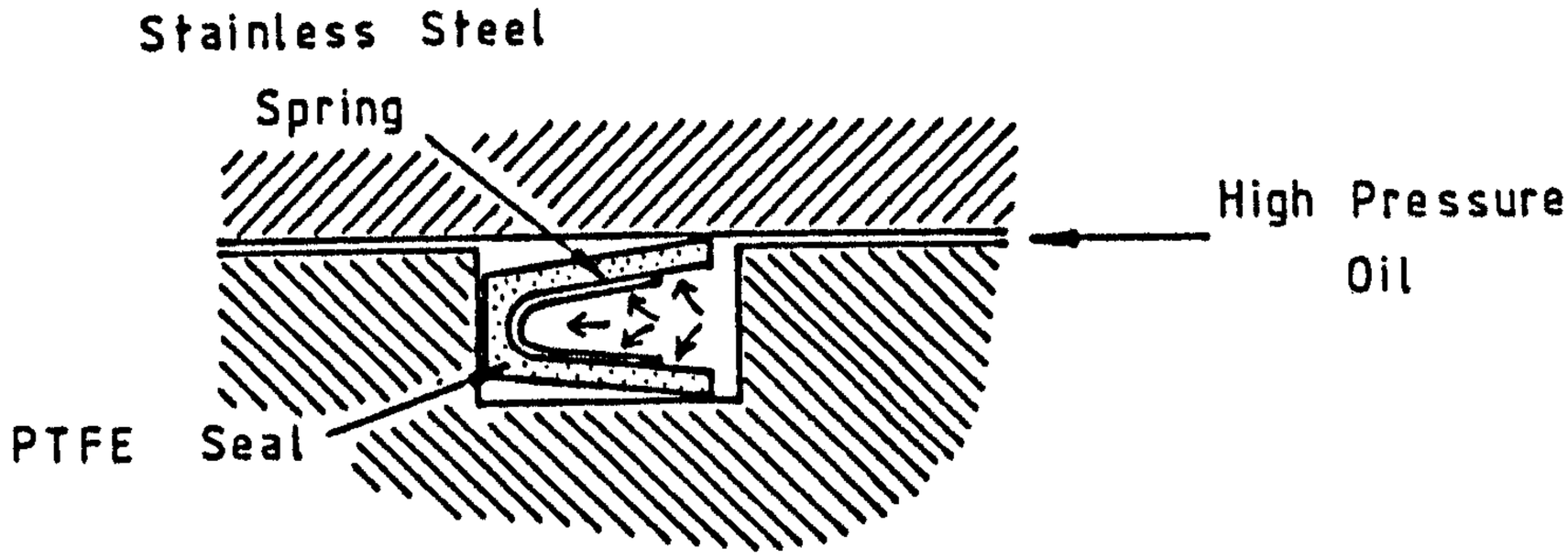

a) Top and bottom plate seals

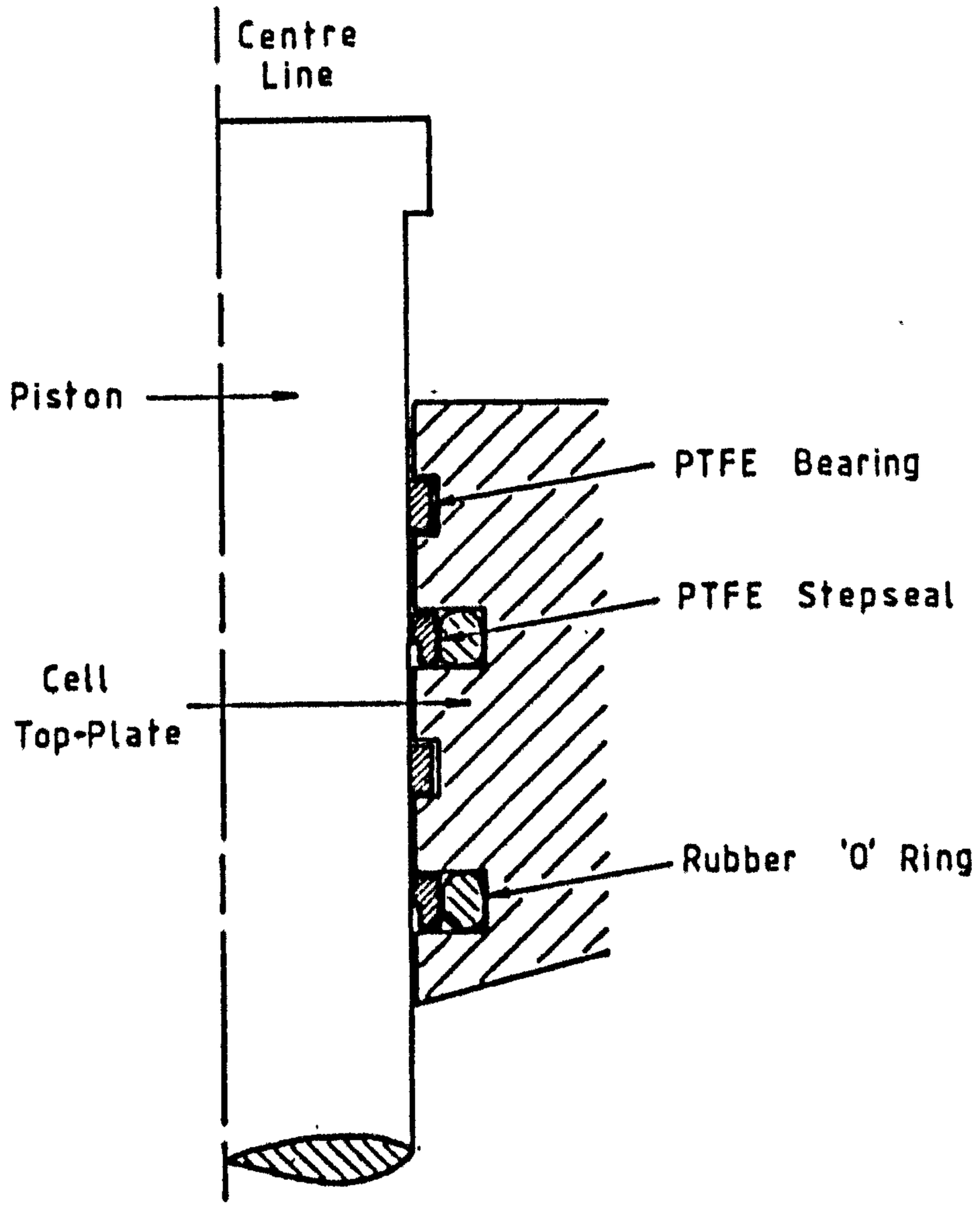

b) Piston seals and bearings

Fig. 4·6 Arrangement of seals in HPCC cell

4.4.3 Refrigeration

The method of refrigeration of the new cell is very similar to that described for the other computer controlled cell and the UNC and Hoek cells. The coil of copper pipe is situated inside the cell with Enots fittings forming a pressure tight connection to ducts through the base plate. Flexible pipes direct fluid to and from a Churchill refrigeration unit as described in section 4.3. A methanol solution is circulated in a circumferential manner from the bottom to the top of the coil and the high conductivity of both copper and silicon oil ensure good thermal contact between the refrigerant and the test specimen. Armaflex insulation around the cell and pipes ensure that temperatures down to -20°C can be achieved within close tolerances. The base plate is insulated from the test machine by a 50mm thick Tufnol plate. The fully insulated HPCC cell is shown in Plate 5.

4.4.4 Loading system

Unlike the existing cell with its dedicated bellofram loading cylinder, the new cell is essentially portable and can be used in conjunction with any loading press. At the time of design and manufacture, the only device of suitable load capacity available within the Civil Engineering Department was a top loading model 301 Farnell machine. The overall dimensions of the cell were limited to fit within the confines of this machine.

The Farnell model 301 is a 5 ton (50 kN) capacity machine which operates at constant deformation rates between 0.00033 and 4.064mm/min. The speed is selected on a manually operated gear box and a three phase contactor box stops and starts the drive motor. Additional electrical circuitry allows the on/off switch to be by-passed and the machine operated remotely by computer controlled relays. Other loading presses can be similarly adapted for computer control, allowing a range of loading methods to be employed and offering the opportunity to match the

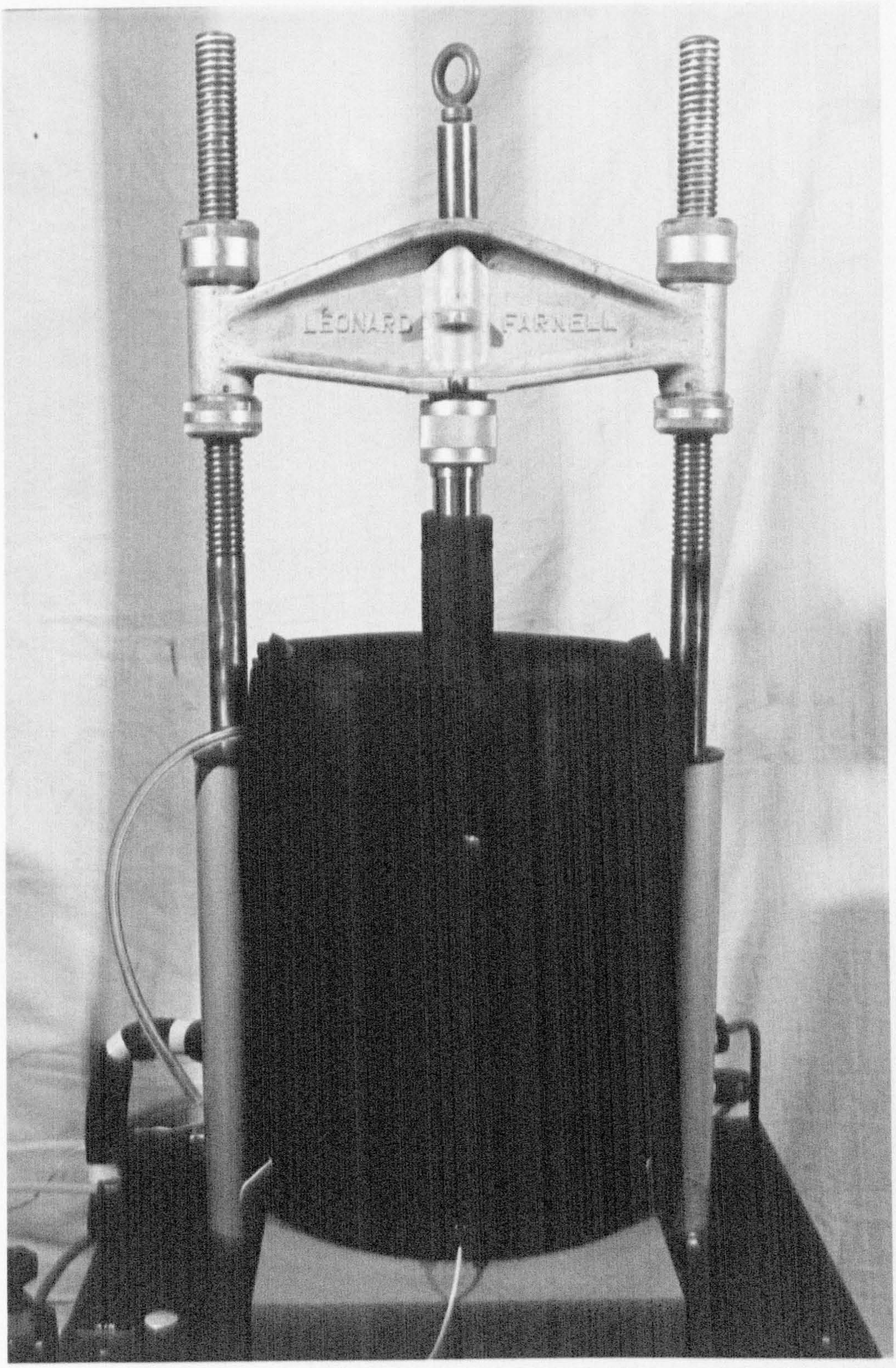

Plate 5 HPCC Triaxial Cell

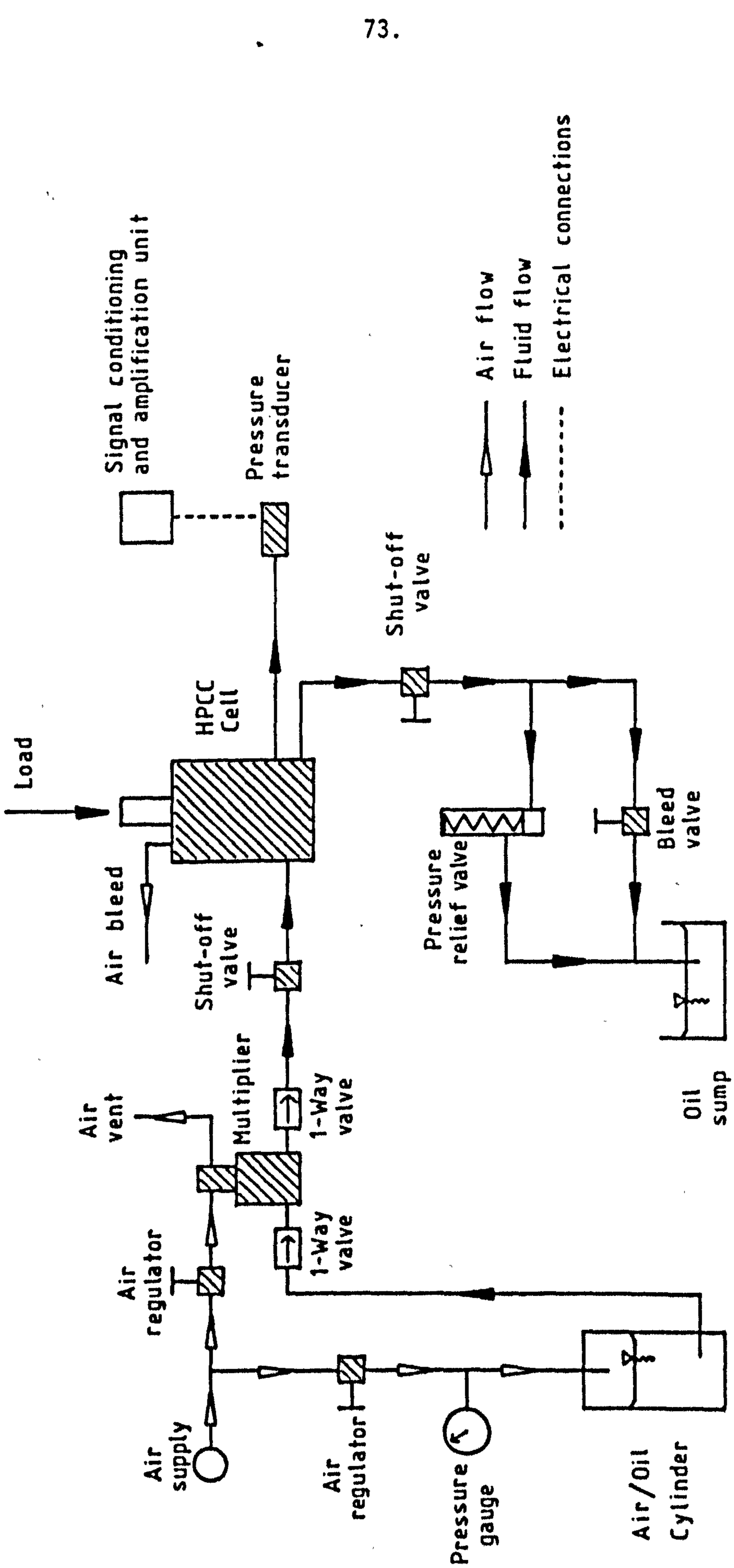

Fig. 4-7 Pressure system for the HPCC cell

strength of the material to a machine of suitable sensitivity.

4.4.5 Instrumentation

The cell has been designed to determine the strength and deformation properties of frozen soils in terms of total stress and strain. This is achieved through the use of instruments installed in the cell for measuring vertical load, confining pressure, vertical deformation and temperature. All four types of instrument supply electrical analogue outputs.

The load cell is designed to be easily removed from the cell so that the operating range and sensitivity of the installed device can be matched to the material being tested. The load cell used in the current suite of tests was designed for a capacity of 60 kN. It consists of a cylinder of grade 817M40 (EN24) steel with square faces milled and polished on the centre section to provide four flat surfaces for the attachment of strain gauges (Fig. 4.8, Plate 6). The gauges used are type FCL-6-350, with a nominal resistance of 350 ± 1.0 Ω, and they are bonded to the steel so that strain induced in the steel by load on the test specimen causes a change in electrical resistance. The cross-sectional area of the load cell is reduced by drilling a hole along the vertical axis such that a load of 60 kN induces 1000 microstrain in the gauges. The gauges are connected into a bridge circuit which, with a DC supply of 10V, gives an output of 20mV at 1000 microstrain. All the wires from this circuit are collected into a 6-pin DIN plug which matches a socket in the base plate of the cell.

The load cell is 30mm in diameter and stands 82mm high in a central recess in the base plate.

Specimen deformation in the triaxial cell is measured by a linear motion potentiometer (LMP) mounted on a support bracket. The LMP consists of a strip of resistive plastic supplied with 12 V DC and a wiper arm which taps off a voltage dependent on

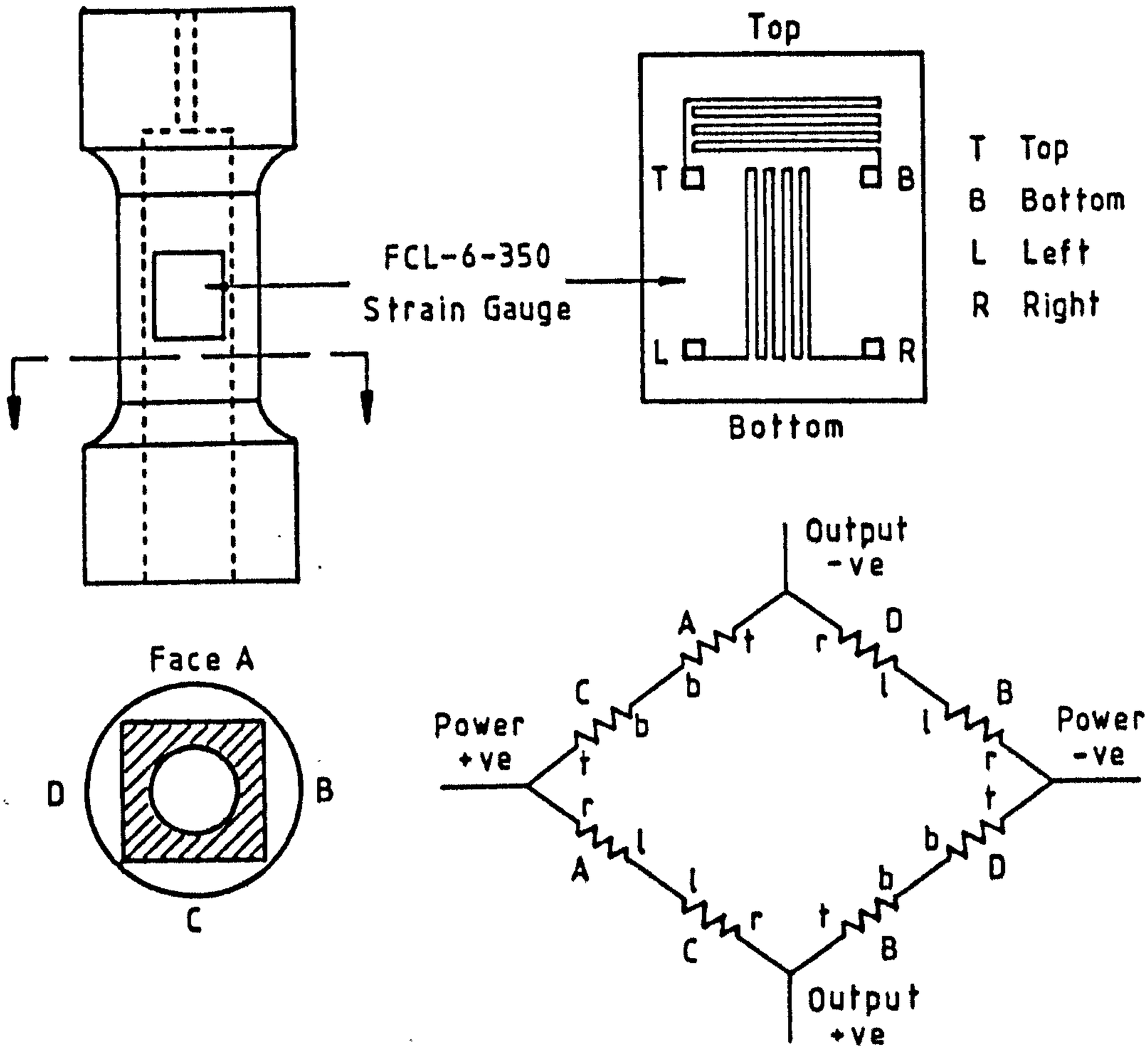

Fig. 4·8 HPCC cell load cell and wiring diagram

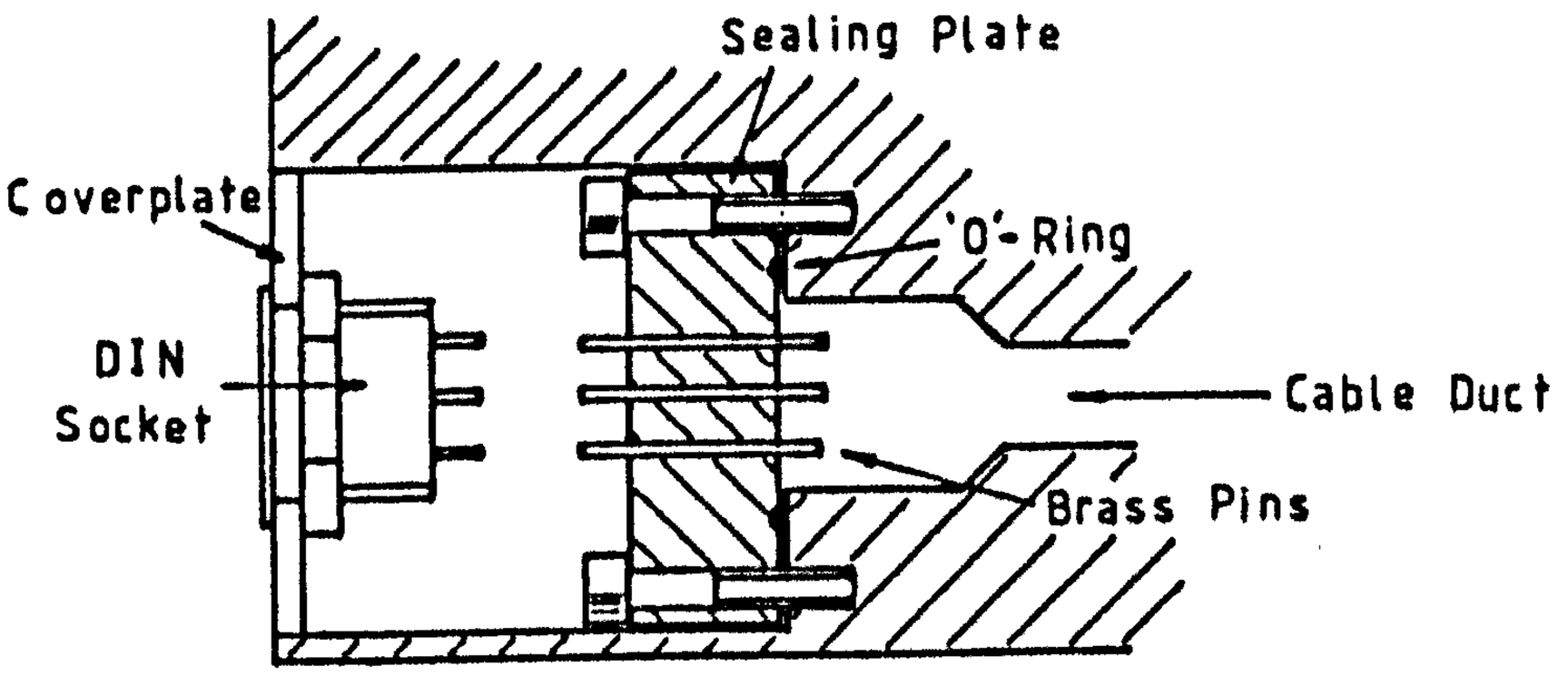

Fig. 4·9 Cable duct sealing plate in base of HPCC cell

the position of the push rod. The mounting bracket holds the LMP adjacent to the specimen so that the push rod bears on a plate held between the specimen top platen and the piston. The three wires from the LMP are collected into a DIN plug for location in a socket in the base plate. Although only one LMP was used in the completed test programme, provision has been made for the installation of a second assembly to allow measurements of tilt to be taken during a test. Restrictions on space within the cell have resulted in the LMPs being sited in loading positions such that during compression testing, the push rods enter the LMPs, and risk damage, should the limit of travel be exceeded. A failsafe device is incorporated in the control software to prevent this occurrence.

Test temperatures are measured by thermocouples which are secured to the outside of the specimen after it has been surrounded by a membrane and positioned in the cell. Copper/constantan thermocouples are used with the free ends of the wires collected into miniature thermocouple plugs which enter sockets set into the base plate.

The confining pressure transducer is described in section 4.4.2. The use of internal instrumentation introduces the problem of leakage of fluid through the cable ducts and along the electrical insulation. Attempts to seal the ducts by injection of silicon rubber were unsuccessful as the bond between the hardened rubber and stainless steel was unreliable. This led to the design of two alternative solutions.

The thermocouple sockets were held in place in the cell by a high strength Araldite cement and by ensuring that this cement also covered the electrical contacts at the back of each socket, an effective but permanent seal was made. For the LMP and load cell connections, which terminate in DIN sockets, a concealed sealing plate method was devised (Fig. 4.9). The sealing plate consists of a disc of Tufnol which houses a rubber 'o' ring. The 'o' ring is compressed against a recessed face of the base plate by clamping the Tufnol disc with six securing bolts. Through the

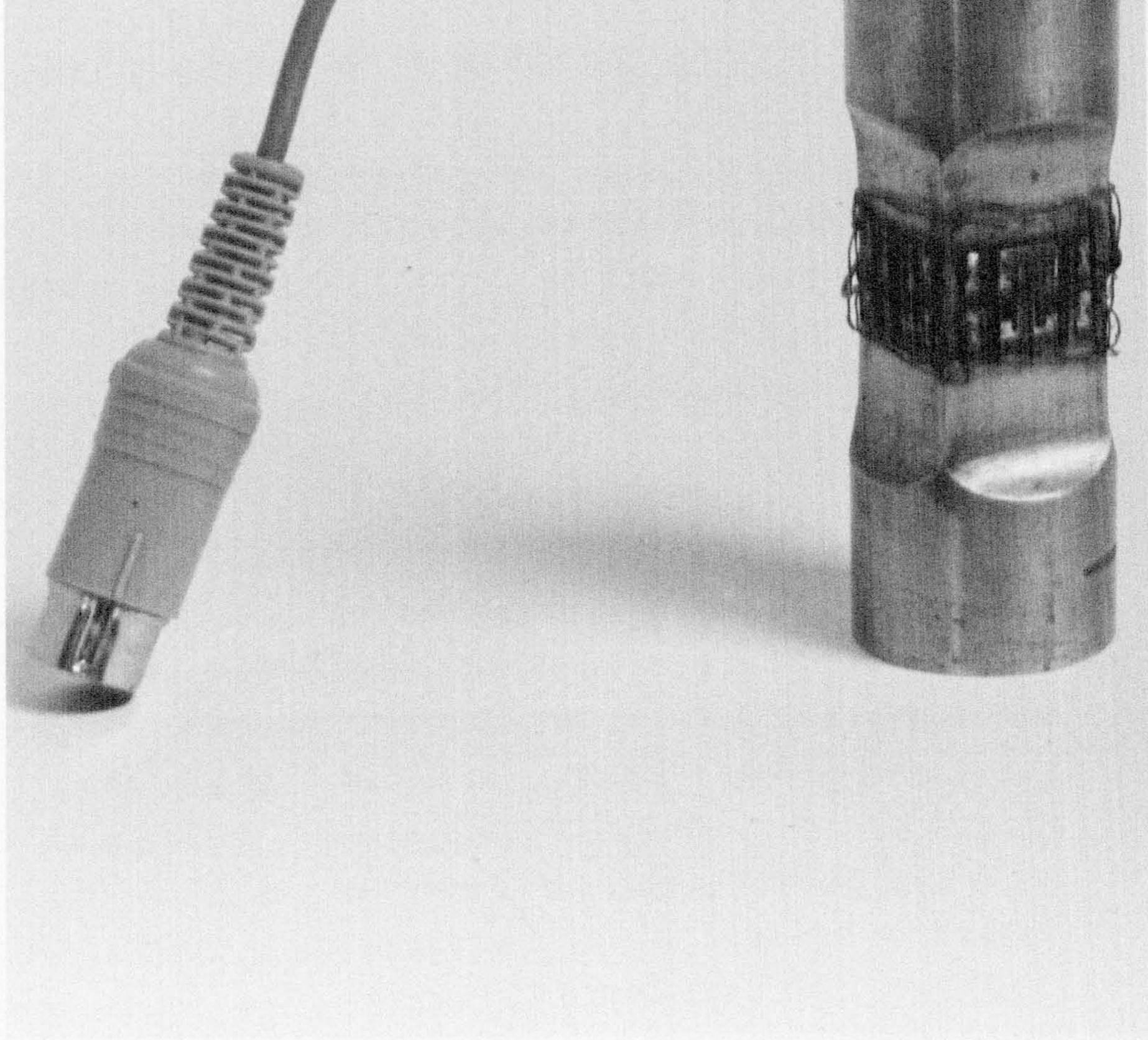

Plate 6 HPCC Cell Load Transducer

centre of each plate, a series of holes were drilled and tapped and then threaded brass pins were cemented in position with Araldite so that they protruded from each face. With wires soldered to each end of the pins, leakage of fluid was prevented through both the cable duct and along the electrical insulation. The DIN sockets on the outside of the base were attached to mounting plates which fit over the sealing plate recess. The sealing plate method could be adapted for use with thermocouples by replacing the brass pins with, in this case, copper and constantan.

Plate 7 shows all the instruments installed in the base plate. A specimen is shown in position on the load cell and is topped by the LMP bearing plate and spherical platen.

4.4.6 Monitoring and control of tests

Analogue outputs, from the instruments inside the triaxial cell, need to be converted into digital signals before being sent to the computer. The analogue to digital (A-D) conversion unit is included in a CIL model 6380 multifunction instrument which is linked to the computer by an IEEE-488 general purpose interface bus. The complete monitoring and control circuit is shown in block form in Fig. 4.10.

The instruments inside the triaxial cell all require a DC stabilised supply which is provided by a Farnell model FT 15/2 power unit. The output of this unit is adjustable in the range 12 to 15 volts and is currently set at the lower bound. The supply is connected directly to the LMP resistive strip and also to conditioning units for the load cell, pressure transducer and thermocouple signals. CIL model SGA 701 miniature strain gauge conditioning units reduce the supply voltage to the load cell and pressure transducer bridge circuits to the required 10 volts, then amplify the mV output signals to a level determined by an adjustable gain set potentiometer. The thermocouple signals are sent to CIL model TA 100 conditioning units, which

incorporate the warm junction of the couple, where amplification of the mV signal is again determined by a manually set potentiometer.

The amplified conditioning unit signals and those coming directly from the LMPs enter the A-D convertor on shielded co-axial cables terminating in bnc plugs. Eight input channels are available on the CIL 6380, each with a 16 bit resolution of the converted signal. Signals transmitted along the bus therefore range between -32767 and +32768 bits.

A sharp MZ-80B microcomputer with integral monitor and cassette deck is used to interpret the signals on the bus line, and software allows their conversion into recognisable units. A listing of the control programme used for creep testing in the new triaxial cell is given in appendix A.

The CIL 6380 instrument incorporates four relays and a four channel digital to analogue (D-A) convertor as well as the eight channel A-D. Two of the relay channels are used to control the Farnell machine which currently provides the load to the specimen (section 4.4.4). A microprocessor within the 6380 can operate the relay channels in response to changes in input to the A-D channels and use is made of this function in two ways. The first is a failsafe device which protects the LMPs from damage due to excessive specimen deformation by activating relay R0, which switches off the Farnell machine. The second use is to control the load on the specimen by activating relays R0 and R1 to switch the Farnell machine off and on in response to readings from the load cell. This comparator function is initially activated by the computer.

The MZ-80B is used to calculate the load required to maintain a constant stress as the specimen deforms and the 6380 comparators are periodically reset to compensate. The current status of the test can be displayed on the computer screen in a continually updated status table or as a graphical display of strain against time. At regular intervals, readings are sent to the MZ-80P4

Plate 7 Instrumentation on HPCC Cell Base

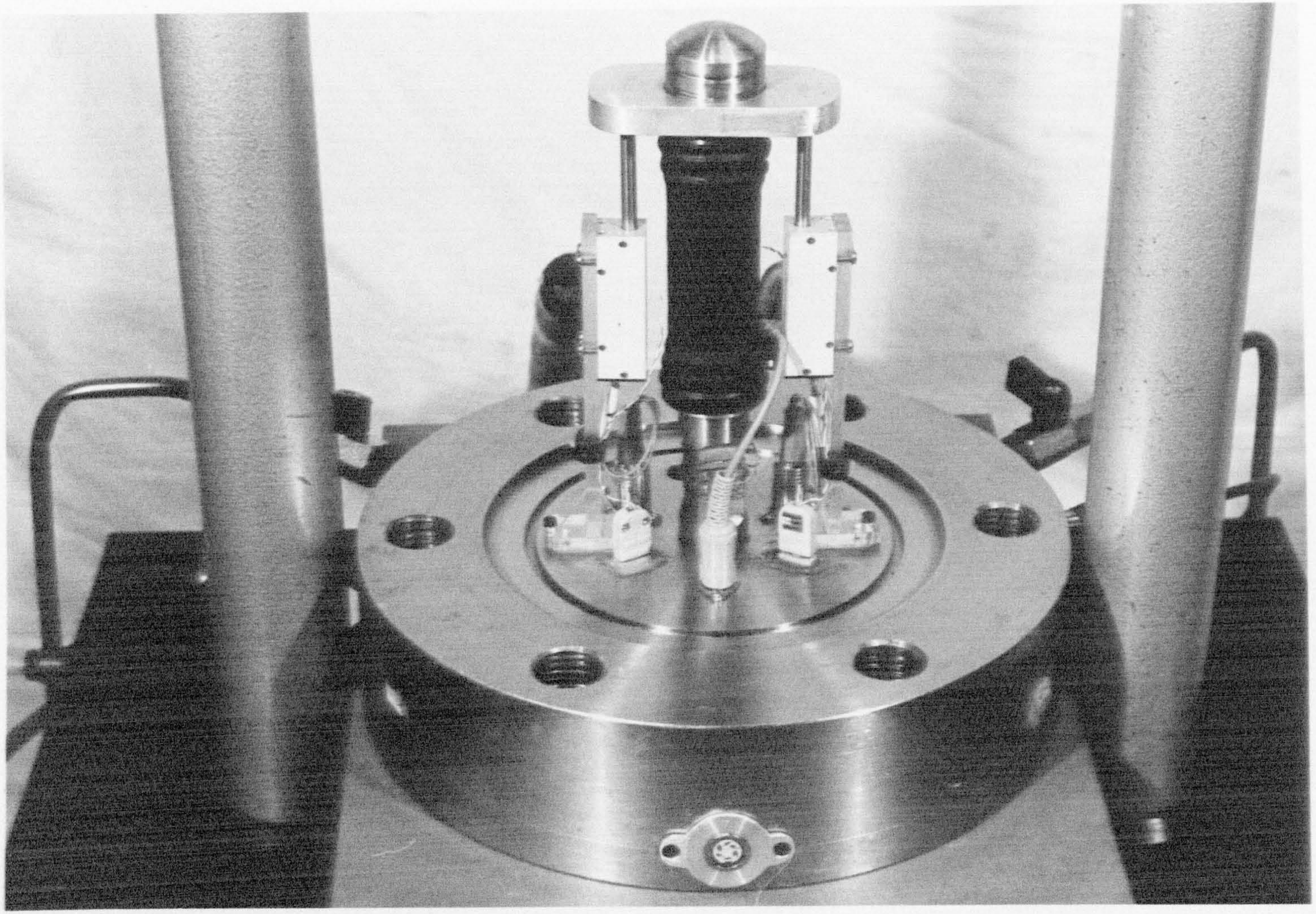

LC Load Cell
PT Pressure Transducer
T Thermocouple
LMP Linear Motion Potentiometer

440 v Mains
220 v Mains
Analogue Signals
Digital Signals

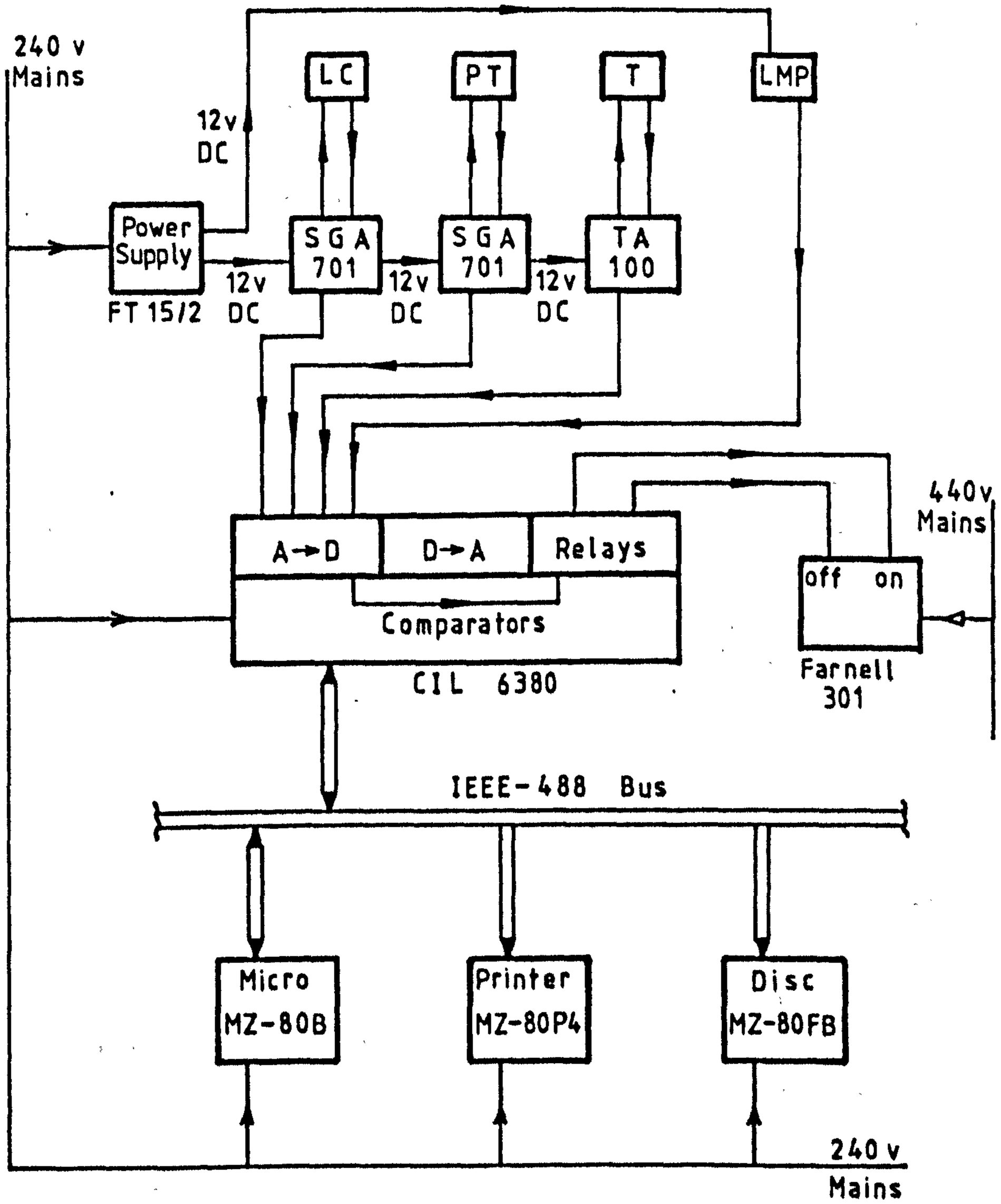

Fig 4·10 Monitoring and control circuits for HPCC cell

printer to provide a hard copy of the results, and it is also possible to record the data onto floppy discs using an MZ-80FB dual disc drive unit.

The main problems encountered during the development of this system were due to electrical noise on the data lines. The three-phase contactor on the Farnell machine was responsible for sending spikes down the relay lines and disrupting the electronics within the 6380. This noise was considerably reduced by the inclusion of contact arc suppressors across the relay terminals. The suppressors are rated at 200 to 250 volts AC with a maximum r.m.s. load current of 50A. The weakness now lies in the manual change gearbox of the Farnell machine which needs to be periodically altered at the start of each creep test. A more recent model with a load capacity of 100 kN and an electronic gearbox is now available within the Civil Engineering Department, and electronic circuitry is currently being installed to allow the computer to control the speed. The speed will be determined by the voltage output from the D-A channels of the 6380 unit.

4.5 Applicability to rocks, sands and clays

To prove the suitability of the short and long term strength facilities, a series of tests on a range of materials followed the equipment development. The UNC and Hoek cells were initially used to test 30mm diameter rock specimens at both -16°C and ambient temperature. The rocks are described in section 3.2 and their variability in composition was demonstrated by the range of peak stresses obtained. The cells were used to test at a deformation rate of 4mm/min and a stress rate of 1 MPa/s, with confining pressures upto 8 MPa kept to within the limits ± 4% by the hand pump and bleed valve.

Three different sands, B, LAF and LAL (section 3.2), have been used at various stages in the research programme. Tests on B sand in the LPCC cell have been reported by Gardner (1985) and

used to prove the apparatus during its development. LAF sand was introduced as the UNC and Hoek cells were developed and 38mm diameter specimens have been tested at -10°C in a constant deformation rate machine. Confining pressures in the Hoek cell reached 12 MPa. All the creep and strength tests in the new HPCC cell have involved LAF sand at -10°C with the creep tests proving the pressure system and seals upto 11.2 MPa.

Saturated LAF sand is significantly stronger than 21% saturated B sand at -10°C and the LAF creep test programme in the LPCC cell therefore extended its proven operating range. Saturated LAL sand further extended the range of applied deviator stresses to 7 MPa in LPCC cell creep tests after the UNC and Hoek cells had yielded short term strength characteristics. KM clay highlighted the difficulties of testing plastic materials in the Hoek cell where the large deformations before failure reduced efficiency. The failed frozen clay specimens could not be extruded through the aperture in the steel Hoek cell end plates and removal was effected only by melting the specimen with a jet of warm water. This raised the temperature of the whole cell and re-refrigeration was necessary before placement of a new specimen. The HPCC cell is better suited to testing these plastic materials.

4.6 Summary

In 1982, the frozen soil strength testing facility at Nottingham University consisted of a single self-contained low pressure computer controlled (LPCC) refrigerated triaxial cell. Testing of specimens had been limited to one soil (B) at confining pressures upto 1 MPa and with peak deviator stress reaching 8.7 MPa. Software was available for running constant strain rate, constant stress rate and constant stress creep tests.

The available apparatus has now been extended to four pieces of equipment, two cells for measuring short term strength and two versatile computer controlled cells. One of the short term

strength test cells is suitable for measuring unconfined compressive strength (UNC cell) and the other triaxial strength (Hoek cell). The pressure system for the Hoek cell is currently limited by the pressure transducer to 14 MPa. Both the UNC and Hoek cells are refrigerated by externally mounted copper coils through which is circulated a methanol refrigerant.

The second computer controlled cell (HPCC) has been designed and built to withstand confining pressures upto 12 MPa. Unlike the LPCC cell, this cell relies on an external device for applying the deviator stress and in this respect, is portable. The loading device can be chosen to suit the particular type of test to be executed. Many aspects of the design for the computer control system of the HPCC cell are similar to those for the LPCC cell, the main differences currently being the choice of computer and the devices through which it communicates with the analogue instruments. The HPCC cell uses a Sharp MZ-80B microcomputer and a CIL 6380 multifunction instrument which combines eight A-D channels, four D-A channels and four relays.

The suitability of the equipment to determine the mechanical properties of frozen ground materials has been demonstrated by the testing of triassic rocks, three types of sand and a clay. Table 4.1 summarises the limits to which each piece of equipment has been taken for the respective materials.

Table 4.1 Limits of application of the test cells to five frozen materials

		UNC	Hoek	LPCC	HPCC
Triassic Rocks	T σ_3 $\Delta\sigma$	+20, -16 N/A 143.7	+20, -16 10 106.9		
B Sand	T σ_3 $\Delta\sigma$			-5, -10 1.0 8.74	
LAF Sand	T σ_3 $\Delta\sigma$	-10 N/A 12.9	-10 12 21.7	-10 1.0 5.2	-10 11.2 6.9
LAL Sand	T σ_3 $\Delta\sigma$	-10 N/A 15.8	-10 10.3 28.9	-10 1.0 7	
KM Clay	T σ_3 $\Delta\sigma$	-10 N/A 4	-10 10 10.7	-10 1.0 3.2	

T - Temperature (°C) σ_3 - Confining Pressure (MPa)
$\Delta\sigma$ - Deviator stress (MPa)

CHAPTER 5

SHORT TERM STRENGTH

5.1 INTRODUCTION

In Chapter 2, two equations (2.1 and 2.2) are listed and their practical usage in ice wall design is described. These equations, based on the elastic and elasto-plastic response of a hollow cylinder to external stresses, require some knowledge of the mechanical behaviour of the materials involved. This is frequently provided by short term strength tests in the laboratory. Equations 2.1 and 2.2 require a value for the unconfined compressive strength, K, of the frozen soil, while more complicated formulae make use of the Mohr-Coulomb failure parameters c and ϕ when calculating ice wall thicknesses (Auld, 1985).

Short term strength tests involve the rapid application of stress to a specimen. This stress is normally applied along the vertical axis of an upright cylinder of the soil mounted in a triaxial test cell. Details of such cells, suitable for testing frozen materials, have been given in the previous chapter. Stress application can be controlled in a number of ways and this can affect the response of the test specimens. The most frequently used test involves deforming the specimen at a constant rate and monitoring the induced stress. Variations include constant strain rate, constant load rate and constant stress rate tests. In each case, it is the stress-strain response which is monitored. The shape of the stress-strain curve is dependent on the mode of failure of the specimen. Brittle failure is characterised by a peak stress being obtained at fairly low strain, while plastic failure allows the stress to continue to increase at a decreasing rate through to very high strains.

The stress measured during these tests is the total stress σ, which is distributed within the soil as a pore ice pressure u, and an effective stress σ'. The instantaneous response of the frozen soil on application of a stress is to increase the pore pressure. With time, this pressure may dissipate as a result of localised pressure melting of the ice. In this thesis, the

apparatus for measuring the pore pressure within the ice is not available and all analysis of results is necessarily made in terms of total stress.

The short term strength test has been widely used in the investigation of the mechanical properties of frozen soils. The results of these tests are well documented in the literature. The behaviour of a particular soil varies with both the specimen properties and with the test conditions imposed. Section 5.2 reviews the general behaviour of one such soil, Ottawa sand (a standard sand in the USA), and includes a summary table of the results published by various authors. This serves to highlight the difficulties incurred in comparative studies of results without the inclusion of a comprehensive reference test schedule.

The strength tests on triassic rocks are discussed in section 5.3. The results are used primarily to establish the gain of uniaxial strength on freezing of saturated rocks. As equipment limitations prevented the more slake susceptible rocks from being resaturated, the specimens obtained from these samples were tested in their unsaturated states. The results are used in an analysis of the effects of degree of saturation on uniaxial strength of both unfrozen and frozen rocks. A limited number of triaxial strength tests yield Mohr-Coulomb failure parameters.

The test programme for the three soils LAF, LAL and KM was devised to establish their creep characteristics at -10°C. As a preliminary to creep testing, short term strength tests establish an upper limit for possible creep stresses and results from these tests are analysed in section 5.4. Included in the strength test programme on LAF sand is an exploratory study into the use of non-destructive testing to identify defective specimens and predict frozen soil strengths. The system used measures the transmission time of an ultrasonic pulse through the specimen, and from the specimen dimensions this can be readily converted to a pulse velocity. A discussion of the non-destructive test results is included in section 5.5.

The chapter closes with a summary.

5.2 Strength of frozen soils

In unfrozen soils, the strength is dependent on cohesion and on friction and interlocking between particles. These three factors also have an effect on the behaviour of frozen soils but bonding of the particles by ice becomes dominant. Bonding is complicated by the presence of unfrozen water films around the particles, which restrict the number of interparticle contacts, and play an important role in the strength of low ice content soils.

The deformation process is dictated by pressure melting of the ice under the influence of hydrostatic and deviator stresses. Pressure melting develops from stress concentrations on the ice between soil particles, and deformation is a result of the flow of the water to regions of lower stress where it refreezes.

The strength attained by a frozen soil is a function of both internal and external constraints. Principal amongst these are temperature, density, ice content, degree of saturation, unfrozen water content, hydrostatic pressure and strain rate.

5.2.1 Effect of temperature

The temperature dependence of the strength of frozen soils is mainly due to the behaviour of the interparticle ice and the relative proportions of ice and unfrozen water. The behaviour of various materials over the temperature range 0 to -180°C was reported by Sayles (1966) and by Wolfe and Thieme (1964). A summary plot of their results is reproduced as Fig. 5.1. Over this temperature range, a largely non-linear relationship exists for unconfined compressive strength.

Attempts have been made (Alkire and Andersland 1973, Goughnour

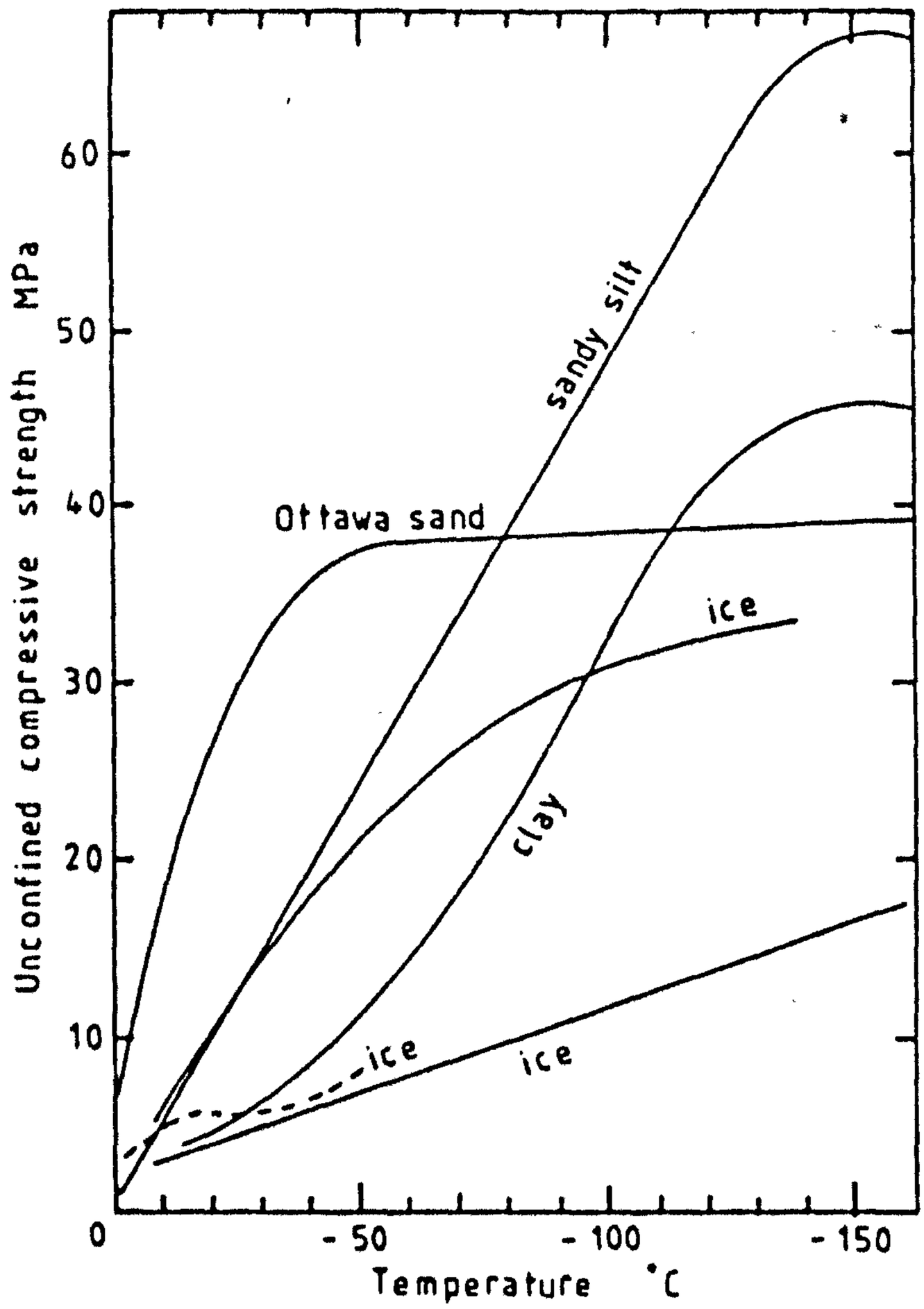

Fig. 5·1 Temperature dependence of unconfined compressive strength for several frozen soils and ice. (After Sayles, 1966)

and Andersland 1968) to explain this temperature dependence using the theory of rate processes proposed by Glasstone et al (1941). This theory is applicable to processes involving time and temperature dependent rearrangement of matter.

An expression of the form

$$\dot{\epsilon} = C\,\sigma^{n} \exp(-\Delta G/RT) \qquad 5.1$$

was proposed for frozen soils where ΔG is the activation energy, R the gas constant, T the absolute temperature and σ the applied stress. Parameswaran (1980) showed that the activation energy, ΔG, in this equation was not constant for Ottawa sand but varied with both stress and temperature.

Equation 5.1 breaks down for ice above -10°C when the deformation process is governed by grain boundary flow (Glen 1955). Parameswaran suggests that stress concentrations between particles in frozen soils could extend this effect to lower temperatures and account for the behaviour of frozen Ottawa sand.

An alternative relationship, proposed by Tsytovich (1975) and supported by Parameswaran, takes the form of a power law

$$\sigma \propto \Theta^{s} \qquad 5.2$$

where Θ is the temperature below freezing in degrees celsius and the constant s was attributed the value 0.5 by Tsytovich and 0.44 by Parameswaran.

5.2.2 Effect of density and ice content

The failure mechanism in frozen soils is greatly affected by the

relative proportions of soil and ice. At high ice content levels, the frozen material relies on the cohesive nature of the ice for its strength but as the proportion of soil particles increases, both friction and dilatancy begin to contribute. Dilatancy acts against both the cohesion of the ice matrix and the adhesion between sand grains and ice, creating an effect analogous to higher effective stresses. The mobilization of frictional resistance is a direct result of the increased number and greater magnitude of contact stresses between soil particles. Goughnour and Andersland (1968) found that a 42% volume of Ottawa sand was the minimum needed for the contributions of frictional resistance and dilatancy to affect the frozen shear strength.

For frozen sands and silts, an optimum ice content exists at which a maximum peak stress is found. Kaplar (1971) showed this to be at an ice:soil volume ratio of 0.58 for Manchester fine sand. At this ratio, the best possible combinations of the simultaneous effects of ice cohesion, intergranular friction and dilatancy occur.

Alkire and Andersland (1973) show that the initial deformation of Ottawa sand samples is dominated by the cohesion of the ice maxtrix. Frictional effects only become significant in the later stages of the deformation process. This work hardening nature of deformation has been observed by Parameswaran and Roy (1982). Small changes in the density of specimens has an effect on both the initial tangent modulus and the cohesive and frictional components of strength, combining to lead to an increase of failure strain with lower specimen densities.

5.2.3 Effect of degree of saturation

The degree of ice saturation is defined as the ratio of ice volume to void volume and it affects the strength of a frozen soil specimen by affecting the cohesion of the ice matrix. A reduction in ice saturation is accompanied by a decrease in

strength of frozen sand (Alkire and Andersland, 1973). The decrease in strength is in proportion to the volume of ice in the sand voids.

Data produced by Alkire (1973) also showed a decrease in Young's modulus to accompany a decrease in ice saturation. This behaviour supports the observations of Alkire and Andersland (1973) on the predominant influence of the ice matrix on initial response to load (section 5.2.2).

5.2.4 Effect of unfrozen water content

Unfrozen water is generally bound to soil particles in layers a few molecules thick. The quantity of unfrozen water is therefore related to the total surface area of soil particles within a specimen, and at a given temperature, fine grained soils, such as clays, will have higher unfrozen water contents than coarser sands and silts. This accounts for many of the differences in behaviour of these materials.

Coarse grained sands generally fail in a brittle manner at low strains whilst clay soils, with their higher unfrozen water contents, undergo large plastic deformations. Alnouri (1969) reports 12% strain at failure in frozen Sault Ste. Marie clay while Ottawa sand will typically fail at close to 2% strain.

Unlike frozen sands, where the soil particles tend to contribute to the strength by adding a frictional component to the cohesion of the ice, frozen silts and clays may be weaker than the pure ice at temperatures close to 0°C. This is directly attributable to the high unfrozen water content in these soils (Tsytovich 1975).

5.2.5 Effect of hydrostatic pressure and strain rate

Hydrostatic pressure on a frozen soil tends to suppress failure

mechanisms and this often shows itself in the form of greater strains at failure. The failure mechanism becomes more plastic and at high confining pressures, dilatancy may be both suppressed and reversed due to fracture of sand grains. These effects are similar to those of unfrozen soils.

The effect of a confining pressure on the strength envelope for ice saturated soil is related to both the density of the specimens and the strain rate applied. At low strain rates, the behaviour is analogous to that of unfrozen water-saturated soil in a drained test. At high strain rates and as long as the ice matrix does not fail, behaviour becomes analogous to that of an unfrozen undrained test.

In frozen sands at low strain rates frictional resistance is dominant and the frozen angle of frictional resistance may be only a few degrees less than the unfrozen (Sayles 1973, Andersland and Alnouri 1970, Neuber and Walters 1970, Alkire and Andersland 1973, Chamberlain et al 1972). However, for frozen clays, the effects of hydrostatic pressure on strength are usually very low due to the presence of unfrozen water and the lack of friction and particle interlocking.

Very high hydrostatic pressure may lead to pressure melting of the ice matrix and an increase in unfrozen water content. Chamberlain et al (1972) observed this for both sand and silt and above a confining pressure of about 34.5 MPa, pressure melting contributed to a decrease in frozen strength.

5.2.6 Summary with reference to a medium sand

The strength obtained for a particular frozen soil is dependent on material, specimen and test conditions. In Table 5.1, the strength results obtained for Ottawa sand, a medium sand used in the USA, are presented against the conditions adopted by each investigator.

Author / Source	Grading Curve	Particle Size Range	Specific Gravity	Maximum Dry Density	Optimum Moisture Content	Dry Density	Moisture Content	Degree of Saturation	Porosity	Height / Diameter	Temperature	Strain Rate	Confining Pressure	Maximum Deviator Stress	Strain at Peak Stress	Young's Modulus	Shear Angle	Apparent Cohesion
		mm	G_s Mgm^{-3}	MDD Mgm^{-3}	OMC %	ρ_{d_3} Mgm^{-3}	w %	S_r %	n %	H/D mm	θ °C	$\dot{\varepsilon}$ s^{-1}	σ_3 MPa	$\Delta\sigma_{max}$ MPa	ε_f %	E MPa	ϕ °	c MPa
1 Parameswaran 1980	✓	0.16 0.6	-	1.70	14	-	20	100	-	127 /50.8	- 2 - 6 -10 -15	$1.0\ 10^{-7}$ to $1.0\ 10^{-2}$	0	6 -12.5 10 -20 11.5 -25 12 -29	4	520 to 4800	-	-
2 Sayles 1966		0.2 0.6	-	-	-	-	-	100	-	-	-40 to -186	$5.5\ 10^{-4}$	0	38.6 35.9	-	-	-	-
3 Sayles & Epanchin 1966		0.2 0.6	-	-	-	-	-	100	-	-	- 3 -6.5 -10 -30	$3.33\ 10^{-4}$ to $2.5\ 10^{-2}$	0	10.35-15.86 13.79-20.69 17.93-27.58 28.96-48.27	-	-	-	-
4 Sayles 1968	×	0.2 0.6	-	-	-	-	-	100	-	-	-9.4 -3.9 -1.7 -.56	$5.5\ 10^{-4}$	0	17.44 10.10 9.10 5.14	-	-	-	-
5 Goughnour & Andersland 1968	×	0.2 0.6	2.65	-	-	0.64 & 1.64	-	100	76 & 38	57.4/28.7	-3.9 -12 -7.6	$2.2\ 10^{-6}$ to $4.4\ 10^{-6}$	0 to 0.7	5.38 to 9.38	3 to 4	690 to 17000	-	-
6 Chamberlain, Groves & Perham 1972	✓	0.074 0.149	2.63	-	-	1.65	21	100	38	-	-10	$8.7\ 10^{-4}$ to $1.0\ 10^{-3}$	3.45 to 276	21 -28	-	-	19.3 6.91 (σ_3=0-5)	
7 Parameswaran & Jones 1979		-	-	-	-	-	-	100	-	-	-12	$1.0\ 10^{-5}$ to $1.0\ 10^{-2}$	5	16 -28	-	-	-	-
8 Parameswaran & Roy 1982	×	0.16 0.6	-	1.70	14	-	20	100	-	115 /51	-30	$5.0\ 10^{-7}$ to $1.0\ 10^{-2}$	0	15 -42	3.9 to 4.4	2300 to 5577	-	-
9 Alkire & Andersland 1973	×	0.59 0.84	-	-	-	-	-	97 55	-	57.4/28.7	-12	$2.66\ 10^{-3}$	0 to 6.9	11 -19 5 -17	-	-	31.4 2.9 31.4 1.5	
10 Andersland & Alnouri 1970	×	0.6 0.85	2.65	-	-	1.72	19	99	36	57.4/28.7	-12	$5.0\ 10^{-5}$	0.2 to 0.62	10.3	2	-	25.1 2.9	
11 Sayles 1973 & 1974	×	0.6 0.85	2.65	-	-	1.67	21	100	37	153 /70	-3.9	$5.0\ 10^{-4}$	0.34 to 8.2	8 -23	-	-	31 2.0 σ_3=2.6-7	

TABLE 5.1 THE STRENGTH PROPERTIES OF OTTAWA SAND UNDER VARYING MATERIAL , SAMPLE AND TEST CONDITIONS

cont.....

Author / Source	Grading Curve	Particle Size Range	Specific Gravity	Maximum Dry Density	Optimum Moisture Content	Dry Density	Moisture Content	Degree of Saturation	Porosity	Height / Diameter	Temperature	Strain Rate	Confining Pressure	Maximum Deviator Stress	Strain at Peak Stress	Young's Modulus	Shear Angle	Apparent Cohesion
		mm	G_s Mgm^{-3}	MDD Mgm^{-3}	OMC %	ρ_d Mgm^{-3}	w %	S_r %	n %	H/D mm	θ °C	$\dot{\varepsilon}$ s^{-1}	σ_3 MPa	$\Delta\sigma_{max}$ MPa	ε_f %	E MPa	ϕ °	c MPa
12 Parameswaran & Jones 1981	×	0.2 0.6	-	1.70	14	-	20	100	-	108 /50.8	-10	$7.7\ 10^{-5}$	0.1 to 75	17-35-26	4 to 8	1250 to 2000	12.7 σ_3=0-17	7.4
13 Baker 1978	×	-	-	-	14	1.68	19	100	37	150 /75	-5.5	$1.0\ 10^{-7}$ to $1.0\ 10^{-2}$	0	5 -20	0.8 to 9	-	-	-
14 Baker,Jones & Parameswaran 1982	×	0.16 0.6	-	1.70	14	1.67	19 to 20	100	32 to 41	100 /50 & 150 /75	-2 to -15	$1.0\ 10^{-7}$ to $1.0\ 10^{-2}$	0 to 76	8 -15	3.5 to 5	-	-	-
15 Jones & Parameswaran 1983	×	0.2 0.6	-	-	-	-	-	100	37 to 96	108 /51	-11	$7.7\ 10^{-5}$	0.1 to 85	4-13- 5	1 to 3	-	-	-
16 Simonsen,Jones & Green 1974	×	-	-	-	-	1.91 bulk	-	100	46	-	-10	$1.0\ 10^{-4}$ to $1.0\ 10^{0}$	0 to 200	10 -16	2	100 to 4000	-	-

TABLE 5.1 THE STRENGTH PROPERTIES OF OTTAWA SAND UNDER VARYING MATERIAL , SAMPLE AND TEST CONDITIONS

The table divides into four main sections which detail the material properties, the specimen properties, the test conditions and the strength parameters obtained. Comparisons of work from various research centres becomes difficult when so many variables are involved, as the effects generated by variations in one property, may be masked by those of another. This highlights the need for the inclusion of reference tests in a test programme and the ISGF working group on testing methods for frozen soils (Baker et al 1983) has produced guidelines for this purpose. The main points referring to strength of frozen soils are as follows:

1) The soil description should include a grading curve, total density, moisture content and Atterberg limits, where applicable.
2) The aspect ratio of test specimens should be 2:1 or greater.
3) Uniaxial strength tests at 1% per minute constant strain rate should be included.
4) Tests at temperatures of -2°C and -10°C should be included.

5.3 Strength tests on triassic rocks

The tests on samples of triassic rock formed part of a commercial testing schedule to investigate the triaxial strength gain on freezing. Each sample was received as a number of AX sized specimens (30mm diameter, 60mm high) of variable quality. The use of the saturation apparatus described in Chapter 4 was limited by susceptibility to slaking to nine (all sandstones) of the twenty two samples available. The subsequent development of an improved apparatus for saturating and freezing specimens under the influence of a confining pressure, is reported by Marchina (1984).

5.3.1 Saturated rocks

The results obtained from these tests are affected by the

variability of the rock structure within the small specimens. Individual test results are included in Appendix B, and in Table 5.2, mean values of the unconfined compressive strengths for both unfrozen and frozen specimens, are presented.

The strength gain on freezing is largely due to the increase in cohesion afforded by the ice matrix. Excluding the result for sandstone 107, where sufficient material was available for just one test at each temperature, the average strength gain ratio on freezing is 2.64. In unfrozen rocks, the water acts as a lubricant between the solid grains, but, on freezing to ice, becomes a bonding agent. Fig. 5.2 shows both unfrozen and frozen triaxial data for three of the sandstone samples with sandstones 90 and 118 clearly demonstrating the gain in strength to be almost entirely due to increased cohesion. The friction angles for these two samples remain almost constant with change of temperature. The unfrozen data for sample 105, at a confining pressure of 7.3 MPa, is unaccountably low.

5.3.2 Unsaturated rocks

The rock samples not included in Table 5.2 were all tested in an unsaturated condition as received from the client. Although the individual AX sized specimens were sealed in plastic, the moisture contents measured after testing indicated that considerable moisture loss had occurred during the coring and end preparation procedures. In the extreme case, mudstone 114 had degrees of saturation estimated to be as low as 3%.

The effect of increased degree of saturation on unfrozen rocks is to decrease the strength, as the lubricating nature of the pore water acts against the frictional component. The strength asymptotically approaches that of the fully saturated condition (Fig. 5.3). In the frozen state, the strength of dry rocks may be slightly greater than that unfrozen but, after initially following the same trend, the strength increases to a maximum in the fully saturated condition (Mellor, 1973). The initial

Table 5.2 Mean values of unfrozen and frozen strengths of saturated rocks tested in uniaxial compression

Rock Sample		Unfrozen			Frozen			Strength Gain Ratio
No.	Material †	No. of tests	mean UCS	S.D. *	No. of tests	mean UCS	S.D. *	
82	Sa	4	22.45	3.43	4	27.7	2.31	1.23
83	Sa	4	21.5	3.06	4	34.55	2.69	1.61
90	Sa	3	13.7	1.35	3	36.33	2.09	2.65
98	Sa	3	20.97	2.21	4	32.1	2.70	1.53
105	Sa	3	3.27	1.21	3	15.9	1.82	4.86
107	Sa	1	3.7	-	1	24.3	-	6.57
111	Sa	4	9.68	1.86	4	35.6	1.80	3.68
115	Sa	4	12.7	1.71	4	34.5	2.81	2.72
118	Sa	3	12.23	1.40	3	34.37	1.70	2.81

† Sa = Sandstone

* S.D. = Standard Deviation

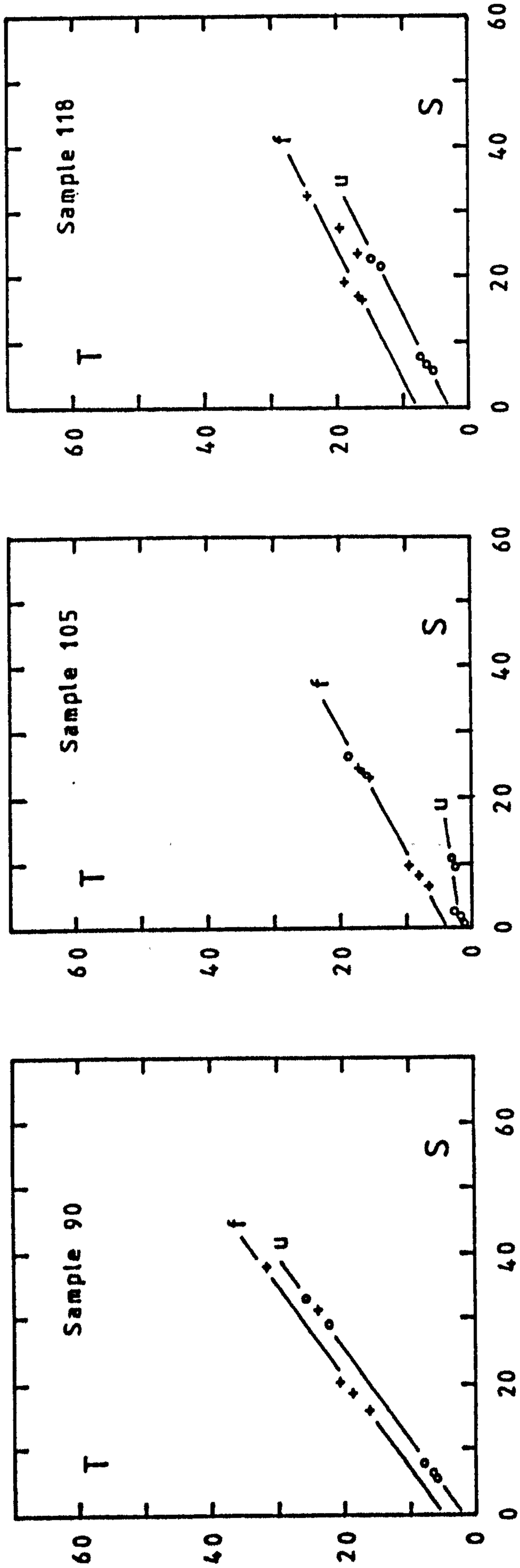

Fig. 5.2 Comparisons between unfrozen (u) and frozen (f) strength for three sandstones triaxial

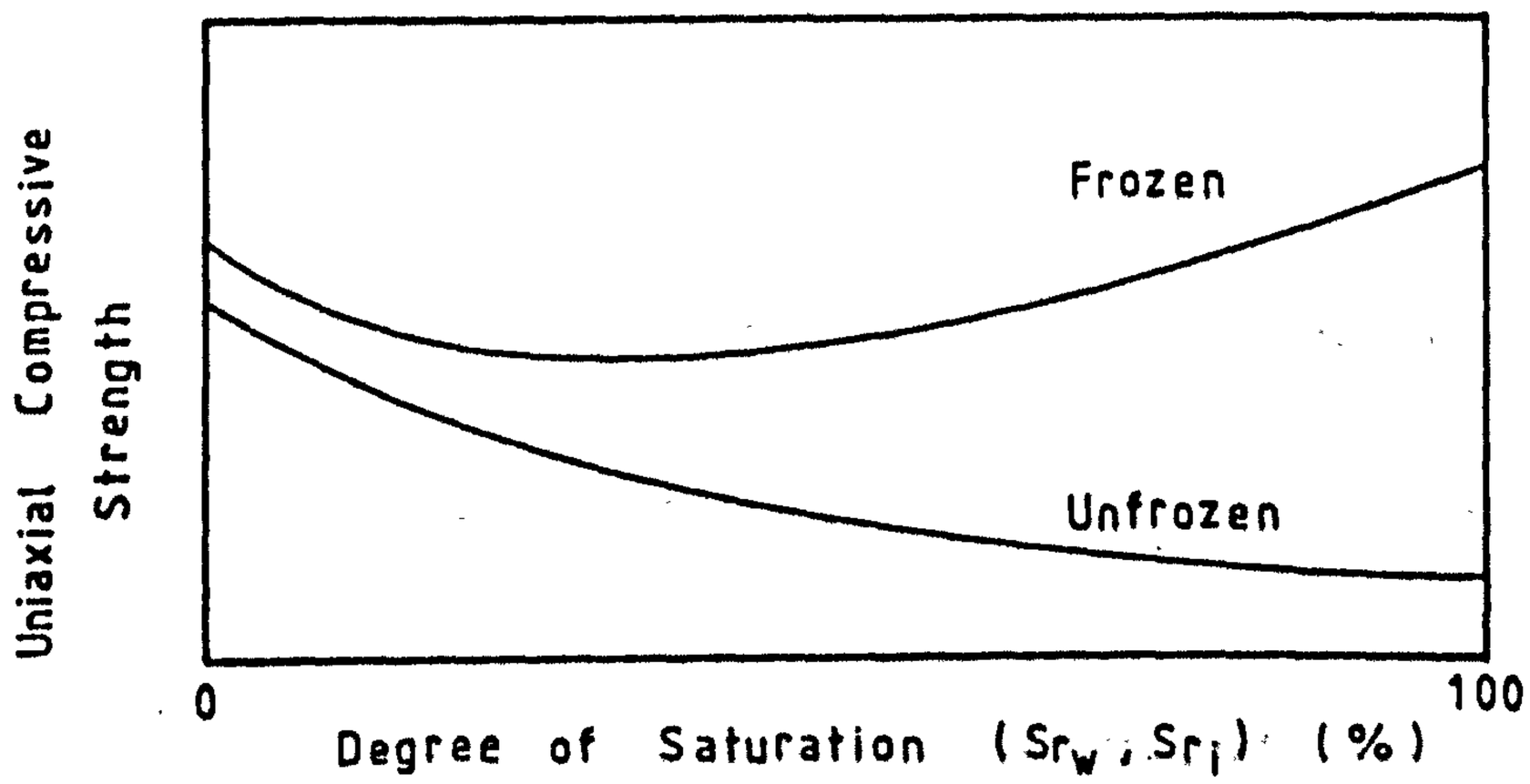

Fig. 5·3 Idealised variation of uniaxial compressive strength with degree of saturation in unfrozen and frozen rocks.

decrease is due to the presence of unfrozen bound water surrounding the rock grains and acting against the frictional strength component. At higher saturations, the ice matrix cohesion is dominant.

For the tests reported here, the range of degrees of saturation are too small and the variations in properties of specimens within each sample, too great to observe a distinct relationship in most cases. Siltstone sample 77 covering the range 69% to 100% saturated for both unfrozen and frozen specimens, shows some support of the theory and is included with the other results in Fig. 5.4.

5.4 Strength tests on frozen soils

The short term strength testing programme was devised to establish the stress limits during the subsequent creep tests. Instantaneous loading to failure could not be readily applied and an arbitrary constant deformation rate of 1mm/min was used as an alternative. The failure of LAL sand was taken as the peak stress reached during the test and was well defined. The plastic nature of the failure of frozen LAF and KM required that a nominal failure strain limit was imposed as no distinct peak was reached. For KM, the limit was set at 20% strain, which is accepted practice in unfrozen soil mechanics, but the excessive lateral deformation produced at this limit made the Hoek cell difficult to use. LAF sand showed similar behaviour through to 20% strain and to increase the efficiency of the facility, tests were terminated after 15% strain had been reached. A table showing the strength test results at -10°C for the three soils LAF, LAL and KM is presented in Appendix B.

A triaxial test programme was devised to investigate the soil strengths upto 12 MPa. The K_f failure lines at -10°C are shown in Fig. 5.5 for all three soils. Table 5.3 summarises the slopes, α, and intercepts, a, for each line and also lists the corresponding Mohr-Coulomb failure parameters ϕ and c. At a

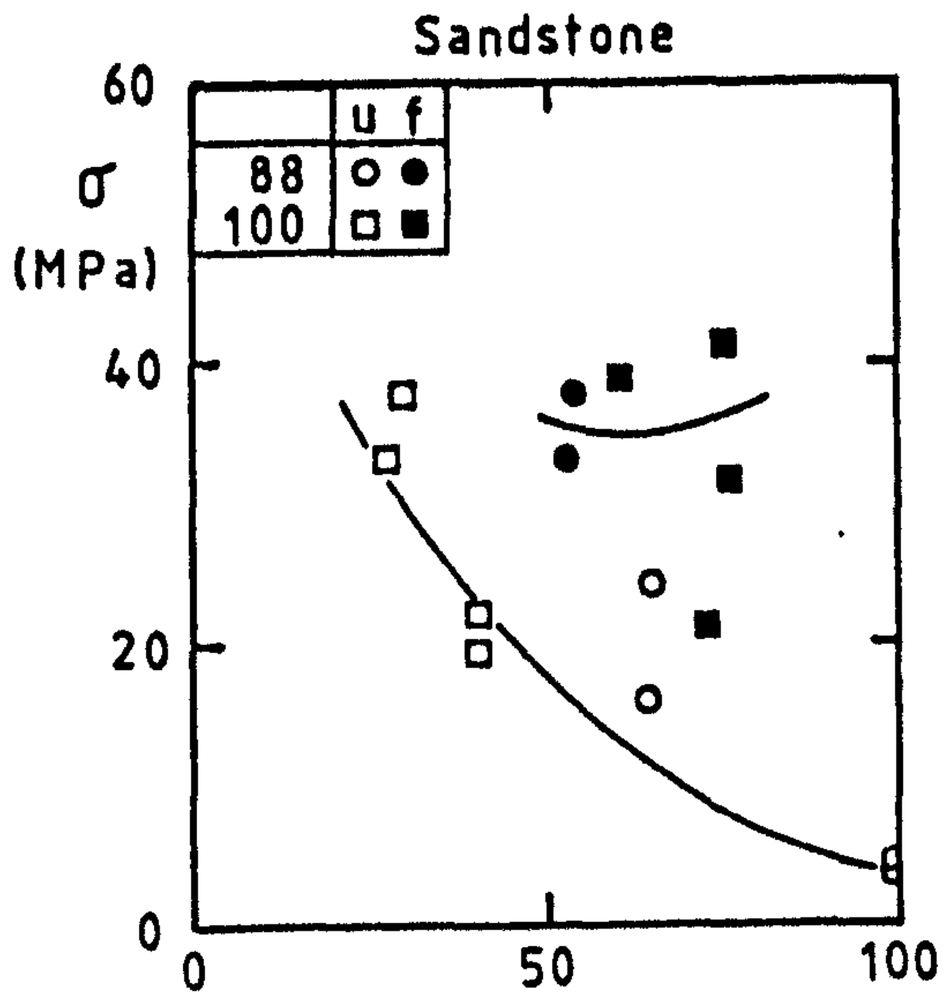

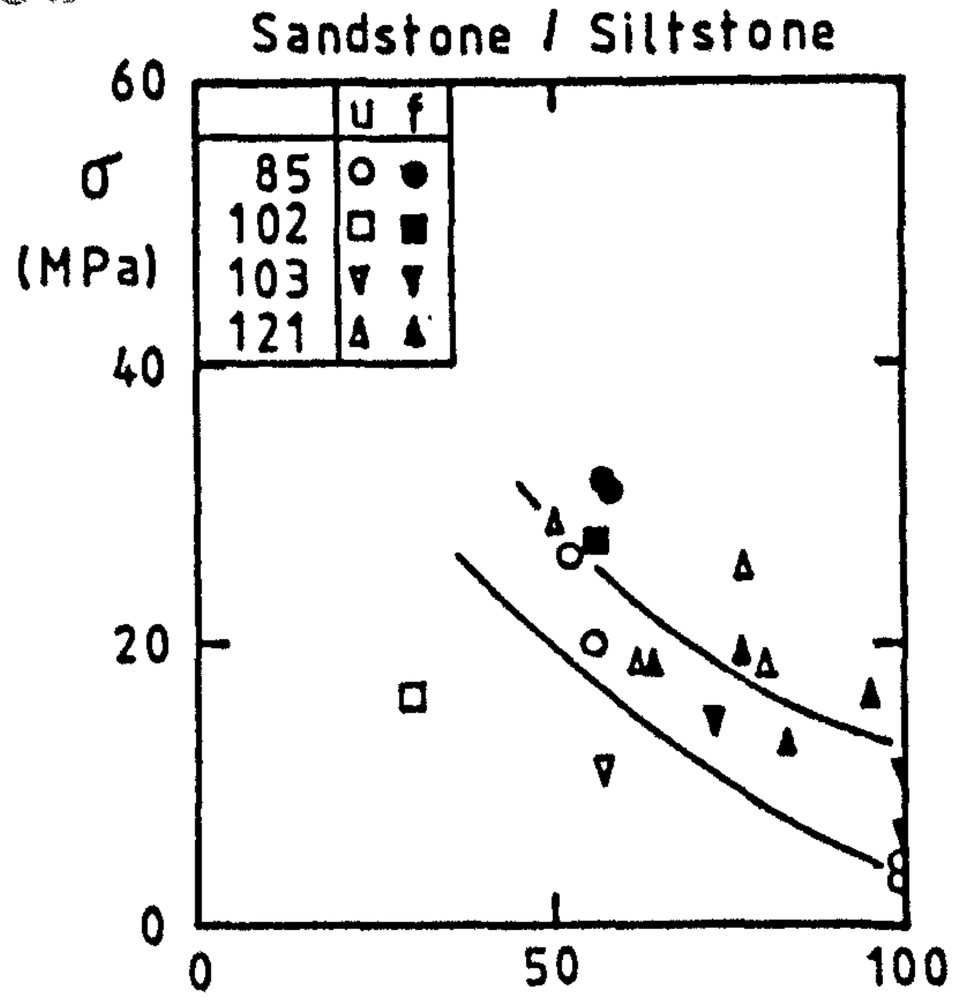

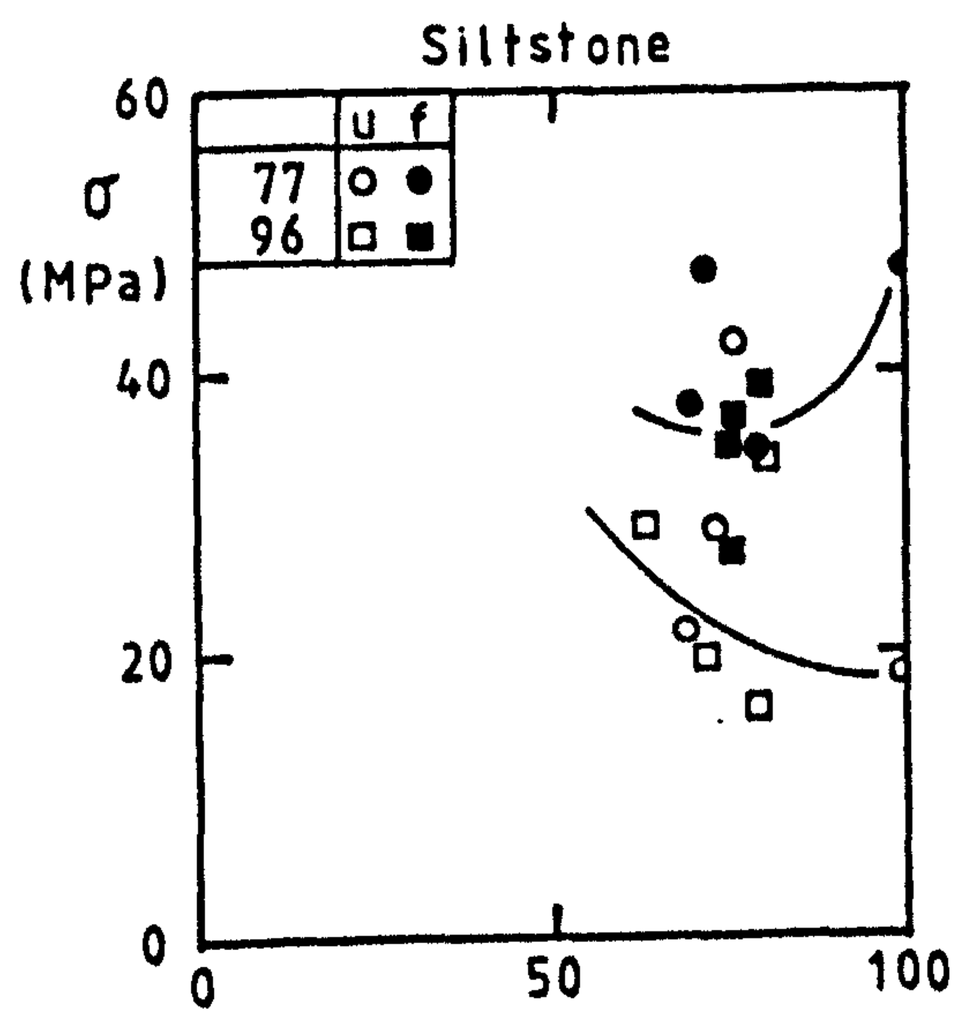

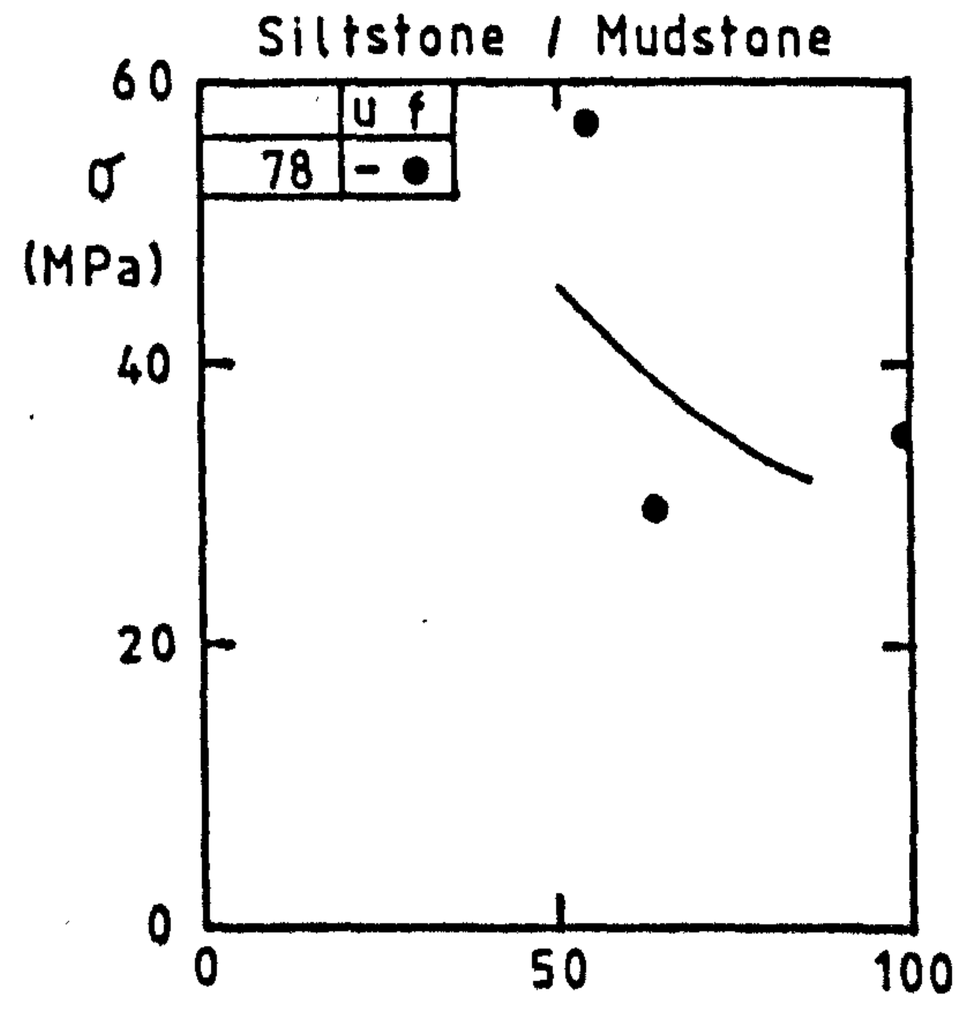

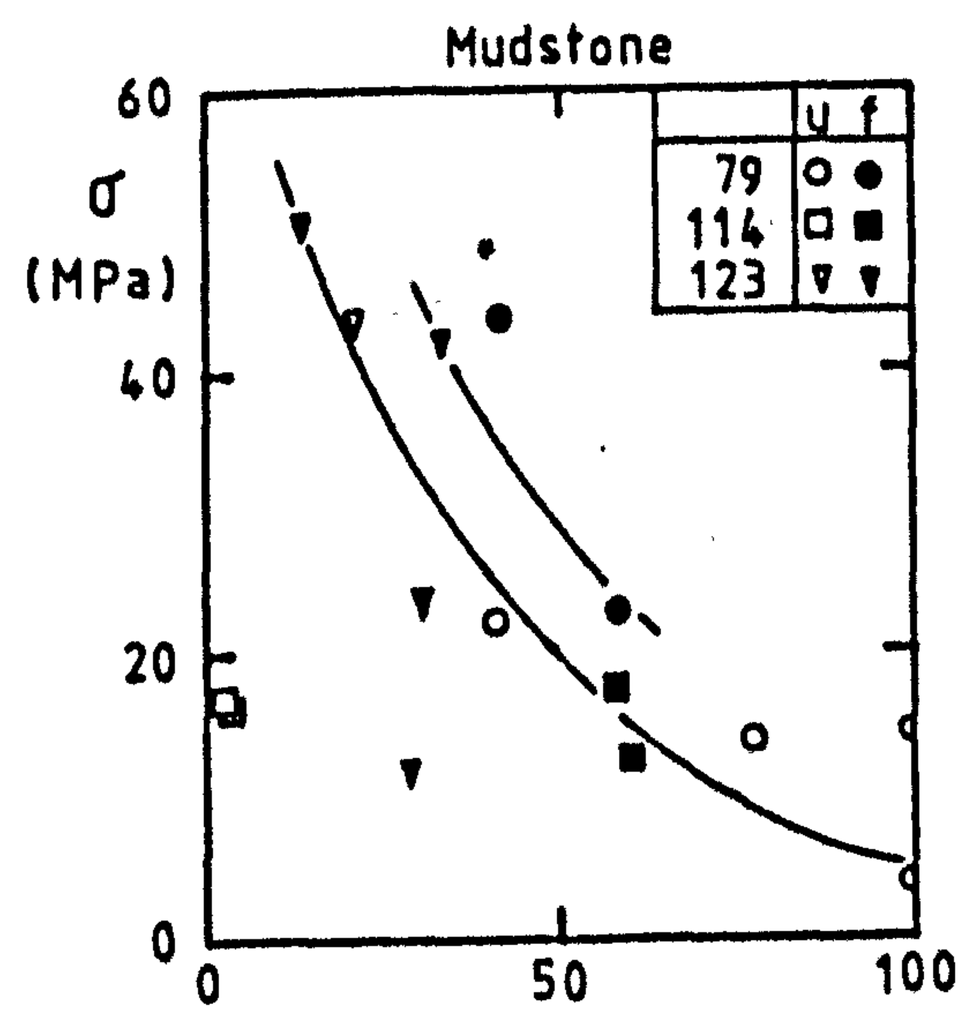

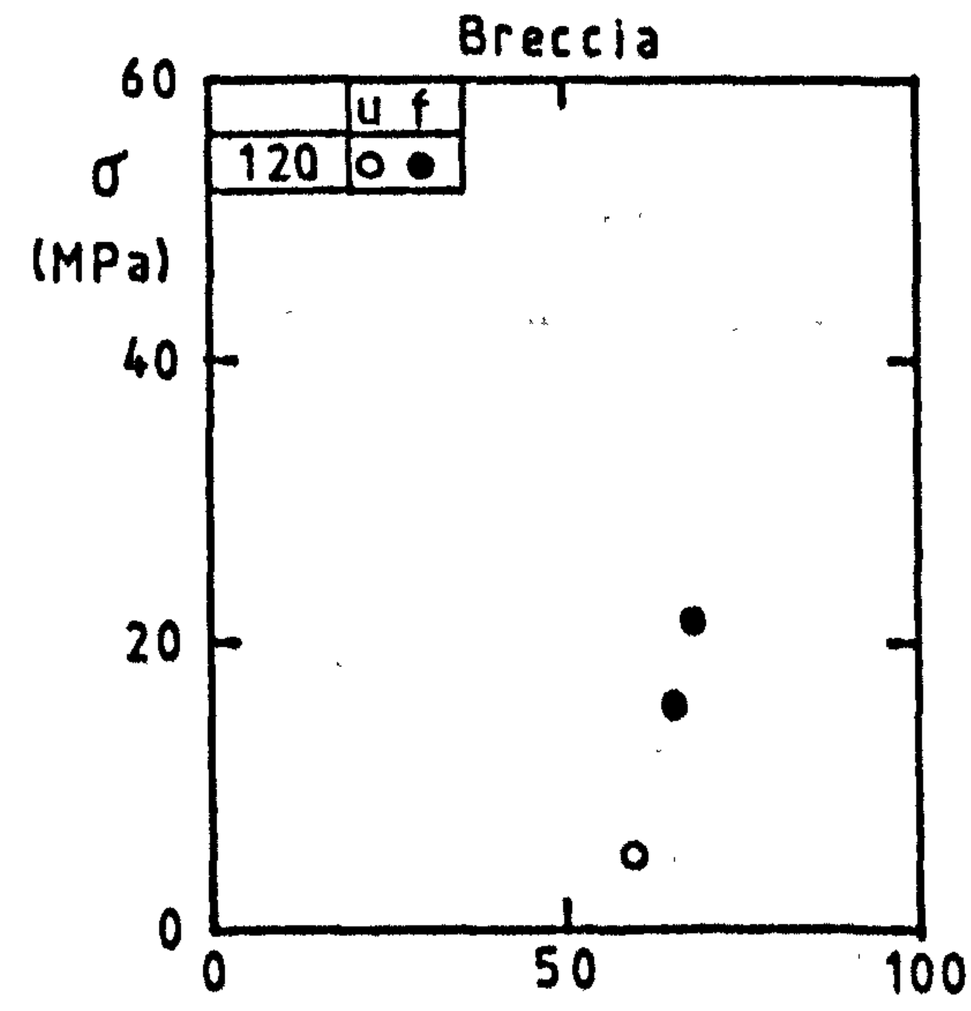

Fig. 5·4 Summary plots showing variations of uniaxial rock strength with degree of saturation.

given confining pressure, the expected deviator stress at failure can be calculated from the expressions:

$$\Delta\sigma_f = 2 \frac{(a + \sigma_3 \text{ Tan } \alpha)}{(1 - \text{Tan } \alpha)} \qquad 5.3$$

or $$\Delta\sigma_f = 2 \frac{(c \text{ Cos } \phi + \sigma_3 \text{ Sin } \phi)}{(1 - \text{Sin } \phi)} \qquad 5.4$$

Table 5.3 Shear strength parameters of the test materials at -10°C and 1mm/min deformation rate

Material	No. of Tests	σ_3 range	a (MPa)	α (°)	c (MPa)	ϕ (°)
LAF	14	0-12	1.6	10.0	1.6	10.2
LAL	26	0-10.3	4.8	20.5	5.2	22.0
KM	4	0-10	1.3	14.6	1.4	15.0

For creep testing, a deviator stress less than that calculated by equations 5.3 and 5.4 will generally be applied and this can be readily expressed as an applied stress ratio (ASR):

$$ASR = \Delta\sigma/\Delta\sigma_f \times 100\% \qquad 5.5$$

Because $\Delta\sigma_f$ is not an instantaneous failure stress, ASR values greater than 100% can be applied in creep tests without inducing an immediate collapse.

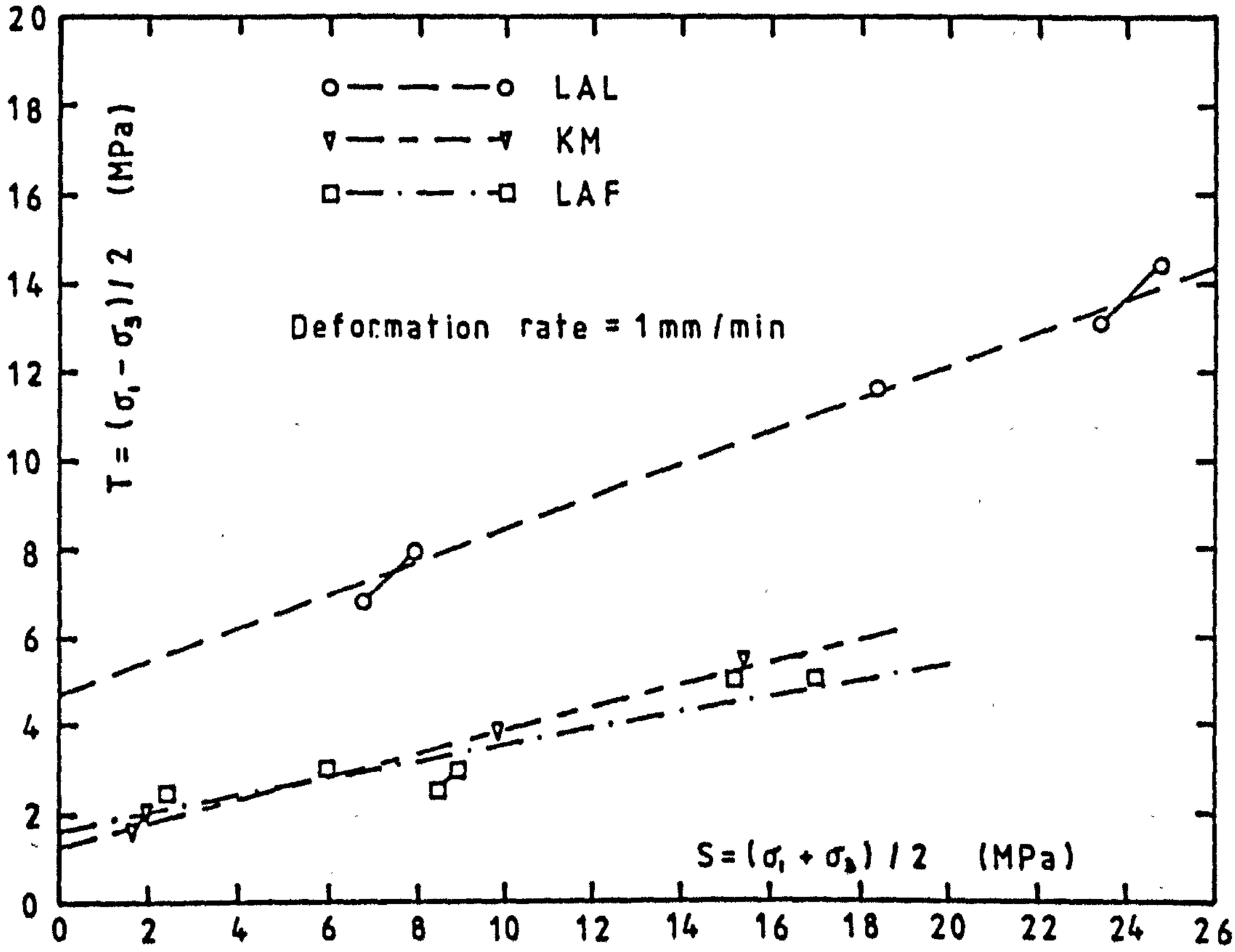

Fig. 5·5 K_f failure lines for LAF, LAL and KM at a temperature of -10°C.

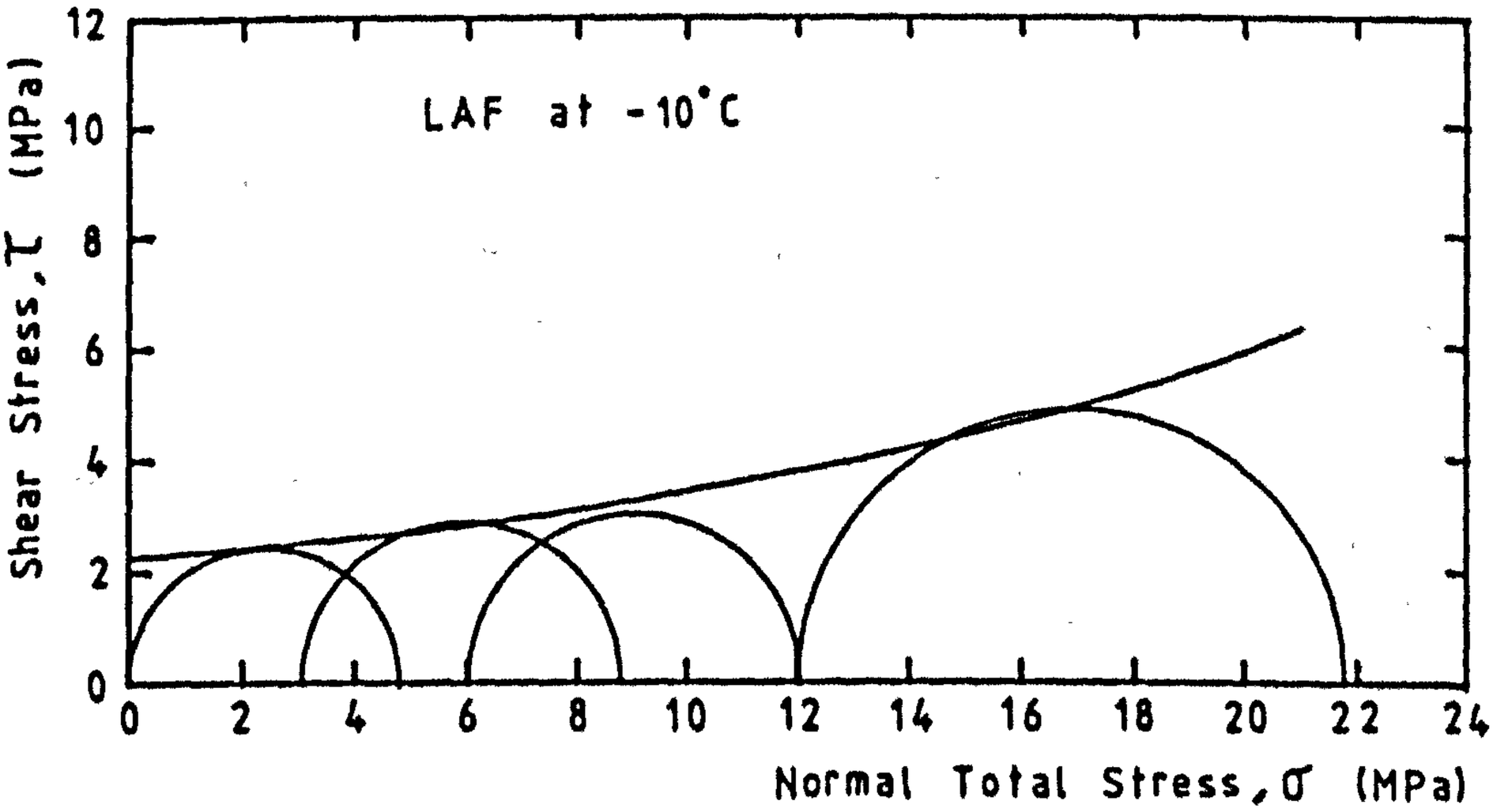

Fig. 5·6 Mohr circle plot for frozen LAF sand in units of total stress.

5.5 Discussion

The shape of the failure envelope resulting from triaxial compression tests on frozen soils and rocks can be greatly affected by the range of confining pressures applied. The ø value obtained for frozen KM clay is fairly high at 15°. Previous works have indicated that ø values of frozen clays are effectively zero but the confining pressure range in such studies have generally been small (Andersland and Alnouri, 1970). For example, the 100 psi confining pressure applied by Andersland and Alnouri is only one quarter of the unconfined compressive strength as compared to the 2.8 ratio in this study. Comparisons between the two results should be tentative.

The results in this study are all expressed in units of total stress, as no provision was made for measuring the pressures within the pore ice. Drainage from the specimens is possible with both the UCS and Hoek cells but the pore ice pressure is still expected to rise during the rapid deformation rate tests.

The failure envelope for a frozen frictional soil in CSR compression, when expressed in terms of total stress, is non-linear and can only be quoted for specific ranges of normal stress. This is due to the progressively smaller increase in deviator stress at failure as the air voids are compressed (Andersland and Anderson, 1978). The envelope is normally approximated to a straight line for the stated pressure range and the amount of smoothing involved in this process for a particular soil will be a function of this pressure range.

The brittle nature of the failure of LAL specimens becomes increasingly plastic as the confining pressure increases and dilatancy is suppressed. Uniaxial failure typically occurs around 4% strain but this increases to around 10% with σ_3 at 10.3 MPa.

For LAF, the effect of the confining pressure at low strains is to increase the strength rapidly and this manifests itself as a

confining pressure dependent Young's modulus. The repeatability of tests was checked by three tests at 3 MPa and six at 6 MPa confining pressure. One test at each of these pressures in the Hoek cell produced similar results to those in the HPCC cell and confirmed that apparatus effects were not influencing the results.

Subsequent tests in the Hoek cell at σ_3 = 10 MPa and 12 MPa showed a significant increase in strength over those at lower pressures. Specimen behaviour is similar to that during the consolidation period in a consolidated undrained triaxial test on unfrozen soil. This can be explained in terms of the creep of the ice matrix during isotropic compression. The confining pressure is applied to the specimens well in advance of the commencement of the test to allow the cell temperature to reach its equilibrium position. During this period, the pore pressures are relieved by the gradual creep of the ice matrix which allows the effective stresses to increase. The amount of creep is determined by the level of the confining pressure and results in an increased number of interparticle contacts. The frictional component of strength therefore increases with confining pressure and this is shown in terms of total stress in Fig. 5.6 for LAF sand. A straight line approximation to this data is reasonable over the pressure range investigated. The similar behaviour of a sandy silt is reported by Lade et al (1980) at -14°C over the confining pressure range 0 to 6 MPa.

In an attempt at further investigating the structure of the specimens used in strength testing, the ultrasonic pulse velocity (UPV) along the major axis was measured, before destructive testing. The results are shown in Fig. 5.7 as plots of deviator stress vs UPV and dry density vs UPV. No clear pattern emerges in either case. This lack of correlation may be a function of poor contact between the frozen specimen and the ultrasonic pulse transmitter and receiver. The UPV is particularly sensitive to air gaps at these interfaces and the specimen preparation technique is not currently able to produce end faces of sufficient quality for this test. Baker and

Kurfurst (1985) report acoustic test results on specimens of frozen Ottawa sand which clearly show that the UPV increases directly with density. These results were obtained over a greater density range (1.55 to 1.78 Mg/m^3) than in this study (1.50 to 1.55 Mg/m^3), and specimen preparation was completed by end facing in a lathe. The gradient of the Ottawa sand results was 0.5 $(Mg/m^3)/(kms^{-1})$ and an extrapolation of this result is shown on Fig. 5.7b. Further work on the development of the UPV system for frozen soils is needed before non-destructive testing of this sort can be used to accurately predict strength behaviour. This is beyond the scope of this thesis.

5.6 Summary

This chapter has presented a review of the mechanical behaviour of frozen soils during short term strength tests. Specific reference has been made to their response to changes in temperature, density, ice content, degree of ice saturation, unfrozen water content, confining pressure and strain rate. This review is based on published literature and is centred around tests on Ottawa sand. Table 5.1 is used to summarise the effects, and highlights the need for the inclusion of reference tests to allow a comparison of results.

The results obtained from short term strength tests on the materials of Chapter 3 are examined in detail. The rock specimens were tested under constant stress rate conditions (1 MPa/s) to obtain a comparison in strengths of the unfrozen and frozen materials. Test temperatures were +20°C and -16°C. Sandstone specimens were resaturated before testing or freezing to compensate for moisture loss since removal from the ground. The remaining rocks were susceptible to slaking and consequently were tested in an unsaturated condition. The saturated samples showed that, on freezing, the gain of strength is almost entirely due to the cohesion of the ice matrix. The angle of internal friction remains effectively unchanged. The average strength gain ratio on freezing of the sandstones tested in

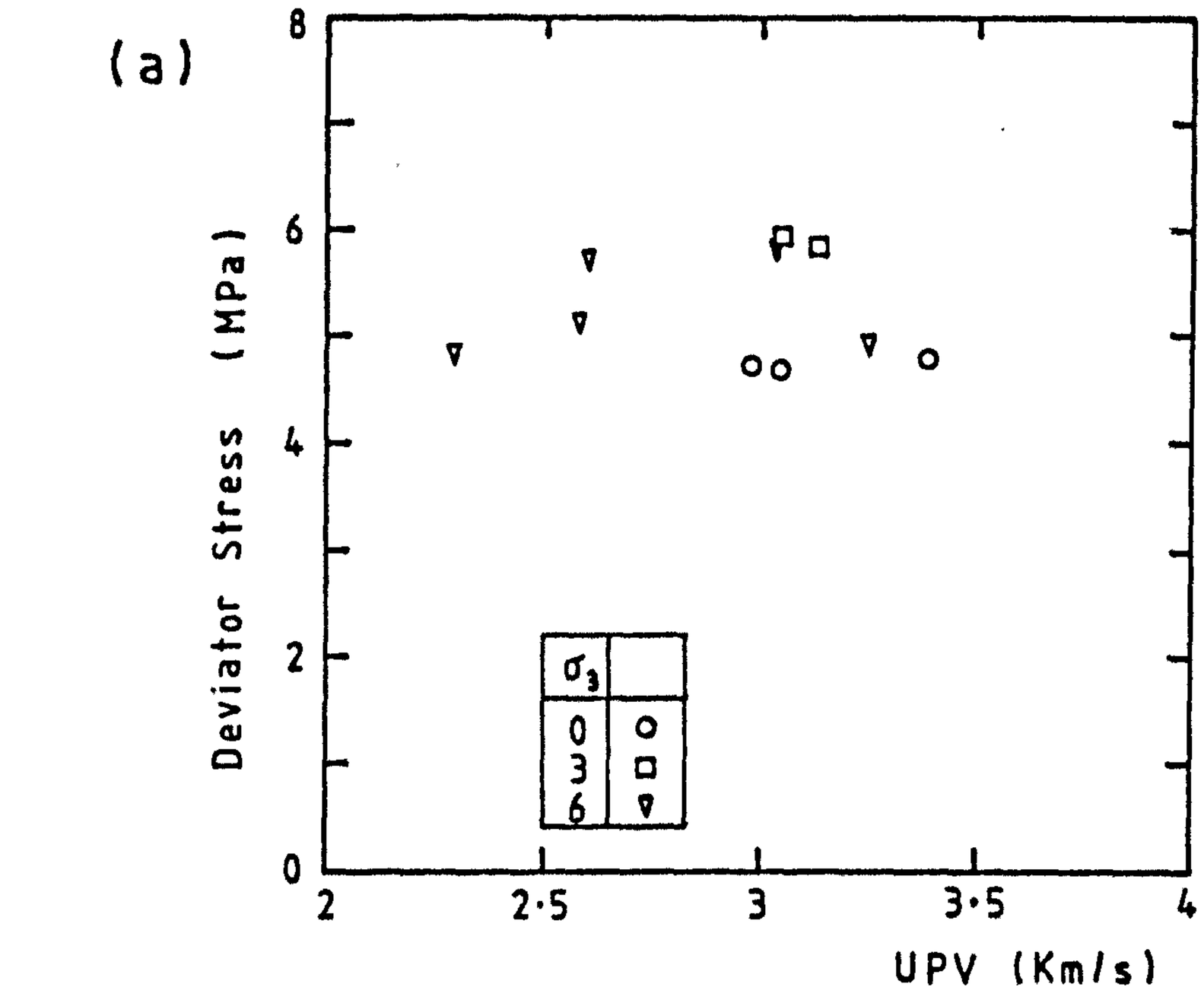

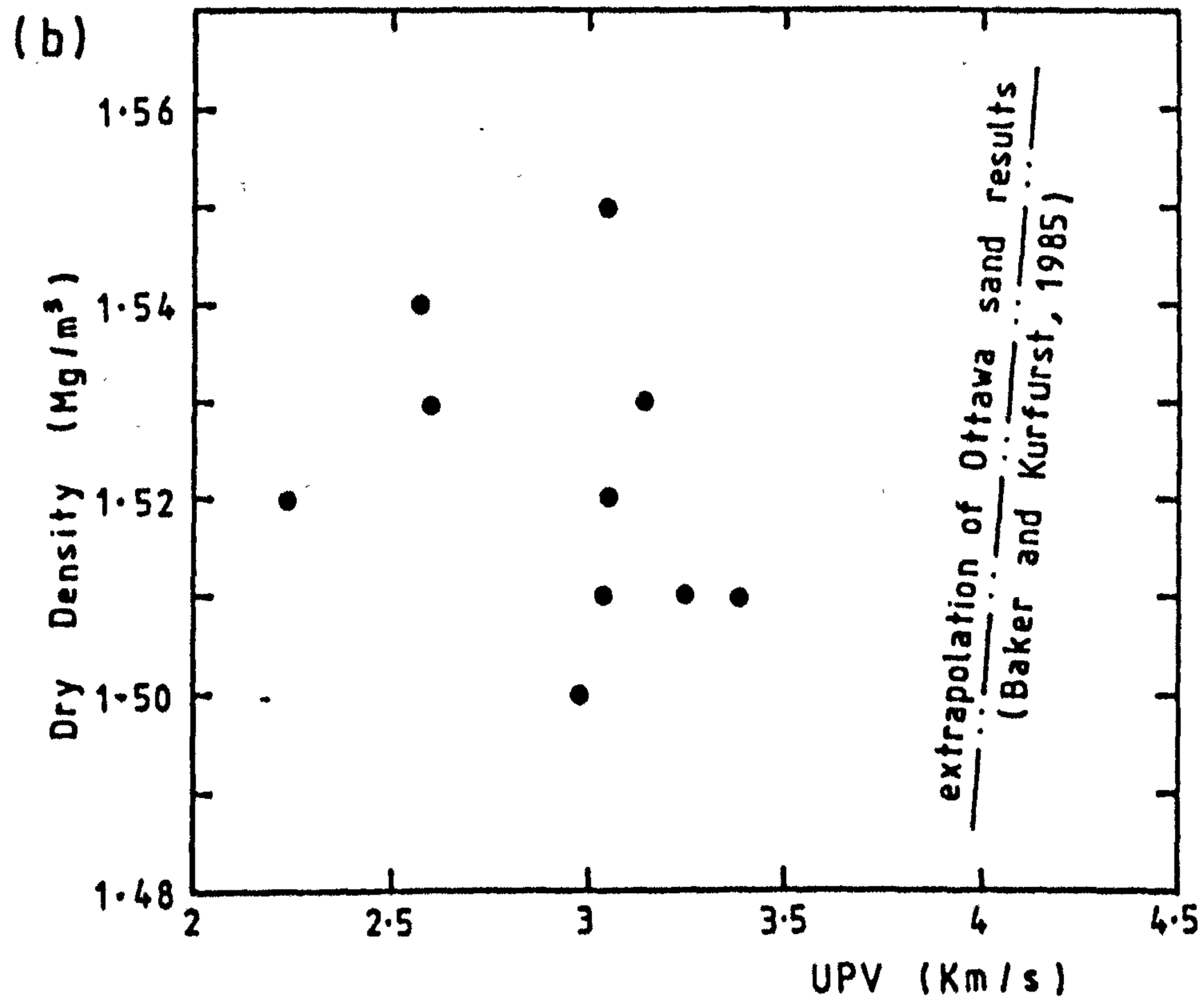

Fig. 5·7 Distribution of a) deviator stress and b) dry density with ultrasonic pulse velocity (UPV) for LAF strength test specimens at -10°C.

uniaxial compression, was 2.64.

The unsaturated rocks also showed greater strength when frozen, although at low ice contents, this effect is minimal. The variation of uniaxial strength with degree of saturation is examined over fairly limited ranges of moisture content for each sample. As no control of moisture content was effected, the findings of this study were limited.

The three soils LAF, LAL and KM were tested to obtain reference strengths for the creep tests to follow. For this purpose, the applied stress ratio (ASR) is defined by equation 5.5.

LAL exhibits a brittle failure at low strain (4%) in uniaxial compression, increasing to 10% at 10.3 MPa confining pressure. LAF and KM both deform plastically to high strains, and failure strains are defined at 15% and 20% respectively. The effects of isotropic compression at high confining pressure is observed to produce a curved failure envelope for LAF sand, but a straight line approximation gives minimal errors for the range covered.

Non-destructive testing by transmission of ultrasonic pulses along the major axis of a frozen specimen has been studied briefly. Difficulties arising from the inclusion of air gaps between the pulse transmitter, specimen and receiver are identified as potentially masking monotonic relationships between the ultrasonic pulse velocity (UPV) and specimen density and strength.

CHAPTER 6

THE CHARACTERISATION OF CREEP

6.1 INTRODUCTION

Creep is the time dependent plastic deformation of a material under a constant load or stress. It has been most extensively studied in relation to metals. Creep deformation occurs in metals at all temperatures but is generally only significant at higher temperatures, well above those normally experienced in aeroengines, chemical plants and electricity generating stations. The main mechanism involved is the movement of vacancies and dislocations through the crystal lattice and grain boundaries (Evans and Wilshire, 1985).

Frozen soils are also affected by creep deformation. Stresses between the pore ice and soil particles cause pressure melting of the ice. This unfrozen water is then moved to regions of lower stress by differences in surface tension (Andersland and Anderson, 1978) where it refreezes. The accompanying breakdown of the ice and its bonds with the soil particles results in plastic deformation of the pore ice and a readjustment in particle arrangement.

The creep process has traditionally been represented by a strain-time curve consisting of three distinct phases; primary, secondary, and tertiary. Shown in Fig. 6.1, these phases correspond to periods of strain deceleration, constant strain rate and strain acceleration respectively. Recent interpretations have moved away from this concept to classify creep in just two stages, the secondary stage being replaced by a momentary minimum strain rate represented by an inflection point (m) on the strain-time curve. Engineering failure (as opposed to rupture) is defined at the onset of tertiary creep in both classifications and is therefore at the inflection point in the two stage interpretation.

This chapter looks at the ways in which the creep strain curve is appropriate to engineering and to artificial ground freezing in particular. A review is included of the many attempts made to model all or part of the curve for frozen soils and ice. The

results from laboratory creep tests, on the materials described in Chapter 3, are then introduced prior to being used for more detailed examination of two of the uniaxial creep equations. Leading on from this, a new triaxial creep equation is proposed and shown to be consistent with the laboratory results over a wide range of confining pressures.

6.2 Creep in relation to AGF

Open excavations in frozen ground will be subject to creep deformation which may impair the construction of permanent linings. It is therefore important that these deformations are kept within predefined limits and for this purpose, knowledge of the creep strain-time characteristics of the frozen soil, is needed.

Creep deformation is a rate process and as such is best expressed in terms of strain rate and time. Some empirical approaches to the problem of modelling creep behaviour have directly produced strain-time relationships. The alternative is to transform a strain rate expression using mathematical integration. For AGF deformation analysis (Section 2.5), the acceptability of a particular model may depend on the complexity of the resulting equation.

Two demands are made of the creep model. Firstly, it shall predict the limit of long term strength of the frozen ground water under the imposed loading regime. This enables the time (t_m) to engineering failure of the material to be defined and imposes an absolute upper limit to the period in which the excavation is supported solely by the ice wall. The second requirement is that good predictions of strain are made during the early stages of creep, nominally upto half the time to failure. This is the portion of the creep curve which should affect a well designed ice wall, making serviceability the limiting factor and not engineering failure.

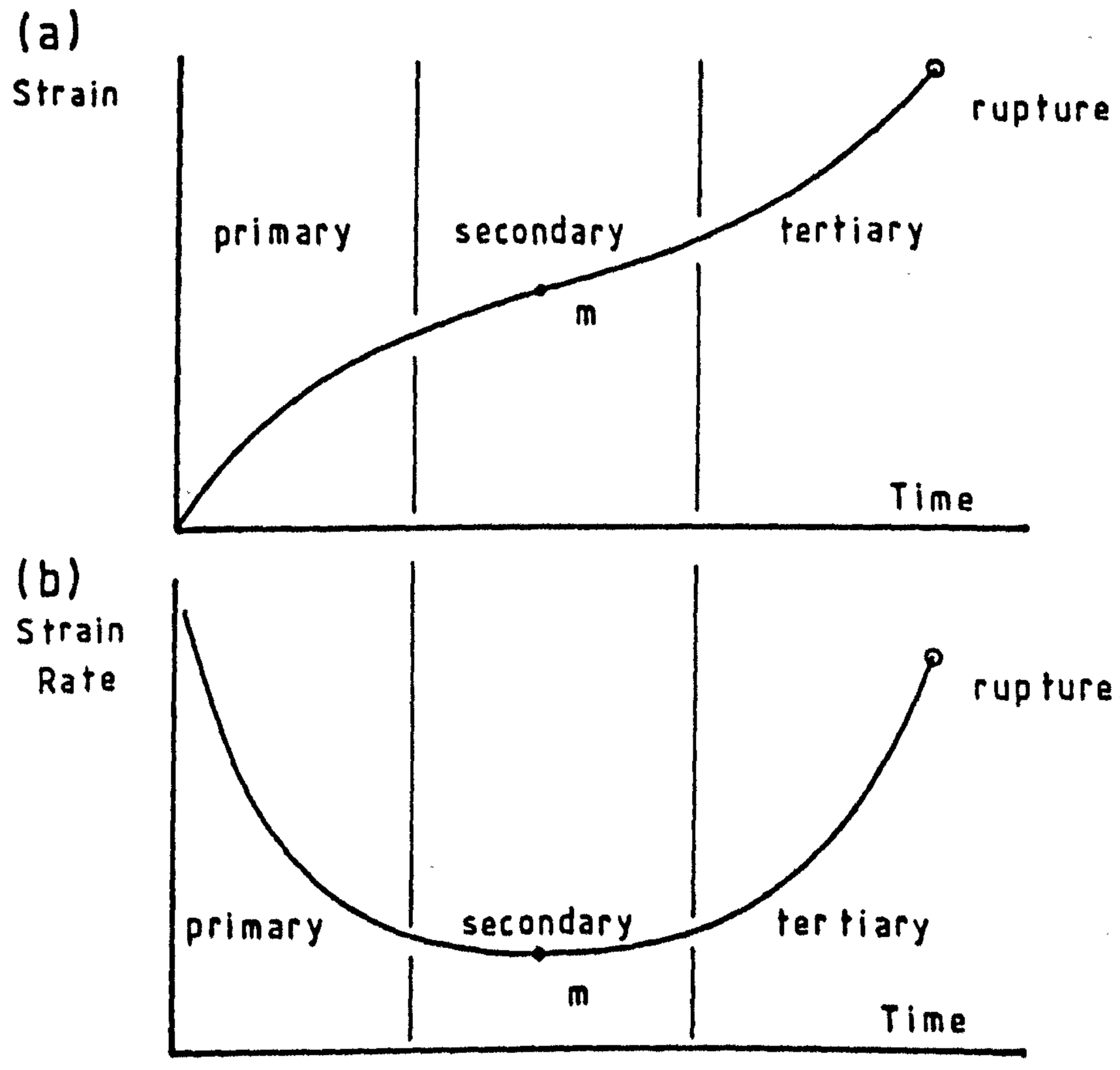

Fig 6·1 Interpretation of creep curves

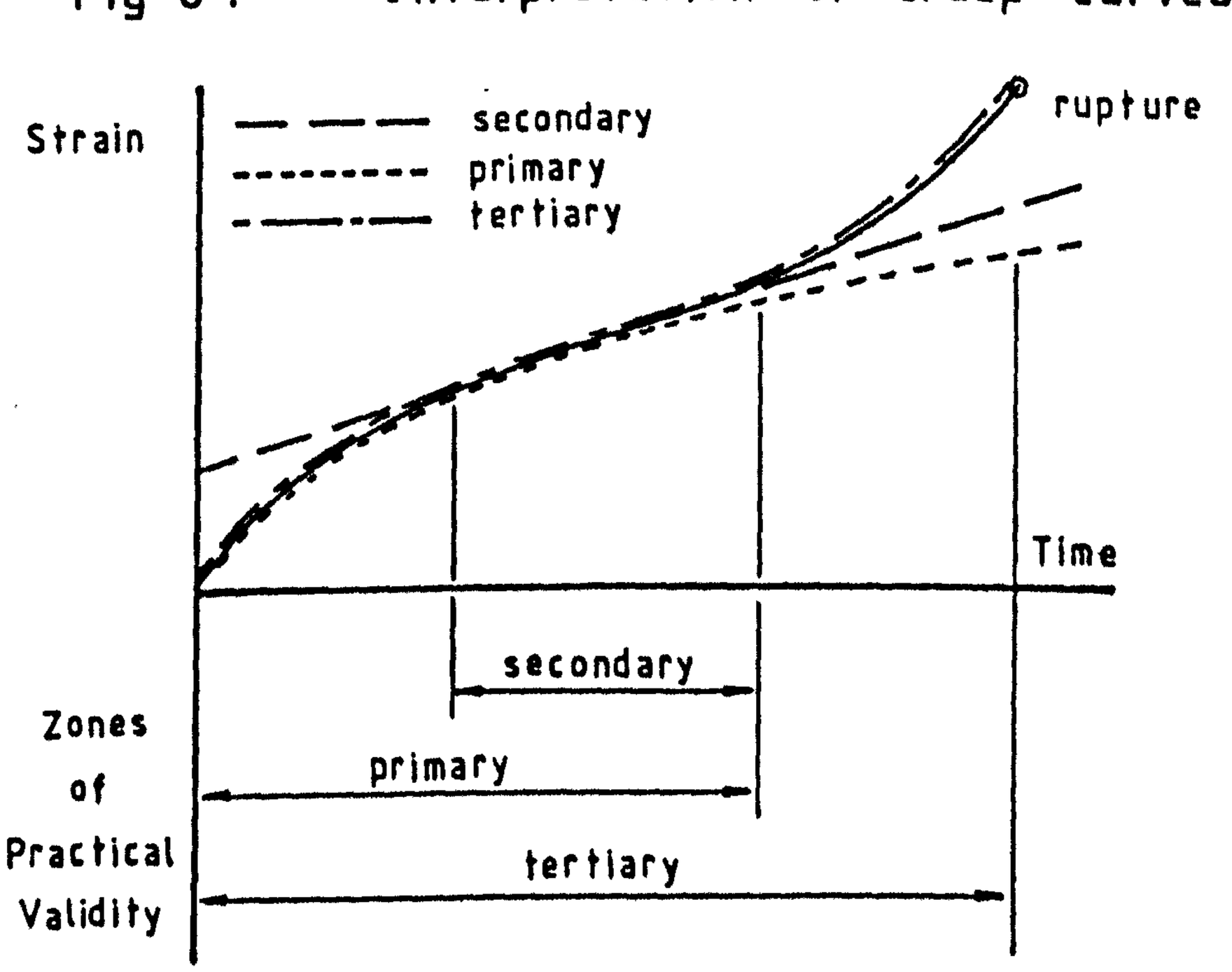

Fig 6·2 Creep model classifications and their zones of practical validity

6.3 Creep model classification

The three stage interpretation of the creep process has led to three basic types of model being developed. The simplest form approximates the process to an instantaneous strain, ε_o, followed by a period of constant strain rate, $\dot{\varepsilon}$, such that:

$$\varepsilon = \varepsilon_o + \dot{\varepsilon}t \qquad 6.1$$

A model of this form, known as a Secondary model for its close modelling of the secondary creep period, is described by Hult (1966). Ladanyi (1972) has shown the usefulness of such equations when dealing with step stress loading and used in conjunction with a stress dependency expression. One such expression (Alkire and Andersland, 1973) shows the secondary strain rate to be a function of deviator stress ($\Delta\sigma$),

$$\dot{\varepsilon} = b \exp(m\Delta\sigma) \qquad 6.2$$

where b and m are material constants.

Secondary creep models overestimate strain in the early stages of creep and, as such, do not meet the requirements of AGF engineering. Closer predictions of creep strain prior to failure can be obtained from Primary creep models which feature a power term to simulate strain deceleration. The general form of Primary equations is:

$$\varepsilon = f(\sigma)\ t^C \qquad 6.3$$

with constant C less than unity. Vyalov (1965) proposed a power law function for stress and incorporated another power term to

account for the effects of temperature. Vyalov's equation was simplified by Klein (1978) to a temperature dependent equation,

$$\varepsilon = A\sigma^{B}t^{C} \qquad 6.4$$

with the three parameters A, B and C determined empirically.

Primary creep models can give good predictions of strain upto the onset of tertiary creep but, like Secondary models, are not able to identify this failure point. In practical terms they are useful beyond the inflection point (Fig. 6.2) for providing approximate solutions to the strain-time relationship.

The third type of model attempts to predict deformation behaviour throughout the creep process. These Tertiary creep models typically include both power and exponential terms for time and take the form,

$$\varepsilon = f(\sigma)\ t^{Y} \exp(Zt) \qquad 6.5$$

Y and Z are material constants. Tertiary creep models have been proposed by Assur (1980), Fish (1982,1983), Ting (1983) and Gardner et al (1984). Assur and Fish used an analytical approach to arrive at essentially the same equation, but expressed it in different forms. The Fish version is examined in more detail in section 6.5.

Gardner's equation, based on the approach of Assur and Fish, can be expressed in the form,

$$\varepsilon = \varepsilon_m \left(\frac{t}{t_m} \right)^{c} \exp\left[(c^{\frac{1}{2}}-c) \left(\frac{t}{t_m} - 1 \right) \right] \qquad 6.6$$

t_m and ε_m refer to conditions at the inflection point (Fig. 6.1), and c is a material parameter,

$$c = \left(\frac{\dot{\varepsilon}_m \, t_m}{\varepsilon_m} \right)^2 \qquad 6.7$$

$\dot{\varepsilon}_m$ is the strain rate at failure. Equation 6.6 provides a simpler expression for creep strain than those proposed by Assur and Fish and, as such, has advantages in engineering applications. The Gardner model could be extended to represent a family of creep curves by defining the variation with stress of the three main parameters t_m, ε_m and c.

None of the Tertiary creep models mentioned have been observed closely to predict creep strain through to rupture, and cannot predict the point of rupture itself. However, they can give close strain predictions into the tertiary creep zone and are able to identify the failure point m. Fig. 6.2 summarises the regions of practical validity for all three types of creep model and shows both Primary and Tertiary models to be well suited to AGF engineering requirements.

6.4 Experimental results

Three series of creep tests have been completed to provide the experimental data necessary to investigate the applicability of the various creep models. The results were obtained using the two microcomputer controlled test rigs (Chapter 4) which nominally provide constant deviatoric stress. The failure point details for each of the test series, corresponding to the three materials LAF, LAL and KM (Chapter 3), are listed in Appendix C.

The variation with applied stress ratio (ASR) of each of the failure parameters is shown in Figs. 6.3 through 6.5. A fairly high scatter of results highlights the difficulties in

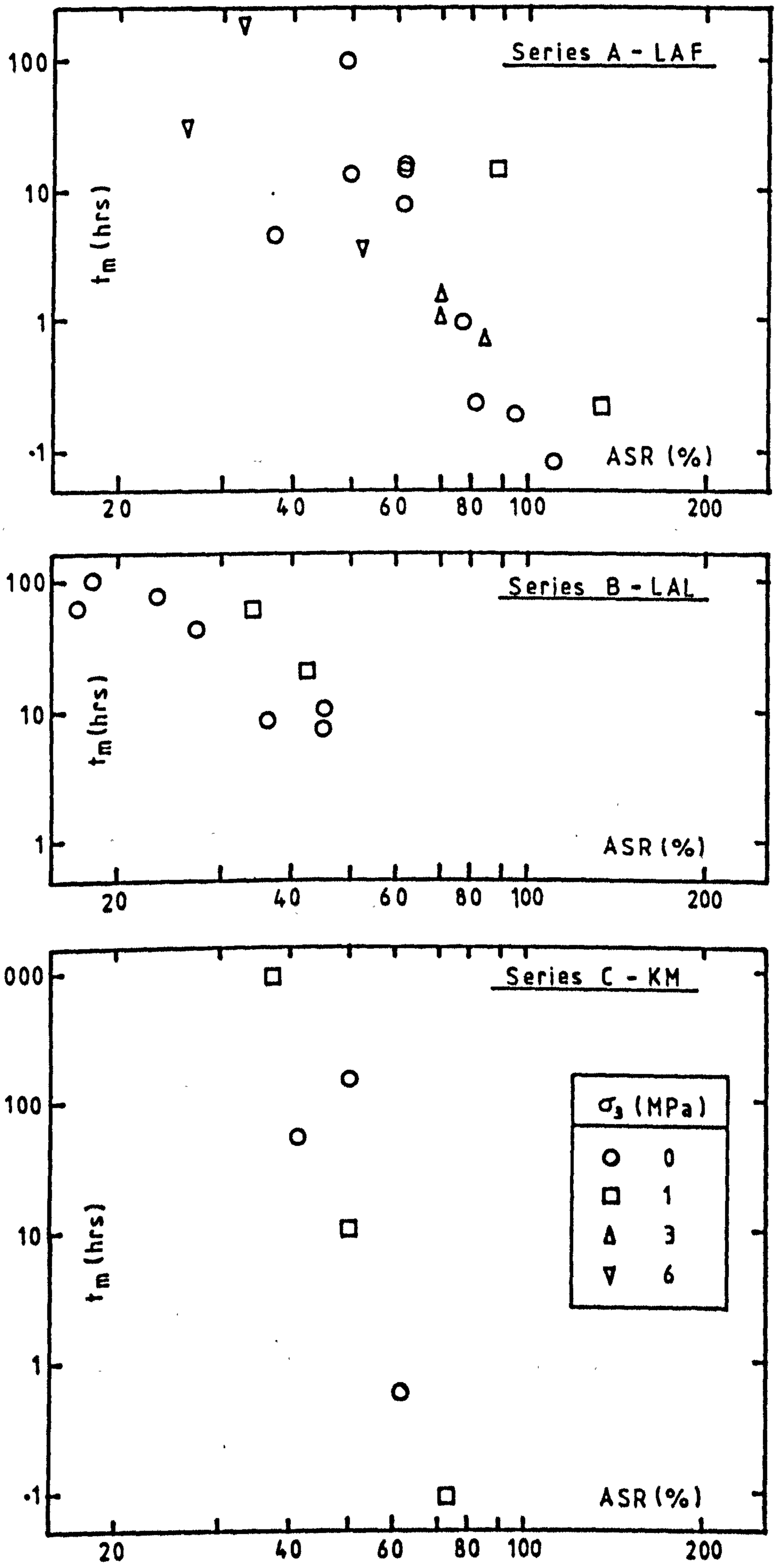

Fig 6·3 The time to failure (t_m) - applied stress ratio (ASR) relationship for test series A, B & C

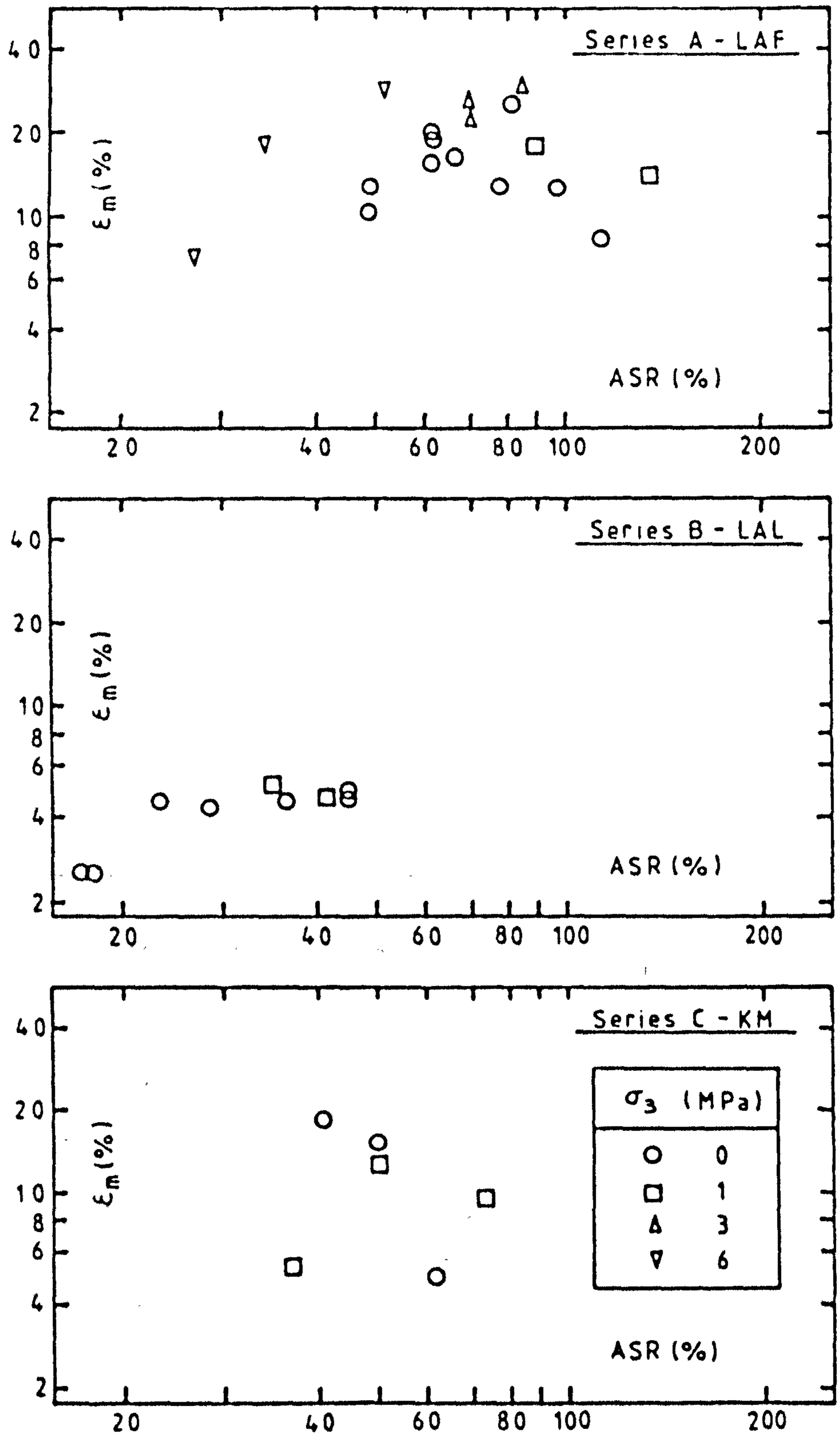

Fig 6·4 The strain at failure - applied stress ratio (ASR) relationship for test series A,B & C

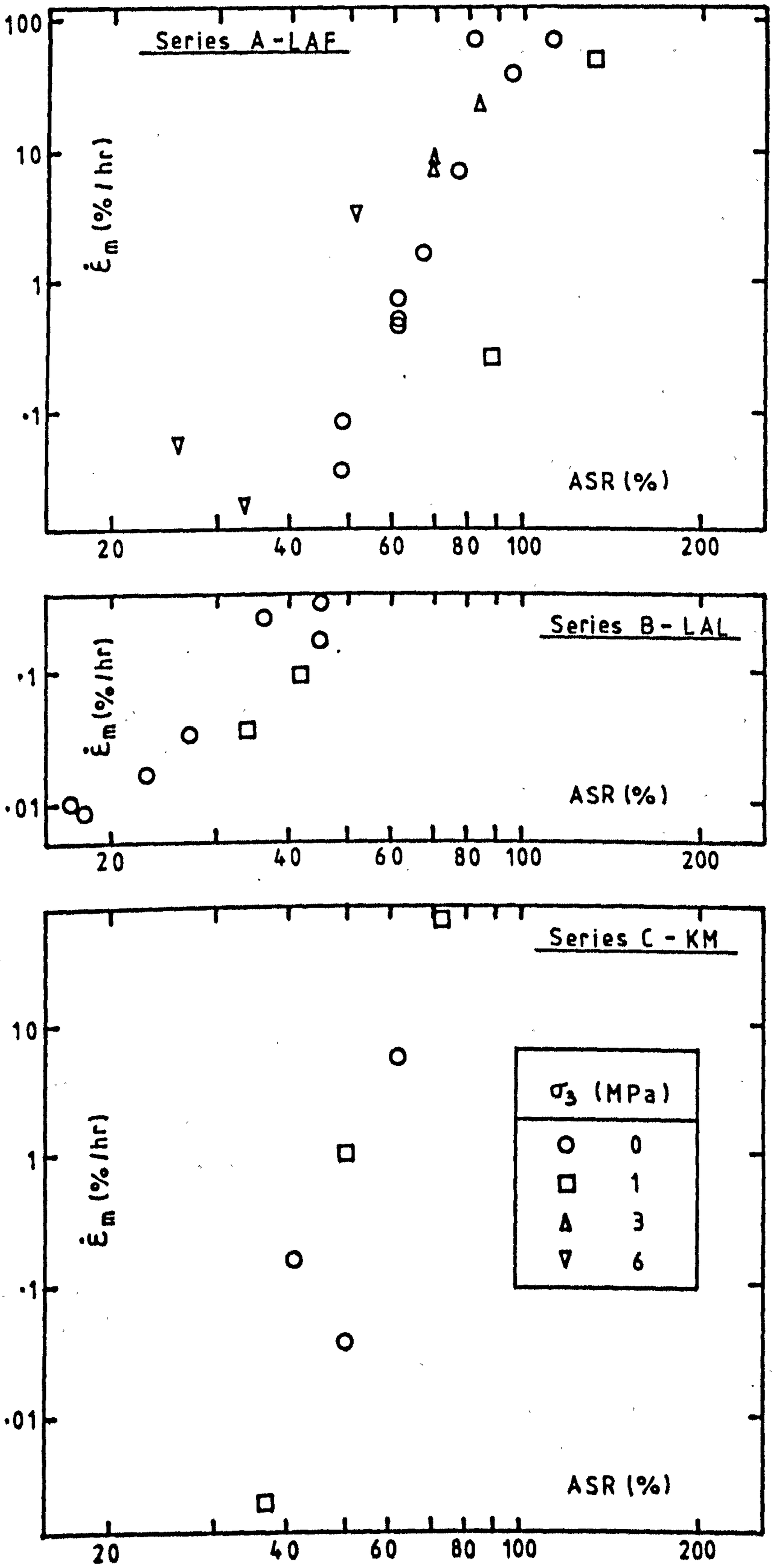

Fig 6·5 The strain rate at failure - applied stress ratio (ASR) relationship for test series A, B & C

establishing unique relationships between parameters, and results from the non-uniform distribution of soil grains and ice through the test specimens. Failure strain does not appear to be constant, as previously claimed by Zhu and Carbee (1983) and Gardner (1985) when the creep stress range is increased, as in this study. However, no unique variation with stress is observable. The effect of stress on the failure strain of frozen sands has been studied by Rein and Hathi (1978). They observe a decrease in ε_m with stress increase for all three sands tested, but this effect is only minor for the coarsest sand. Vyalov (1965) provides data on Callovian sandy loam and Bat-baioss clay which also shows a dependence on stress. Figs. 6.3 and 6.5 show that the time to failure (t_m) and failure strain rate ($\dot{\varepsilon}_m$) decrease and increase respectively with stress level. However, the deviation about any best fit line is considerable.

Fig. 6.6 presents the failure parameters $\dot{\varepsilon}_m$ and t_m in a form which suggests that although individual parameters are affected by specimen variations, a unique failure criterion may exist. The minimum strain rate-time correlation was looked at in detail by Ting (1983) and observed to be linear in logarithmic co-ordinates for uniaxial tests on soil, ice and frozen soil. This relationship was demonstrated to be temperature independent in the range -0.5°C to -10°C by Zhu and Carbee (1983) testing Fairbanks silt. Ting gives further evidence of the correlation by referring to high temperature creep of metals (Garofalo 1965). Fig. 6.6 shows that this relationship can also be extended into the triaxial regime without any significant scatter from a single linear relationship.

Mellor and Cole (1982) suggest that the slope of the $Ln(\dot{\varepsilon}_m)$ - $Ln(t_m)$ correlation is 'close to' -1 for ice, which implies that the failure strain is constant. For the three soils in Fig. 6.6, the gradients are all less than -1 which is indicative of the fact that failure strain is not constant for these materials.

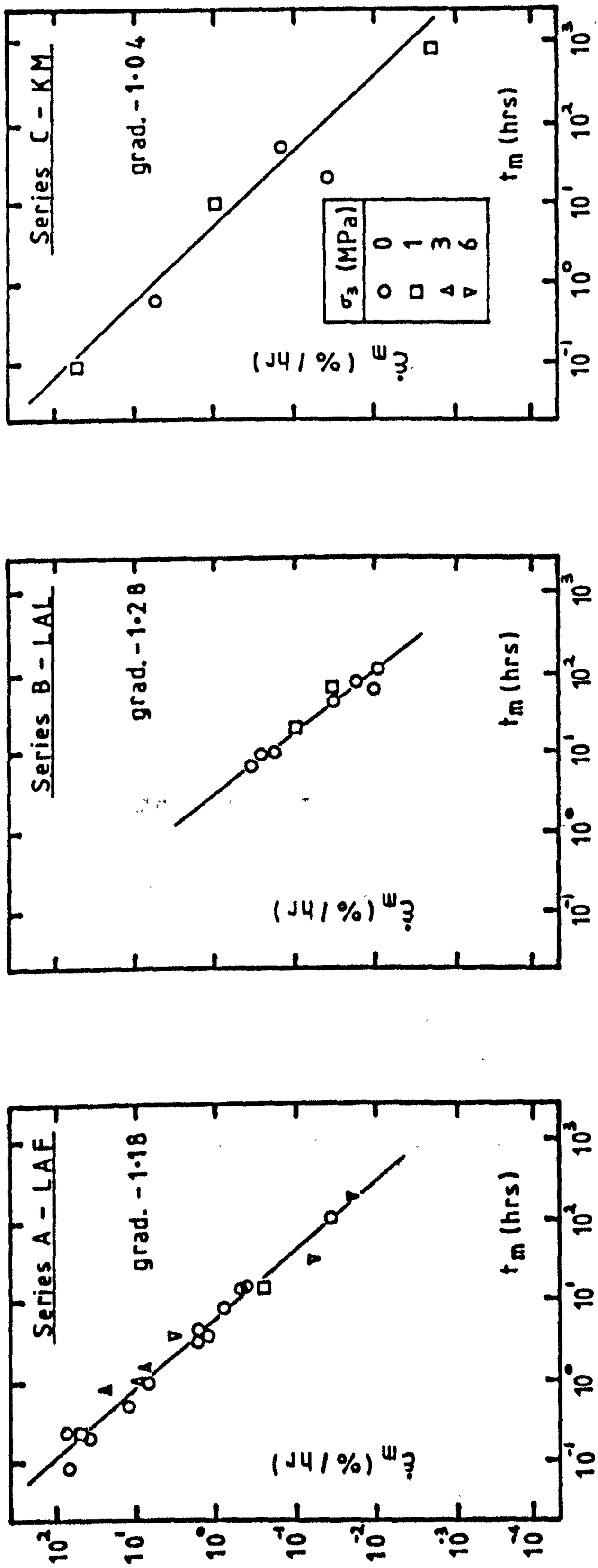

Fig 6·6 The failure strain rate - time to failure relationship for creep tests over a range of confining pressures.

6.5 Uniaxial Creep Equations

6.5.1 Analytical approach

The strength and deformation characteristics of frozen soils have traditionally been determined from constant strain rate (CSR) and constant stress (CS) creep tests respectively. Failure is defined at the peak stress in CSR tests and the minimum strain rate in CS tests, but Fish (1983) recognised the fact that the physico-mechanical properties of the material are similar in each case. The resulting thermodynamic model of creep is given in equation 6.8:

$$\dot{\varepsilon} = \tilde{C}\left(\frac{KT}{h}\right) \exp\left(\frac{-E}{RT}\right) \exp\left(\frac{\Delta S}{K}\right)\left(\frac{\sigma}{\sigma_o}\right)^{n+m} \qquad 6.8$$

where $\tilde{C}$, $n \geqslant 0$, and $m \geqslant 1$ are dimensionless parameters independent of temperature.

σ_o = temperature dependent ultimate strength of soil (MPa)
E = activation energy (KJ/mole)
K = Boltzmann's constant, 1.38×10^{-23} J/°K
h = Planck's constant, 6.63×10^{-34} Js
R = gas constant, 8.31×10^{-3} KJ/mole °K
T = absolute temperature (°K)
ΔS = change of entropy

Fish expresses the entropy term as a function of normalised time (τ) such that,

$$\frac{\Delta S}{K} = \delta f(\tau) = \delta (\tau - Ln\ \tau - 1) \qquad 6.9$$

where δ is a temperature independent dimensionless parameter.

At the failure point, i.e. $t = t_m$ and $\tau = 1$, the RHS of equation 6.9 and, hence, the change of entropy, becomes zero which is the thermodynamic failure criterion.

Fish also defined relationships for the time to failure and corresponding minimum strain rate. Time to failure is expressed as a function of normalised stress,

$$t_m = t_o \left(\frac{\sigma}{\sigma_o} \right)^{-m} \qquad 6.10$$

where t_o is Frenkel's relaxation time,

$$t_o \backsimeq \left(\frac{h}{KT} \right) \exp \left(\frac{E}{RT} \right) \qquad 6.11$$

and σ_o the stress giving failure at $t_m = t_o$

Strain rate at failure, in the general case when $0 < n \neq 1$, can be expressed as:

$$\dot{\varepsilon}_m = \frac{C}{t_r} \qquad 6.12$$

where C is a constant and t_r the time to rupture of the sample,

$$t_r = \exp(\delta)\ t_m \left(\frac{\sigma}{\sigma_o} \right)^{-n} \qquad 6.13$$

In the special case where n = 0, Fish arrives at the expression:

$$\dot{\epsilon}_m = \frac{\tilde{C}}{t_m} \qquad 6.14$$

with $\tilde{C}$ a constant. This equation gives a slope of -1 to the $\mathrm{Ln}(\dot{\epsilon}_m)$ - $\mathrm{Ln}(t_m)$ plot and n = 0 implies that failure strain is constant.

To obtain an expression for creep strain, equation 6.8 can be integrated to,

$$\epsilon = \tilde{C} \left(\frac{\sigma}{\sigma_o} \right)^n \psi \, \tau \, \exp \, (\delta \, f(\tau)) \qquad 6.15$$

where ψ is a tabulated integral for $\delta \neq 1$

$$\psi = \frac{1}{\lambda} \left[1 - \frac{\delta\tau}{1+\lambda} + \frac{(\delta\tau)^2}{(1+\lambda)(2+\lambda)} - .... \right] \qquad 6.16$$

and $\lambda = 1 - \delta$

For frozen soils, Fish suggests that $0 < \delta < 1$ but does not comment on the effect on the predicted creep strain when δ is greater than unity. Fig. 6.7 shows the integration factor ψ as a three dimensional plot of δ and τ. At failure (τ = 1), ψ is relatively insensitive to δ below δ = 0.5.

6.5.2 Empirical approach

Observations made on experimental data by Vyalov et al (1962) led

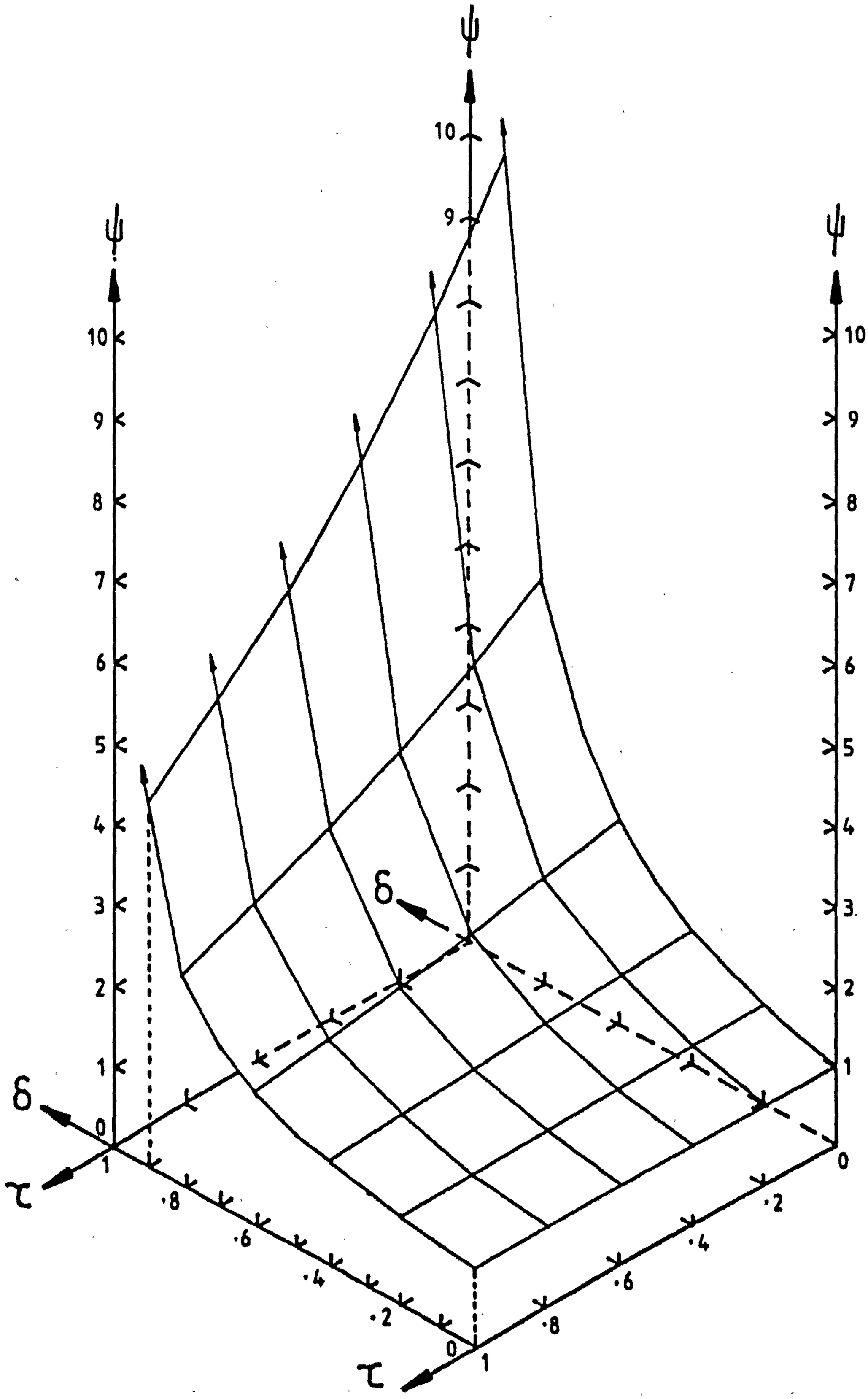

Fig. 6·7 Variation of integration factor ψ with normalised time ($0 \leq \tau \leq 1$) and parameter δ

to the development of a primary creep equation,

$$\varepsilon = \left[\frac{\sigma t^{\lambda}}{w\ (1 + \Theta)^{K}} \right]^{1/m} \qquad 6.17$$

where Θ is the temperature below 0°C in °C and λ, m, w and K are creep parameters. Klein (1978) simplified this to the temperature dependent expression of equation 6.4,

$$\varepsilon = A\sigma^{B}t^{C} \qquad 6.4$$

with parameters A, B and C.

Differentiation of equation 6.4 leads to a strain rate expression,

$$\dot{\varepsilon} = A\sigma^{B}Ct^{C-1} \qquad 6.18$$

As primary creep equations do not inflect, no expressions are available for determining the time to failure or the minimum strain rate.

6.5.3 Determination of parameters

The Fish equation (6.15) and the Klein equation (6.4) each require the determination of three parameters to enable the prediction of creep Strain. If creep strain rates are required, then a fourth parameter, m, is needed for Fish's equation (6.8).

Fish equation parameters can be determined from one short term (instantaneous) strength test and three constant stress creep

tests. The 'instantaneous' test should be conducted at a fast loading rate to provide an approximate value for σ_o. The creep tests then determined parameters $\tilde{C}$, m, n and δ, and also provide a value for the activation energy, E. E will be sensitive to the value of σ_o and it is unlikely that either of these will be true values.

Combining and rearranging equations 6.8, 6.10 and 6.11 gives:

$$T \text{ Ln} \left(\frac{t_m \, KT}{h} \right) = \frac{E}{R} + m \, T \text{ Ln} \left(\frac{\sigma_o}{\sigma} \right) \qquad 6.19$$

which can be used to determine values for E/R and m by plotting T Ln(t_mKT/h) vs T Ln(σ_o/σ) using the time to failure, t_m, and the applied stress, σ, from each test.

Fish determines parameter δ as the gradient of the Ln($\dot{\varepsilon}/\dot{\varepsilon}_m$) vs $f(\tau)$ graph for individual tests. The integration factor ψ can then be calculated from equation 6.16. A combination of equations 6.8, 6.10, 6.11 and 6.15 with $\tau = 1$ give:

$$\psi_m = \varepsilon_m / \dot{\varepsilon}_m t_m \qquad 6.20$$

which can be used directly to calculate the integration factor at failure. In conjunction with Fig. 6.7, the parameter δ may be obtained from ψ_m and by this method, less information is required from the creep test than by the method suggested by Fish.

As δ is constant for all tests at any sub zero temperature, an average value is taken.

A combination of equations 6.12 and 6.13, with the substitution $\tilde{C}$ = C exp (-δ), gives:

$$Ln(\dot{\varepsilon}_m t_m) = Ln(\tilde{C}) + n\ Ln\left(\frac{\sigma}{\sigma_o}\right) \qquad 6.21$$

and the parameters $\tilde{C}$ and n determined from a plot of $Ln(\dot{\varepsilon}_m t_m)$ vs $Ln(\sigma/\sigma_o)$. Fig. 6.8 shows the relevant plots for determining the Fish parameters for LAF sand. The applied stress ratio (ASR) was used in place of σ/σ_o in these plots and also in the determination of the parameters for LAL and KM. Results for all three materials are shown in Table 6.1.

For a single constant stress creep test, the Klein equation (6.4) can be expressed as:

$$\varepsilon = K\ t^C \qquad 6.22$$

and strain rate obtained from,

$$\dot{\varepsilon} = KC\ t^{C-1} = \varepsilon\ C\ t^{-1} \qquad 6.23$$

Traditionally, equation 6.22 has been used to determine parameter C by plotting data in co-ordinates of Ln ε vs Ln t,

$$Ln\ \varepsilon = Ln\ K + C\ Ln\ t \qquad 6.24$$

Both Vyalov and Klein obtain a series of parallel lines with gradient C from this plot. Parameters A and B are subsequently found by plotting the intercept Ln K against Ln σ,

$$Ln\ K = Ln\ A + B\ Ln\ \sigma \qquad 6.25$$

to obtain a linear relationship.

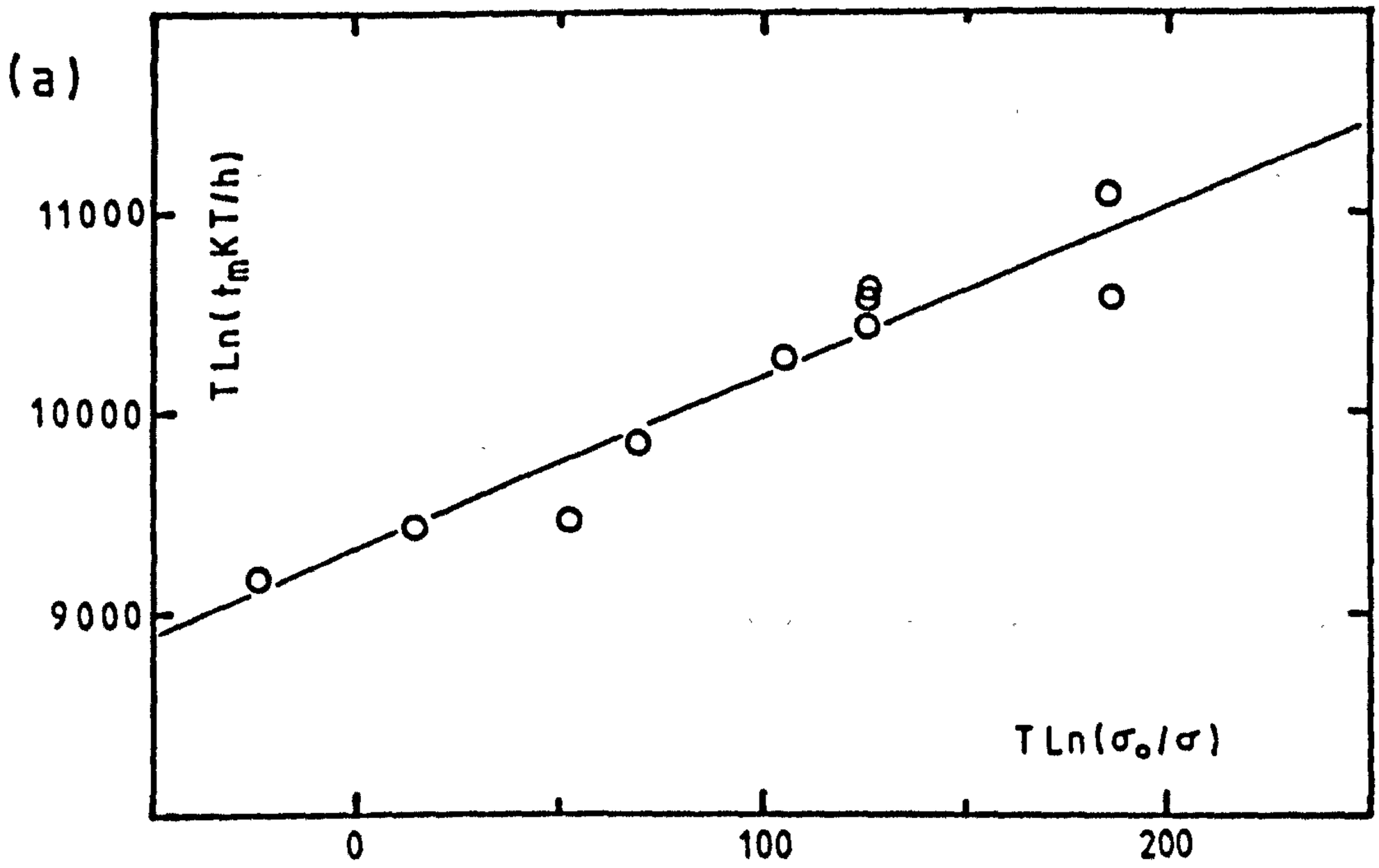

Fig.6·8 Fish equation parameter determination for LAF sand (CS creep tests)

132

Table 6.1 Creep test parameters for FISH model (equations 6.8 and 6.15)

Material	σ_o (approx) MPa	E KJ/ mole	m	δ	ψ_m	$\tilde{C}$	n
LAF	12.9	77.5	8.6	0.74	2.18	0.07	0.15
LAL	15.4	82.0	2.6	0.81	2.72	0.53	1.1
KM	4.0	70.9	11.4	0.72	2.07	(0.01)*	(-2.3)*

* Best fit to data yields n value < 0

Table 6.2 Creep test parameters for KLEIN model (equation 6.4)

Material	A -B -C MPa hrs	B	C
LAF	0.49	3.08	0.43
LAL	0.44	0.79	0.36
KM	1.37	1.78	0.47

Less information is required from each creep test if C is calculated from equation 6.23 and K from equation 6.22, at any time during the test. An average value of C is assumed, to account for variations between tests. Fig. 6.9 shows the Ln K - Ln σ plot for LAF, and the three parameters A, B and C determined for each material are listed in Table 6.2.

6.5.4 Comments on uniaxial creep models

Both the Fish and Klein models make assumptions about the acceptable values for the various creep parameters, based either on theory or on observation. Experimental results obtained in this study question the validity of these assumptions.

Fish suggests that his parameter δ is a material constant, independent of both stress and temperature, but values of δ obtained from individual creep tests on LAF sand, all at -10°C, show a strong dependence on the applied stress (Table 6.3, Fig. 6.10). Choosing a mean value for δ will lead to a significant disparity between experimental and predicted strains in the early stages of creep.

A similar problem is found with Klein parameter C. Table 6.3 also lists the C values calculated for uniaxial LAF tests and once more a clear variation with stress is apparent. Thus, it would appear that the assumption by both Vyalov and Klein, that C is a material constant independent of stress, is an overgeneralization and not applicable to the three series of tests reported here.

6.6 Triaxial creep model

The parameter C, calculated from equation 6.23, has been seen to vary with applied stress and, hence, ASR. For LAF this is shown in Fig. 6.11a, which includes both uniaxial and triaxial test data. The confining pressure range covered is 0 to 6 MPa. A

Table 6.3 Calculated creep parameters for individual LAF tests

Test No.	ASR	FISH		KLEIN	
		δ	ψ_m	C	K
S30	110	0.60	1.65	0.60	40.8
S31	77	0.68	1.90	0.53	13.4
S32	95	0.63	1.74	0.58	33.1
S43	82	0.58	1.61	0.62	66.6
S66	62	0.81	2.66	0.38	6.6
S67	62	0.82	2.77	0.36	7.8
S68	49	0.81	2.69	0.37	3.8
S69	62	0.81	2.66	0.38	7.1
S70	49	0.87	3.71	0.27	3.8
S73	67	0.77	2.35	0.43	8.8
Mean		0.74		0.43	

Table 6.4 Parameters for modelling triaxial creep behaviour using equation 6.27

Material	A -B -C* MPa hrs	B	N	H
LAF	0.75	2.56	0.015	0.80
LAL	0.54	0.60	0.042	0.62
KM	0.06	5.60	0.019	0.82

* $C = N(ASR)^H$ $\therefore$ units of A vary with ASR

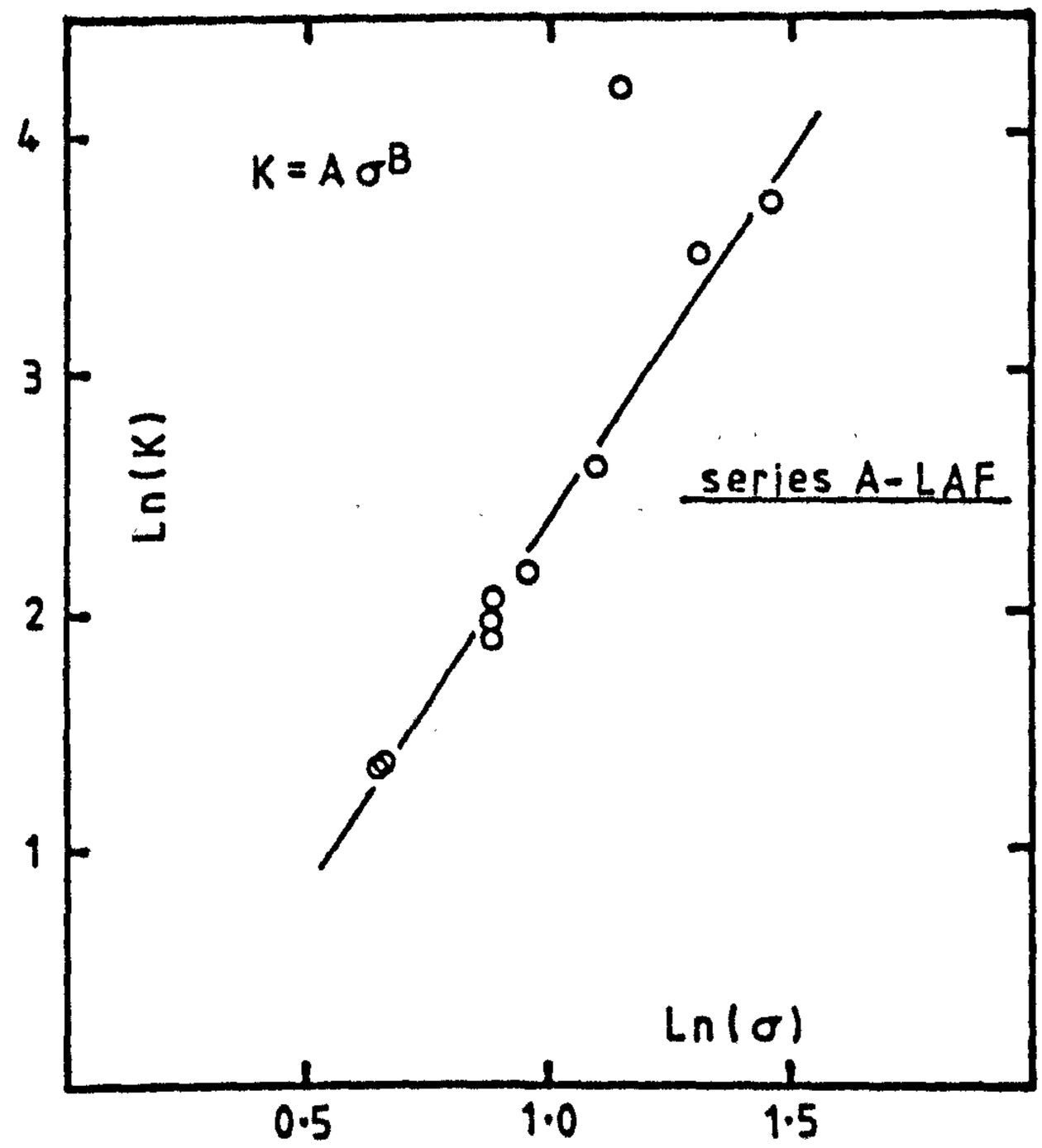

Fig. 6·9 Determination of stress dependent parameters in Klein equation

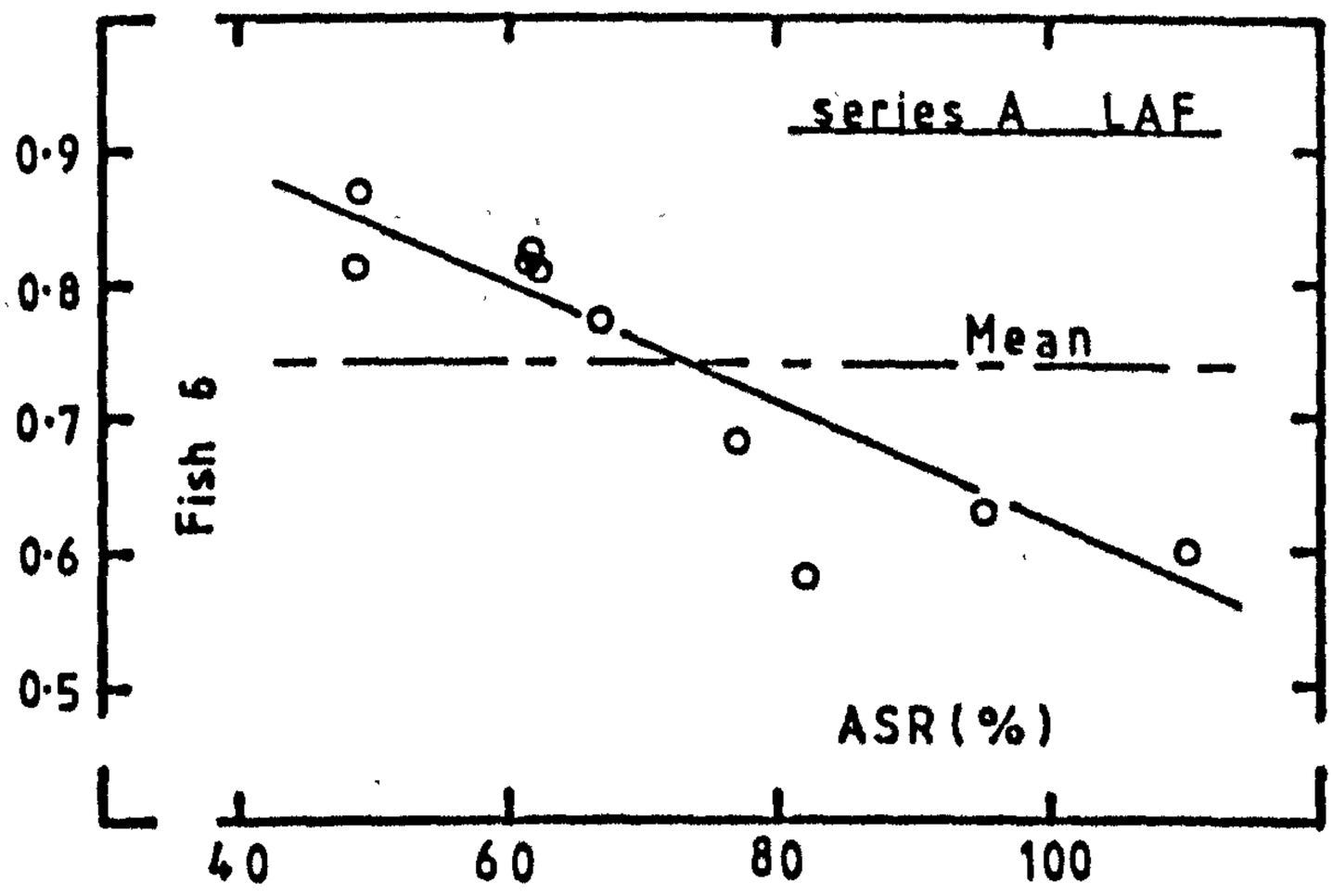

Fig. 6·10 Variation of Fish parameter 6 with ASR for LAF sand

relationship of the form,

$$C = N\ (ASR)^{H} \qquad 6.26$$

where N and H are temperature dependent constants, can be fitted to this data. Equation 6.26 is seen to be independent of confining pressure over the range tested.

This leads to the development of a new triaxial creep equation,

$$\epsilon = A\ (\Delta\sigma)^{B}\ t^{N(ASR)^{H}} \qquad 6.27$$

based on the uniaxial models of Vyalov and Klein. Fig. 6.11b shows how substitution of the deviator stress, $\Delta\sigma$, for the uniaxial stress, σ, reduces equation 6.25 to a unique triaxial relationship. Parameters A and B, in equation 6.27, are nominally the same as those in equation 6.4. Creep test data for the confining pressure range 0 to 1 MPa is presented in Figs. 6.12 and 6.13 for LAL sand and KM clay respectively, and the parameters obtained from these plots are collected into Table 6.4.

By incorporating the effects of confining pressure into the dimensionless stress ratio (ASR), equation 6.27 becomes valid under both uniaxial and triaxial stress conditions. This is an important advance on the triaxial equation proposed by Diekmann and Jessberger (1982),

$$\epsilon = m\ (\Delta\sigma)^{P}\ \sigma_3{}^{n}\ t^{s} \qquad 6.28$$

which reduces to $\epsilon = 0$ under uniaxial conditions.

137

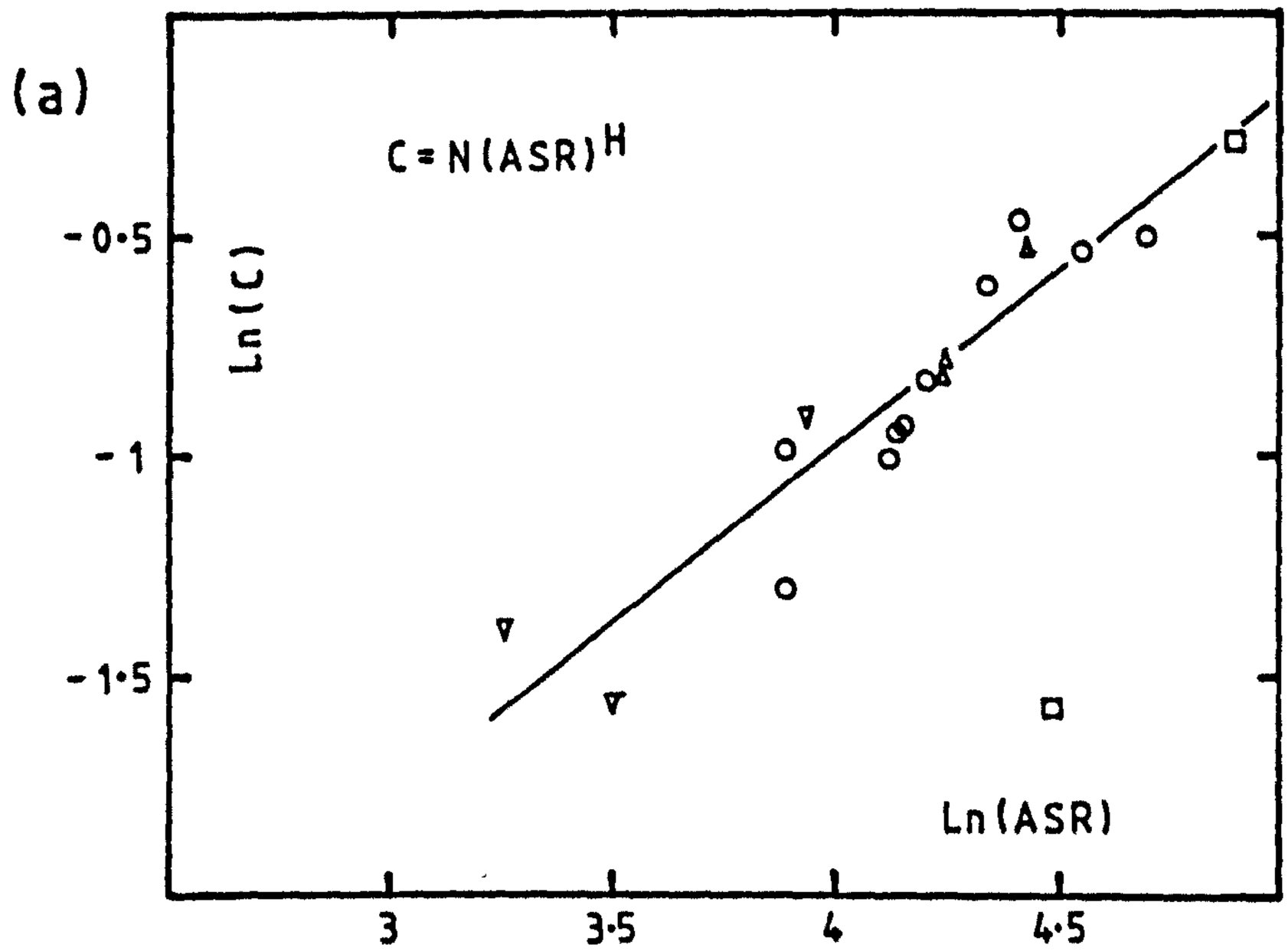

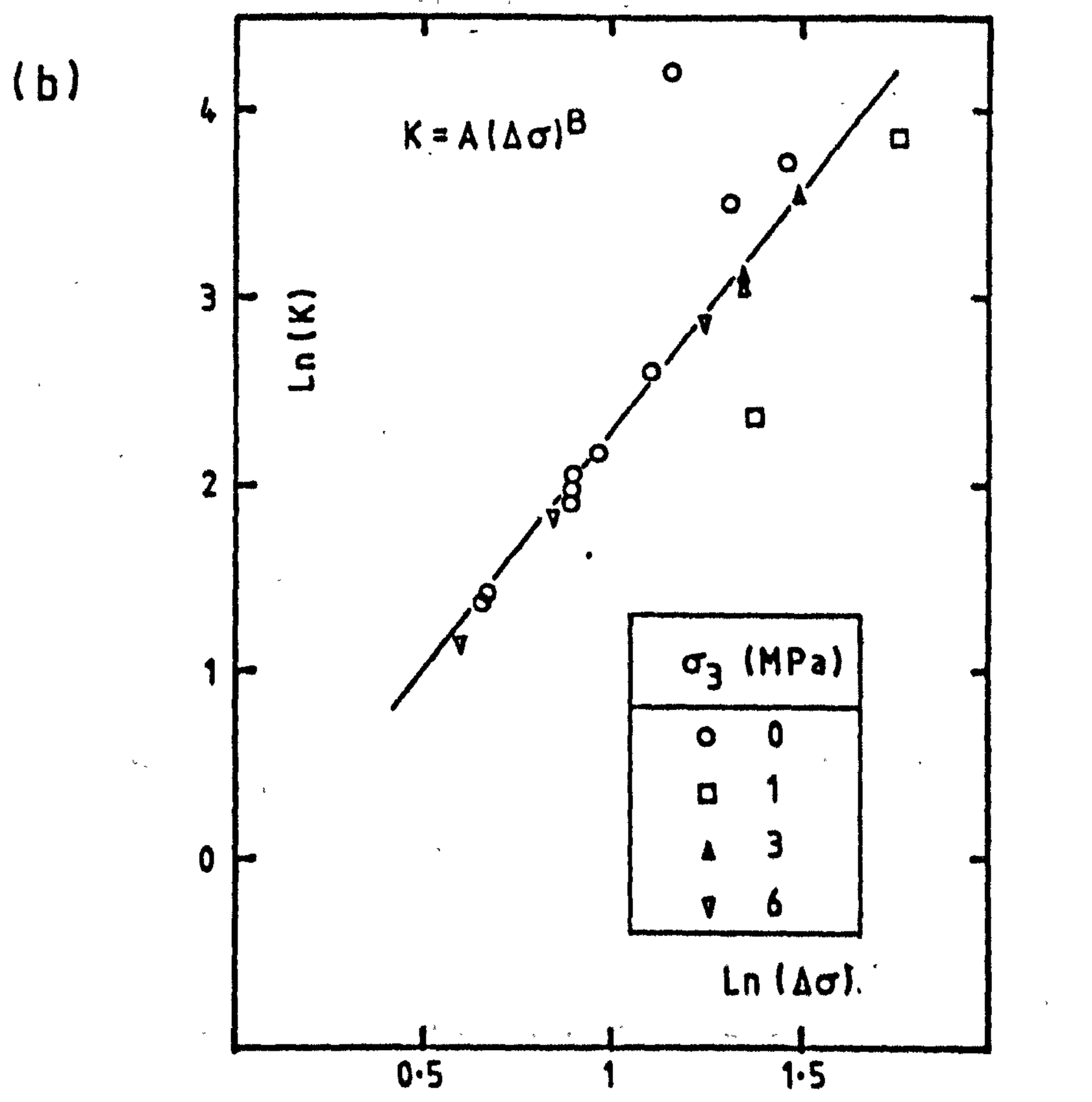

Fig. 6·11 Parameter determination for equation 6·27 using triaxial LAF data

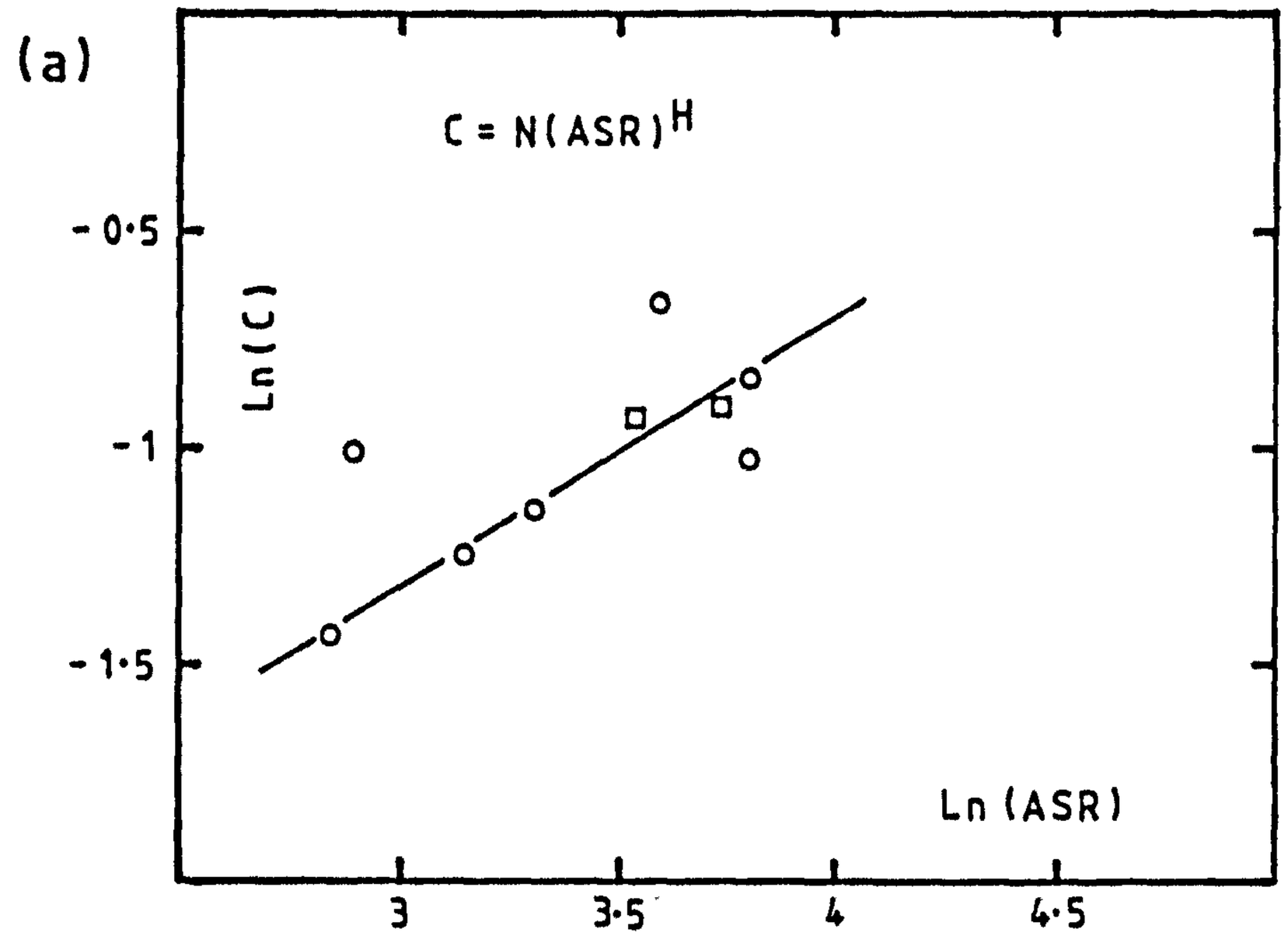

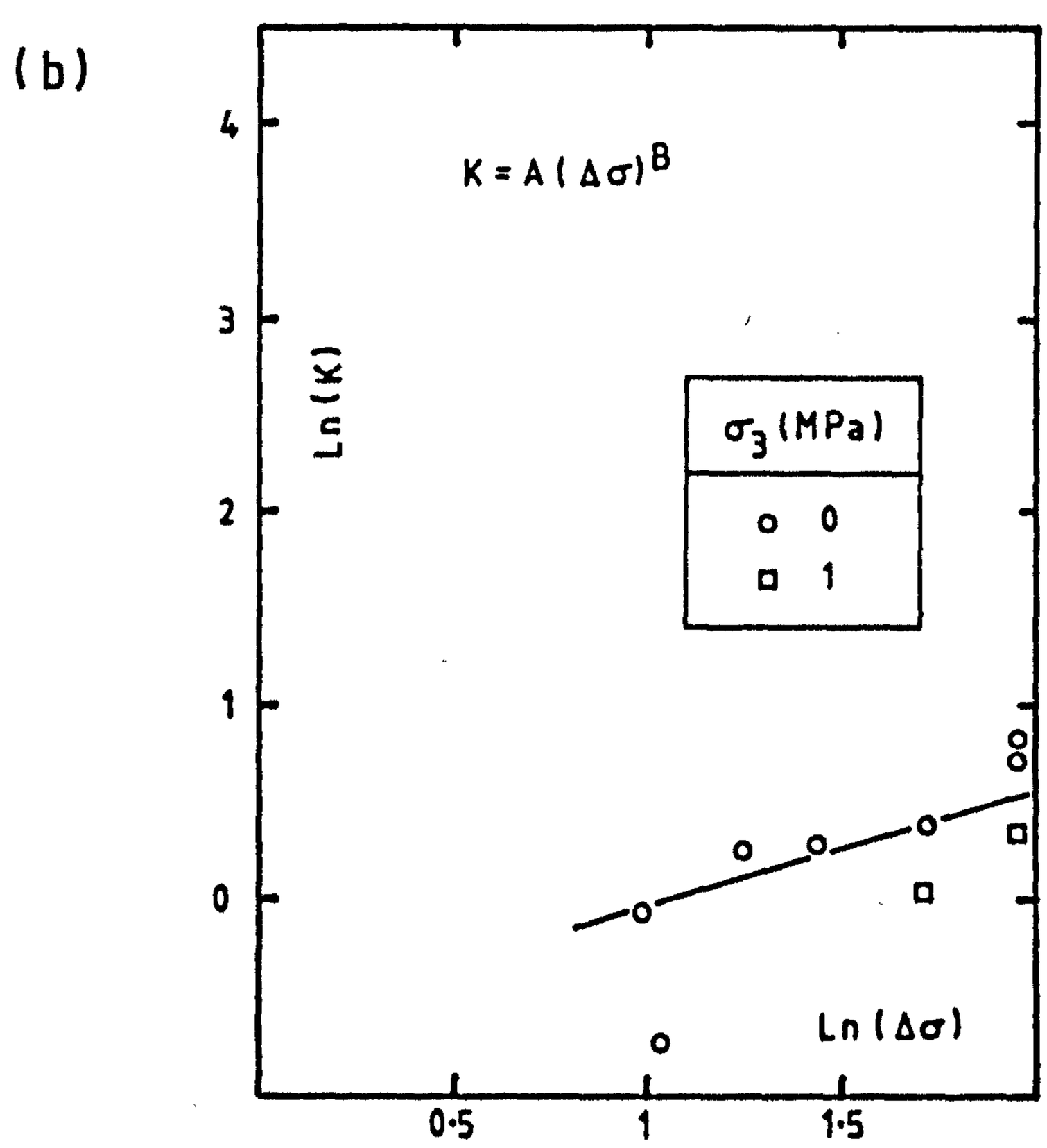

Fig. 6·12 Parameter determination for equation 6·27 using triaxial LAL data

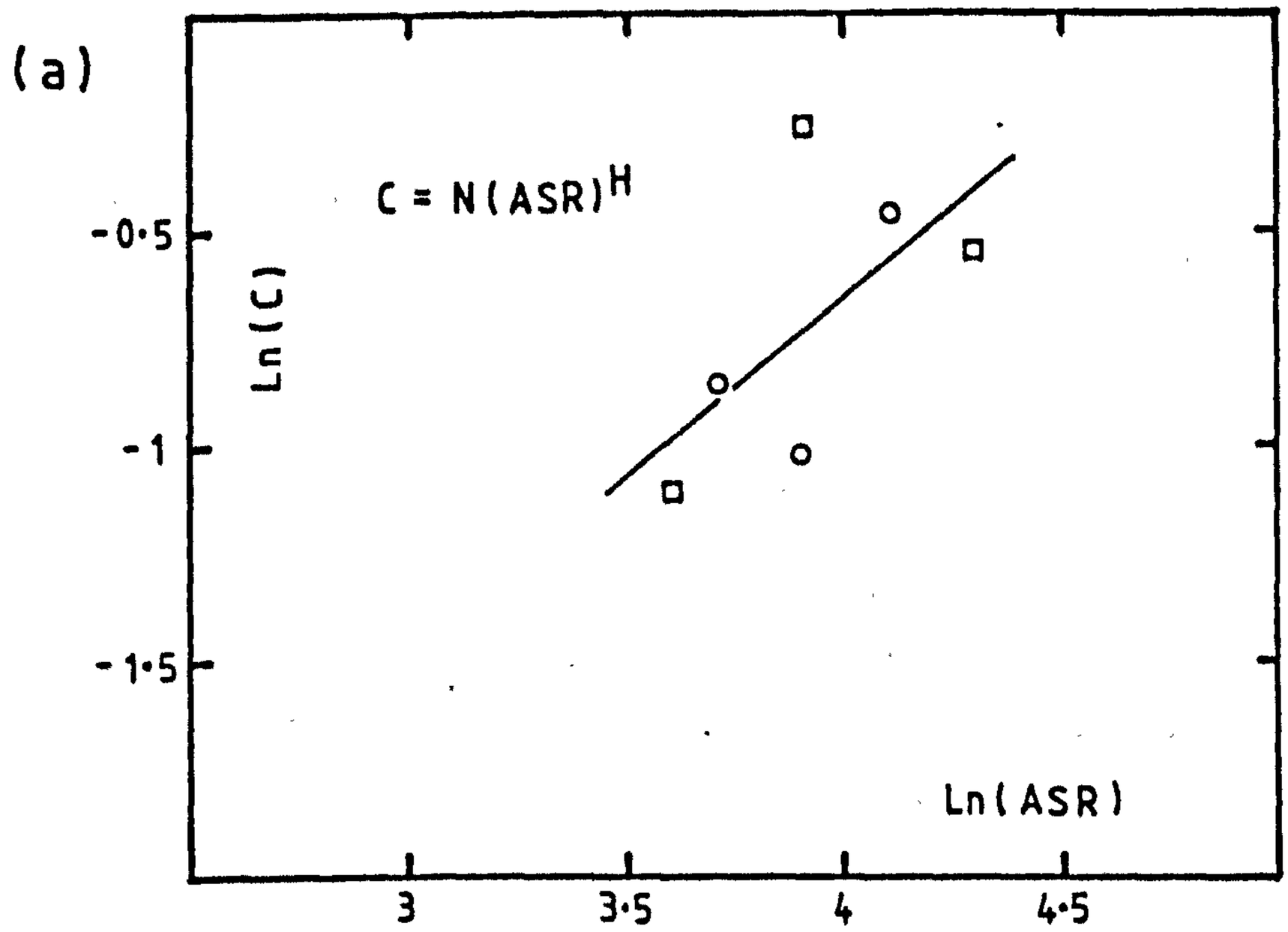

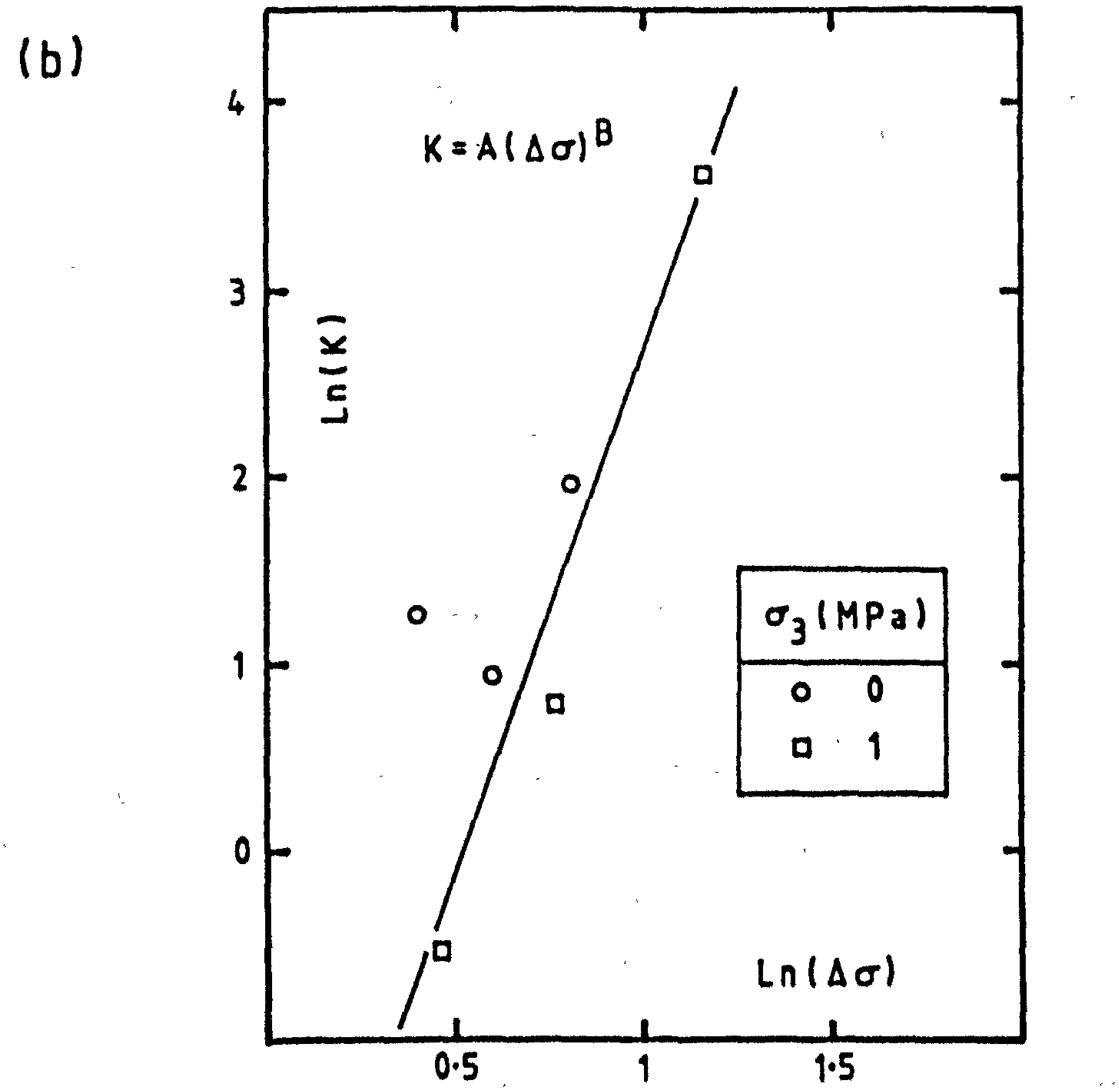

Fig. 6·13 Parameter determination for equation 6·27 using triaxial KM data

Equations 6.27 and 6.28 are empirically based primary creep equations capable of predicting creep upto the failure point. An empirical approach by Orth and Meissner (1982) produced another triaxial model which took account of heat and water flow rates through the soil. The resulting tertiary creep model involves a complex series of equations to evaluate parameters and requires data input on material properties such as void ratio, permeability, thermal conductivity and volumetric heat capacity.

The new creep equation (6.27) requires just four laboratory tests to determine all the parameters, as both equations 6.25 and 6.26 are independent of confining pressure. A plot of Ln(K) vs Ln($\Delta\sigma$) will yield parameters A and B and a plot of Ln(C) vs Ln (ASR) yields N and H. A uniaxial constant strain rate test can provide the normalising stress to define three ASR values for subsequent uniaxial creep tests. Thus, although equation 6.27 predicts triaxial creep strain, the parameters may be defined by uniaxial tests in the laboratory.

6.7 Analysis of models

To investigate the quality of fit of the individual models, normalised strain-time curves can be used. The axes in these plots are normalised with respect to the strain and time at the failure point m, so that experimental data will pass through the point (1,1). The creep equations 6.15, 6.4 and 6.27 are also normalised with respect to the experimental failure conditions to show deviations from the actual results for the duration of the test.

Examples of normalised plots for LAF creep tests are shown in Figs. 6.14 to 6.17. The lower diagram in these figures shows the quality of fit of each equation by plotting the ratio calculated strain:measured strain against normalised time.

From the uniaxial creep tests shown in Figs. 6.14 and 6.15, it is clear that no single creep equation consistently provides the

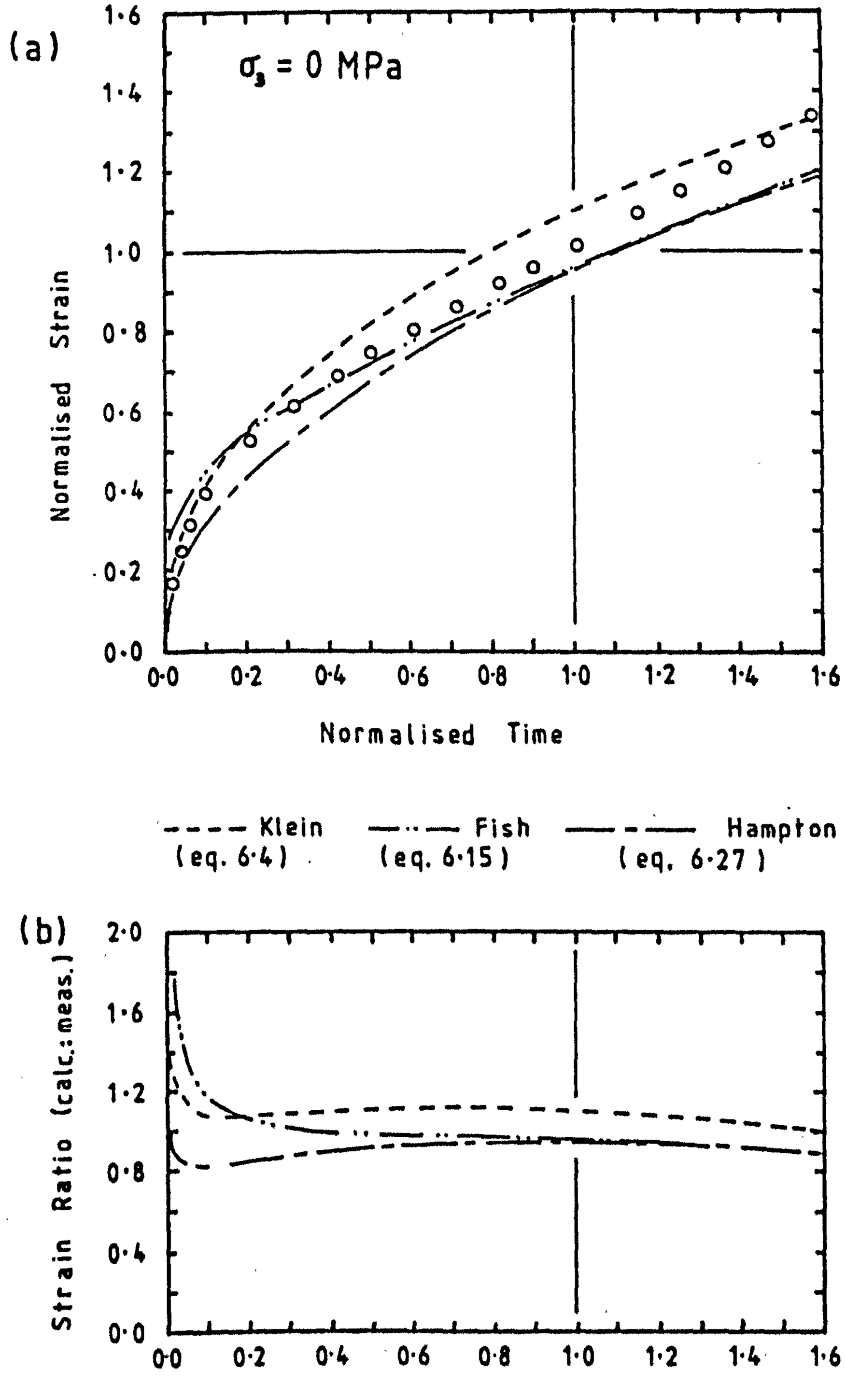

Fig. 6·14 a) Normalised creep strain curve and b) model fit analysis for test S31

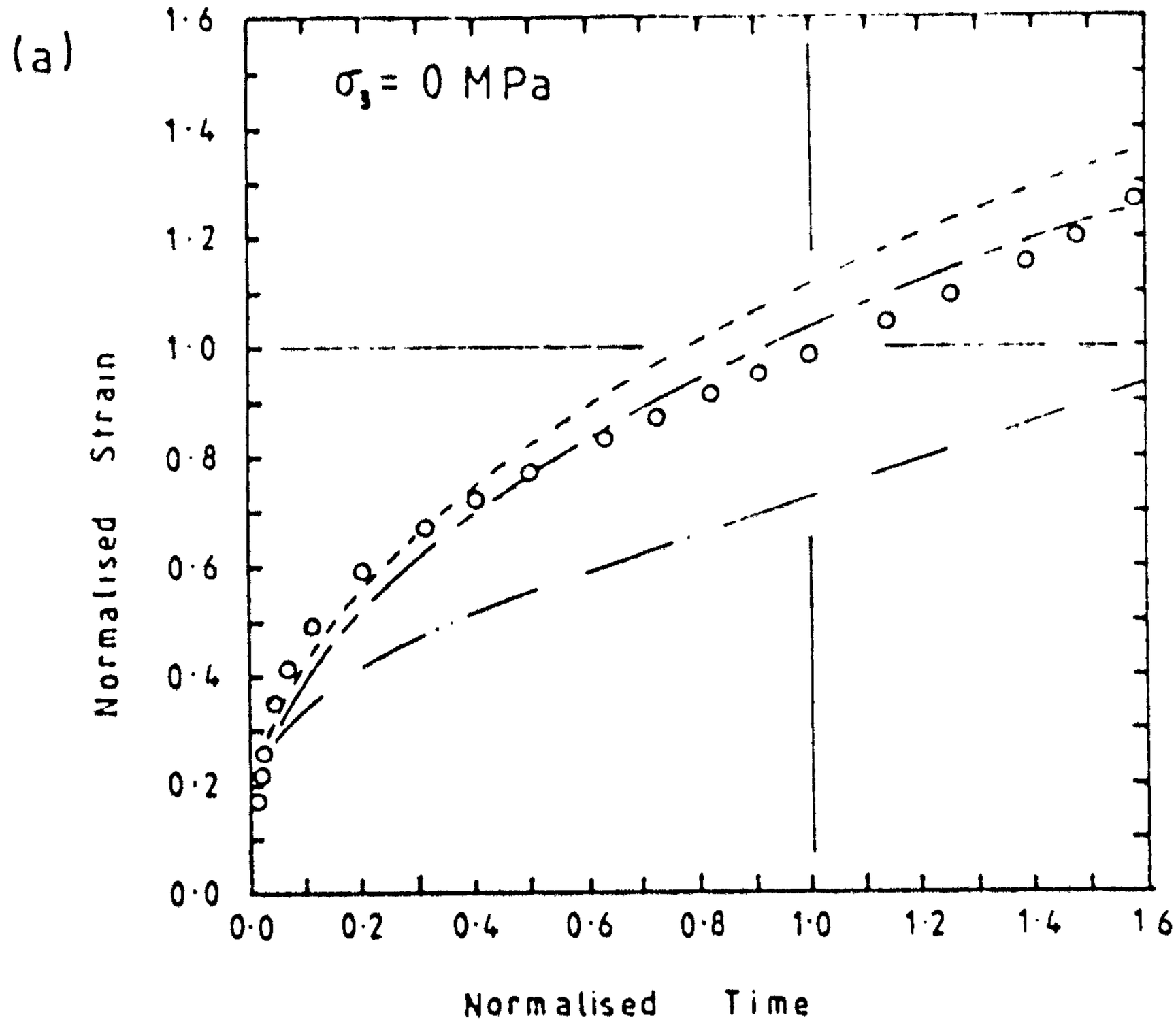

Fig. 6·15 a) Normalised creep strain curve and b) model fit analysis for test S73

best model of the creep process. This is as much due to the variability of the soil structure as to the approximations made in determining the equation parameters. The errors in the models are generally generated in the early stages of creep when the strain rate is high and this is reflected by the calculated: measured strain ratio staying approximately constant beyond t/t_m = 0.3.

Figs. 6.16 and 6.17 show triaxial creep tests at 3 and 6 MPa confining pressure. Equation 6.27 is once again seen to settle to a fairly constant error after an early deviation. The quality of fit of the triaxial creep equation to test data at σ_3 = 3 MPa (S78) and σ_3 = 6 MPa (S64) is seen to be excellent in the range of normalised time plotted.

6.8 Summary

The classical three stage interpretation of the creep strain vs time curve has been superseded by a two-stage interpretation. The inflection point between the two stages marks the onset of strain acceleration and is, thus, the failure point for engineering design. In engineering applications, serviceability is the limiting factor in design and the primary creep stage is the main consideration.

Equations to model the creep process can be divided into three categories: Secondary, the simplest form which approximates creep to an instantaneous strain followed by a period of constant strain rate; Primary, which allows strain to build up at a decreasing rate, and Tertiary, which includes both strain acceleration and deceleration to approximate the whole process. Only Primary and Tertiary models are able to map onto creep data in the primary creep stage.

Creep data from both uniaxial and triaxial tests on three materials (LAF and LAL sands, KM clay) is presented in the form of the inflection point details t_m, ϵ_m and $\dot{\epsilon}_m$. Taken

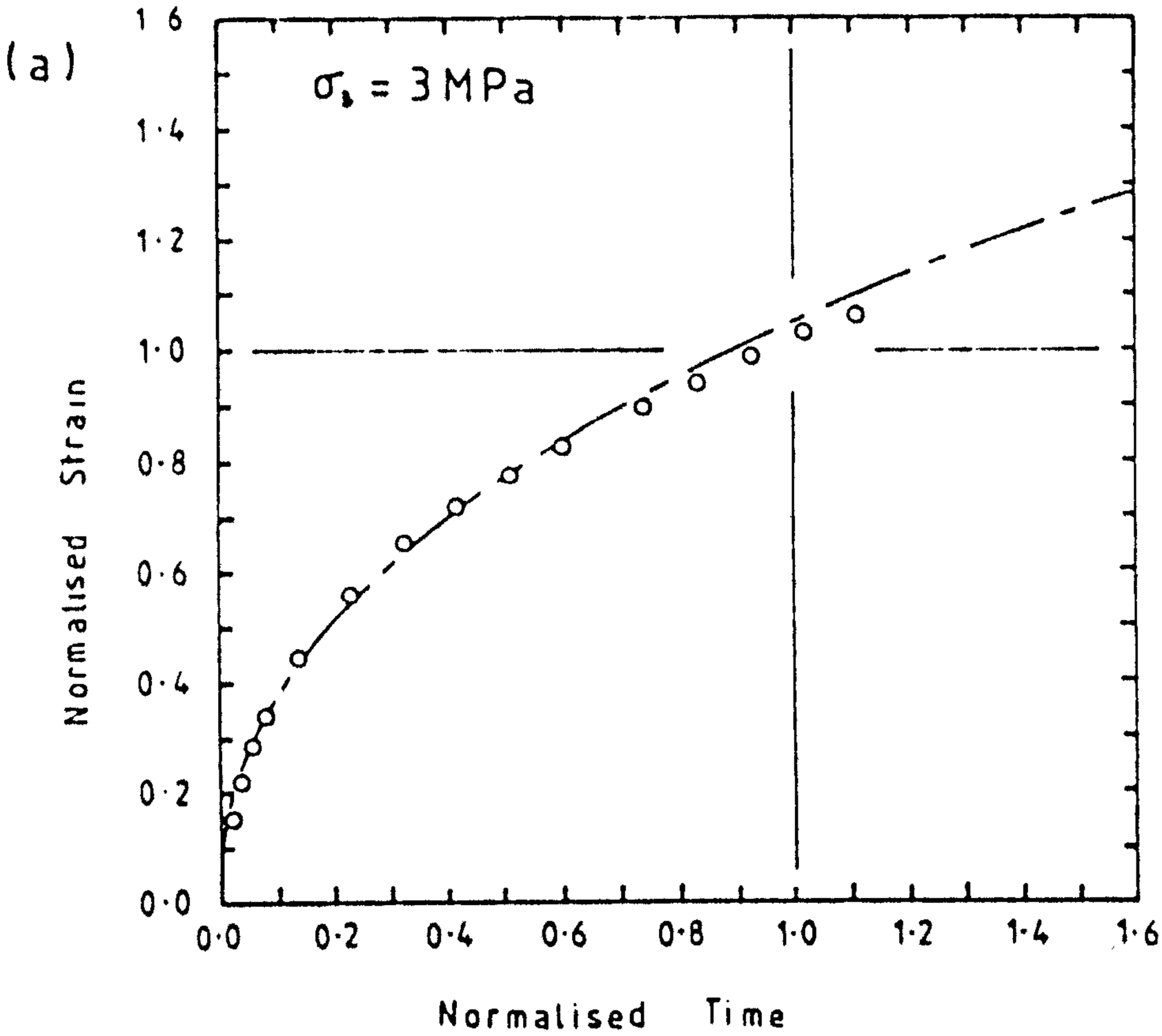

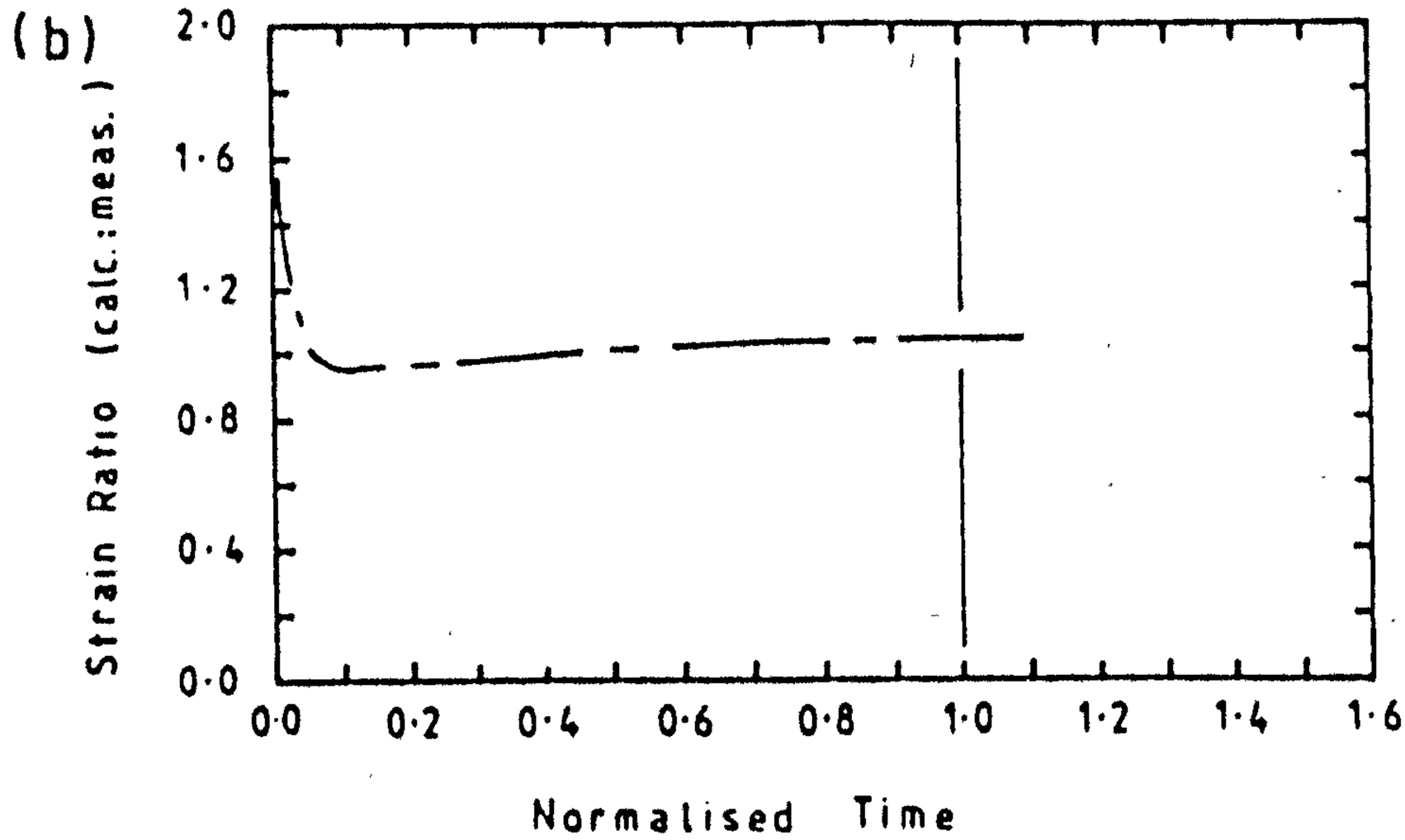

Fig. 6·16 a) Normalised creep strain curve and b) model fit analysis for test S78

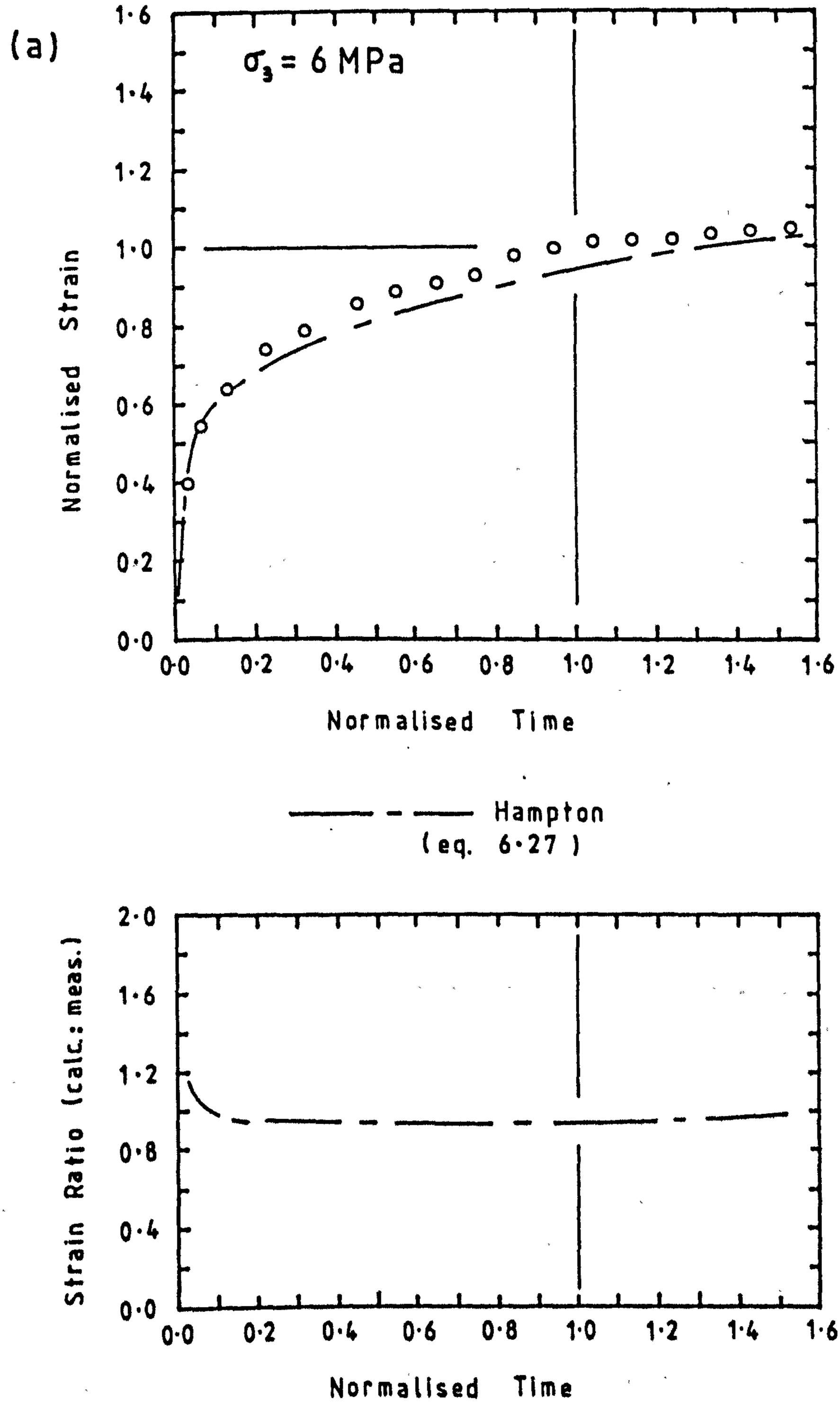

Fig. 6·17 a) Normalised creep strain curve and b) model fit analysis for test S 64

individually, these parameters show a high degree of scatter when plotted against the applied stress ratio (ASR) but distinct relationships are shown in Fig. 6.6, $Ln(\dot{\epsilon}_m)$ vs $Ln(t_m)$, and Figs. 6.11a, 6.12a and 6.13a, $Ln(\dot{\epsilon}_m t_m/\epsilon_m)$ vs Ln(ASR), where the inflection point details are combined. $Ln(\dot{\epsilon}_m)$ vs $Ln(t_m)$ plots, previously shown to be linear and independent of temperature, are now shown to be independent of confining pressure.

Uniaxial creep equations devised by Fish (1983) and Klein (1978) have been examined and the required parameters have been determined from the LAF creep test data. Methods other than those proposed by the original authors have been devised to determine the necessary parameters. The new methods reduce the amount of experimental data needed. The Fish parameter δ and Klein parameter C are seen to be stress dependent and not constant, as suggested by the authors.

Based on the uniaxial Klein equation and observations of the variation of C with ASR, a new triaxial creep equation is proposed which is valid for both uniaxial and triaxial test conditions,

$$\epsilon = A\ (\Delta\sigma)^B\ t^{N(ASR)^H} \qquad 6.27$$

The parameters A and B are nominally the same as for the Klein equation and, as such, it is possible to determine them from uniaxial tests alone. Least squares fits through the uniaxial data (Fig. 6.9) and combined uniaxial/triaxial data (Fig. 6.11b) yield different values for A and B with LAF sand, but the net effect is negligible over the deviator stress range covered. Equation 6.27 has been shown to be valid upto confining pressures of 6 MPa.

All three creep equations give adequate predictions of strain under uniaxial conditions but none of them is consistently superior. The physical structure of the specimens has a considerable effect on the mechanical properties and may be the main contributor to this erratic behaviour.

CHAPTER 7

IMPLICATIONS OF FINDINGS

7.1 INTRODUCTION

The work presented in this thesis has covered the equipment available for testing frozen soils in the laboratory, and the results obtained from a range of materials subjected to two types of loading. In this chapter, the implications of these results and the subsequent methods of analysis will be examined.

The triaxial creep equation developed in Chapter 6 is well suited to engineering applications where pre-failure conditions are to be modelled. The parameters for this equation were shown to be obtainable from a limited number of short and long term strength tests in the laboratory. Having been developed from the uniaxial creep equation of Klein, the parameters A and B are theoretically the same as when calculated from uniaxial data only. The results quoted do, however, vary considerably and in this chapter the effect this may have on the ability of the equation to model creep strain is investigated.

A further set of values of the four parameters A, B, N and H are presented in section 7.2. These parameters are determined at an earlier stage of the creep process (pre-failure) to demonstrate the flexibility available in this model. This approach enables laboratory tests to be terminated before failure is reached, which in turn, extends the applicability of test equipment to a greater range of materials. It also allows tests at high confining pressures, typically associated with high strains at failure, to be included in the analysis.

The chapter goes on to show how the new triaxial equation may affect design by considering a simplified analysis of a shaft sunk through frozen ground. In section 7.4, the results are compared with those obtained with the uniaxial Klein equation when applied across the same ice wall. The lower strains predicted by the new equation are attributable to the way the applied stress ratio (ASR) is able to accommodate changes in strength with confining pressure and temperature.

7.2 Advantages of empirical creep equations

The classic shape of a uniaxial creep curve (Fig. 6.1) has allowed an analytical approach to modelling based on the stress dependence of the failure point, m. Under triaxial stress conditions, the mode of failure becomes more plastic, leading to an extended period of primary creep before failure.

In a triaxial cell, the applied stress is kept constant during a creep test by assuming the soil deforms as a right cylinder of constant volume. At high strains this is not the case for most frozen soils and a meaningful failure point may not be reached under high confining pressures.

The empirical triaxial equation (6.27), introduced in the previous chapter, does not rely on the laboratory tests reaching an inflection point on the strain-time curve in order that its parameters be determined. In Figs. 6.11 and 6.13, the parameters C and K were obtained at the failure point of each of 18 tests on LAF sand. A further eight tests were excluded as no definite failure was observed. These eight tests included two at σ_3 = 10.2 MPa and one at σ_3 = 11.2 MPa. Equation 6.27 models the creep deformation through the primary stage and into what is effectively a period of near constant strain rate at high confining pressures. For a perfect correlation with the test data, the parameters C and K will be constant at all points along the curve and may be calculated from any set of t, ϵ and $\dot{\epsilon}$ data. As correlation is not perfect, some standardisation is needed, such as the failure point on each curve. A useful alternative is the transition point between primary and secondary creep (subscript ps),

$$C_{ps} = \dot{\epsilon}_{ps}\ t_{ps}/\epsilon_{ps} \qquad 7.1$$

$$K_{ps} = \epsilon_{ps}\ t_{ps}^{-C} \qquad 7.2$$

Parameters K_{ps} and C_{ps} obtained from each test are plotted on logarithmic scales against Ln($\Delta\sigma$) and Ln(ASR) in Fig. 7.1. The four parameters A, B, N and H obtained from the slopes and intercepts of straight lines through this data, are collected into Table 7.1.

Table 7.1 Parameters for equation 6.27 obtained from primary-secondary transition point data

Material	Eqn 6.27 Parameters			
	A	B	N	H
LAF	1.65	1.94	0.0033	1.06

In Figs. 7.1a and 7.1b, four tests have been distinguished by arrows. The values of K and C plotted for these tests were calculated from the conditions prevailing at the end of the test. These tests had not entered the apparent secondary creep period and the data plotted is not truely consistent with the primary-secondary transition point. Two other specimens appeared much weaker (S43) and stronger (S19) than the rest. Full details of the time, strain and strain rate data used in this analysis appear in Appendix B.

7.3 Sensitivity analysis for triaxial creep model

During the analysis of the creep behaviour of LAF sand, three tables have been presented which include values of the parameters A and B for use in both equations 6.4 and 6.27. Table 6.2 is

based on uniaxial data and includes parameter C (eqn 6.4) which is given a constant mean value. Tables 6.4 and 7.1 are based on triaxial data at the inflection point and primary-secondary transition point respectively. The latter two tables include parameters N and H for equation 6.27. Table 7.2 summarises these results.

Table 7.2 Summary of creep equation parameters determined for LAF sand

Original Table No.	Method of Evaluation*	No. of Tests	Parameters				
			A	B	C	N	H
6.2	Uniaxial(m)	10	0.49	3.08	0.43	-	-
6.4	Triaxial(m)	18	0.75	2.56	-	0.015	0.80
7.1	Triaxial(ps)	26	1.65	1.94	-	0.0033	1.06
Mean Values			0.85^{+}	2.53	0.43	0.007^{+}	0.93

* (m) = at inflection point, (ps) = at end of primary

\+ Based on mean values of Ln(A) and Ln(N)

Each method of analysis has produced a different value for each parameter. To investigate the effect this has on strains calculated by equation 6.27, the following sensitivity analysis is based on an imaginary soil (soil X) with properties similar to those of LAF sand. The creep behaviour of soil X can be exactly modelled by equation 6.27 with parameters having the values shown in Table 7.3.

Fig. 7.2 shows a creep test at $\Delta\sigma$ = 2 MPa (ASR = 50%) in both

153

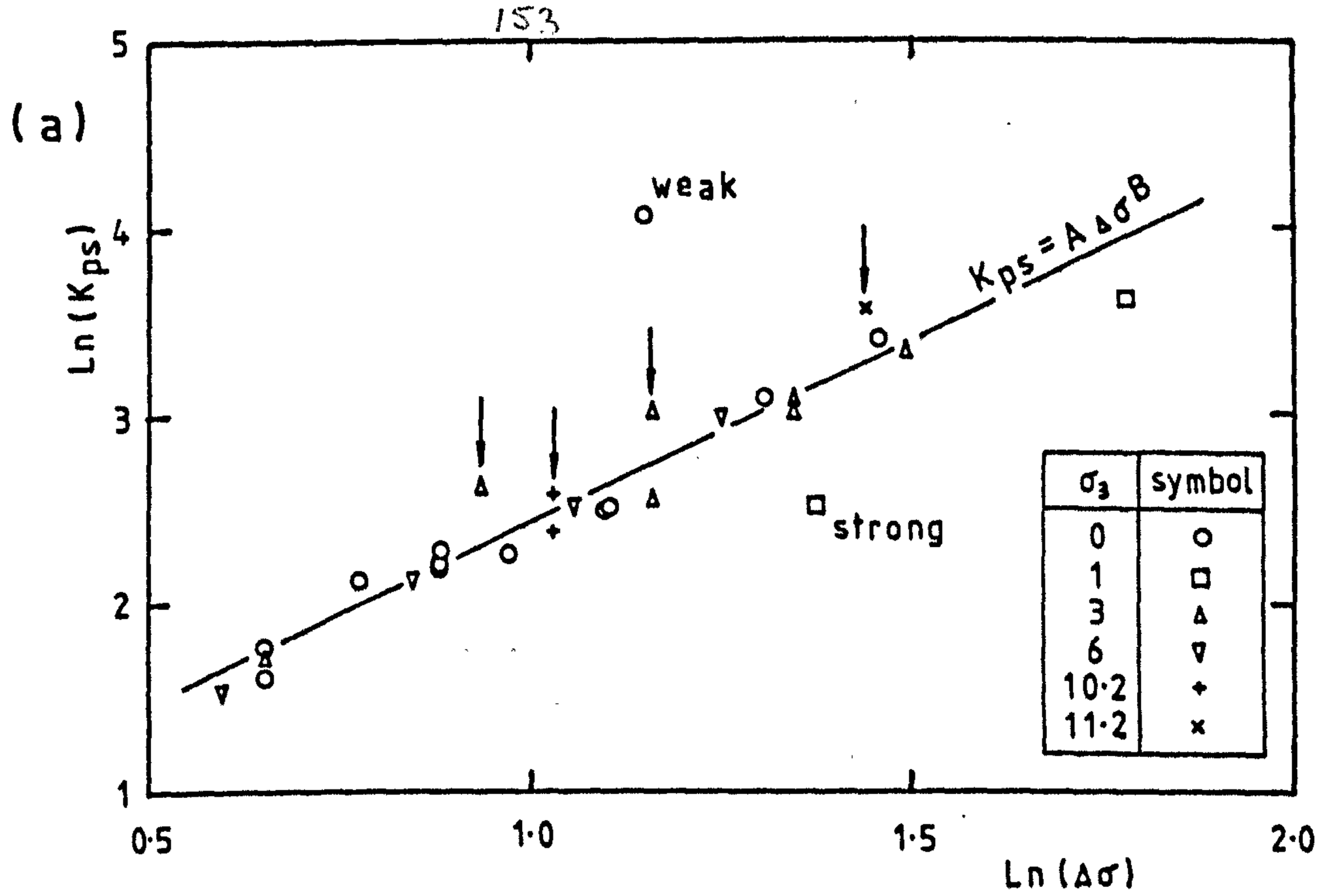

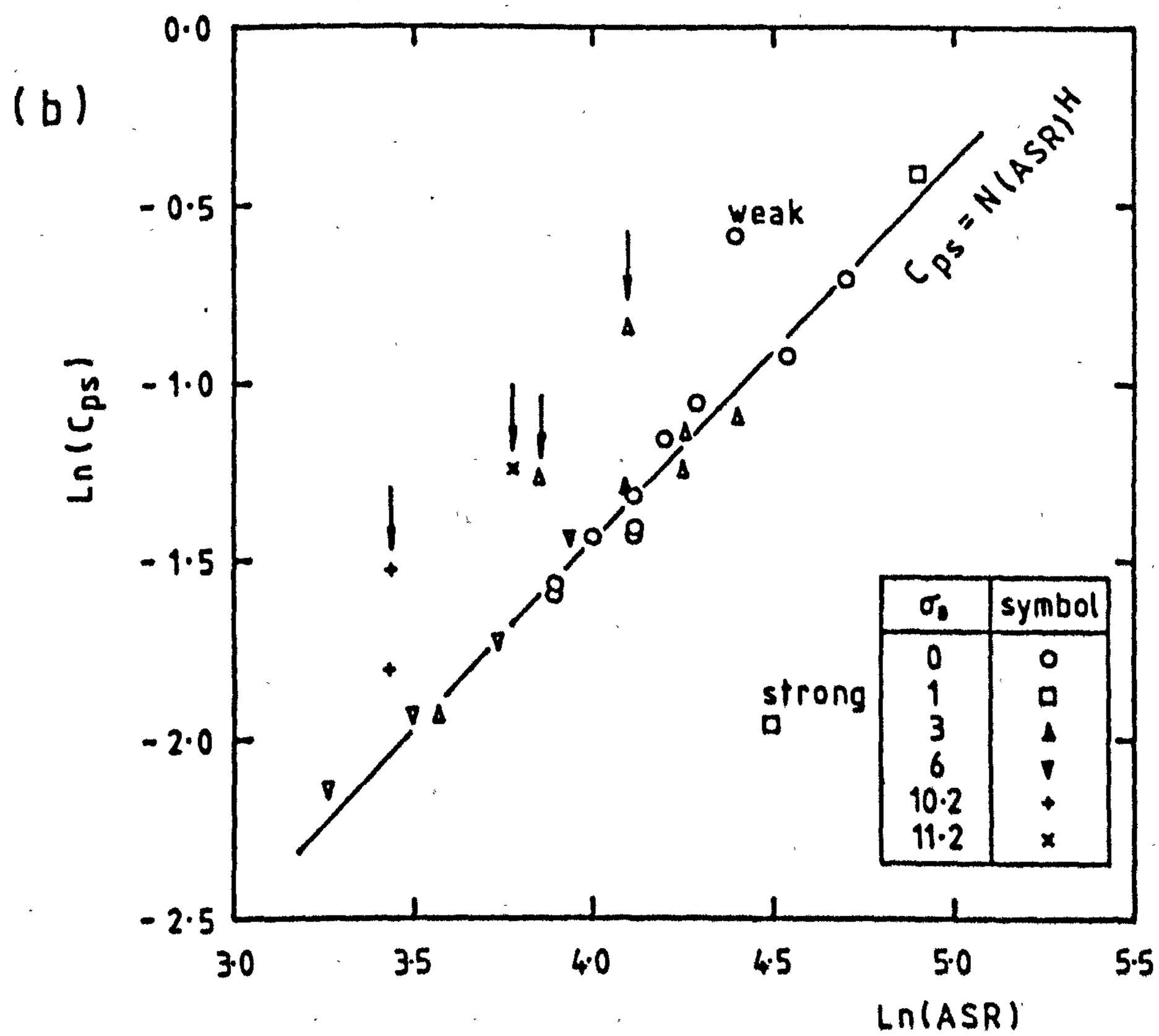

Fig. 7·1 Primary - secondary transition point data for LAF sand, used to determine parameters in equation 6·27.

strain vs time and Norm strain vs Norm time plots. Failure occurs at t_m = 8 hrs and equation 6.27 is shown to map perfectly onto the data upto this point. Strain at failure is 16%.

The effects on the calculated strain of varying each parameter in turn are shown in Fig. 7.3. The abscissa of each plot is the variable parameter normalised with respect to the true values listed above. The ordinate (ε_{Nt}) is the calculated strain normalised with respect to the true strain at the same normalised time, t_N. Figs. 7.3a and 7.3b show single relationships for all values of t_N, while Figs. 7.3c and 7.3d show that the errors incurred by incorrect values of N and H, accumulate with time.

Errors in the determination of parameters will commonly result from experimental errors during testing and from variability amongst specimens. The scatter of results when plotted on Ln(K) vs Ln($\Delta\sigma$) and Ln(C) vs Ln(ASR) axes may lead to the incorrect choice of straight line fits. The error produced is likely to be of a pivotal nature (Fig. 7.4) which pairs high values of A or N with low values of B or H. The nett effect of errors of this nature is significantly smaller than single errors in any one parameter. Deviations from the true value of strain are of opposite sign and result in a certain amount of cancellation of errors.

In Fig. 7.5, the pivotal errors shown in Fig. 7.4 are converted to strain by equation 6.27 and superimposed on the plots of ε_{Nt} vs Norm A (for all t_N values) and ε_{Nt} vs Norm N (for t_N = 1). Induced errors are seen to be minimal. Comparing Figs. 7.5a and 7.5b also shows that errors in determining A and B have a far greater affect on strain than do similar errors in N and H. This may be accounted for by reference to the ranges of $\Delta\sigma$ and ASR marked on Fig. 7.4. The pivotal errors on each plot are of the same angular magnitude but the error in Ln(K) at 2 MPa is seen to be significantly greater than that in Ln(C) at ASR = 50%.

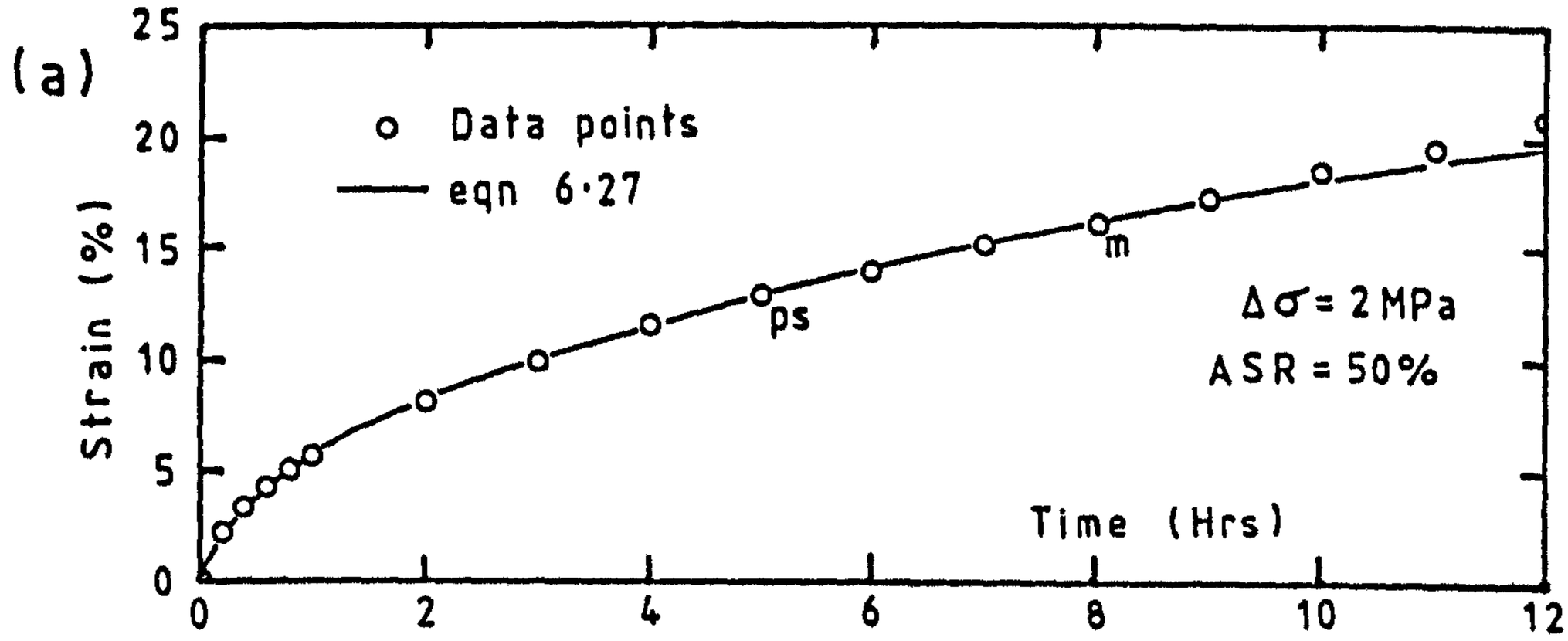

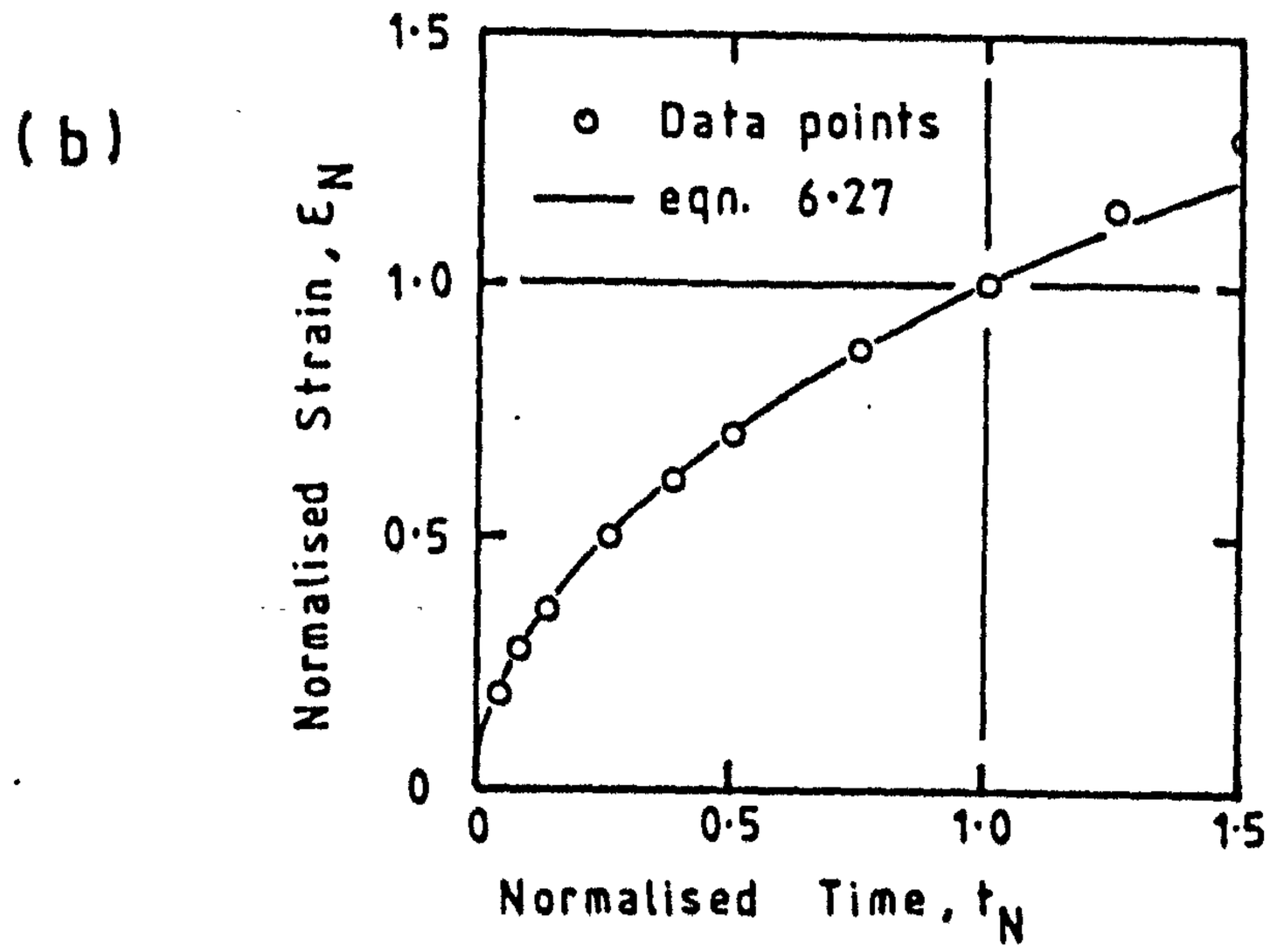

Fig. 7·2 (a) Strain vs Time and (b) Normalised strain vs Normalised time plots of imaginary creep test data for soil X

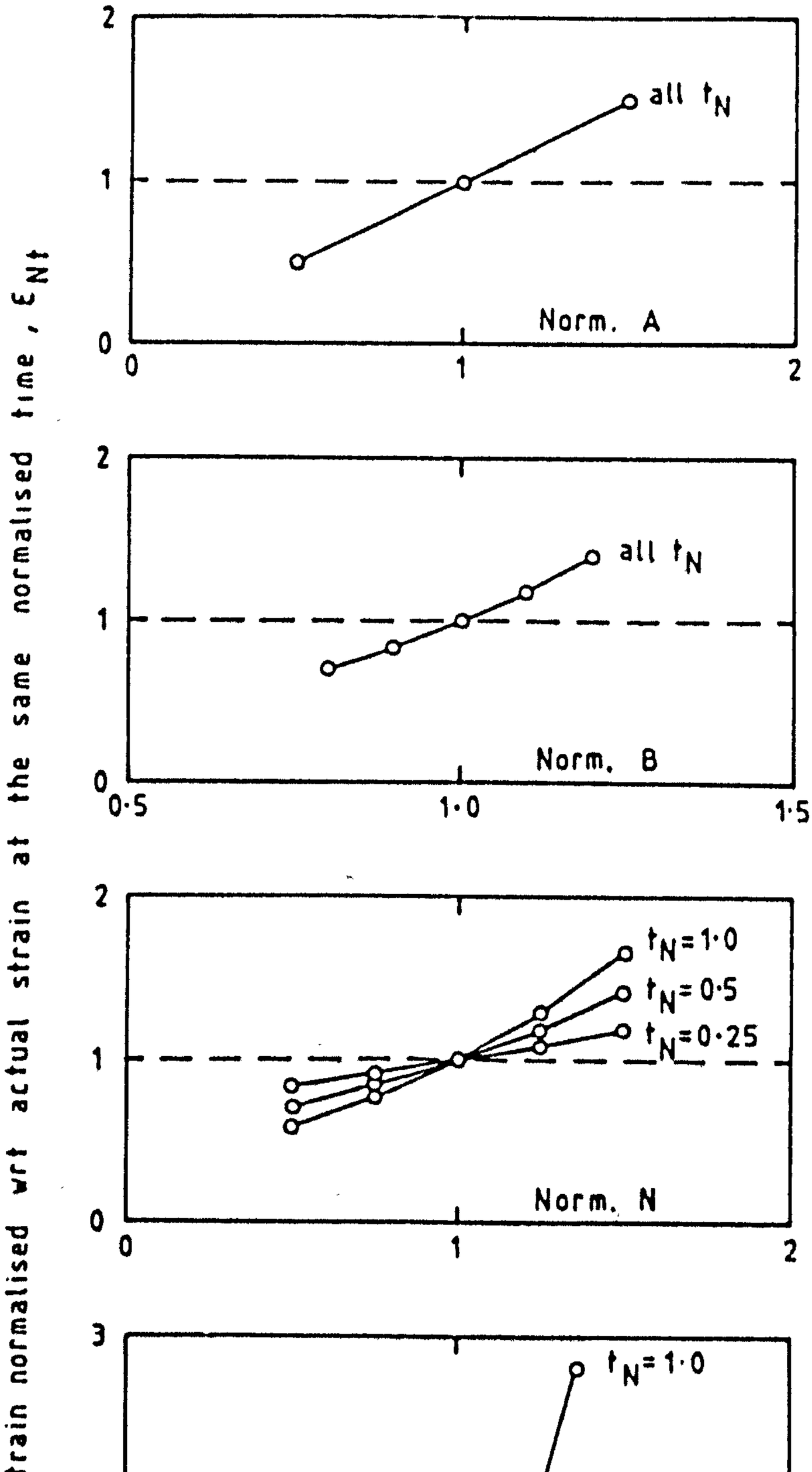

Fig.7·3 Sensitivity analysis of strain predictions by eqn. 6·27. Axes are normalised w.r.t. actual values of strain and parameters A, B, N and H.

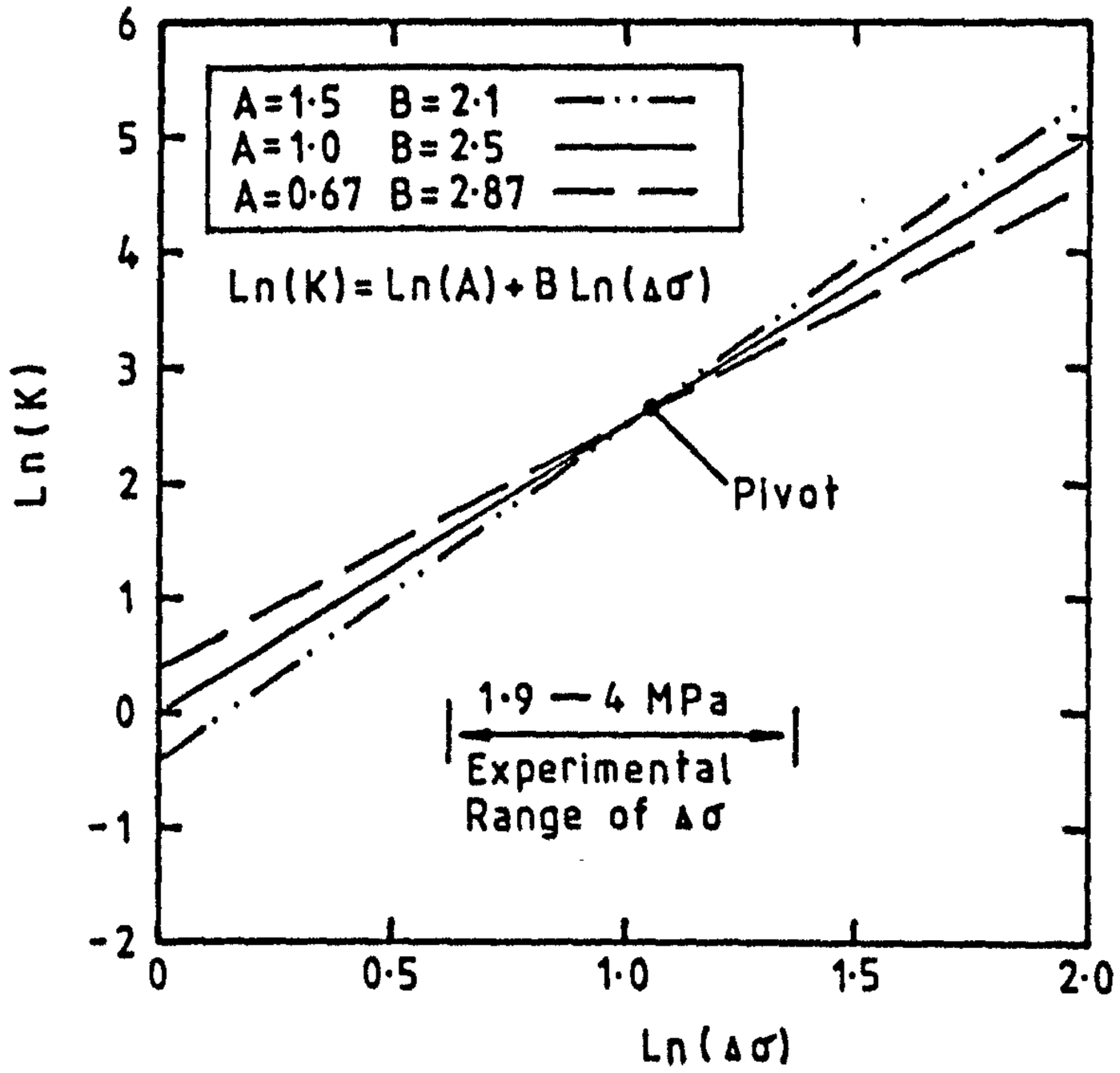

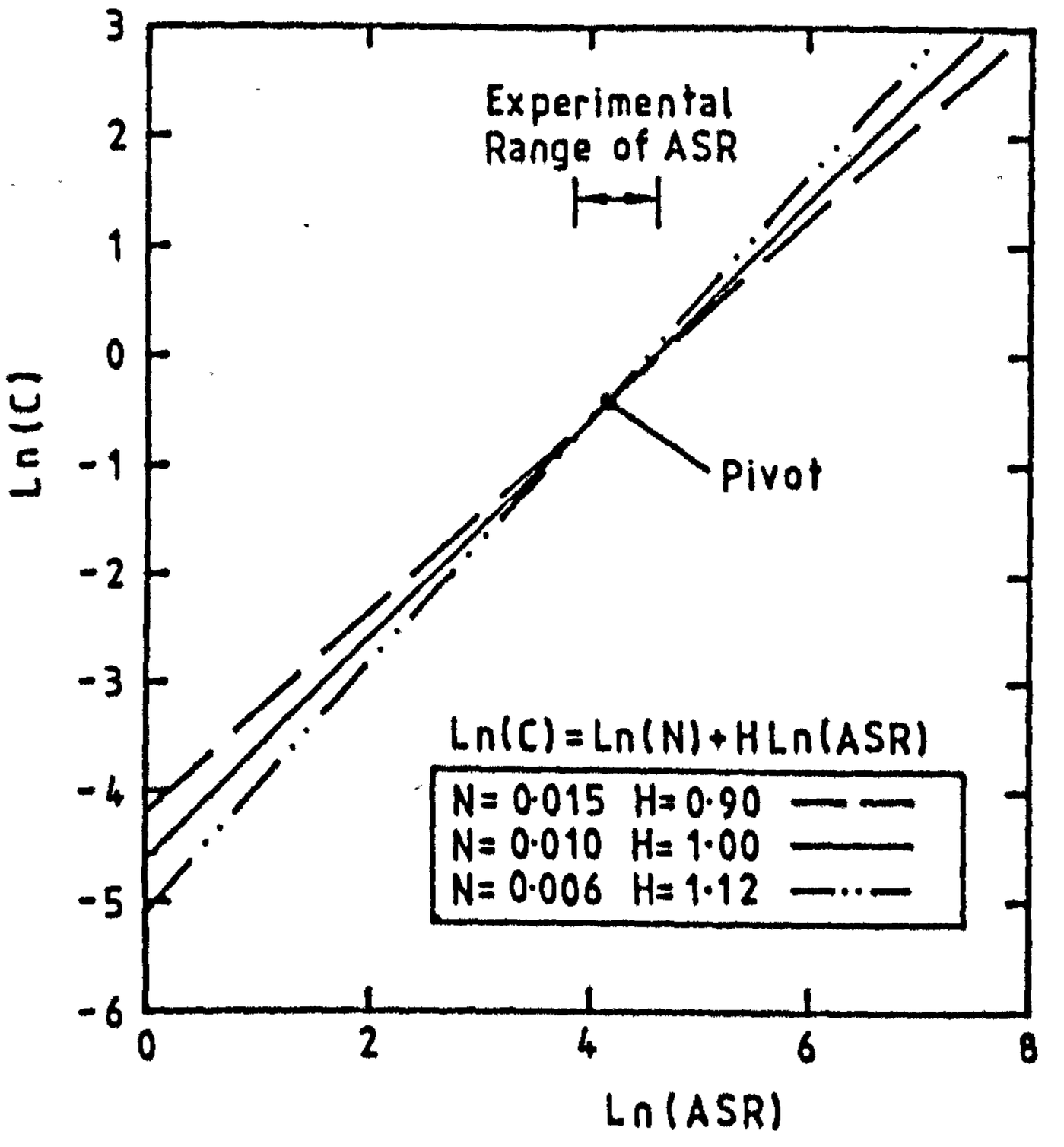

Fig. 7·4 Pivotal errors and their affect on the determination of parameters for eqn. 6·27.

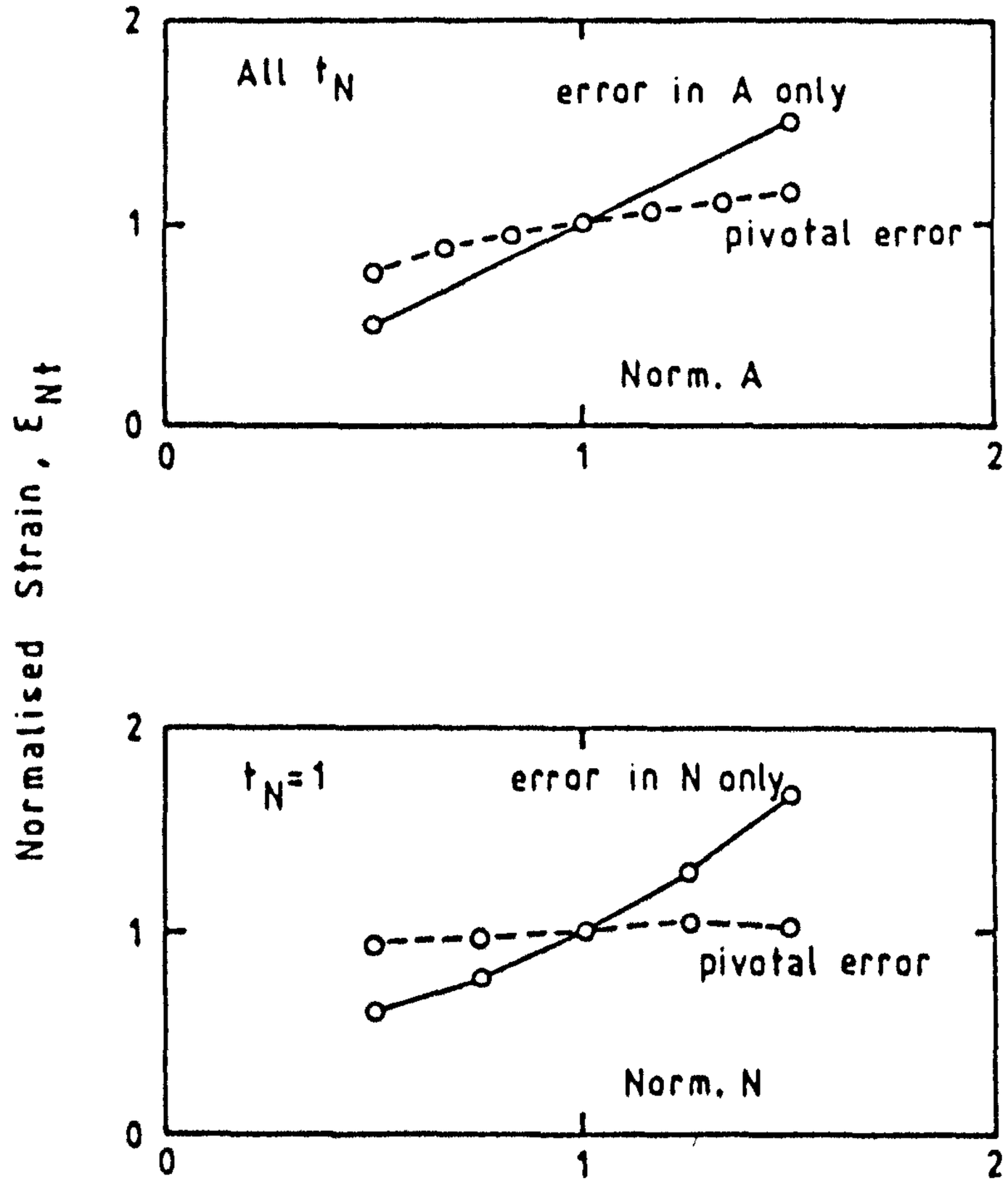

Fig.7·5 Comparison of the effect on calculated strain of translational and pivotal errors incurred during parameter determination

7.4 Creep analysis of a frozen shaft

The triaxial creep equation (6.27) may be incorporated into a simplified ice wall analysis for comparison with the uniaxial creep equation (6.4) due to Klein. The analysis is based on the excavation of a shallow shaft through soil X, the relevant properties of which are listed in Table 7.3 along with the physical dimensions of the shaft.

Table 7.3 Physical and mechanical properties of soil x with relevant details for the analysis of a shallow shaft

Material Properties			Construction Details	
Soil X			Shaft Depth H = 20m	
Unit Weight	γ = 20 kN/m²		Inner Radius a = 5m	
Shear Angle	ϕ = 12°		Outer Radius b = 8.5m	
			Freeze Circle Radius 7m	
Cohesion	c = 1.5 MPa	At -10°C		
Creep Parameter	A = 1			
" "	B = 2.5			
" "	N = 0.01			
" "	H = 1			
" "	C = 0.43			

The ground pressure P_o is $K_o\gamma H$ which at this depth has a value of 0.4 MPa if K_o is assumed equal to one. The pressure (q) on the outside of the ice wall after excavation will probably be at a level below P_o and will be assumed to be 0.35 MPa in this analysis.

The radial stress, σ_r, and tangential stress, σ_θ, at any radius

within the ice wall may be calculated on the basis of the instantaneous elastic response of a thick walled hollow cylinder to external loading,

$$\sigma_r = qb^2 \ (1 - a^2/r^2)/(b^2 - a^2) \qquad 7.3$$

$$\sigma_\Theta = qb^2 \ (1 + a^2/r^2)/(b^2 - a^2) \qquad 7.4$$

The radial stress corresponds to the minor principal stress and the tangential stress the major. The deviator stress follows from $\sigma_\Theta - \sigma_r$.

The variation of temperature through an ice wall was shown in Fig. 2.6. The strength of frozen ground is known to be temperature dependent (Fig. 5.1) and in section 5.3, it was shown that this can be accounted for by changes in the cohesive strength contributed by the ice matrix. Assuming the behaviour of soil X to be similar to the sand shown in Fig. 5.1, over the temperature range 0 to -25°C, the cohesion, c, may be expressed as:

$$c = 0.5 - 0.1 \ \Theta \qquad 7.5$$

where Θ is the temperature in degrees celsius and c is in MPa. The failure strength as a function of temperature and confining pressure (i.e. position within the ice wall) follows from:

$$\sigma_f = 2 \ (c \ \mathrm{Cos} \ \phi + \sigma_3 \ \mathrm{Sin} \ \phi)/(1 - \mathrm{Sin} \ \phi) \qquad 7.6$$

Deviator stress and σ_f can be combined to determine ASR values at each point in the ice wall. Equation 6.27 then calculates the creep strain due to the imposed loading at any time, t, after excavation.

Table 7.4 shows the values of stress, strength, ASR and temperature obtained for the present example. Strains have been calculated at t = 1, 10, 100 and 1000 hrs, assuming that the imposed stresses remain constant throughout these time periods. The strain at t = 1000 hrs, as calculated by equation 6.4, is included for comparison.

The assumption of constant stress with no relaxation accompanying creep deformation is a worst possible loading case. The variations of strain with radial position through the ice wall are shown in Fig. 7.6. By taking account of the confining pressure effect ($C = N(ASR)^H$) equation 6.27 shows the strain to be considerably lower, away from the excavation wall, than was previously assumed (equation 6.4). The strain after 1000 hrs is only 1% at a radius of 6.25m from the centre line of the shaft. Beyond this point, the ground is effectively stable.

The stress relaxation characteristics of frozen soils have not been studied here but would significantly reduce the magnitude of the calculated strains at the excavation wall. To demonstrate this, a second analysis has been followed through with the inner radius of the shaft decreasing in response to the calculated circumferential strain. The effect of decreasing radius a is to decrease the size of the stresses calculated by equations 7.3 and 7.4, thus approximating the stress relaxation process. In Fig. 7.7, the strain vs time relationship at the excavation boundary is plotted for both analyses. The slower rate of increase of strain under stress relaxation conditions is apparent.

For the full analysis of the strain generated in an ice wall, these approaches are over-simplistic. They do, however, serve to demonstrate the effects of confining pressure and stress relaxation on strain calculated by equations 6.4 and 6.27. A fuller solution may be obtained through a finite element analysis which is able to take into account the continuity of the structure.

Table 7.4 Stress, strength, temperature and strain through the ice wall of a frozen shaft

Eqn. No.		Radial Position (m)							
		5	5.5	6	6.5	7	7.5	8	8.5
7.3	σ_3 (MPa)	0	0.09	0.16	0.22	0.26	0.30	0.33	0.35
7.4	σ_1 (MPa)	1.07	0.98	0.91	0.85	0.81	0.77	0.74	0.72
	$\Delta\sigma$ (MPa)	1.07	0.89	0.75	0.63	0.55	0.47	0.41	0.37
	θ °C	-5	-8.8	-13.2	-18.8	-25	-13.5	-5.6	0
7.5	c (MPa)	1	1.38	1.82	2.36	3	1.85	1.06	0.5
7.6	σ_f (MPa)	2.47	3.46	4.58	5.94	7.55	4.73	2.79	1.42
5.5	ASR (%)	43	26	16	11	7	10	15	26
6.27	ϵ_1 (%)	1.18	0.75	0.49	0.32	0.22	0.15	0.11	0.08
6.27	ϵ_{10} (%)	3.19	1.36	0.70	0.41	0.26	0.19	0.15	0.15
6.27	ϵ_{100} (%)	8.58	2.47	1.02	0.52	0.31	0.24	0.21	0.28
6.27	ϵ_{1000} (%)	23.1	4.50	1.47	0.67	0.36	0.30	0.30	0.50
6.4	ϵ_{1000} (%)	23.1	14.6	9.50	6.14	4.37	2.95	2.10	1.62

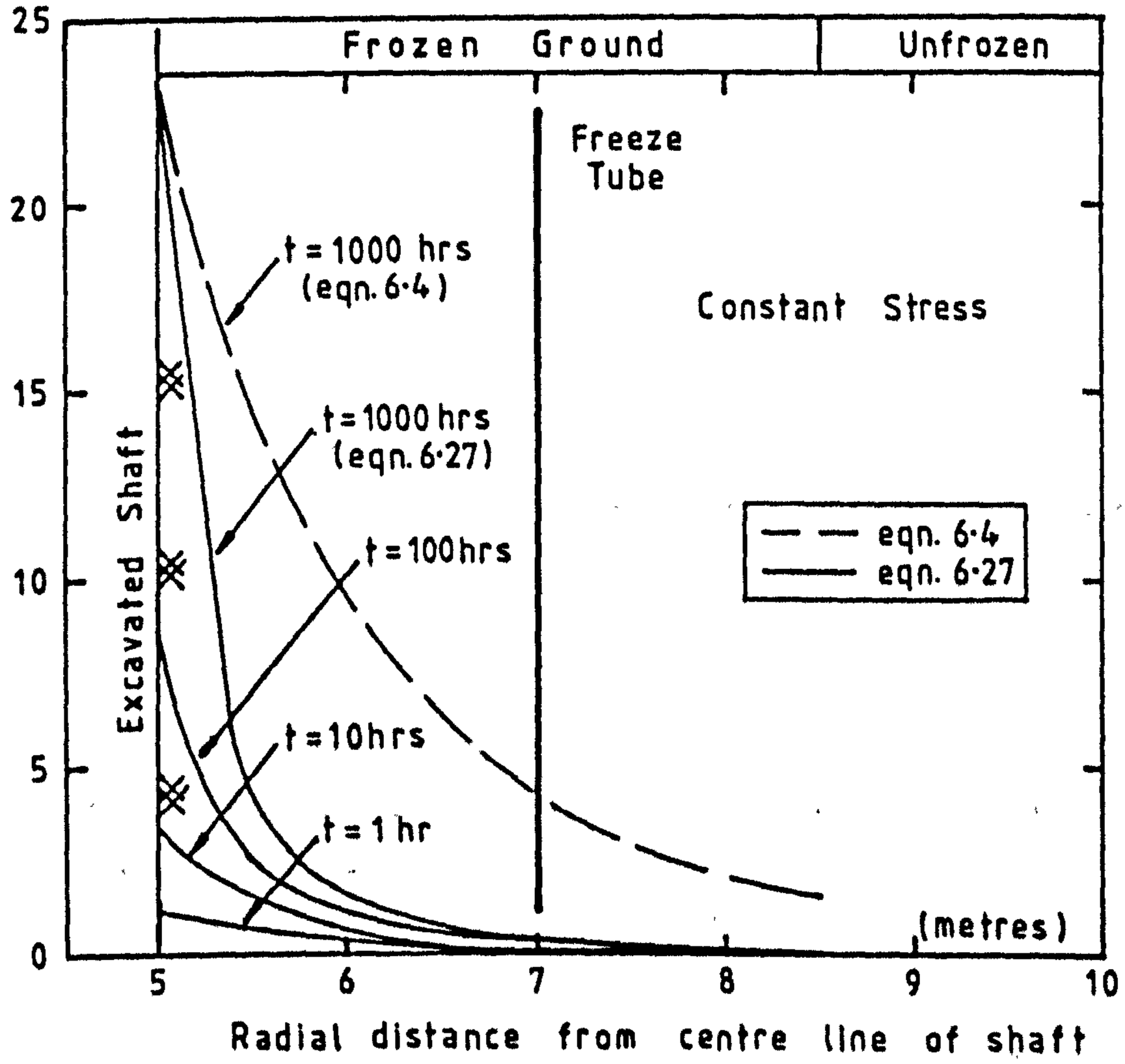

Fig. 7·6 Predicted variations in strain, with time and radial position, within the ice wall of a frozen shaft

7.5 Summary

Creep equations, which have evolved from analytical approaches to modelling, commonly refer to the conditions at failure when calculating strain and strain rate. It may also be necessary to take laboratory creep tests beyond the failure point to enable the equation parameters to be evaluated. Empirical equations which model primary creep, do not require this. This is an advantage when the material exhibits large strains to failure, an effect which is exaggerated at higher pressures.

The parameters for the new triaxial equation (6.27) may be evaluated from time, strain and strain rate sets at any point upto failure. In section 7.2, the apparent transition point between primary and secondary creep is used and the relationships between C and ASR, and between K and $\Delta\sigma$ are consistent with previous results.

The parameters A and B have been evaluated for LAF sand at the inflection point, from uniaxial and combined uniaxial/triaxial test data, and from the primary/secondary transition point using the uniaxial/triaxial results. The latter two analyses also yield values of N and H. The results from each analysis have yielded different values. The effect this has on strain predictions has been investigated by considering an imaginary soil with properties similar to LAF but with a perfect correlation between test data and equation 6.27. In section 7.3, the sensitivity of equation 6.27 to variations in each parameter is demonstrated. Translational errors such as these are shown to give large errors in strain predictions. The most likely errors are considered to be pivotal and to result from the incorrect choice of a straight line through data with a limited amount of scatter. The pivotal error pairs high values of A or N with low values of B and H (and vice versa). The resulting errors in strain are seen to be minimal.

The effect that equation 6.27 may have on the design of an ice wall is demonstrated in section 7.4. This simple analysis, which

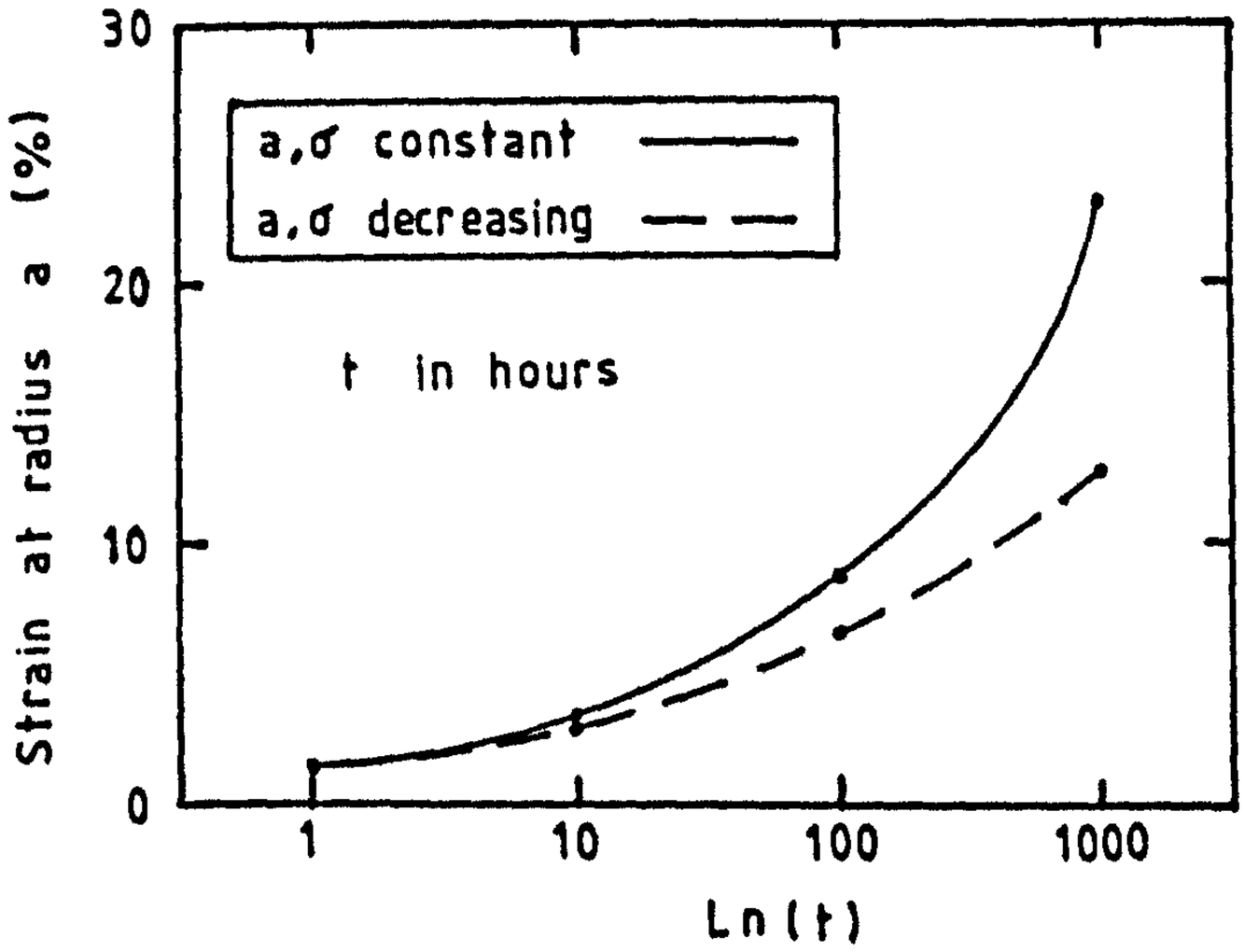

Fig. 7·7 Comparison of strains at the excavation boundary calculated assuming constant and relaxing stress conditions.

is based on the initial stress levels expected within a hollow elastic cylinder, show that the creep strain is likely to be negligible beyond the middle of the ice wall. This is a function of the confining pressure and the increase in soil strength, the latter being a function of the soil temperature which is lowest near the freeze tubes. Equation 6.27 is easily able to account for these variations through the ASR term.

CHAPTER 8

CONCLUSIONS AND SUGGESTIONS FOR FURTHER WORK

8.1 CONCLUSIONS

This thesis has been concerned with the development of laboratory resources for investigating the deformation behaviour of frozen soils and rocks and the way in which this behaviour can be characterised for the purposes of AGF design. The main conclusions reached are as follows:

1. Three soils and a selection of triassic rocks have been described and tested. The soils were LAF, a fine silty sand from the Lenton Abbey formation of the lower mottled sandstone; LAL, a uniform rounded sand from Loch Aline in Scotland, and Keuper Marl (KM), a clay which overlies LAF in the Nottinghamshire region.

2. A computer controlled refrigerated triaxial cell has been developed and used for strength and creep testing of saturated sand and clay. Tests at -10°C have been completed in the confining pressure range 0 - 11.2 MPa.

3. A simple uniaxial apparatus and a standard Hoek cell have been modified to operate at sub-zero temperatures. These cells are suitable for short term strength tests and enable the computer controlled apparatus to be reserved for more complex tests. Short term strength tests at a constant deformation rate of 1mm/min have established failure deviator stresses for LAF, LAL and KM using these apparatus. The confining pressure range covered was 0 - 12 MPa.

4. Small soil specimens do not consistently fail in the same manner during creep tests. LAF sand specimens have shown evidence of shear planes, barrelling and double barrelling at failure but the mode of failure appears to be unrelated to the applied stress. Larger specimens may be less susceptible to these effects but specimen size must be compatible with the practical aspects of recovery of material from the field.

5. The scatter of results obtained from the non-destructive test programme were such that no correlation was observed between ultrasonic pulse velocity and LAF specimen density or strength. Better results may lead from improved end preparation methods.

6. An engineering model for creep of frozen soils should require a minimum of experimental work to determine the equation parameters. Servicability rather than failure of the ice wall is the limitation in design. Therefore, for engineering purposes a creep model need only predict prefailure strains.

7. The traditional creep curve consists of three stages where strain rate decreases, maintains a constant minimum and then accelerates to rupture. These stages are termed primary, secondary and tertiary creep.. A more recent interpretation has the secondary creep period replaced by a momentary minimum strain rate which appears as an inflection point on the strain-time curve. The inflection point is recognised as the point of material failure. The two stage (primary-tertiary) creep concept allows for an analytical approach to modelling which adheres to physical principles.

8. The analytical approach of Fish to uniaxial creep modelling can be expressed in the form of equation 6.15:

$$\varepsilon = \tilde{C} \left(\frac{\sigma}{\sigma_o}\right)^n \psi \tau \exp(\delta f(\tau)) \qquad 6.15$$

which is difficult to use for an engineering model. The results obtained with LAF sand do not fit the model as parameter δ, which Fish finds to be a constant, varies linearly with the applied uniaxial stress.

9. The empirical approach of Klein to uniaxial creep can be expressed in the form of equation 6.4:

$$\varepsilon = A\sigma^B t^C \qquad 6.4$$

which can model strains in the primary creep region but does not uniquely define the failure point. Beyond the failure point, equation 6.4 will underestimate strain but errors may be minimal until strain acceleration is well established. The results obtained with LAF sand data do not fit the model as parameter C, which Klein finds to be a constant, varies with the applied uniaxial stress.

10. The new computer controlled triaxial cell allowed LAF sand creep test data to be obtained over a wide range of confining pressures. The deviator stress applied during each creep test can be expressed as an applied stress ratio (ASR) based on the short term strength at the same confining pressure:

$$ASR = \Delta\sigma/\Delta\sigma_f \times 100\% \qquad 5.5$$

$\Delta\sigma_f$ was measured at a deformation rate of 1mm/min in this study. For LAF sand and KM clay, where no peak stress was reached in short term strength tests, $\Delta\sigma_f$ was taken at 15% and 20% strain respectively.

11. Parameter C in the Klein equation can be calculated from the failure point conditions (denoted by subscript m):

$$C_m = \dot{\varepsilon}_m t_m / \varepsilon_m$$

Plotting C against ASR for each test gives a confining pressure independent relationship:

$$C_m = N\ (ASR)^H$$

where N and H are dimensionless parameters.

12. An empirical triaxial creep equation, based on the uniaxial equation of Klein, is proposed:

$$\epsilon = A\ (\Delta\sigma)^B t^{N(ASR)^H} \qquad 6.27$$

The effect of confining pressure is absorbed by the ASR term. Equation 6.27 has been shown to model creep deformation of all three test materials.

13. For engineering purposes the new creep equation improves on that of Diekmann and Jessberger (equation 6.28) which requires a separate expression for the unconfined condition. Both equations 6.27 and 6.28 are developed from the uniaxial model of Klein. Equation 6.27 is also easier to use than the triaxial model of Orth and Meissner (1982) which requires considerably more data input and consequently involves a greater amount of laboratory testing.

14. Parameters A, B, N and H may be defined by a minimum of one short term strength test and three long term creep tests, all at the same confining pressure. Parameters A and B are defined in the same manner as for the uniaxial Klein equation. A strength envelope is needed when using equation 6.27 and this increases the number of short term strength tests required to three.

15. Application of a confining pressure tends to suppress creep deformation and practical interpretation of the strain-time relationship has primary creep being followed by an extended period of secondary creep. Inflection point details are not then available and this affects the determination of parameters for the creep model (equation 6.27). The value of C, and hence N and H, can be defined at another earlier point on the creep curve such as the transition between primary and secondary creep (denoted by subscript ps):

$$C_{ps} = \dot{\epsilon}_{ps}\ t_{ps}/\epsilon_{ps}$$

C_{ps} varies with ASR in a similar manner to C_m. LAF sand results over the confining pressure range 0 - 11.2 MPa, confirm this relationship.

8.2 Suggestions for further work

The facility for strength and creep testing of frozen soils has been extended to cover a wide range of confining pressures and is now able to provide data for the modelling of frozen ground behaviour. Further work on the development of equipment can be kept to a minimum and the emphasis moved to the methods used for analysis. The following items of further work are suggested:

1. The new triaxial creep equation (6.27) should be incorporated into the method of analysis of frozen soil structures. By taking account of the suppresion of creep deformation by the influence of a confining pressure, it can be expected that ice wall thickness calculations will decrease. This emphasizes the potentially conservative nature of current ice wall design procedures which rely on uniaxial creep equations.

2. To support further analysis work there is an urgent need for

the monitoring of ground conditions during construction in frozen ground. Field measurements have provided information on the temperature profile through the soil, and similar information on stress levels is now needed to justify some of the assumptions made in the design procedure. An investigation of this sort would necessarily involve a considerable investment in both time and money.

3. To support the objectives of 1) and 2) above, it may be necessary to develop new control software for the triaxial test apparatus which will enable different stress paths to be applied to the frozen soils. Stress relaxation tests are appropriate for materials undergoing creep deformation and the relaxation characteristics may need to be considered during modelling of an excavation. Consideration should also be given to the development of multistage creep test techniques, as it is often necessary to maximise the information gained from field samples.

4. To further establish the new triaxial apparatus, it should be used to investigate triaxial creep properties over a wider range of materials, material properties and test conditions (e.g. temperature). This will also extend the current data base on frozen soil creep behaviour. Future research programmes should include reference tests in agreement with the recently published guidelines of the ISGF working group. The development of a non- destructive testing technique, to run in parallel with these experiments, should also lead to an optimisation of information gained from the resources available.

APPENDIX A

COMPUTER CONTROL PROGRAMME FOR CREEP

```
1 REM
2 REM
3 REM
4 REM
5 REM
6 REM
7 REM
8 REM
9 REM
10 REM
11 REM
12 REM
13 REM
100 REM
101 REM
102 REM
110 ON ERROR GOTO 25000
999 REM
1000 REM
1001 REM
1010 ICL:REN:DCL
1020 DIM A$(3),B$(5),T(25),TY(25),E(25),EX(25)
1030 XT=0.2:YE=0.2:KX=XT/5:KY=YE/5:CT=XT/50:CE=YE/25
1040 ED=0:TH=0:PN=0:PS=5:PD=0:PM=0:TI$="000000":DP=40.1
1050 A$(1)=CHR$($3F):A$(2)=CHR$($5F)
1060 WRT9,"A,CR,IF I4>31000 R01,IF I5>31000 R01,CE,R00,R10":CMDW A$(1)
1070 CONSOLEC80:GRAPHI1,C,01
1999 REM
2000 REM
2001 REM
2010 PRINTCHR$(6):GRAPH C
```

```
┌──────────────────────────┐
│                          │
│   CREEP CONTROL PROGRAMME│
│                          │
│          for the         │
│                          │
│      CNH Triaxial Cell   │
│                          │
└──────────────────────────┘

┌──────────────────────────┐
│↓↓↓↓↓↓ Error Processing ↓↓↓↓↓↓│
└──────────────────────────┘

┌──────────────────────────┐
│↓↓↓↓↓↓↓↓↓ Initiation ↓↓↓↓↓↓↓↓↓│
└──────────────────────────┘

┌──────────────────────────┐
│↓↓↓↓↓↓↓↓↓ Data Input ↓↓↓↓↓↓↓↓↓│
└──────────────────────────┘
```

```
2020 CURSOR 31, 0:PRINT"CONSTANT STRESS TEST"
2030 CURSOR 31, 1:PRINT"                    "
2040 CURSOR  2, 2:PRINT"┌──────────────────────┬──────────────────────┬──────────────────────┐"
2050 CURSOR  2, 3:PRINT"| Date (DD/MM/YY):    | Title :              | % Instantaneous Stress|"
2060 CURSOR  2, 4:PRINT"|                      |                      |                      |"
2070 CURSOR  2, 5:PRINT"|                      |                      |                      |"
2080 CURSOR  2, 6:PRINT"|                      |                      |                      |"
2090 CURSOR  2, 7:PRINT"├──────────────────────┼──────────────────────┼──────────────────────┤"
2100 CURSOR  2, 8:PRINT"| Initial Diameter (mm):| Initial Height (mm):| Mass (g):            |"
2110 CURSOR  2, 9:PRINT"|                      |                      |                      |"
2120 CURSOR  2,10:PRINT"|                      |                      |                      |"
2130 CURSOR  2,11:PRINT"|                      |                      |                      |"
2140 CURSOR  2,12:PRINT"├──────────────────────┴──────────┬───────────┴──────────────────────┤"
2150 CURSOR  2,13:PRINT"| Confining Pressure (MPa):       | Deviator Stress (MPa):           |"
2160 CURSOR  2,14:PRINT"|                                 |                                  |"
2170 CURSOR  2,15:PRINT"|                                 |                                  |"
2180 CURSOR  2,16:PRINT"|                                 |                                  |"
2190 CURSOR  2,17:PRINT"├─────────────────────────────────┼──────────────────────────────────┤"
2200 CURSOR  2,18:PRINT"| Test Temperature (C):           | Maximum Duration (Hrs):          |"
2210 CURSOR  2,19:PRINT"|                                 |                                  |"
2220 CURSOR  2,20:PRINT"|                                 |                                  |"
2230 CURSOR  2,21:PRINT"|                                 |                                  |"
2240 CURSOR  2,22:PRINT"└─────────────────────────────────┴──────────────────────────────────┘"
2250 CURSOR  8, 5:INPUT DT$:DT$=LEFT$(DT$, 8)
2260 CURSOR 33, 5:INPUT  A$: A$=LEFT$( A$,16)
2270 CURSOR 61, 5:INPUT PS$:PS$=LEFT$(PS$, 4)
2280 CURSOR 10,10:INPUT  D$: D$=LEFT$( D$, 4): D=VAL( D$)
2290 CURSOR 38,10:INPUT  H$: H$=LEFT$( H$, 4): H=VAL( H$)
2300 CURSOR 61,10:INPUT  M$: M$=LEFT$( M$, 5)
2310 CURSOR 18,15:INPUT CP$:CP$=LEFT$(CP$, 4):CP=VAL(CP$):CP$=STR$(CP)
```

```
2320 CURSOR 56,15:INPUT C 2320 CURSOR 56,15:INPUT CS$:CS$=LEFT$(CS$, 5):CS=VAL(CS$):CS$=STR$(CS)
2330 CURSOR 18,20:INPUT  T$: T$=LEFT$( T$, 5): T=VAL( T$): T$=STR$( T)
2340 CURSOR 56,20:INPUT MD$:MD$=LEFT$(MD$, 4):MD=VAL(MD$):MD$=STR$(MD)
2350 YC=0:OK$="OK"
2360 CURSOR 23,23:PRINT"..... Data ";OK$;" ? Y or N ....."
2370 GET G$:IF G$="N" THEN CURSOR 23,23:PRINT"... Correct or Verify Data ...":GOTO 2250
2380 IF G$="Y" THEN 2420
2390 YC=YC+1:IF YC>10 THEN OK$="OK"
2400 IF YC>20 THEN 2350
2410 GOTO 2360
2420 AS$=STR$(INT(π*D^2/4))
2430 V$=STR$(INT(VAL(AS$)*VAL(H$)/100+.5)/10)
2440 BD$=STR$(INT(VAL(M$)/VAL(V$)*100+.5)/100)
2450 CURSOR0,0
2999 REM                    ┌──────────────────────────┐
3000 REM                    │↓↓↓↓↓↓↓↓↓↓ Menu Card ↓↓↓↓↓↓↓↓↓↓│
3001 REM                    └──────────────────────────┘
3005 IF PS=PN THEN 3015
3010 PRINTCHR$(6):GRAPH 00
3015 PS=PN
3020 REM                      :CURSOR 38, 2:PRINT"MENU"
3030 REM                      :CURSOR 38, 3:PRINT"────"
3040 CURSOR 15, 4:PRINT"┌──────────┬──────────────────────────────────────┐"
3050 CURSOR 15, 5:PRINT"│ Page No. │              Function                │"
3060 CURSOR 15, 6:PRINT"├──────────┼──────────────────────────────────────┤"
3070 CURSOR 15, 7:PRINT"│    1     │    Initial Data                      │"
3080 CURSOR 15, 8:PRINT"│          │                                      │"
3090 CURSOR 15, 9:PRINT"│    2     │    Current Status                    │"
3100 CURSOR 15,10:PRINT"│          │                                      │"
3120 CURSOR 15,11:PRINT"│    3     │    Start Test                        │"
```

```
3130 CURSOR 3130 CURSOR 15,12:PRINT"|          |                                  |"
3140 CURSOR 15,13:PRINT"└──────────┘                                  ┘"
3150 CURSOR 15,19:PRINT"..... Select Page by Depressing Number Key ....."
3160 REM
3200 POKE 4470,255:POKE 4476,255:POKE 4471,255:GET G$
3210 PN=PEEK(4470):QN=PEEK(4476):BK=PEEK(4471)
3215 IF BK=253 THEN PN=0:GOTO 3990
3220 IF QN<>255 THEN PN=QN
3230 IF PN=255 THEN PN=PS:GOTO 3990
3240 FOR I=1 TO 3
3250 IF (255-PN)<(2^I+.1)THEN PN=I:I=3
3260 NEXT I
3270 IF PN>3 THEN PN=0
3990 GOSUB 4000:GOTO 7000
3999 REM                    ┌──────────────────────────────┐
4000 REM                    |↓↓↓↓↓↓↓↓↓ Data Acquisition ↓↓↓↓↓↓↓↓↓|
4001 REM                    └──────────────────────────────┘
4010 FOR I=0 TO 5
4020 A$(3)="A,G0,F1,I"+STR$(I)
4030 WRT9,A$(3):CMDW A$(1)
4040 RED9,B$(I):CMDR A$(2)
4050 NEXT I
4060 WRT9,"R00,R10,R20,R30":CMDW A$(1)
4070 L=(-VAL(B$(0))-10280)/435.5
4075 REM Zero error 5/6/86 (was -10250..429.5)*** Alter Calibration on lines 6032,6035,22010 & 22020 ***
4080 P3=(VAL(B$(1))+158)/2381
4090 T2=(VAL(B$(2))+55)/127.8
4100 T3=(VAL(B$(3))+20)/111.1
4110 D4=(VAL(B$(4)))/1285
4120 D5=(VAL(B$(5)))/1331
4999 REM                    ┌──────────────────────────┐
```

```
5000 REM                    |↓↓↓↓↓↓↓↓↓↓ Time ↓↓↓↓↓↓↓↓|
5001 REM                    └──────────────────────────┘
5010 TN$=TI$
5020 IF LEFT$(TN$,2)="01" THEN TH=TH+1:TI$="00"+RIGHT$(TN$,4)
5040 TM=VAL(MID$(TN$,3,2))
5050 TS=VAL(RIGHT$(TN$,2))
5060 HR=TH+TM/60+TS/3600
5999 REM                    ┌──────────────────────────────────┐
6000 REM                    |↓↓↓↓↓↓↓↓↓ Processing of Data ↓↓↓↓↓↓↓↓↓|
6001 REM                    └──────────────────────────────────┘
6010 REM IF BT=0 THEN DI=D5
6020 DF=ABS(D5-DI)
6030 AI$=STR$(INT(VAL(AS$)*H/(H-DF)+.5))
6032 LB=-((P3*.*DP^2/4+CS*VAL(AI$))/1000*435.5+10280):REM --- Reqd. load in bits for external load cell ---
6035 REM LB=-(CS*VAL(AI$)/1000*435.5+10280):REM ----- Reqd. load in bits -----
6040 Q=(L*1000-P3*.*DP^2/4)/VAL(AI$)
6050 Z=T2:GOSUB 6140:T2$=Z$
6060 Z=T3:GOSUB 6140:TT$=Z$
6070 Z=P3:GOSUB 6170:PP$=Z$
6080 Z=L:GOSUB 6170:LL$=Z$
6090 Z=Q:GOSUB 6170:QQ$=Z$
6100 Z=DF:GOSUB 6170:DF$=Z$
6110 TS=LN(H/(H-DF))*100
6120 Z=TS:GOSUB 6170:EE$=Z$
6130 Z=HR:GOSUB 6230:EH$=Z$
6135 GOTO 6998
6140 REM ************ 1 DECIMAL PLACE FORMAT ************
6150 Z=INT(Z*10+.5)/10:Z$=STR$(Z):IF Z=INT(Z) THEN Z$=Z$+".0"
6160 RETURN
6170 REM ************ 2 DECIMAL PLACE FORMAT ************
6180 Z=INT(Z*100+.5)/100:Z$=STR$(Z):IF Z=INT(Z) THEN Z$=Z$+".00":GOTO 6220
```

```
6190 Z$=Z$+"00":IF VAL(Z$)>=10 THEN 6210
6200 Z$=LEFT$(Z$,4):GOTO 6220
6210 Z$=LEFT$(Z$,5)
6220 RETURN
6230 REM ************ 3 DECIMAL PLACE FORMAT ************
6240 Z=INT(Z*1000+.5)/1000:Z$=STR$(Z):IF Z=INT(Z) THEN Z$=Z$+".000":GOTO 6300
6250 IF VAL(Z$)<=.9E-02 THEN 6300
6260 Z$=Z$+"000"
6270 IF VAL(Z$)>=10 THEN 6290
6280 Z$=LEFT$(Z$,5):GOTO 6300
6290 Z$=LEFT$(Z$,6)
6300 RETURN
6998 RETURN
6999 REM                    ┌──────────────────────────────────────┐
7000 REM                    │↓↓↓↓↓↓↓↓↓ Page Selection ↓↓↓↓↓↓↓↓↓│
7001 REM                    └──────────────────────────────────────┘
7010 IF PS=PN THEN 7060
7020 IF PN=3 THEN 10000
7030 ON PN GOSUB 8000,9000
7040 IF PN=0 THEN 3000
7050 GOTO 7998
7060 ON PS GOSUB 8998,9500
7998 GOTO 3200
7999 REM                    ┌──────────────────────────────────────┐
8000 REM                    │↓↓↓↓↓↓↓↓↓↓ Initial Data ↓↓↓↓↓↓↓↓↓↓│
8001 REM                    └──────────────────────────────────────┘
8010 PRINTCHR$(6):GRAPH00
8020 PS=PN
8030 CURSOR 26, 0:PRINT"University of Nottingham"
8040 CURSOR 23, 2:PRINT"Department of Civil Engineering"
8050 CURSOR 25, 5:PRINT"CONSTANT STRESS CREEP TEST"
```

```
8060 CURSOR 25, 6:PRINT"──────────────────────────────────────"
8070 CURSOR  1, 7:PRINT"┌──────────────────┬──────────────────┐"
8080 CURSOR  1, 8:PRINT"| DETAILS OF SAMPLE |                  |"
8090 CURSOR  1, 9:PRINT"├──────────────────┴──────────────────┤"
8100 CURSOR  1,10:PRINT"| Mean Diameter (mm)     :           |"
8110 CURSOR  1,11:PRINT"|                                    |"
8120 CURSOR  1,12:PRINT"| Mean Height   (mm)     :           |"
8130 CURSOR  1,13:PRINT"|                                    |"
8140 CURSOR  1,14:PRINT"| Mean X-Section (mm^2)  :           |"
8150 CURSOR  1,15:PRINT"|                                    |"
8160 CURSOR  1,16:PRINT"| Volume         (cm^3)  :           |"
8170 CURSOR  1,17:PRINT"|                                    |"
8180 CURSOR  1,18:PRINT"| Mass           (g)     :           |"
8190 CURSOR  1,19:PRINT"|                                    |"
8200 CURSOR  1,20:PRINT"| Bulk Density  (Mg/m^3) :           |"
8210 CURSOR  1,21:PRINT"└──────────────────────────────────────┘"
8270 CURSOR 41, 7:PRINT"┌──────────────────────────────────────┐"
8280 CURSOR 41, 8:PRINT"|          DETAILS OF TEST             |"
8290 CURSOR 41, 9:PRINT"├──────────────────────────────────────┤"
8300 CURSOR 41,10:PRINT"| Start Date              :          |"
8310 CURSOR 41,11:PRINT"|                                    |"
8320 CURSOR 41,12:PRINT"| Confining Stress (MPa) :           |"
8330 CURSOR 41,13:PRINT"|                                    |"
8340 CURSOR 41,14:PRINT"| Deviator Stress  (MPa) :           |"
8350 CURSOR 41,15:PRINT"|                                    |"
8360 CURSOR 41,16:PRINT"| % of Instaneous Stress :           |"
8370 CURSOR 41,17:PRINT"|                                    |"
8380 CURSOR 41,18:PRINT"| Temperature       (C)  :           |"
8390 CURSOR 41,19:PRINT"|                                    |"
8400 CURSOR 41,20:PRINT"| Maximum Duration (Hrs) :           |"
8410 CURSOR 41,21:PRINT"└──────────────────────────────────────┘"
```

```
8500 CURSOR 22, 8:PRINTA$
8510 CURSOR 28,10:PRINTD$
8520 CURSOR 28,12:PRINTH$
8530 CURSOR 28,14:PRINTAS$
8540 CURSOR 28,16:PRINTV$
8550 CURSOR 28,18:PRINTM$
8560 CURSOR 28,20:PRINTBD$
8570 CURSOR 68,10:PRINTDT$
8580 CURSOR 68,12:PRINTCP$
8590 CURSOR 68,14:PRINTCS$
8600 CURSOR 68,16:PRINTPS$
8610 CURSOR 68,18:PRINTT$
8620 CURSOR 68,20:PRINTMD$
8630 CURSOR  7,23:PRINT"..... Press <SPACE> to return to MENU ....."
8998 RETURN
8999 REM
9000 REM                  |↓↓↓↓↓↓↓↓↓ Current Status Display ↓↓↓↓↓↓↓↓↓|
9001 REM
9010 PS=PN
9020 PRINTCHR$(6):GRAPH00
9030 CURSOR 25, 2:PRINT"Current Status of Test"
9040 CURSOR 25, 3:PRINT"                        "
9050 CURSOR  2, 5:PRINT"Duration"          :CURSOR 22, 5:PRINT"(Hrs)   :"
9060 CURSOR  2, 7:PRINT"Deformation"       :CURSOR 23, 7:PRINT"(mm)   :"
9070 CURSOR  2, 9:PRINT"Mean Area"         :CURSOR 21, 9:PRINT"(mm^2)   :"
9080 CURSOR  2,11:PRINT"Strain"            :CURSOR 24,11:PRINT"(%)   :"
9090 CURSOR  2,13:PRINT"Load"              :CURSOR 23,13:PRINT"(KN)   :"
9100 CURSOR  2,16:PRINT"Temperature"       :CURSOR 24,16:PRINT"(C)   :"
9110 CURSOR  2,18:PRINT"Confining Pressure":CURSOR 22,18:PRINT"(MPa)   :"
9120 CURSOR  2,20:PRINT"Stress"            :CURSOR 22,20:PRINT"(MPa)   :"
9130 REM ---------------------------
```

```
9140 REM                                    :CURSOR 55,4:PRINT"┌──────────┐"
9150 CURSOR 42, 5:PRINT"(";MD$;" max)"      :CURSOR 55,5:PRINT"0|          |";MD$
9160 REM                                    :CURSOR 55,6:PRINT"├──────────┤"
9170 CURSOR 42, 7:PRINT"(25 max)"           :CURSOR 55,7:PRINT"0|          |25"
9180 REM                                    :CURSOR 55,8:PRINT"├──────────┤"
9190 CURSOR 42, 9:PRINT"(";AS$;" init)":CURSOR 55,9:PRINT"i|          |*2"
9200 REM                                    :CURSOR 55,10:PRINT"├──────────┤"
9210 CURSOR 42,11:PRINT"(25 max)"           :CURSOR 55,11:PRINT"0|          |25"
9220 REM                                    :CURSOR 55,12:PRINT"├──────────┤"
9230 CURSOR 42,13:PRINT"(50 max)"           :CURSOR 55,13:PRINT"0|          |50"
9240 REM                                    :CURSOR 55,14:PRINT"└──────────┘"
9250 REM                                    :CURSOR 55,15:PRINT"┌─────┬────┐"
9260 CURSOR 42,16:PRINT"(";T$;" reqd)"  :CURSOR 55,16:PRINT"w|     |    |c"
9270 REM                                    :CURSOR 55,17:PRINT"├─────┼────┤"
9280 CURSOR 42,18:PRINT"(";CP$;" reqd)":CURSOR 55;18:PRINT"1|     |    |h"
9290 REM                                    :CURSOR 55,19:PRINT"├─────┼────┤"
9300 CURSOR 42,20:PRINT"(";CS$;" reqd)":CURSOR 55,20:PRINT"1|     |    |h"
9310 REM                                    :CURSOR 55,21:PRINT"└─────┴────┘"
9320 REM                                    :CURSOR 55,22:PRINT"      ↑      "
9330 REM                                      :CURSOR 56,23:PRINT"    (reqd)    "
9340 CURSOR  7,23:PRINT"..... Press <SPACE> to return to MENU ....."
9500 CURSOR 34, 5:PRINT EH$;"  "
9510 CURSOR 34, 7:PRINT DF$;"  "
9520 CURSOR 34, 9:PRINT AI$;"  "
9530 CURSOR 34,11:PRINT EE$;"  "
9540 CURSOR 34,13:PRINT LL$;"  "
9545 IF VAL(TT$)>=0 THEN CX=34:GOTO 9550
9546 CX=33
9550 CURSOR 34,16:PRINT TT$;"  "
9560 CURSOR 34,18:PRINT PP$;"  "
9570 CURSOR 34,20:PRINT QQ$;"  "
```

```
9600 GP=INT(VAL(EH$)/VAL(MD$)*13):IF GP>13 THEN GP=13
9605 IF GP<0 THEN GP=0
9610 GS$="|"+STRING$("■",GP)+STRING$(" ",(13-GP))+"|":CURSOR 56, 5:PRINT GS$
9620 GP=INT(VAL(DF$)/25*13):IF GP>13 THEN GP=13
9625 IF GP<0 THEN GP=0
9630 GS$="|"+STRING$("■",GP)+STRING$(" ",(13-GP))+"|":CURSOR 56, 7:PRINT GS$
9640 GP=(VAL(AI$)/VAL(AS$)-1)*13:IF GP>13 THEN GP=13
9645 IF GP<0 THEN GP=0
9650 GS$="|"+STRING$("■",GP)+STRING$(" ",(13-GP))+"|":CURSOR 56, 9:PRINT GS$
9660 GP=INT(VAL(EE$)/25*13):IF GP>13 THEN GP=13
9665 IF GP<0 THEN GP=0
9670 GS$="|"+STRING$("■",GP)+STRING$(" ",(13-GP))+"|":CURSOR 56,11:PRINT GS$
9680 GP=INT(VAL(LL$)/50*13):IF GP>13 THEN GP=13
9685 IF GP<0 THEN GP=0
9690 GS$="|"+STRING$("■",GP)+STRING$(" ",(13-GP))+"|":CURSOR 56,13:PRINT GS$
9700 GP=INT(-(VAL(TT$)-VAL( T$))*10+.5):IF GP<=-6THEN GP=-6
9710 IF GP>=6 THEN GP=6
9720 GS$="|"+STRING$(" ",(6+GP))+"■"+STRING$(" ",(6-GP))+"|"
9730 CURSOR 56,16:PRINT GS$
9740 GP=INT((VAL(PP$)-VAL(CP$))*10+.5):IF GP<=-6THEN GP=-6
9750 IF GP>=6 THEN GP=6
9760 GS$="|"+STRING$(" ",(6+GP))+"■"+STRING$(" ",(6-GP))+"|"
9770 CURSOR 56,18:PRINT GS$
9780 GP=INT((VAL(QQ$)-VAL(CS$))*10+.5):IF GP<=-6THEN GP=-6
9790 IF GP>=6 THEN GP=6
9800 GS$="|"+STRING$(" ",(6+GP))+"■"+STRING$(" ",(6-GP))+"|"
9810 CURSOR 56,20:PRINT GS$
9998 RETURN
9999 REM
10000 REM
10001 REM
```

```
┌──────────────────────────────────┐
|↓↓↓↓↓↓↓↓↓ Test Start ↓↓↓↓↓↓↓↓↓|
└──────────────────────────────────┘
```

```
10010 PRINTCHR$(6):PS=PN
10020 CURSOR 18, 4:PRINT"CHECK POSITION OF PAPER ......."
10030 CURSOR 25, 7:PRINT".... PRESS 'P' WHEN CORRECTLY SET"
10040 CURSOR 41,11:PRINT"|"
10050 CURSOR 39,12:PRINT"o |"
10060 CURSOR 13,13:PRINT"FAN - FOLD PAPER            |"
10070 CURSOR 39,14:PRINT"o |"
10080 CURSOR 41,15:PRINT"|----------------|"
10090 CURSOR 39,16:PRINT"o |                |"
10100 CURSOR 11,17:PRINT"----------------------------|----------------|"
10110 CURSOR 39,18:PRINT"o |                | PLATEN"
10120 CURSOR 12,19:PRINT"PERFORATION                |                |"
10130 CURSOR 39,20:PRINT"o |----------------|"
10140 CURSOR 41,21:PRINT"|"
10150 CURSOR 39,22:PRINT"o |"
10160 CURSOR 41,23:PRINT"|"
10170 GET G$:IF G$<>"P" THEN 10170
10180 PRINTCHR$(6):CURSOR 10,10:PRINT"Wait for Printer"
10190 PRINT/P:PRINT/P:PRINT/P:PRINT/P:PRINT/P
10200 PRINT/P CHR$(18);TAB(28);"University of Nottingham"
10210 PRINT/P:PRINT/P TAB(25);"Department of Civil Engineering"
10220 PRINT/P:PRINT/P:PRINT/P TAB(27);"CONSTANT STRESS CREEP TEST"
10230 PRINT/P TAB(27);"------------------------------"
10240 PRINT/P:PRINT/P:PRINT/P
10250 PRINT/P TAB( 5);"Sample Code                  :  "; A$
10260 PRINT/P
10270 PRINT/P TAB( 5);"Initial Diameter             :  "; D$;TAB(47);"(mm)"
10280 PRINT/P
10290 PRINT/P TAB( 5);"Initial Height               :  "; H$;TAB(47);"(mm)"
10300 PRINT/P
10310 PRINT/P TAB( 5);"Mass                         :  "; M$;TAB(47);"(g)"
```

```
10320 PRINT/P
10330 PRINT/P TAB( 5);"Bulk Density                    :  ";BD$;TAB(47);"(Mg/m^3)"
10340 PRINT/P:PRINT/P
10350 PRINT/P TAB( 5);"TEST START DATE                 :  ";DT$
10360 PRINT/P
10370 PRINT/P TAB( 5);"CONFINING PRESSURE              :  ";CP$;TAB(47);"(MPa)"
10380 PRINT/P
10390 PRINT/P TAB( 5);"DEVIATOR STRESS                 :  ";CS$;TAB(47);"(MPa)"
10400 PRINT/P
10410 PRINT/P TAB( 5);"% OF INSTANTANEOUS STRENGTH     :  ";PS$;TAB(47);"(%)"
10420 PRINT/P
10430 PRINT/P TAB( 5);"TEMPERATURE                     :  "; T$;TAB(47);"(C)"
10440 PRINT/PCHR$(5)
10450 PRINT/P CHR$(19)
10460 PRINT/P:PRINT/P
10470 PRINT/P TAB(27);"CONFINING";TAB(66);" TRUE "
10480 PRINT/P:PRINT/P TAB(9);"TIME";TAB(27);"PRESSURE";TAB(48);"DEFORMATION";
10485 PRINT/P TAB(66);"STRAIN";TAB(84);"LOAD";TAB(95);"STRESS";TAB(113);"TEMPERATURE"
10490 PRINT/P:PRINT/P TAB(9);"(Hrs)";TAB(29);"(MPa)";TAB(52);"(mm)";TAB(68);
10495 PRINT/P"(%)";TAB(84);"(KN)";TAB(96);"(MPa)";TAB(117);"(C)"
10500 PRINTCHR$(6)
10510 CURSOR 10,10:PRINT"START TEST Y OR N ?"
10520 GET G$:IF G$="Y" THEN 10550
10530 IF G$="N" THEN 23998
10540 IF G$<>"Y" THEN 10520
10550 REM <WOPEN#4,A$>
10560 TI$="000000":EH$="0.000":DI=D5:TH=0:B0=VAL(B$(0))
10570 PRINT/P TAB(15-LEN(EH$));EH$;TAB(33-LEN(PP$));PP$;TAB(56-LEN(DF$));DF$;TAB(71-LEN(EE$));EE$;
10575 PRINT/P TAB(88-LEN(LL$));LL$;TAB(100-LEN(QQ$));QQ$;TAB(121-LEN(TT$));TT$
10600 REM <PRINT#4,EH$(I),EE$(I)>
10998 REM RETURN ?
```

```
10999 REM
11000 REM          |↓↓↓↓↓↓↓↓↓ Data Aquis , Time , Data Processing ↓↓↓↓↓↓↓↓↓|
11001 REM
11010 GOSUB 4000
11999 REM
12000 REM                    |↓↓↓↓↓↓↓↓↓ Display Time & Stresses ↓↓↓↓↓↓↓↓↓|
12001 REM
12005 IF PS=4 THEN 12020
12010 CONSOLEC40:PS=4
12020 CURSOR  8,10:PRINT"Time                          ";EH$;"      "
12030 CURSOR  8,12:PRINT"Confining Pressure      ";PP$;"      "
12040 CURSOR  8,14:PRINT"Deviator Stress ("+CS$+")";QQ$;"      "
12050 CURSOR  5,19:PRINT"Press << SPACE >> to engage"
12060 CURSOR 10,21:PRINT"Automatic control"
12999 REM
13000 REM                    |↓↓↓↓↓↓↓↓↓ Print Data ↓↓↓↓↓↓↓↓↓|
13001 REM
13010 IF HR<= 0.01 THEN PI=0.001:GOTO 13060
13020 IF HR<= 0.1  THEN PI=0.005:GOTO 13060
13030 IF HR<= 1    THEN PI=0.01 :GOTO 13060
13040 IF HR<=10    THEN PI=0.05 :GOTO 13060
13050 IF HR> 10    THEN PI=0.1
13060 IF HR<PD+PI THEN 13998
13070 PD=PD+PI
13080 PRINT/P TAB(15-LEN(EH$));EH$;TAB(33-LEN(PP$));PP$;TAB(56-LEN(DF$));DF$;TAB(71-LEN(EE$));EE$;
13090 PRINT/P TAB(88-LEN(LL$));LL$;TAB(100-LEN(QQ$));QQ$;TAB(121-LEN(TT$));TT$
13998 REM
13999 REM                    |↓↓↓↓↓↓↓↓↓ Automatic Control ↓↓↓↓↓↓↓↓↓|
14000 REM
14001 REM
14010 POKE 4471,255:GET G$
```

```
14020 IF PEEK(4471)=253 THEN 15000
14030 GOTO 11000
14999 REM                  ┌──────────────────────────┐
15000 REM                  │↓↓↓↓↓↓↓↓↓↓ Menu ↓↓↓↓↓↓↓↓↓↓│
15001 REM                  └──────────────────────────┘
15010 CONSOLE80:GRAPH 00
15015 PS=PN
15020 REM                     :CURSOR 38, 2:PRINT"MENU"
15030 REM                     :CURSOR 38, 3:PRINT"────"
15040 CURSOR 15, 4:PRINT"┌──────────┬──────────────────────────────────────┐"
15050 CURSOR 15, 5:PRINT"│ Page No. │              Function                │"
15060 CURSOR 15, 6:PRINT"├──────────┼──────────────────────────────────────┤"
15070 CURSOR 15, 7:PRINT"│    1     │    Initial Data                      │"
15080 CURSOR 15, 8:PRINT"│          │                                      │"
15090 CURSOR 15, 9:PRINT"│    2     │    Current Status                    │"
15100 CURSOR 15,10:PRINT"│          │                                      │"
15120 CURSOR 15,11:PRINT"│    3     │    Strain vs Time Graph              │"
15130 CURSOR 15,12:PRINT"│          │                                      │"
15140 CURSOR 15,13:PRINT"│    4     │    Press [S] to Stop Test            │"
15150 CURSOR 15,14:PRINT"│          │                                      │"
15160 CURSOR 15,15:PRINT"└──────────┴──────────────────────────────────────┘"
15170 CURSOR 15,19:PRINT"..... Select Page by Depressing Number Key ....."
15180 REM ---- repeat key function -----
15200 POKE 4470,255:POKE 4476,255:POKE 4471,255:POKE4474,255:GET G$
15210 PN=PEEK(4470):ON=PEEK(4476):BK=PEEK(4471)
15215 IF BK=253 THEN PN=0:GOTO 15990
15220 IF ON<>255 THEN PN=ON
15230 IF PN=255 THEN PN=PS:GOTO 15990
15240 FOR I=1 TO 3
15250 IF (255-PN)<(2^I+.1)THEN PN=I:I=3
15260 NEXT I
```

```
15270 IF PN>3 THEN PN=0
15990 REM
15999 REM                 ┌──────────────────────────────────────┐
16000 REM                 │↓↓↓↓↓↓↓↓↓↓ End of Test ↓↓↓↓↓↓↓↓↓↓│
16001 REM                 └──────────────────────────────────────┘
16010 IF VAL(B$(4))>31000    THEN ET=1:GOTO 16080
16020 IF VAL(B$(5))>31000    THEN ET=2:GOTO 16080
16030 IF          L>50       THEN ET=3:GOTO 16080
16040 IF         TS>30       THEN ET=4:GOTO 16080
16050 IF         HR>VAL(MD$) THEN ET=5:GOTO 23000
16060 IF         G$="S"      THEN ET=6:GOTO 23000
16070 GOTO 16999
16080 GOSUB 4000
16090 ON ET GOTO 16100,16110,16120,16130
16100 IF VAL(B$(4))>31000    THEN ET=1:GOTO 23000
16105 ET=0:GOTO 16999
16110 IF VAL(B$(5))>31000    THEN ET=2:GOTO 23000
16115 ET=0:GOTO 16999
16120 IF          L>50       THEN ET=3:GOTO 23000
16125 ET=0:GOTO 16999
16130 IF         TS>30       THEN ET=4:GOTO 23000
16135 ET=0
16999 REM                 ┌──────────────────────────────────────┐
17000 REM                 │↓↓↓↓↓↓↓↓↓ Screen Displays ↓↓↓↓↓↓↓↓↓│
17001 REM                 └──────────────────────────────────────┘
17010 IF PS=PN THEN 17050
17020 IF PN=0 THEN 15000
17030 ON PN GOSUB 8000,9000,18000
17040 GOTO 17998
17050 ON PS GOSUB 8998,9500,18998
17998 GOTO 19000
```

```
17999 REM
18000 REM                ┌──────────────────────┐
18001 REM                │↓↓↓↓↓↓↓↓↓ Graph ↓↓↓↓↓↓↓↓↓│
18015 PRINTCHR$(6):GRAPH I1,01                └──────────────────────┘
18020 LINE 60,15,60,142:LINE 58,140,310,140
18030 FOR I=0 TO 4
18040 LINE 58,(25*I+15),60,(25*I+15):LINE (50*I+110),140,(50*I+110),142
18050 NEXT I
18110 CURSOR  0, 7:PRINT"STRAIN"
18120 CURSOR  1, 9:PRINT"(%)"
18130 CURSOR 47,21:PRINT"TIME (Hrs)"
18140 FOR I=1 TO 5
18150 X$=STR$(I*YE):Y$=STR$(I*XT)
18160 CURSOR (12-LEN(X$)),(17-3*I):PRINTX$
18170 CURSOR (13+13*I-LEN(Y$)/2),19:PRINTY$
18180 NEXT I
18190 CURSOR  7,23:PRINT"..... Press <SPACE> to return to MENU ....."
18200 PS=PN
18998 RETURN
18999 REM                ┌──────────────────────┐
19000 REM                │↓↓↓↓↓↓↓↓↓↓ Print Data ↓↓↓↓↓↓↓↓↓│
19001 REM                └──────────────────────┘
19010 IF HR<= 0.01 THEN PI=0.001:GOTO 19060
19020 IF HR<= 0.1  THEN PI=0.005:GOTO 19060
19030 IF HR<= 1    THEN PI=0.01 :GOTO 19060
19040 IF HR<=10    THEN PI=0.05 :GOTO 19060
19050 IF HR> 10    THEN PI=0.1
19060 IF HR<PD+PI THEN 19998
19070 PD=PD+PI
19080 PRINT/P TAB(15-LEN(EH$));EH$;TAB(33-LEN(PP$));PP$;TAB(56-LEN(DF$));DF$;TAB(71-LEN(EE$));EE$;
19090 PRINT/P TAB(88-LEN(LL$));LL$;TAB(100-LEN(QQ$));QQ$;TAB(121-LEN(TT$));TT$
```

```
19998 REM
19999 REM
20000 REM                    |↓↓↓↓↓↓↓↓↓↓ Plot Data ↓↓↓↓↓↓↓↓↓|
20001 REM
20010 X=VAL(EH$)/CT+60:Y=140-TS/CE
20020 IF(X<310)*(Y>15)THEN 20120
20040 IF X>=310 THEN XT=XT*2:IF Y<65 THEN YE=YE*2
20050 IF Y<=15 THEN YE=YE*2:IF X>210 THEN XT=XT*2
20060 CT=XT/50:CE=YE/25
20070 GRAPHC:IF PS=3 THEN PS=0:PRINTCHR$(6)
20080 FOR I=1 TO 25:SET (T(I)/CT+60),(140-TY(I)/CE):NEXT I
20090 FOR I=1 TO 25:SET (EX(I)/CT+60),(140-E(I)/CE):NEXT I
20100 DIM T(25),TY(25),EX(25),E(25)
20110 GOTO 20010
20120 X=VAL(EH$)/CT+60:Y=140-TS/CE
20130 SET X,Y
20140 IF VAL(EH$)>KX THEN T(KX/XT*5)=VAL(EH$):TY(KX/XT*5)=TS:KX=KX+XT/5
20150 IF TS>KY THEN E(KY/YE*5)=TS:EX(KY/YE*5)=VAL(EH$):KY=KY+YE/5
20999 REM       |↓↓↓↓↓↓↓↓↓↓ Data Aquis , Time , Data Processing ↓↓↓↓↓↓↓↓↓↓|
21000 REM
21001 REM
21010 GOSUB 4000
21999 REM                  |↓↓↓↓↓↓↓↓↓↓ Stress Control ↓↓↓↓↓↓↓↓↓↓|
22000 REM
22001 REM
22010 WRT9,"CR,IF I0>"+STR$(LB*.98-206)+" R11,R00,IF I4>31000 R01,R10":CMDW A$(1):REM - 205.6 = 2% of 10280 -
22020 WRT9,"IF I0<"+STR$(LB*1.02+206)+" R01,R10,IF I5>31000 R01,R10,CE":CMDW A$(1)
22030 GOTO 22130
22040 IF M0=1 THEN 22060
22050 GOTO 22130
22060 WRT9,"R01":CMDW A$(1)
```

```
22070 MO=0
22080 GOTO 22130
22100 IF MO=1 THEN 22130
22110 WRT9,"R11":CMDW A$(1)
22120 MO=1
22130 GOTO 15200
22999 REM
23000 REM                    |↓↓↓↓↓↓↓↓↓ End Routine ↓↓↓↓↓↓↓↓↓|
23001 REM
23010 WRT9,"CD,R00,R10":CMDW A$(1)
23020 ON ET GOTO 23030,23050,23070,23090,23110,23130
23030 CURSOR 7,23:PRINT"LMP 4 NEAR LIMIT OF TRAVEL                    "
23035 PRINT/P:PRINT/P"LMP 4 NEAR LIMIT OF TRAVEL                    "
23040 GOTO 23998
23050 CURSOR 7,23:PRINT"LMP 5 NEAR LIMIT OF TRAVEL                    "
23055 PRINT/P:PRINT/P"LMP 5 NEAR LIMIT OF TRAVEL                    "
23060 GOTO 23998
23070 CURSOR 7,23:PRINT"LOAD CELL CAPACITY REACHED                    "
23075 PRINT/P:PRINT/P"LOAD CELL CAPACITY REACHED                    "
23080 GOTO 23998
23090 CURSOR 7,23:PRINT"TRUE STRAIN OF 30% REACHED                    "
23095 PRINT/P:PRINT/P"TRUE STRAIN OF 30% REACHED                    "
23100 GOTO 23998
23110 CURSOR 7,23:PRINT"TEST STOPPED - OUT OF TIME                    "
23115 PRINT/P:PRINT/P"TEST STOPPED - OUT OF TIME                    "
23120 GOTO 23998
23130 CURSOR 7,23:PRINT"TEST STOPPED BY OPERATOR                    "
23135 PRINT/P:PRINT/P"TEST STOPPED BY OPERATOR                    "
23998 END
25000 REM                    |↓↓↓↓↓↓↓ Error Processing ↓↓↓↓↓↓↓|
25001 REM
```

```
25002 REM
25010 IF ERN=36 THEN ICL:REN:DCL:PRINT/P ERN:RESUME
25020 IF ERN=39 THEN ICL:REN:DCL:PRINT/P ERN RESUME
25100 PRINT"ERROR ";ERN;" IN ";ERL
25110 END
```

APPENDIX B

STRENGTH TEST RESULTS

199

Table B1 Strength test results for rock specimens at +20°C and -16°C

Sample No.	Rock Type	ρ_d Mgm^{-3}	w %	S_r %	σ_3 MPa	$\Delta\sigma$ MPa +20°C	$\Delta\sigma$ MPa -16°C
77	Si	2.31	7.5	100	0	18.2	
		2.31	7.3	100	0		47.5
		2.31	5.1	69	0		37.1
		2.35	5.3	79	0		34.2
		2.34	4.9	71	0		47.4
		2.38	4.3	69	0	21.5	
		2.35	4.9	73	0	28.8	
		2.35	5.0	75	0	41.9	
78	Mu/Si	2.36	4.0	63	0		29.6
		2.19	9.5	99	0		34.7
		2.38	3.2	54	0		57.1
		2.36	4.6	73	6.3	72.4	
		2.39	3.2	56	6.3		93.7
79	Mu/Si	2.40	6.5	100	0	14.7	
		2.37	7.9	100	0	3.4	
		2.41	2.8	41	0		43.9
		2.35	4.5	58	0		22.9
		2.26	7.4	78	0	13.8	
		2.38	3.0	41	0	22.3	
		2.40	2.8	40	6.8	45.2	
		2.44	1.6	26	6.8	83.7	
		2.41	2.2	32	6.8		55.9
		2.32	4.9	58	6.8		45.3
		2.36	2.6	34	6.8		33.8
82	Sa	2.34	6.1	100	0	9.3	
		2.28	9.3	100	0		23.9
		2.30	6.2	100	0		24.8
		2.35	5.0	100	0		26.6
		2.36	4.6	100	0		35.5
		2.37	4.3	100	0	32.6	
		2.38	4.2	100	0	15.8	
		2.37	4.2	100	0	32.1	
83	Sa	2.24	7.5	100	0	15.4	
		2.26	8.0	100	0	16.8	
		2.23	7.5	100	0		34.5
		2.24	6.7	100	0		25.3

Table B1 ..... cont

Sample No.	Rock Type	ρ_d Mgm^{-3}	w %	S_r %	σ_3 MPa	$\Delta\sigma$ MPa +20°C	$\Delta\sigma$ MPa -16°C
83		2.31	4.6	100	0		43.0
		2.22	6.8	100	0		35.4
		2.29	6.6	100	0	18.4	
		2.26	6.6	100	0	35.4	
85	Sa/Si	2.45	6.1	100	0	3.0	
		2.34	7.7	100	0	4.6	
		2.41	3.5	53	0	26.7	
		2.46	3.2	55	0	19.9	
		2.37	4.2	57	0		31.4
		2.50	2.7	52	0		10.5
		2.51	2.9	58	0		30.7
88	Sa	2.39	6.6	100	0	4.0	
		2.36	7.3	100	0	3.4	
		2.41	4.1	65	0	24.3	
		2.39	4.2	64	0	16.0	
		2.40	3.5	54	0		37.3
		2.43	3.1	53	0		33.1
90	Sa	2.27	7.0	100	0	12.7	
		2.26	6.7	100	0	15.8	
		2.22	7.2	100	0	12.6	
		2.27	6.0	100	0		36.7
		2.33	6.1	100	0		40.5
		2.29	7.2	100	0		31.8
		2.35	4.6	83	6.8	51.3	
		2.27	5.7	81	6.8	58.4	
		2.31	3.9	62	6.8		54.6
		2.29	3.6	54	6.8		69.1
96	Si	2.35	4.9	72	0	19.5	
		2.35	5.4	79	0	16.0	
		2.36	5.0	75	0		35.5
		2.35	5.2	76	0		27.2
		2.36	5.3	79	0		39.1
		2.35	5.2	76	0		36.8
		2.36	4.2	63	0	29.7	
		2.36	5.4	81	0	33.8	
98	Sa	2.45	1.7	59	0	28.5	
		2.33	6.8	100	0		21.4
		2.38	4.2	100	0	26.2	

Table B1 ..... cont

Sample No.	Rock Type	ρ_d Mgm^{-3}	w %	S_r %	σ_3 MPa	Δσ MPa +20°C	Δσ MPa -16°C
98		2.36	4.8	100	0		37.1
		2.34	4.7	100	0		33.6
		2.40	4.3	100	0		36.3
		2.37	3.8	100	0	16.5	
		2.40	3.8	100	0	20.2	
100	Sa	2.44	1.8	39	0	19.4	
		2.42	1.5	30	0	38.0	
		2.43	1.3	27	0	33.1	
		2.34	4.7	73	0		21.8
		2.40	4.0	75	0		41.2
		2.37	4.4	76	0		31.9
		2.39	3.3	60	0		39.0
		2.40	2.1	40	0	22.5	
102	Sa/Si	2.34	3.5	55	0		27.1
		2.40	1.6	30	0	16.0	
		2.37	0.0	0	7.3	51.3	
		2.30	2.4	34	7.3		53.6
103	Sa/Si	2.37	3.3	57	0	10.5	
		2.32	4.8	72	0		14.8
		2.36	5.8	100	0		10.7
		2.30	7.3	100	0		4.5
105	Sa	2.30	8.1	100	0		19.2
		2.35	5.2	100	0	3.5	
		2.28	8.1	100	0	1.7	
		2.27	8.9	100	0		12.6
		2.24	11.5	100	0		15.9
		2.36	5.4	100	0	4.6	
		2.36	4.8	64	7.3	44.9	
		2.35	7.5	99	7.3	12.3	
		2.32	7.6	94	7.3	12.9	
		2.33	4.7	60	7.3		38.5
		2.37	4.7	66	7.3		41.8
		2.36	5.0	69	7.3		39.8
106	Sa	1.90	11.5	91	7.6	37.9	
		1.92	6.1	50	7.6		48.0
		1.91	7.2	58	7.6		46.3

Table B1 ..... cont

Sample No.	Rock Type	ρ_d Mgm^{-3}	w %	S_r %	σ_3 MPa	$\Delta\sigma$ MPa +20°C	$\Delta\sigma$ MPa -16°C
107	Sa	1.87	12.7	100	0	3.7	
		1.89	12.5	100	0		24.3
110	Br	2.26	5.9	100	0		20.5
111	Sa	2.19	6.9	100	0	6.7	
		2.21	6.5	100	0	11.1	
		2.16	7.5	100	0	13.9	
		2.09	8.7	100	0	7.0	
		2.07	9.9	100	0		33.7
		2.18	7.9	100	0		36.6
		2.19	8.3	100	0		39.7
		2.05	9.9	100	0		32.4
114	Mu	1.94	0.5	3	0	16.9	
		1.92	0.6	4	0	16.6	
		1.81	11.1	58	0		17.8
		1.95	9.1	60	0		12.4
		2.12	0.7	6	7.6	58.3	
		2.15	0.9	9	7.6	47.6	
		1.82	6.3	33	7.6		53.4
		2.06	3.6	29	7.6		33.0
115	Sa	2.08	9.4	100	0	11.1	
		2.11	9.0	100	0	9.6	
		2.08	10.2	100	0	14.0	
		2.10	8.7	100	0	16.1	
		2.06	10.6	100	0		42.0
		2.05	10.1	100	0		39.8
		2.06	9.7	100	0		31.3
		2.25	5.7	100	0		24.9
118	Sa	2.06	9.2	100	0	10.3	
		2.11	9.9	100	0	14.2	
		2.13	8.7	100	0	12.2	
		2.15	8.1	100	0		37.7
		2.10	10.7	100	0		32.6
		2.17	7.5	100	0		32.8
		2.08	9.3	94	7.6	35.0	
		2.05	10.1	98	7.6	37.6	
		2.09	3.6	37	7.6		45.9
		2.12	3.6	40	7.6		56.5
		2.03	4.1	37	7.6		40.0

Table B1 ..... cont

Sample No.	Rock Type	ρ_d Mgm^{-3}	w %	S_r %	σ_3 MPa	$\Delta\sigma$ MPa +20°C	$\Delta\sigma$ MPa -16°C
120	Br	2.38	2.2	59	0	4.9	
		2.40	2.2	65	0		15.3
		2.40	2.3	68	0		21.9
		2.43	1.3	21	7.9	67.1	
		2.16	11.1	99	7.9		15.2
121	Sa/Si	2.39	3.3	79	0	18.5	
		2.38	2.7	61	0	18.8	
		2.36	2.4	50	0	28.8	
		2.36	3.7	77	0		19.2
		2.40	3.4	83	0		13.1
		2.39	4.0	95	0		16.2
		2.33	3.4	64	0		18.8
		2.41	3.0	77	0	25.5	
123	Mu	2.41	1.3	21	0	43.4	
		2.40	0.9	14	0	50.9	
		2.36	2.2	31	0		23.6
		2.36	2.4	33	0		42.0
		2.37	2.0	29	0		11.7
		2.40	1.1	17	8.0	61.7	
		2.40	1.1	17	8.0	70.0	
		2.37	1.8	26	8.0		15.4
		2.37	2.5	36	8.0		24.4

constant stress rate = 1 MPa/s

Br - Breccia
Mu - Mudstone
Sa - Sandstone
Si - Siltstone

ρ_d - Dry Density

w - Moisture Content

S_r - Degree of Saturation

σ_3 - Confining Pressure

Table B2 Strength test results at -10°C for soil specimens subjected to constant deformation rate of 1mm/min ($\dot{\epsilon}$= 1.3%/min approx)

Material	Spec. No.	Test App.	ρ_d Mgm^{-3}	w %	σ_3 MPa	$\Delta\sigma$ MPa	ϵ_f %
LAF	S53	HPCC	1.51	25.8	0	4.80	15[a]
	S54		1.52	25.3	0	4.69	
	S55		1.50	25.7	0	4.71	
	S56		1.55	24.0	3	5.98	
	S57		1.53	24.2	3	5.85	
	S59		1.51	24.1	6	5.90	
	S60		1.51	25.3	6	4.92	
	S61		1.52	24.6	6	4.87	
	S62		1.54	23.8	6	5.12	
	S63		1.53	23.6	6	5.75	
	S87	Hoek	1.51	24.3	3	5.49	
	S89		1.54	23.8	6	5.80	
	S91		1.54	23.9	12	9.92	
	S92		1.51	24.5	10	10.14	
KM	K5	Hoek	1.58	21.9	10	10.7	20[b]
	K6	UNC	1.57	22.7	0	4.0	
	K7		1.59	22.3	0	3.3	
	K9	Hoek	1.58	23.1	6	7.7	

Table B2 ..... cont

Material	Spec. No.	Test App.	ρ_d Mgm^{-3}	w %	σ_3 MPa	$\Delta\sigma$ MPa	ε_f %
LAL	W1	Hoek	1.67	19.2	0	14.4	4.6
	W2		1.66	19.6	6.8	23.3	8.2
	W3		1.68	19.0	10.3	27.0	10.5
	W4		1.68	19.2	0	14.4	5.3
	W5		1.67	19.5	0	15.0	4.2
	W6		1.67	19.6	0	13.8	4.7
	W7		1.66	19.1	0	13.7	4.7
	W8		1.67	19.1	0	14.0	4.1
	W9		1.67	19.1	10.3	28.9	10.6
	W10		1.65	19.6	10.3	27.4	10.5
	W11		1.66	19.8	10.3	28.7	9.2
	W12		1.65	20.0	10.3	26.3	10.5
	W13		1.67	19.6	10.3	27.0	9.3
	W14	UNC	1.69	18.2	0	15.8	5.3
	W15		1.67	19.2	0	15.0	4.0
	W16		1.70	18.2	0	14.9	3.3
	W17		1.66	19.1	0	14.2	3.3
	W18		1.64	20.2	0	15.2	3.3
	W19		1.70	18.6	0	14.3	4.0
	W20	Hoek[c]	1.69	19.1	0	13.6	3.3
	W21		1.70	18.5	0	13.9	3.3
	W22		1.65	20.3	0	13.7	3.3
	W23		1.68	19.3	0	13.4	3.6
	W24		1.69	18.8	0	14.0	2.6
	W25		1.68	19.1	0	13.7	3.4
	W26		1.69	20.5	0	13.7	3.3

a - Nominal 15% strain defined as failure
b - Nominal 20% strain defined as failure
c - Membrane removed from Hoek cell

ρ_d - Dry Density, w - Moisture Content, σ_3 - Confining pressure,

$\Delta\sigma$ - Deviator stress, ε_f - Failure strain

APPENDIX C

CREEP TEST RESULTS

Table C1 Creep test results - conditions at failure for LAF, LAL and KM (-10°C)

Series A - LAF Sand

Test No.	σ_3 (MPa)	$\Delta\sigma$ (MPa)	ASR (%)	Failure Point			C_m	K_m
				t_m (hrs)	ε_m (%)	$\dot{\varepsilon}_m$ (%/hr)		
S30	0	4.3	110	0.076	8.6	68.4	0.60	40.4
S31	0	3.0	77	0.95	13	7.2	0.53	13.4
S32	0	3.7	95	0.184	12.5	39.1	0.58	33.4
S43	0	3.17	82	0.212	25.4	74.5	0.62	66.5
S66	0	2.4	62	15.9	18.6	0.44	0.38	6.5
S67	0	2.4	62	14.94	20.7	0.5	0.36	7.8
S68	0	1.92	49	14.75	10.3	0.26	0.37	3.8
S69	0	2.4	62	7.81	15.4	0.74	0.38	7.1
S70	0	1.92	49	100	13	0.035	0.27	3.7
S73	0	2.64	67	4.39	16.5	1.6	0.43	8.7
S18	1	5.88	134	0.209	14.1	51.2	0.76	46.3
S19	1	3.92	89	14.2	18.1	0.26	0.20	10.6
S78	3	3.81	70	1.08	22.6	9.56	0.46	21.8
S80	3	4.45	83	0.75	30	24.1	0.60	35.7
S84	3	3.81	70	1.51	26.8	7.95	0.45	22.3
S64	6	1.80	26	30.62	7.2	0.059	0.25	3.1
S85	6	3.48	51	3.38	28.4	3.34	0.40	17.4
S88	6	2.32	33	194	18.4	0.02	0.21	6.1

Table C1 ..... cont

Series B - LAL Sand

Test No.	σ_3 (MPa)	$\Delta\sigma$ (MPa)	ASR (%)	Failure Point			C_m	K_m
				t_m (hrs)	ϵ_m (%)	$\dot{\epsilon}_m$ (%/hr)		
UC1	0	2.68	17	59.5	2.5	0.01	0.24	0.9
UC2	0	2.8	18	101	2.5	0.009	0.36	0.5
UC3	0	4.2	27	42.3	4.4	0.033	0.32	1.3
UC4	0	3.5	23	77.6	4.6	0.017	0.29	1.3
UC5	0	5.6	36	8.9	4.5	0.26	0.51	1.5
UC6	0	7	45	6.5	5.1	0.34	0.43	2.3
UC10	0	7	45	9.9	4.7	0.17	0.36	2.1
CC4	1	7	42	20.1	4.7	0.094	0.40	1.4
CC5	1	5.6	34	62.3	5.3	0.034	0.40	1.0

Series C - KM Clay

Test No.	σ_3 (MPa)	$\Delta\sigma$ (MPa)	ASR (%)	Failure Point			C_m	K_m
				t_m (hrs)	ϵ_m (%)	$\dot{\epsilon}_m$ (%/hr)		
K8	0	1.48	41	51.9	18.4	0.15	0.42	3.5
K10	0	2.22	61	0.56	5.0	5.58	0.62	7.2
K11	0	1.8	50	149.5	15.1	0.036	0.36	2.5
K12	1	3.18	74	0.09	9.4	60	0.57	37.1
K13	1	1.59	37	900	5.5	0.002	0.33	0.6
K19	1	2.15	50	9.98	12.7	0.98	0.77	2.2

Table C2 Creep test results for LAF sand - data taken at apparent transition point between primary and secondary creep (-10°C)

Test No.	σ_3 (MPa)	$\Delta\sigma$ (MPa)	ASR (%)	Prim.- Sec. Point			C_{ps}	K_{ps}
				t_{ps} (hrs)	ε_{ps} (%)	$\dot{\varepsilon}_{ps}$ (%/hr)		
S68	0	1.92	49	11	9.6	0.175	0.20	5.9
S70	0	1.92	49	70	12	0.036	0.21	4.9
S76	0	2.16	55	1.2	8.8	1.73	0.24	8.4
S66	0	2.40	61	7.2	14.4	0.475	0.24	9.0
S67	0	2.40	61	9.5	17.9	0.504	0.27	9.8
S69	0	2.40	61	4	12.5	0.75	0.24	9.0
S73	0	2.64	67	2.6	13.3	1.6	0.31	9.9
S31	0	3.01	77	0.475	9.5	7	0.35	12.3
S43	0	3.17	81	0.145	20.1	77.2	0.56	58.9
S32	0	3.70	94	0.08	8.15	40.3	0.40	22.1
S30	0	4.30	110	0.054	7.2	65.6	0.49	30.3
S19	1	3.92	88	10	17	0.236	0.14	12.3
S18	1	5.88	133	0.11	8.8	52.5	0.66	37.5
S83	3	1.91	35	10	8.15	0.117	0.14	5.9
S82	3	2.54	47	0.44	10.8	7	0.29	13.6
S77	3	3.18	59	1.2	13.9	5.04	0.44	12.8
S81	3	3.18	59	0.54	17.2	8.71	0.27	20.4
S78	3	3.81	70	0.58	17.9	9.93	0.32	21.3
S84	3	3.81	70	0.59	19	9.41	0.29	22.2
S80	3	4.45	82	0.22	17.3	26.1	0.33	28.6
S64	6	1.80	26	140	8.3	0.007	0.12	4.6
S88	6	2.32	33	110	16.5	0.021	0.14	8.5
S86	6	2.90	42	3.7	15.5	0.741	0.18	12.3
S85	6	3.48	51	1.25	21.1	4.04	0.24	20.0
S97	10.2	2.80	31	0.6	12	4.6	0.23	13.5
S98	10.2	2.80	31	2.1	11.9	0.92	0.16	10.5
S96	11.2	4.20	44	0.21	22.8	31.2	0.29	35.7

REFERENCES

AERNI, K. and METTIER, K. (1980) 'Ground freezing for the construction of the three lane Milchbruck road tunnel in Zurich, Switzerland', Proc. 2nd Int. Symp. on Ground Freezing, Trondheim, preprints, pp 889-895.

AKAGAWA, S., GOTO, S. and RYOKAI, K. (1982) 'Review and findings of laboratory tests on the mechanical properties of artificially frozen soils', Shimizu Tech. Res. Bull., No. 1, Mar. 1982, pp 7-17.

ALKIRE, B.D. (1972) 'Mechanical properties of sand-ice materials', Unpublished Ph.D. thesis, Mich. State Univ., East Lansing.

ALKIRE, B.D. and ANDERSLAND, O.B. (1973) 'The effect of confining pressure on the mechanical properties of sand-ice materials', Jnl. Glaciology, 12(16), pp 469-481.

ALNOURI, I. (1969) 'Time dependent strength behaviour of two soil types at lowered temperatures', Unpublished Ph.D. thesis, Mich. State Univ., East Lansing.

ALTOUNYAN, P.F.R., BELL, M.J., FARMER, I.W. and HOPPER, C.J. (1982) 'Temperature, stress and strain measurements during and after construction of concrete linings in frozen sandstones', Proc. 3rd Int. Symp. on Ground Freezing, USACRREL, preprints, pp 343-348.

ANDERSLAND, O.B. and ALKILI, W. (1967) 'Stress effect on creep rates of frozen clay soil', Geotechnique (London), 17, No. 1, pp 27-39.

ANDERSLAND, O.B. and ALNOURI, I. (1970) 'Time dependent strength behaviour of frozen soils', Proc. ASCE, 96, No. SM4, pp 1249-1266.

ANDERSLAND, O.B. and ANDERSON, D.M., (eds) (1978) 'Geotechnical engineering for cold regions', McGraw-Hill, New York, 566 pp.

ASSUR, A. (1980) 'Some promising trends in ice mechanics', Physics and Mechanics of Ice, I.U.T.A.M. Symp., Copenhagen, Per Tryde (ed.), Springer-Verlag, Berlin, pp 1-15.

AULD, F.A. (1985) 'Freeze wall strength and stability design problems in deep shaft sinking. Is current theory realistic?', Proc. 4th Int. Symp. on Ground Freezing, Sapporo, preprints, pp 343-349.

BAKER, T.H.W. (1976) 'Transportation, preparation and storage of frozen soil samples for laboratory testing', Soil Specimen Preparation for Laboratory Testing, A.S.T.M. STP 599, pp 88-112.

BAKER, T.H.W. (1978) 'Effect of end conditions on the uniaxial compressive strength of frozen sand', Proc. 3rd Int. Conf. on Permafrost, Edmonton, Vol. 1, pp 608-614.

BAKER, T.H.W., GALLAVRESI, F., JESSBERGER, H.L., KINOSITA, S., SAYLES, F.H., SADOVSKIY, A.V., SEGO, D. and VYALOV, S.S. (1983) 'Guidelines for classification and laboratory testing of artificially frozen ground', Findings of ISGF working ground on testing methods for frozen soils, Proc. 3rd Int. Symp. on Ground Freezing, USACRREL, Vol. 2 (In Press).

BAKER, T.H.W., JONES, S.J. and PARAMESWARAN, V.R. (1982) 'Confined and unconfined compression tests on frozen sands', Proc. 4th Can. Permafrost Conf., Roger J.E. Brown mem. vol. , pp 387-393.

BAKER, T.H.W. and KONRAD, J.M. (1985) 'Effect of sample preparation on the strength of artificially frozen sand', Proc. 4th Int. Symp. on Ground Freezing, Sapporo, Vol. 2, pp 171-176.

BAKER, T.H.W. and KURFURST, P.J. (1985) 'Acoustic and mechanical properties of frozen sand', Proc. 4th Int. Symp. on Ground Freezing, Sapporo, preprints, pp 227-234.

BERNASCONI, G. and PIATTI, G., (eds) (1978) 'Creep of engineering materials and structures', Proc. Joint Res. Centre of the Commission of the European Communities, Italy, App. Sci. Publishers Ltd, London, 420 pp.

BOURBONNAIS, J. and LADANYI, B. (1985) 'The mechanical behaviour of frozen sand down to cryogenic temperatures', Proc. 4th Int. Symp. on Ground Freezing, Sapporo, preprints, pp 235-244.

BOURBONNAIS, J. and LADANYI, B. (1985) 'The mechanical behaviour of a frozen clay down to cryogenic temperatures', Proc. 4th Int. Symp. on Ground Freezing, Sapporo, Vol. 2, pp 237-244.

BRAUN, B., SHUSTER, J. and BURNHAM, E. (1978) 'Ground freezing for support of open excavations', Proc. 1st Int. Symp. on Ground Freezing, Bochum, Vol. 2, pp 137-155.

BROWN, E.T., (ed) (1983) 'Suggested methods for determining the strength of rock materials in triaxial compression', revised version, Suggested Methods for Triaxial Compression Testing, Int. Soc. for Rock Mechs, 211 pp.

BS 1377 (1975), 'Methods of test for soils for Civil engineering purposes', 143 pp.

CHAMBERLAIN, E., GROVES, C. and PERHAM, R. (1972) 'The mechanical behaviour of frozen earth materials under high pressure triaxial test conditions', Geotechnique (London), 22, No. 3, pp 469-483.

DIEKMANN, N. and JESSBERGER, H.L. (1982) 'Creep behaviour and strength of an artificially frozen silt under triaxial stress state', Proc. 3rd Int. Symp. on Ground Freezing, USACRREL, Seperate, 8 pp.

DOMKE, O.A. (1915) 'Uber die beanspruchungen der frostmauer beim schachtabteufen nach dem gefrierverfahren', Gluckauf, 51, No. 47, pp 1129-1135 (in German).

ECKARDT, H. (1979) 'Creep behaviour of frozen soils in uniaxial compression tests', Eng. Geology, 13, pp 185-195.

ECKARDT, H. (1982) 'Creep tests with frozen soils under uniaxial tension and uniaxial compression', Proc. 4th Can. Permafrost Conf., Roger J.E. Brown mem. vol., pp 394-405.

EVANS, R.W. and WILSHIRE, B. (1985) 'Creep of metals and alloys', The Inst. of Metals, Book No. 304, 314 pp.

FAROUKI, O.T. (1981) 'The thermal properties of soils in cold regions', Cold Regs Sci. and Tech. 5, No. 1, pp 67-76.

FISH, A.M. (1982) 'Comparative analysis of the USSR construction codes and the US army technical manual for design of foundations on permafrost', US Army CRREL, Report 82-14, 20 pp.

FISH, A.M. (1983)a 'Comparison of USSR codes and US Army manual for design of foundations on permafrost', Cold Regs Sci. and Tech. 8, No. 1, pp 3-24.

FISH, A.M. (1983)b 'Thermodynamic model of creep at constant stresses and constant strain rates', US Army CRREL, Report 83-33, 18 pp.

FISH, A.M. and SAYLES, F.H. (1981) 'Acoustic emissions during creep of frozen soils', A.S.T.M. STP 750, pp 194-206.

FUNCKEN, R., GONZE, P., VRANKEN, P., MANFROY, P. and NEERDAEL, B. (1983) 'Construction of an experimental laboratory in deep clay formation', Eurotunnel 83, Basle, Paper 9, pp 79-86.

FUNCKEN, R., HEREMANS, R., MANFROY, R., MAYENCE, M. and VANHAELEWYN, R. (1980) 'Experimental program during the construction of an underground laboratory in a plastic clay at 215m depth', Proc. Int. Symp. Rockstore 80, Stockholm.

GARDNER, A.R. (1985) 'The creep behaviour of frozen ground in relation to artificial ground freezing', Ph.D. thesis, Univ. of Nottingham, 331 pp.

GARDNER, A.R., JONES, R.H. and HARRIS, J.S. (1982) 'Strength and creep testing of frozen soils', Proc. 3rd Int. Symp. on Ground Freezing, USACRREL, preprints, pp 53-60.

GAROFALO, F. (1965) 'Fundamentals of creep and creep-rupture in metals', MacMillan Co., New York, 258 pp.

GITTUS, J. (1975) 'Creep, viscoelasticity and creep fracture in solids', App. Sci. Publishers Ltd, London, 725 pp.

GLASSTONE, S., LAIDLER, K.J. and EYRING, H. (1941) 'The theory of rate processes: the kinetics of chemical reactions, viscosity, diffusion and electrochemical phenomena', Int. Chem. Series, McGraw Hill, New York, 611 pp.

GLEN, J.W. (1955) 'The creep of polycrystalline ice', Proc. Royal Soc., London, No. A228, pp 519-538.

GONZE, P., LEJEUNE, M., THIMUS, J. and MONJOIE, A. (1985) 'Sand ground freezing for the construction of a subway station in Brussels', Proc. 4th Int. Symp. on Ground Freezing, Sapporo, preprints, pp 277-283.

GOUGHNOUR, R.R. and ANDERSLAND, O.B. (1968) 'Mechanical properties of a sand-ice system', Proc. ASCE, 94, No. SM4, pp 923-950.

GREGORY, O. and MAISHMAN, D. (1973) 'Motorway construction meets an unusual problem in old shaft treatment', Inst. of Mining Engs, Geol. and Min. Soc. Branch meeting, Manchester, 8th Feb 1973, 26 pp.

HANNA, T.H. (1973) 'Foundation instrumentation', Series on Rock and Soil Mechanics, 1, No. 3, Trans. Tech. Publ. 365 pp.

HARRIS, J.S. (1985) 'Ground Freezing', In: Underpinning, Surrey University Press, Thorburn, S. and Hutchinson, J.F. (eds), pp 222-241.

HARRIS, J.S. and POLLARD, C.A. (1985) 'Some aspects of groundwater control by the ground freezing and grouting methods', Geolsoc Eng. Group Symp., Sheffield, Sept 1985, 21 pp.

HOEK, E. and FRANKLIN, J.A. (1968) 'Simple triaxial cell for field or laboratory testing of rock', Trans. Section A, Inst. of Mining and Metallurgy, Vol. 77, pp A22-A26.

HULT, J.A.H. (1966) 'Creep in engineering structures', Blaisdell Publ. Co., Massachusetts, 115 pp.

JESSBERGER, H.L. (1977) 'Strength and time dependent deformation of artificially frozen soil', Proc. Int. Symp. on Frost Action in Soils, Univ. of Lulea, Sweden, pp 157-167.

JESSBERGER, H.L. (1980) 'State-of-the-art-report. Ground freezing: mechanical properties, processes and design', Proc. 2nd Int. Symp. on Ground Freezing, Trondheim, preprints, pp 1-33.

JESSBERGER, H.L. and JORDAN, P. (1982) 'Frozen saline sand subjected to dynamic loads', Proc. 3rd Int. Symp. on Ground Freezing, USACRREL, preprints, pp 19-25.

JONES, R.H. (1982) 'Closing remarks to ISGF 82', Proc. 3rd Int. Symp. on Ground Freezing, USACRREL, Seperate, 4 pp.

JONES, R.H. (1984) 'Role of field observations in bridging the gap between theory and practise in artificial ground freezing', Proc. Symp. on Relating Theory to Practise in Artificial Ground Freezing, Nottingham, Sept. 1984, pp 49-54.

JONES, S.J. and PARAMESWARAN, V.R. (1983) 'Deformation behaviour of frozen sand-ice materials under triaxial compression', Proc. 4th Int. Conf. on Permafrost, Univ. of Alaska, pp 560-565.

KAPLAR, C.W. (1971) 'Some strength properties of frozen soil and effect of loading rate', US Army CRREL, Special Report 159, pp 20.

KLEIN, J. (1978) 'Nichtlineares kriechen von kunstlich gefrorenem Emschermergel', Ruhr-Universitat, Bochum, Heft 2, Serie G, 123 pp (in German: Summary in English).

LADANYI, B. (1972) 'An engineering theory of creep of frozen soils', Can. Geot. Jnl, 9, No. 1, pp 63-80.

LADE, P.V., JESSBERGER, H.L. and DIEKMANN, N. (1980) 'Stress-strain and volumetric behaviour of frozen soil', Proc. 2nd Int. Symp. on Ground Freezing, Trondheim, preprints, pp 48-64.

LAME and CLAPEYRON, (1833) 'Memoire sur l'equilibre interieur des corps solides homogenes', Mem. divers savans, Vol. 4.

LEONARDS, G.A. (1955) 'Strength characteristics of compacted clays', Trans. ASCE, 120, pp 1420-1454.

MARCHINA, P. (1984) 'The influence of specimen preparation on the response of rocks and aggregates to freezing', M.Phil thesis, Univ. of Nottingham, 181 pp.

MELLOR, M. (1973) 'Mechanical properties of rocks at low temperatures', Proc. 2nd Int. Conf. on Permafrost, North American Contribution, Yakutsk, pp 334-344.

MELLOR, M. and COLE, D.M. (1982) 'Deformation and failure of ice under constant stress or constant strain-rate', Cold Regs Sci. and Tech. 5, No. 3, pp 201-219.

NEERDAEL, B., BUYENS, M., LEJEUNE, M., THIMUS, J.F., FUNCKEN, R. and DETHY, B. (1983) 'Field measurements during the construction of an underground laboratory in a deep clay formation', Proc. Int. Symp. on Field Measurements in Geomechanics, Zurich, Vol. 2, pp 1419-1430.

NEUBER, H. and WOLTERS, R. (1970) 'Mechanical behaviour of frozen soils under triaxial compression', Tech. translation by Robert Serre, Can. Inst. for Scientific and Techanical Information, 53 pp.

O'CONNOR, M.J. and MITCHELL, R.J. (1982) 'A comparison of triaxial and plane strain tests on frozen silt', Proc. 4th Can. Permafrost Conf., Roger J.E. Brown mem. vol. , pp 382-386.

ORTH, W. and MEISSNER, H. (1982) 'Long term creep of frozen soil in uniaxial and triaxial tests', Proc. 3rd Int. Symp. on Ground Freezing, USACRREL, preprints, pp 81-87.

PARAMESWARAN, V.R. (1980) 'Deformation behaviour and strength of frozen sand', Can. Geot. Jnl, 17, No. 1, pp 74-88.

PARAMESWARAN, V.R. and JONES, S.J. (1981) 'Triaxial testing of frozen sand', Jnl. of Glaciology, 27(95), pp 147-156.

PARAMESWARAN, V.R. and ROY, M. (1982) 'Strength and deformation of frozen saturated sand at -30°C', Can. Geot. Jnl., 19, No. 1, pp 104-107.

PERKINS, T.K. and RUEDRICH, R.A. (1973) 'The mechanical behaviour of synthetic permafrost', Soc. of Petroleum Engs Jnl., 13, No. 4, pp 211-220.

REIN, R.G. and HATHI, V.V. (1978) 'The effect of stress on strain at the onset of tertiary creep of frozen soils', Can. Geot. Jnl., 15, No. 3, pp 424-426.

REIN, R.G., HATHI, V.V. and SLIEPCEVICH, C.M. (1975) 'Creep of sand ice system', Proc. ASCE, 101, No. GT2, pp 115-128.

SANGER, F.J. (1968) 'Ground freezing in construction', Proc. ASCE, 94, No. SM1, pp 131-158.

SANGER, F.J. and KAPLAR, C.W. (1963) 'Plastic deformation of frozen soils', Proc. 1st Int. Conf. on Permafrost, Lafayette, pp 305-315.

SAYLES, F.H. (1963) 'Constant stress compression type creep apparatus', US Army CRREL, Tech. Note IR 254, 18 pp.

SAYLES, F.H. (1966) 'Low temperature soil mechanics', US Army CRREL, Tech. Note.

SAYLES, F.H. (1968) 'Creep of frozen sands', US Army CRREL, Tech. Report 190, 54 pp.

SAYLES, F.H. (1973) 'Triaxial and creep tests on frozen Ottawa sand', Proc. 2nd Int. Conf. on Permafrost, North American contribution, Yakutsk, pp 384-391.

SAYLES, F.H. and EPANCHIN, N.V. (1966) 'Rate of strain compression tests on frozen Ottawa sand and ice', US Army CRREL, Tech. Note IR 238, 89 pp.

SCHMID, L. (1981) 'Milchbuck tunnel: Application of the freezing method to drive a three-lane highway tunnel close to the surface', Rapid Excavation and Tunnelling Conf. Proc. Vol. 1, Chap. 27, pp 427-445.

SIMONSON, E.R., JONES, A.H. and GREEN, S.J. (1974) 'High pressure mechanical properties of three frozen materials', Proc. 4th Int. Conf. on High Pressure, Physico-chemical Soc. of Japan, Kyoto, pp 115-121.

SULLY, A.H. (1949) 'Metallic creep and creep resistant alloys', Robert Maclehouse and Co. Ltd., Glasgow, 278 pp.

TAN, A.O. (1985) 'Laboratory strength and creep testing of frozen LAL sand', Internal Report, Civil Eng. Dept., Univ. of Nottingham, pp 28.

TING, J.M. (1983) 'On the nature of the minimum creep rate-time correlation for soil, ice and frozen soil', Can. Geot. Jnl., 20, No. 1, pp 176-182.

TSYTOVICH, N.A. (1975) 'The mechanics of frozen ground', McGraw Hill Series in Modern Structures: Systems and Management, New York.

VYALOV, S.S. (ed) (1965) 'The strength and creep of frozen soils and calculations for ice-soil retaining structures', US Army CRREL, Translation No. 76.

WOLFE, L.M. and THIEME, J.O. (1964) 'Physical and thermal properties of frozen soil and ice', Jnl. of the Soc. of Petroleum Engineers, pp 67-72.

ZHU YUALIN and CARBEE, D.L. (1983) 'Creep behaviour of frozen silt under constant uniaxial stress', Proc. 4th Int. Conf. on Permafrost, Univ. of Alaska, pp 1507-1512.